Batch to continuous vinyl chloride suspension polymerization process : a feasibility study

Emeline Lobry

Université de Toulouse

THÈSE

En vue de l'obtention du

DOCTORAT DE L'UNIVERSITÉ DE TOULOUSE

Délivré par :
Institut National Polytechnique de Toulouse (INP Toulouse)

Discipline ou spécialité :

Génie des procédés et de l'Environnement

Présentée et soutenue par :
Emeline LOBRY

le : vendredi 14 septembre 2012

Titre :

Batch to continuous vinyl chloride suspension polymerization process : a feasibility study

---

Ecole doctorale :
Mécanique, Energétique, Génie civil et Procédés (MEGeP)

Unité de recherche :
Laboratoire de Génie Chimique

Directeur(s) de Thèse :
Christophe GOURDON, Professeur INP-ENSIACET
Catherine XUEREB, Directrice de recherche CNRS-LGC

Rapporteurs :
Michel SARDIN, Professeur à l'ENSIC, Université de LORRAINE, Nancy
Timothy McKENNA , Directeur de recherche CNRS-LCPP/ESCPE-Lyon

Membre(s) du jury :
Timothy McKENNA , Directeur de recherche CNRS-LCPP/ESCPE-Lyon
Michel SARDIN, Professeur à l'ENSIC, Université de LORRAINE, Nancy
Marc BRANLY , Manager Technologie PVC et Développement, Ineos ChlorVinyls
Gilbert CASAMATTA , Professeur INP-ENSIACET, Toulouse
Thierry LASUYE , Responsable Département Qualité Innovation PVC, Ineos ChlorVinyls
Xiong-Wei NI, Professeur, Heriot Watt University

Remerciements

A l'issue de la rédaction de ce manuscrit et de ces trois années de thèse, je suis convaincue que je n'aurais jamais pu réaliser ce travail sans le soutien d'un grand nombre de personnes dont la générosité et la bonne humeur m'ont permis de progresser. Je tiens à remercier chaleureusement toutes ces personnes qui m'ont entourée au cours de ces dernières années.

Tout d'abord, mes remerciements s'adressent à mes directeurs de thèse, Christophe Gourdon et Catherine Xuereb. Christophe, je te remercie pour nos discussions, tes conseils et tes encouragements. Cathy, je te remercie pour ton soutien et tes remarques pertinentes. Je tiens à vous remercier tous les deux pour votre confiance au cours de ces années.

J'adresse également mes remerciements à Thierry Lasuye et Marc Branly pour m'avoir fait confiance pour ce projet ainsi que pour leur disponibilité. Je vous remercie pour votre accueil sur le site de Mazingarbe et également pour m'avoir toujours incluse dans les réunions avec les différents fournisseurs. Les débuts de ma thèse ont ainsi été ponctués par quelques visites de sites de mélangeurs statiques! J'en profite également pour remercier l'équipe du pilote, et plus particulièrement Didier Berlinet et Julien Lionet.

J'adresse ma reconnaissance à Timothy McKenna, directeur de recherche au LCPP et à Michel Sardin, professeur à l'INPL, pour avoir accepté de rapporter ce travail de thèse, pour l'intérêt qu'ils y ont porté et pour leurs remarques et commentaires très constructifs lors de la soutenance. Je remercie également Gilbert Casamatta de m'avoir fait l'honneur de présider ce jury ainsi que Xiongwei Ni pour avoir accepté de participer à ma soutenance.

Je voudrais remercier chaleureusement l'ensemble du personnel du Laboratoire de Génie Chimique. J'ai toujours trouvé une écoute ou des réponses à mes questions et ceci généralement dans la bonne humeur !
Je voudrais remercier toutes les personnes qui nous aident dans notre quotidien de doctorant : Dany et Christine pour leur écoute … et pour avoir sauvé ma soutenance ! Un grand merci à Claudine, Maria et Jean-Luc ! Merci également à Alain Phillip pour sa bonne humeur au détour des couloirs du laboratoire… Désolée encore d'avoir repeint en blanc les murs du hall…

Je m'adresse maintenant aux personnes sans qui ce travail n'auraient pas vus le jour, j'entends par là les personnes de l'équipe technique.
Je souhaiterais remercier tout d'abord Lucien Pollini, pour sa rapidité, sa disponibilité et son intérêt pour mon sujet et pour que tout fonctionne (vite et) bien. Merci aussi à Franck Dunglas et Alec Maunoury pour m'avoir accompagnée à la MEPI pour les essais sur Nitech ! Merci à Alec pour m'avoir également secondée dans ma deuxième session MEPI. Merci pour ton expertise et surtout pour ton écoute ! Merci également d'avoir accepté de jeûner et de m'avoir assistée lors des sessions débouchage !!!!
J'aimerais également remercier Jean-Louis Labbat, Ignace Coghe, Bernard Gally, Alain Pontier et Lacen Fahri pour la bonne humeur autour de la machine à café !
Merci aussi à David Riboul pour les pauses plus tardives !
Mes remerciements iront au service analyses et procédés. Merci à Christine Rey, Marie-Line De Solan, Marie-Line Pern et Gwénaëlle Raimbeaux pour votre disponibilité, vos conseils et votre écoute.

J'adresse également mes remerciements au personnel de la MEPI pour m'avoir accueilli pendant quelques semaines. Je tiens particulièrement à remercier Sophie Cerdan pour m'avoir initiée au Nitech. Je remercie aussi Annelyse Conté pour ses conseils ainsi que Sébastien Elgue.

Je souhaite remercier toutes les personnes de l'équipe RMS avec qui j'ai eu l'occasion de travailler ou d'échanger sur différents sujets ! En particulier, je souhaiterai remercier Philippe Destrac pour son implication, son suivi et ses remarques qui m'ont toujours permis d'avancer. Je remercie aussi Nathalie Le Sauze son intérêt concernant la partie mélangeur statique de ma thèse. Un grand merci à Karine Loubière, pour son écoute, sa curiosité scientifique et ses encouragements. Merci pour ton aide. Je remercie tous les autres membres de l'équipe avec qui j'ai pu discuter au cours de ces trois ans, que ce soit sur le plan professionnel ou non : Laurent Prat, Séverine Camy, Patrick Cognet, Joëlle Aubin.

Un grand merci à tous les doctorants du laboratoire, anciens comme actuels.
Merci à Mallorie pour son écoute et son soutien ! Merci à Carole, Baptiste, Nicolas AbiChebel (et sa douce voix), Edgar, Fatima, Thomas pour les moments agréables passés ensemble.
Mes pensées vont aussi à tous les doctorants du premier étage de Labège : Maxime et Alex.
Céline, merci pour tout ! Je penserai toujours à nos grandes discussions le soir avant de quitter le labo ! Je n'oublierai pas non plus notre escapade au Skybar ;-) ni le jour où j'ai déposé mon manuscrit…Quand tu veux pour un mojito.

Tristan, cette fois-ci je ne t'oublierai pas !!! J'ai pris beaucoup de plaisir à partager mon bureau avec toi cette dernière année de thèse, malgré nos divergences…Je te souhaite plein de bonnes choses pour la suite !

Youen, merci pour toutes les pauses sucrées ! En écrivant ces mots, je pense au kouing aman et au caramel beurre salé… Merci aussi pour ton grand soutien pendant les derniers mois !

Je voudrais également remercier mes amies Tanya, Miruna et Félicie. Nous avons formé un quatuor de choc ! Aujourd'hui nous avons toutes soutenues et l'aventure continue ! Tanya merci pour tes sourires et ta spontanéité ! Miruna, je te remercie pour ton accueil au laboratoire et ta générosité ! Je te souhaite plein de bonheur et de réussite dans la nouvelle aventure qui t'attend ! Félicie, non seulement tu as été une collègue avec qui j'ai aimé (et j'apprécie toujours) travailler, mais en plus tu as été une très grande amie ! Tu m'as soutenue malgré la distance ! Merci de t'être déplacée pour la soutenance !

Je tiens également à remercier Anne-Claire et Charles pour les moments de détente…

Je souhaite également remercier tous mes amis nancéiens, normands, vosgiens, lyonnais, rémois et londoniens…

Enfin, ma dernière pensée ira à ma famille. Je vous remercie pour vos encouragements et pour m'avoir toujours laissé libre de mes choix. Merci pour votre soutien et pour m'avoir donné confiance en moi. Merci de m'avoir appris à donner le meilleur et toujours plus. Merci à Sylvaine pour son soutien en fin de rédaction ! Bonne chance pour ta thèse !

Merci également à Lilian pour m'avoir soutenu et permis de relativiser, pour le réconfort et … pour les chocolats…

Abstract

Les procédés continus par rapport aux procédés batch sont réputés être plus sûrs, plus économiques et plus sélectifs. Au regard de ces avantages, de plus en plus d'industries opérant traditionnellement en batch s'orientent vers des procédés continus. Si beaucoup de recherches ont été menées dans ce domaine en chimie fine, il n'en est pas de même pour les procédés de polymérisation et plus particulièrement pour le procédé de polymérisation en suspension du chlorure de vinyle. Ce procédé est à l'heure actuelle un des procédés batch les plus aboutis tant il a subi d'améliorations au cours des dernières décennies sur les plan chimiques (recette) et technologiques. Cependant, l'exposition au chlorure de vinyle est extrêmement toxique et le procédé présente notamment toujours des limitations en transfert thermique inhérentes à la technologie batch. De plus, l'étape réactionnelle constitue la seule étape batch du procédé total de production. Eu égard à la formation des grains de PVC au cours de la réaction, le procédé peut être divisé en trois principales étapes : une étape de dispersion liquide-liquide dans laquelle les gouttelettes de monomères (diamètre moyen 30-50μm) sont formées et stabilisées, une étape de réaction qui s'accompagne d'un phénomène d'agglomération contrôlée des gouttelettes de monomères et au cours duquel les particules polymérisant s'avèrent collantes et une pure étape réactionnelle au cours de laquelle la polymérisation est menée jusqu'à la conversion désirée. La présente étude se propose d'identifier les technologies adaptées pour chacune des étapes identifiées. Compte tenu des connaissances actuelles sur le comportement et l'évolution des grains avec la conversion et après une étude bibliographique sur les procédés continus de polymérisation, les technologies choisies dans ce travail sont les mélangeurs statiques et différents design de colonnes pulsées utilisées à co-courant. L'étape de dispersion liquide-liquide a été étudiée à l'aide de trois technologies différentes pour des systèmes de phases modèles. Concernant les mélangeurs statiques, les études ont démontré leur capacité à obtenir des gouttelettes de taille contrôlée et de la taille désirée. Dans la gamme étudiée, aucun effet de la concentration en phase dispersée n'a été démontré sur la taille des gouttes. Le paramètre physico-chimique le plus influent est la tension interfaciale. Celle-ci a d'ailleurs été estimée aux temps courts, correspondant aux temps de séjour (40-100 ms) dans les mélangeurs statiques, en modifiant la technique de la goutte pendante. Les résultats en termes de diamètre de goutte ont été corrélés via les nombres adimensionnels caractéristiques du système et de l'écoulement, à savoir les nombres de Reynolds et de Weber. A la lueur de ces résultats, les mélangeurs statiques ont été installés au pilote industriel pour effectuer des chargements de réacteurs batch de polymérisation. En plus de réduire considérablement les temps de chargement, leur utilisation a montré une meilleure répartition des agents de suspension et de l'initiateur au sein du grain. Ensuite, deux design de colonnes pulsées ont été utilisés : la colonne pulsée à disques et couronnes à co-courant ascendant vertical et le COBR (continuous oscillatory baffled reactor, Nitech). Pour le premier design, les influence du matériau de garnissage et de son agencement (type et hauteur), des paramètres physico-chimiques (concentration en phase dispersée, tensioactifs) et des paramètres hydrodynamiques (débit total, amplitude et fréquence d'oscillation) sur la taille des gouttes obtenues ont été examinées. Avec le second design, seuls les paramètres hydrodynamiques ont été étudiés. Une corrélation sur la taille des gouttes est proposée en fonction de nombres adimensionnels caractéristiques de ces appareils. Les trois technologies génératrices de la dispersion sont alors comparées en termes d'énergie dissipée et de puissance dissipée. Pour la suite du procédé, qui correspond à la réaction de polymérisation, le choix de travailler en réacteur tubulaire supposé piston (la colonne pulsée) a été fait. Des études ont alors été menées afin d'évaluer la capacité de la colonne à transporter de façon homogène une suspension de particules de PVC solide sous différentes conditions et une polymérisation en suspension modèle (polymérisation de l'acétate de vinyle) a été menée afin d'identifier la faisabilité du procédé pour la polymérisation

du chlorure de vinyle, notamment pour étudier les problèmes d'encroûtement du réacteur en cours de polymérisation. Les résultats fournissent des premières pistes convaincantes.

Table of contents

Introduction and outline

Continuous processes present the benefit to be safer and more cost saving than batch processes. They allow a better control of the process operating parameters (temperature, selectivity) and of the resulting product properties (Calabrese and Pissavini, 2011). In front of these advantages, lots of industries tend to turn on their current processes from batch to continuous. Fine chemistry industries were the first to sign up in the innovation line. In 2007, a report entitled European roadmap in process intensification recommends concrete actions. The authors list and describe all the equipments foreseen for process intensification.

Few polymerizations are carried out in a continuous way but most of them concern solution or bulk polymerization. From our knowledge, no continuous process is known for continuous suspension polymerization.

Our research in this field comes from the request of Tessenderlo Group, the 6th largest manufacturer of poly(vinyl chloride) PVC in Europe in 2007. In 2011, the group becomes part of Ineos ChlorVinyls which is one of the major chlor-alkyli producers in Europe, a global leader in chlorine derivatives and Europe's largest PVC manufacturer.

PVC is a thermoplastic made of 57% chlorine (derived from industrial grade salt) and 43% carbon (derived predominantly from oil / gas via ethylene). It is less dependent than other polymers on crude oil or natural gas, which are non-renewable. It is one of the most explored polymers in the world, presenting a wide range of properties. It is used in various applications such as pipes, fittings, profiles, packaging, cable insulation, sheets, flooring, medical equipments, bottles…

Nowadays PVC is the third most produced polymer after polyethylene and polypropylene. Every year, 23 millions of tonnes are produced among which one quarter is used exclusively in Europe. The PVC industry represents billions of euros of incomes every year and employs 200,000 people in Europe and in the United States.

Polymerization of vinyl chloride at an industrial scale is exclusively carried out via a free radical mechanism. The main processes of PVC processes are suspension, emulsion, bulk and solution polymerization. The suspension mode represents 80% of the PVC worldwide production. The monomer is the vinyl chloride monomer which is very toxic and gaseous under normal pressure and temperature conditions. It requires drastic precautions mainly related to its handling.

At industrial scale, the PVC suspension polymerization reaction is commonly performed in batch reactors from 2 m^3 to 150 m^3 (Saeki and Emura, 2002). The reaction being carried out in liquid phase, the batch reactor must handle pressure (10-12 bar). The monomer is dispersed into droplets in the continuous phase composed of water and different additives. The monomer droplets act as micro-reactors and turn out into solid particles. The polymerization reaction is initiated by temperature and is highly exothermic. The reaction can lead to thermal runaway. It is one of the main drawbacks of batch polymerization process. Polymerization reaction in batch reactor accounts for almost 50% of the classified accident for which there was a high potential of loss control and runaway (Barton and Nolan, 1989).

The batch suspension polymerization process is intensively described in literature. Lots of works refer to the particle formation and polymerization kinetics. Vinyl chloride is very different from the common monomers such as styrene, methyl methacrylate or vinyl acetate because the monomer is insoluble in its monomer. The bottlenecks for the batch to continuous transposition can be identified by accurately studying literature. They concern mainly the ability to control the droplet/particle size distribution, the porosity properties which depend on the additives and their homogeneity inside the droplets and the encrusting issue due to the sticky stage exhibited by the polymerizing droplets at medium conversion (5-30%). The main steps concern then the liquid-liquid dispersion creation, the sticky-stage process in which the particles agglomerate and reach their final size and the end of the polymerization.

Regarding the characteristic of the continuous intensified equipment and the current batch vinyl chloride suspension polymerization process literature, equipments are proposed to fulfill the objectives of the different steps and raise the identified bottlenecks.

The main objective of this work is to study the abilities of devices to perform suspension polymerization via a continuous process or, at least, to suggest some improvement of the current process. Our research program is then organized around the steps described in the different chapters.

This PhD thesis is structured into six chapters. The first one consists of a short literature review on the suspension vinyl chloride polymerization, analyzing the characteristic points of the batch process and underlining the bottlenecks for the continuous transposition. The methodology is exposed, identifying the different relevant steps relative to the particle morphology evolution with the reaction conversion and the current innovative continuous technology able to fulfill the process requirements.

Chapter two is focused on the different fluids used and experimental techniques developed. Due to monomer toxicity, several fluid models have been used at lab scale to study each polymerization step. The different analytical techniques to characterize the systems and the preliminary studies are described.

The third chapter is dedicated to the liquid-liquid dispersion in static mixers. The aim is to create a monodisperse droplet size distribution, which is at the basis of the suspension polymerization process. The dispersion is generated at very small residence time (from 0.04 s to 0.1 s). The lab tests are described and their results have led to the implementation at the industrial pilot scale of static mixers for the direct batch loading.

The fourth chapter is devoted to the liquid-liquid dispersion in two types of pulsed devices. The goal remains the same as in chapter III but the stabilization of the dispersion is also studied. Two kind of experimental rigs are used: the vertical discs and doughnuts pulsed column and the horizontal continuous oscillatory baffled reactor (COBR, Nitech). They allow to create the liquid-liquid dispersion and to study its stabilization-or not- all along the apparatus. The residence times are then larger (several minutes). Different hydrodynamic and physicochemical parameters are studied leading to the identification of the proper operating conditions to obtain and maintain the expected droplet size. In this chapter, the different liquid-liquid dispersion equipments are also compared in term of energy cost.

At the end of the polymerization, the continuous equipment must be suitable to perform a homogeneous transport of the solid-liquid suspension. Chapter V focuses on this step in a disc and doughnut pulsed column.

Chapter VI presents some feasibility results of continuous suspension polymerization in oscillatory baffled reactor. It reveals promising results for the future development of the continuous process.

CHAPTER I: MOTIVATIONS AND SCIENTIFIC STRATEGY

The PVC, Poly (vinyl chloride) is the third worldwide most produced polymer after polyethylene and polypropylene (www.sfc.fr). This polymer is obtained by radical polymerization of vinyl chloride monomer (VCM). It could be produced by three different ways: bulk polymerization which represents about 5% of the global production, emulsion polymerization (10%) and suspension polymerization, which is the most common way and represents 85% of the global production of PVC. Our interest is focused on suspension polymerization process. This chapter presents a short literature survey of the suspension polymerization PVC process (S-PVC process) particularly focused on the different steps occurring in the reaction and on the bottlenecks to carry out the reaction from batch to continuous.

The current PVC suspension polymerization batch process is first introduced as well as the mechanisms involved in the PVC particles creation. In a second part, a state-of-the-art concerning the continuous suspension and the emulsion processes is presented. This literature survey leads to identify the different steps which take part in the S-PVC process and then to define the hydrodynamic and operating conditions and the bottlenecks to be raised at each step. At the end of this chapter, the scientific strategy developed in the manuscript is introduced.

I. THE CURRENT SUSPENSION POLYMERIZATION PROCESS

PVC (Poly Vinyl Chloride) is a synthetic polymer obtained by the free radical polymerization of vinyl chloride monomer (VCM). The polymer is then formed by the successive additions of the radical building blocks.

The main reactions occurring during radical polymerization include the initiation of the reaction which involves the thermal decomposition of a small molecule (initiator), the propagation which corresponds to the chain growth by radical addition and the termination which induces the reaction of two active polymeric chains by combination (formation of one polymer molecule) or disproportionation (formation of two polymer molecules). The disproportionation is the most important termination mode in radical VCM polymerization. A charge transfer monomer reaction also occurs. It consists in a termination reaction between a growing polymeric radical chain and a monomer molecule.

The polymer obtained is composed by a sequence of —$(CH_2\text{-}CHCl)_n$— motifs with n ranging from 500 to 3500.

The suspension polymerization is a heterogeneous process. In this section, the current S-PVC process is presented.

I.1. ***Description of the batch process***

The S-PVC polymerization (PVC suspension polymerization) is carried out batchwise. At ambient temperature and pressure conditions, the VCM is a gas (boiling point -13.8°C). At the ambient temperature, it is then stored as liquid at a vapor pressure of about 2.5 bar. It is highly flammable and form explosive mixture with oxygen. Moreover, it presents carcinogenic effect. It must be handled carefully.

VCM is partially soluble in water (1100 $mg.kg^{-1}$).

The reaction takes place in pressurized stirred tank because the VCM is at liquid state. Consequently, liquid vinyl chloride under its autogeneous vapor pressure is dispersed in the aqueous phase by vigorous stirring in an autoclave of 25 to 300 m^3capacity (Saeki and Emura, 2002). Each droplet (30-50μm) behaves as a mass polymerization microreactor in which reaction takes place. The reaction is initiated by the thermal decomposition of an initiator soluble in the monomer and the PVC, non-soluble in its monomer, precipitates inside the monomer droplets. The stirred tank is not completely filled and a VCM gas phase filled the free reactor space.

A typical S-PVC recipe is detailed Table I- 1.

S-PVC recipe Polymerization degree 1000 (K value 66)	
VCM	100 parts
Water (de-mineralized)	120 parts
Suspending agents (PVA, etc…)	0.05-0.10 parts
Initiator	0.03-0.16 parts
Polymerization temperature	57°C
Conversion	85-90%
Pressure at the end of the polymerization	5 $kg.cm^{-3}$
Polymerization time	8h

Table I- 1 : Typical S-PVC polymerization recipe (Saeki and Emura, 2002)

The recipe is composed of demineralized water which is the continuous phase. The water is degassed to avoid oxygen introduction in the reactive medium. Indeed, oxygen can cause an induction period in the polymerization process of VCM by forming vinyl chloride polyperoxide. However, the oxygen just delays the polymerization without affecting the polymerization rate. The VCM represents the dispersed phase. The initiators are organic peroxides or azo compounds which are soluble in the monomer and quasi insoluble in water. Their reactivity is imposed by the polymerization temperature (Arrhenius law type rate constant for the decomposition). It is expressed as the half-life time (time necessary for that

half the initiator forms free radicals). Initiators must be well distributed in all the droplets to avoid non homogeneity which leads to quality issues on the final particles.

The protective colloids added inhibit droplets to coalesce. Generally, a mixture of stabilizers is often used: a primary suspending agent which prevents the drop from coalescence and a secondary stabilizer which affects the PVC particles inside the drops and increases polymer porosity (Ormondroyd, 1988). These ones are often polyvinyl acetate (PVAc) partially hydrolysed mentioned as PVA (polyvinyl alcohol). They are characterized by their hydrolysis degree DH and their polymerization degree DP. The primary suspending agent, PVA-I, is soluble in water and presents a high DH (>70%). PVA-I acts on the suspension stability and controls the particles agglomeration. The secondary suspending agent PVA-II has a lower DH ranging from 40 to 55%. Both play a role on the particles porosity. There is of course an interaction between the two suspending agents and their concentrations are set depending on the expected particle size and particle characteristics.

In the classical batch process, the different compounds are loaded in the reactor. The stirring allows the droplets creation and at the same time, the medium is heated until polymerization temperature. The autoclave is equipped of a jacket to control the temperature inside the reactor. Once the polymerization temperature is reached, it is important to maintain it constant. Indeed, the temperature is responsible for the polymerization rate but also for the polymer properties as discussed further (I.4.1). The initiator which is soluble in the monomer starts its decomposition. Polymer chains are formed in the VCM droplets via a free radical polymerization mechanism. They precipitate from the monomer phase due to their limited solubility in VCM. The polymerization occurs in the monomer phase and in the polymer rich phase swollen by VCM (27% weight). The VCM polymerization reaction is highly exothermic (1540 kJ. kg^{-1}_{VCM}). Then the product temperature is maintained constant by monitoring continuously on the jacketed temperature (Figure I- 1(a)). The reaction is carried out at polymerization temperature in the range of 40 – 70°C under the saturated pressure of VCM (10-12 bar). The pressure in the stirred tank remains therefore constant until the monomer liquid phase totally reacts. At this point, a critical conversion X_f is reached and polymerization only occurs in the polymer rich phase swollen with monomer (Figure I- 1(a) and (b)). The pressure gradually decreases. The polymerization rate falls too. At a given pressure drop value, the reaction is stopped either by adding a chain terminator and/or by venting off the unreacted monomer to the recovery plant. The slurry is centrifuged and dried. The PVC particles are then recovered. The pressure drop is measured as the difference between VCM vapor pressure and the pressure in the reactor. It is one of the major control parameter that informs on the final conversion (Xie *et al.,* 1991).

Figure I- 1(b) and Figure I- 2 allow to understand the monomer transfer between the different phases: gas, liquid and polymer. When the amount of free liquid monomer falls at 15-20% (i.e. 55-60% of conversion), the pressure starts to drop. There is still a balance between phases. Before the consumption of the whole liquid monomer, no VCM diffusion from gas phase to polymer occurs. Whereas the VCM mole number in the vapor phase is constant, its volume decreases due to the reaction medium volume shrinkage. It is due to the density difference between the monomer and the polymer.

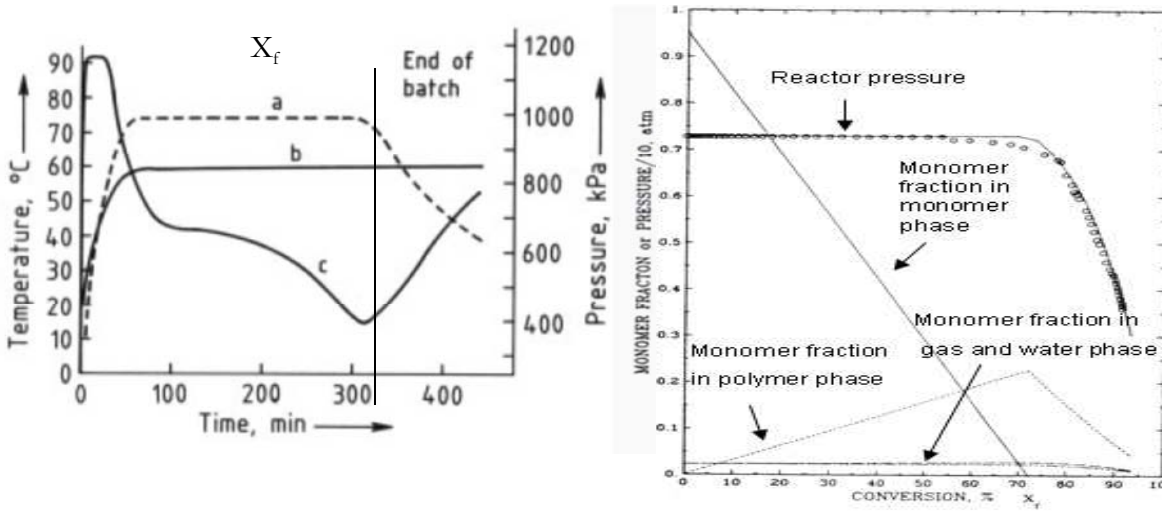

Figure I- 1: (a) a typical suspension polymerization reaction: a) pressure temperature, c) jacketed temperature (i.e. Burgess, 1986) and (b) evolution of reactor pressure and monomer distribution in the different phases

To maintain the pressure constant, the monomer in the liquid phase diffuses through the interface. After X_f, at the moment when the VCM is considerably reduced, the VCM fraction in the polymer phase decreases enabling the monomer transfer from vapor and water phase to polymer phase. The pressure drop corresponds then to high conversion values.

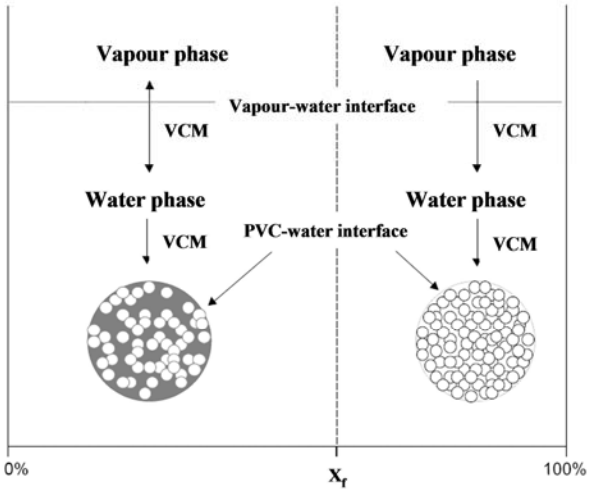

Figure I- 2 : Schematic representation of the monomer transfer before and after the critical conversion X_f (Xie et al., 1991)

Figure I- 3 represents a typical S-PVC process. Except the reactive part of the process, the recovery part and drying are continuous processes.

Our goal is to investigate how to proceed in a continuous mode for the reactive part. The key-steps characterizing the process must be identified. In the following parts, we focus on the liquid-liquid dispersion creation, the reaction kinetics and the PVC grain behaviour in the course of polymerization.

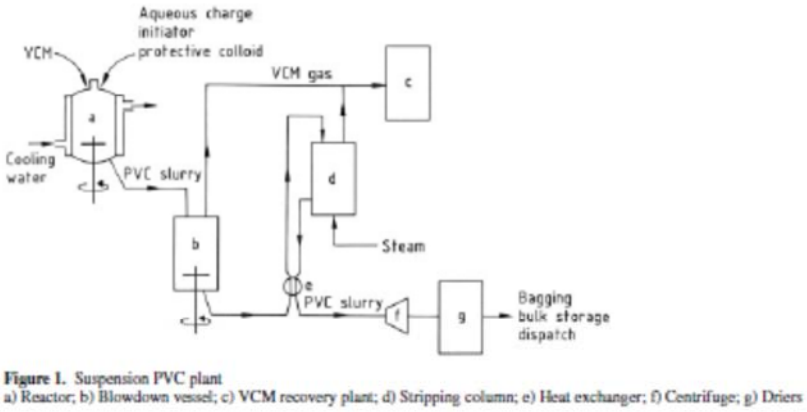

Figure 1. Suspension PVC plant
a) Reactor; b) Blowdown vessel; c) VCM recovery plant; d) Stripping column; e) Heat exchanger; f) Centrifuge; g) Driers

Figure I- 3 : a typical batch VCM suspension polymerization process (i.e. Allsopp 2005)

I.2. ***Creation of the VCM droplets/PVC particles***

The S-PVC process takes place in a jacketed stirred tank reactor. The medium stirring enables first to disperse the VCM in the continuous aqueous phase. The stirring provides the mechanical energy to breakup and disperse the monomer as droplets of mean droplet size ranging from 30 to 50 μm. During the reaction, the VCM droplets become PVC particles and a stirring stop can conduct to a settling of PVC particles (density evolution, ϱ_{VCM}=911 kg.m^{-3} at 20°C and ϱ_{PVC}=1400 kg.m^{-3})

In batch process the stirred tank is in turbulent regime. The hydrodynamics of stirred tank is rather complex and can be modelled by two regions. The region around the impeller has a high turbulence intensity and the region away from the impeller (circulation region) which presents a greater volume has a rather lower turbulence intensity (Coulaloglou and Tavlarides, 1976). If breakage and coalescence are occurring simultaneously then eventually an equilibrium can be achieved. The average droplet size in stirred tank reactor will depend on two processes: breakup in regions of high shear stress (near the impeller blades) or of high turbulent intensity, and coalescence in quiescent regions.

Breakup phenomenon depends on the phase viscosity, the inertial force and surface forces (interfacial tension). A dimensionless number, Weber number We in turbulent flow field,

represents the ratio of inertial forces to surface forces and it is expressed through the following relationship in stirred tank:

$$We = \frac{\rho_c N D_T^{\,2}}{\sigma} \qquad \textbf{(I- 1)}$$

ρ_c represents the continuous liquid phase density ($kg.m^{-3}$), N the stirring velocity (s^{-1}) , D_T the impeller diameter (m) and σ the interfacial tension ($N.m^{-1}$).

The mean droplet size d_{32} evolution is classically represented in literature as a function of the Weber number (Coulaloglou and Tavlarides, 1976 or Zhou and Kresta, 1997 listed the various correlations)

$$\frac{d_{32}}{D_T} = C We^{-0.6} \qquad \textbf{(I- 2)}$$

C is a constant depending on the system, the tank geometry and the impeller.

The liquid-liquid dispersion of VCM in aqueous phase has been studied (Zerfa and Brooks, 1996a and 1996b; Hashim and Brooks, 2002 and 2004) and a mean droplet size prediction is proposed:

$$\frac{d_{32}}{D_T} = 0.027(1 + 3.1\Phi) We^{-0.6} \qquad \textbf{(I- 3)}$$

d_{32} is the classical Sauter diameter, Φ is the dispersed phase hold-up expressed as the ratio of the dispersed phase volume to total liquid volume. This correlation has been established for dispersed phase hold-ups ranging from 0.01 to 0.40.

Expression (I-3) refers to non-reactive liquid-liquid dispersion. In the course of polymerization, the physical state of the droplet is gradually evolved to form solid PVC particles. Saeki and Emura, 2002 predict the evolution of the mean PVC particle diameter d_{50} with the Weber number for industrial reactor from 2 up to 150 m^3 in volume.

$$\frac{d_{50}}{D_T} = 223872 We^{-0.6} \qquad \textbf{(I- 4)}$$

The constant seems really large but in the Weber number ranges from 10^5 to 10^6 for industrial reactors of these sizes.

The mean PVC particle diameter d_{50} presents the same evolution law with the Weber number as the VCM droplet Sauter diameter d_{32}. Consequently it is meaningful to control accurately the initial dispersion in order to manage with the final product granulometry. The PVC grain morphology influences the quality of the final product. It is related to the final properties of the product during the shaping such as plasticizer absorption. The process must be controlled to provide a given mean particle size and porosity.

The final PVC grain depends then first on the initial liquid-liquid dispersion of VCM in the aqueous phase. In batch process, it is influenced by the stirring velocity. As previously mentioned the mean droplet size depends also on the suspending agents and particularly on

the primary one which presents the highest hydrolysis degree of the acetate function (superior to 70%) and controls the droplet coalescence. In our work, it has been decided that the formulation is not a parameter under study and subsequently, the concentrations of the different additives are fixed and will be not further discussed.

Now, let's focus on the non-reactive liquid-liquid dispersion. Some authors have studied the liquid-liquid dispersion of VCM in water by using PVA as surfactant. Figure I- 4 presents the Sauter mean diameter evolution with the stirring time according to the works of Zerfa and Brooks, 1996 and Kotoulas and Kiparissides, 2006.

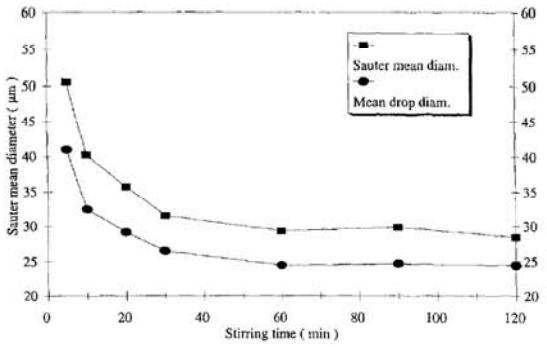

Variation of vinyl chloride Sauter mean diameter and mean drop diameter with stir [volume fraction = 0.1; C_{PVA} (72.5% hydrolysis) = 0.02% and N = 500 rpm].

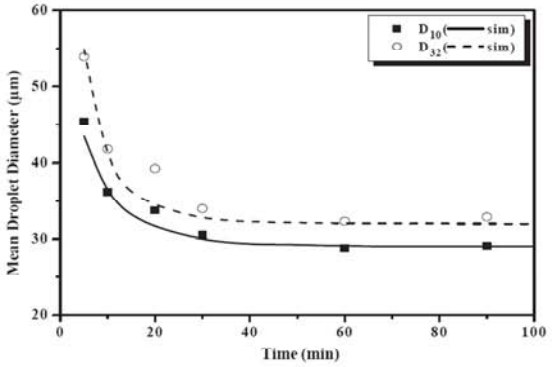

Dynamic evolution of the calculated and measured mean diameter of VCM droplets (non-reactive case: monomer volume fraction = 0.1; C_{PVA} (72.5% degree of hydrolysis) = 0.02%; temperature = 55 °C; N = 500 rpm).

Figure I- 4 : Evolution of the VCM mean droplet size with the stirring time according to literature

The mean droplet size and consequently the droplet size distribution stabilizations are estimated to half an hour. This time is rather long.

The decrease of the mean Sauter diameter is due to the breakage ascendancy over the coalescence. The dispersion tends then to be stabilized according to time. It depends on the diffusion of the surfactant and the rearrangement at the interface.

In case of continuous process, this stabilization time must be accurately defined. Indeed, the reactor length must be evaluated as well as the effect of a non-stabilized dispersion loading in a stirred tank at polymerization temperature. Indeed, it could lead to irregular particles.

If it is important to ensure an adequate stirring velocity, a too high or too low stirring velocity may also induce product quality defects. Saeki and Emura, 2002 present the consequence of three different conditions of stirring and suspending agent concentration on PVC particles obtained. A low agitation and medium surface tension value lead to PVC particle of same size as VCM droplet. The particles are finer resulting in a denser polymer with a low porosity. The low surface tension with a high agitation provides particles expected by the S-PVC producer: coaser PVC particles with high porosity. On the contrary, in case of a too strong agitation, too much agglomeration of the PVC particles causes solid batch.

To summarize, it is important to control the initial mean droplet size to ensure a good final quality product. At the initial stage of the polymerization, the VCM must be dispersed in water by high shear rates or high energy dissipation rate device. Moreover it seems that the granulating suspending agent absorption at the interface is really long and could be a limiting step. The goal is to obtain a narrow droplet size distribution with a mean droplet size ranging from 30-50μm.

During the polymerization reaction, the stirring must be efficient to ensure a good homogeneity and to control the coalescence/agglomeration process. The final particles size distribution is expected to be narrow (63-250μm) with a mean particle size between 120-180μm.

I.3. ***The physical mechanism related to kinetics in the S-PVC process***

It is a complex phenomenon which is described at the macroscopic scale and at drop scale in the literature.

I.3.1. Evolution of the particles: the macroscopic view

At a macroscopic scale, it consists in studying the mean droplet/particle size evolution during the polymerization process. Four intervals can be noticed for suspension polymerization (Jahanzad *et al.*, 2004 and 2005). Figure I- 5 shows a representation of these different successive stages based on the methyl methacrylate (MMA) suspension polymerization.

The four stages identified are described above:

- The **transition stage**: the droplets decrease in size. Droplets finally reach an almost constant average size. This stage can be shortened by increasing the polymerization rate in the droplets (i.e. increasing the initiator concentration or the temperature) and by increasing the stirring velocity or the PVA concentration.
- The **quasi-steady state stage**: the droplet size is rather constant. It is strongly affected by the previous mentioned polymerization conditions. This step is not necessarily observed.
- The **growth stage** corresponds to a sharp increase of the droplet size. It occurs if drops are not sufficiently stable as regards to breakup or coalescence. This stage has been traditionally called a "sticky stage". It is probably because drop coalescence is

boosted with the drops tackiness as a result of drop viscosity build-up with conversion. This agglomeration can be suppressed if dispersions can reach a quasi-steady state at high PVA concentration or high stirring velocity as mentioned before.

- The **identification stage**: all the monomer contained in droplets has reacted. The particles are now solid. It only depends on the parameters affecting the rate of polymerization (initiator concentration and temperature). The particles have reached their final size.

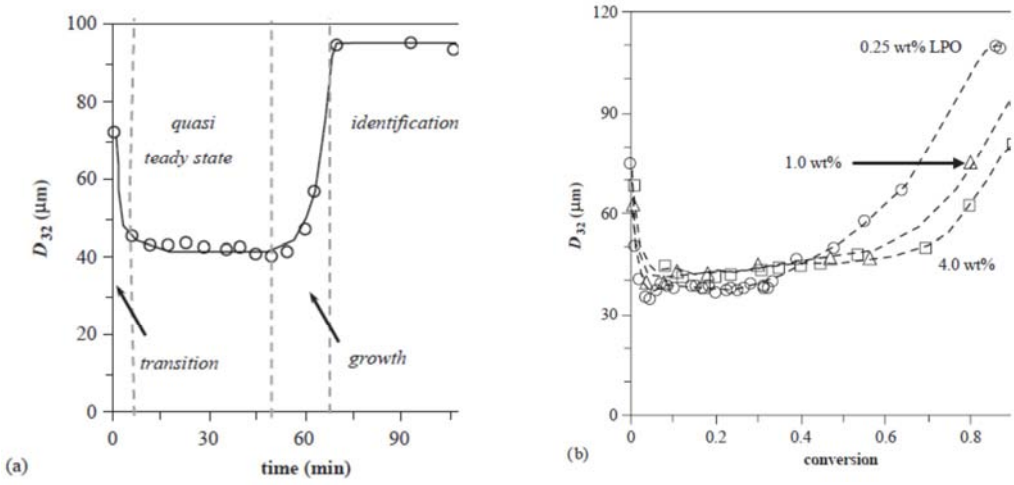

Figure I- 5 : (a) characteristic intervals of mean droplet size (Jahanzad et al. 2005) (b) representation for the MMA suspension polymerization at different initiator concentration

From Figure I- 5-b, it appears that the different steps correspond to different conversion values. These different steps correspond then on one hand to a liquid-liquid dispersion process with a control of the mean droplet size and on the other hand to a reaction step in which the particle exhibit a sticky behaviour at a given conversion depending on the polymerization conditions, and at the end, the reaction proceeds without any particle evolution.

Let's focus now on the S-PVC polymerization. The physical particle behaviour is observed and described at the drop scale.

I.3.2. Identification of the different domains inside particles

PVC is insoluble in its own monomer. VCM polymerization is therefore an heterogeneous process which implies some physical transition during the reaction. The polymerizing system is composed of two phases: the monomer and the polymer rich phase. The precipitated polymer chains initially form unstable nano-domains that rapidly coagulate, leading to the generation of the primary particle nuclei. The primary particles increase in size by both polymerization of the absorbed monomer in the polymer-rich phase and the continuously nucleated unstable nano-domain. The final grain is composed of a number of subgrains (agglomerated droplets) depending on the quality of the stirring and the stability of the VCM droplets.

Five stages have been previously described in literature (Allsopp, 2005; Xie *et al.*, 1991; Kiparissides *et al.*, 1997; Yuan *et al.*,1991; Geil, 1977; Alexopoulos and Kiparissides, 2007, Pauwels, 2004). They are summarized in Table I- 2 and described below.

Based on the morphology evolution with the conversion X, different conversion zones are identified:

- X<0.01%: the radical obtained by thermal decomposition are reacting quickly with the monomer and then produce the first polymeric chain which precipitates instantaneously in the liquid VCM phase. The polymeric chain combines each other to form nano domains swollen by the monomer. Their size ranges from 10 to 20 nm.
- The second phase 0.01 %< X<1% corresponds to the emergence of primary particles nuclei. Indeed, due to the instability of the nano-domains, they agglomerate together. A thousand of nano-domains coagulate all together and the size of the primary particle nuclei obtained ranges from 80-200nm. During this step, the first primary particles grow by a coagulation mechanism with the formed nano-domain instead of growing by polymerization with the absorbed monomer.
- The third polymerization step occurs from 1 to 20% of conversion. The primary particles are growing and aggregate. The nuclei are produced until 5-10%. The primary particle growth is due to the capture of the formed nano-domains but also by the absorbed monomer polymerization. The polymerization becomes the main growth mechanism as long as the polymer mass increases. For a conversion between 7-20%, the primary particles aggregate massively and they produce a continuous and three-dimensional primary particle network.
- The fourth polymerization step arises until 75% of conversion. The primary particles expand thanks to the polymerization process and fuse together in a same primary particle aggregate. The particle porosity decreases. It is an antagonist process

compared to the initial primary particle agglomeration which promotes the high porosity. For a conversion inferior to 30% (sticky stage) the biphasic droplets coalesce and form macro-aggregates of primary particles which correspond almost to the final PVC grains. Above a conversion degree of 30%, the coalescence between primary particles and aggregates tends to zero because the solid surface is less sticky. This conversion is close to the Allsopp value (20%). The primary particle growth carries on by polymerization until 70-75%.

- The last polymerization phase corresponds to the polymerization in the PVC phase swollen by the monomer until it disappears. At the final conversion degree, the final primary particle size is if 1 to 1.5µm whereas the primary particle aggregates ranging from 3 to 10µm. the aggregates of primary particle creates PVC grain of 130µm mean diameter.

The final porosity is controlled thanks to the conversion rate X_c from which the aggregates of primary particle is constructed and by the contraction of this three dimensional network.

It has been demonstrated that the conversion at which the primary particles begin to fuse is the same as that at which the free monomer phase disappears (X_f) (Smallwood *et al.*, 1986).

Bao and Brooks, 2001 note that the mean particle size is established at low conversions (< 20%), implying that the VCM droplets finish their agglomeration at the early stages of polymerization, while the primary particles continue to aggregate inside the droplet producing its shrinkage. This result is in agreement with Allsopp but it is inconsistent with the results of Cebollada, 1989 which suggest a stabilisation of the grain at 70%.

Stage	Description	Size (µm)	X (%)
Coiled macro radicals	Precipitation of growing polymer chains length 10-30 monomer units		<0.01%
Microdomain	Aggregation of precipitated macro radicals and macromolecules about 50 in number	0.01-0.02	<0.1
Domain	Agglomeration of about 10^3 microdomain-primary particle nucleus	0.1-0.3	<1
Primary particle	Formed by continuous growth of domain	0.6-0.8	>5 Up to 15-30
Agglomerate	Coalescence of primary particles and subsequent growth	1-2	Up to 50-70
Fused agglomerate	Gradual fusing of the primary particle named 'intergrowth'	2-10	X_f Up to limiting conversion
Sub-Grain	Fusing of the agglomerates of primary particle inside the droplet-polymerized monomer droplet	10-150	
Grain	Particle made of several polymerized monomer droplet	50-250	

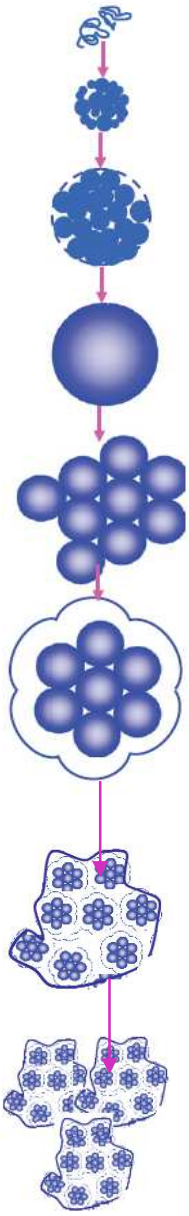

Table I- 2 : PVC grain formation (Pauwels, 2004)

I.4. Identifications of the bottlenecks

I.4.1. Exothermicity of the reaction and polymerization temperature control

As already mentioned, the suspension polymerization of the vinyl chloride is highly exothermic. The enthalpy is estimated to ΔH_R=-71 kJ.mol$^{-1}_{VCM}$ or -1135 kJ.kg$_{VCM}^{-1}$. However, the suspension polymerization process requires a good control of the exothermicity. It is partially ensured thanks to the aqueous continuous phase which can absorb part of the heat released because of its huge calorific capacity. Besides, the small droplet size (30-50µm) allows an instantaneous heat transfer through the continuous phase.

In the suspension process, the heat transfer limiting step relies on the heat exchange at the wall reactor.

In batch process, the poor release of the reaction exothermicity represents a limitation to productivity. Larger quantities should be produced. Indeed, with an increase of the reactor size, the surface to volume ratio decreases (in case of geometrical similitude, Burgess, 1982). In the same way, the polymerization reaction time at the same conversion increases with the reactor volume. Consequently, it is time consuming. The heat removal capacity is considered as a true bottleneck of the polymerization process. Consequently, the initiators currently used in the recipe are adapted to this polymerization duration: they have a half-life time of about one hour at the polymerization temperature.

Batch to continuous will obviously enhance the heat transfer. The surface area to volume ratio is expected to be much larger than in batch. The exothermicity can then be handled and the equipment becomes no longer the limitation.

The polymerization temperature has also an important impact on the porosity of PVC particles. A higher constant polymerization temperature causes a lower porosity, as the internal particles tend to coalesce much more, which results in a more compact internal structure. With increasing temperature, all reaction rate parameters (following Arrhenius type law evolution with temperature) increase, but differently to a certain extent.

Commercial S-PVC is usually manufactured in the temperature range of 40-70 °C. But, some temperature variations inside the reactor may affect negatively the quality of the polymer produced, while increasing the polydispersity (broadening of the molecular weight distribution). As the resulting polymers differ in molecular weight and morphology, they are suitable for different types of application. PVC for commercial applications is denoted with K-values, which is a measure of the relative viscosity of PVC (Table I- 1).

The temperature control is then a key-factor for the product quality and kinetics control. In batch, product temperature is regulated thanks to the jacket temperature. In continuous process, the mass and thermal balances will allow to predict the jacketed temperature profile to be applied in order to maintain the expected polymerization temperature all along the reactor(s).

I.4.2. Fouling problem

During the polymerization process, a PVC deposit appears on the walls. It decreases the reactor heat transfer capacity. Besides this deposit affect also the drying time of the PVC grains as well as the final powder quality ("fish eye" creation). The deposit prevention is then an efficiency and safety requirement and is necessary for the quality product.

The current batch reactor process does not suppress the deposit but some technologies have been developed to limit it. The internal surfaces of the reactor are treated (by coating). A cleaning procedure is performed after each batch. In their review, Saeki and Emura, 2002 suggest several causes for the deposit creation. The first mechanism involves the small solubility of PVC in its own monomer. The PVC particles can then quasi instantaneously precipitate and preferentially on the absorbed VCM layer on the reactor walls. At the beginning of the polymerization, no or few nuclei exist in suspension and this macro radical will tend to precipitate out on any available imperfection on the wall where VCM is more likely absorbed. A second mechanism of deposit is due to the small soluble amount of initiator in the aqueous phase which polymerize with the soluble VCM part in the water. The PVC chains can then precipitate on the reactor wall. Once the PVC has adhered and has a radical activity, it can be swollen by fresh monomer and it keeps growing. The third mechanism involves the material of the reactor wall. Indeed, stainless steel reactors are more concerned by deposition because of the presence of active sites. These sites may act as a polymerization catalyst and play a role of strong adhesion points.

The deposition is also often located at the liquid gas interface in the batch reactor.

In batch process, two ways have been proposed to limit or suppress the deposit: chemical additives in the polymerization recipe or reactor wall coating. The second solution is more common.

I.5. Steps identification for a continuous process

The previous literature study enables us to propose three main steps for our research work. Figure I- 6 depicts these three steps regarding the polymerizing droplet physical behaviour and the conversion progress.

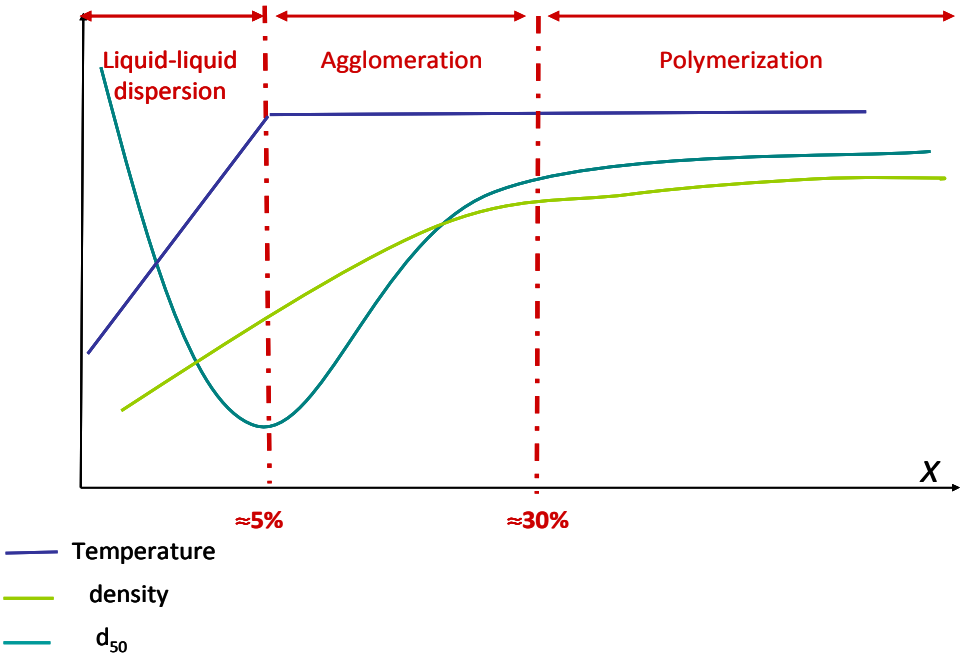

Figure I- 6: Schematic representation of product evolution with conversion

The first step corresponds to the liquid-liquid dispersion. It corresponds to the creation of VCM droplets with a controlled mean droplet size. This step requires a high shear rate or high energy dissipation rate. The surfactant absorption could be a limiting parameter and should be evaluated to create a stable dispersion before starting polymerization.

The second step corresponds to the agglomeration step. The conversion ranges from 5 to 30%. This range is based on the literature study. In this range, the polymerizing droplets agglomerate each other. The emulsion/suspension must be homogeneous and in order to avoid non-homogeneity in the final product properties, the flow must be close to plug-flow. On top of the agglomeration control issue, the heat reaction should be released to ensure a constant temperature in the reactor.

In the third step, the particle size distribution has to be maintained while the polymerization proceeds and heat is released.

The technology in which the continuous S-PVC can take place must be identified for the different steps.

The second part of this chapter is devoted to present the advantages of a continuous process compared to batch and the current continuous polymerization processes.

II. FROM BATCH TO CONTINUOUS

In this section, an overview of the continuous S-PVC process mentioned in the literature and more generally of continuous polymerization process involving two phases are described.

II.1. ***Benefits of continuous and intensification***

An assessment of the batch process demonstrates the advantages of flexibility and polyvalence, coupled with the high degree of knowledge. It is highly flexible for the different operating conditions (throughput, temperature, additives concentration). Indeed depending on the K-value which corresponds to specific grain properties and then powder applications, the operating parameters such as the initiator, the concentration of the different additives and the temperature may be adapted for each batch.

But, batch process is limited by the poor heat transfer capacity. Moreover the productivity can be affected by the reducing of the batch occupation time due to the cleaning step. But one of the main drawbacks of the batch process concerns the safety. The reaction can cause runaway and VCM exposure.

We have reported on Figure I-7 the accidents which occurred between 1962 and 1989 (Barton and Nolan, 1989). The graph highlights that the polymerization is the main reaction responsible for accidents with a rate of 47.80 %. The batch polymerization reactions have a high potential for loss of control and runaway.

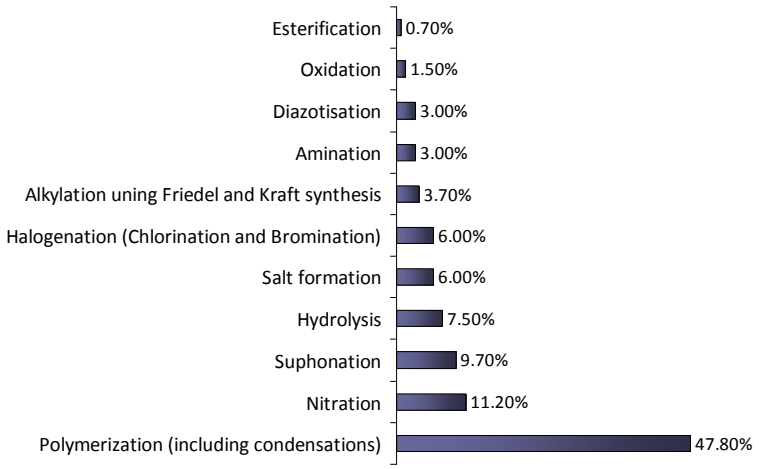

Figure I- 7: accidents between 1962-1989 according to Barton and Nolan, 1989

Besides, the continuous process is expected to provide a better control of the product quality and of the operating conditions, particularly of the temperature in order to avoid any thermal runaway. Moreover continuous processes are interesting from an economical point of view. Calabrese and Pissavini, 2011 compared two reactions performed in batch and in continuous and underline the continuous process benefits in term of safety, costs and quality.

Continuous process limits also the product exposure by removing the daily maintenance operation.

II.2. ***Continuous two-phases polymerization: emulsion and suspension process***

First, some two-phases polymerization processes described in literature are presented in order to provide an overview of the involved equipments.

In this section, the patents available concerning the suspension polymerization of vinyl chloride are then presented. Despite the publication of these patents, the suspension polymerization is still conducted batchwise. From our knowledge, no application of these patents is nowadays available at the industrial plant scale.

II.2.1. Continuous suspension or emulsion polymerization in literature

In literature, two types of reactor are distinguished. On one hand, the emulsion or suspension polymerizations are carried out in stirred tank reactor in series. On the other hand, the polymerization takes place in tubular reactors such as pulsed sieve plate column or pulsed packed column.

This part describes the drawbacks and benefits of such processes.

II.2.1.1. Continuous stirred tank reactor in series (CSTR)

The continuous stirred tanks in series have been studied for **emulsion** polymerization of vinyl acetate, styrene and methylmethacrylate (Kiparissides *et al.*, 1979; Pendilis *et al.*, 1985; Pendilis *et al.*, 1989; Rawling and Ray, 1988). The authors observed that for monomers such as vinyl acetate and vinyl chloride, that is to say for radicals with a high mobility and a high solubility in water, there are sustained oscillations of the conversion and of the polymer

properties. This is due to the polymerization kinetic and high solubility of the monomer radicals in water. Consequently, the steady state is not achieved. Pendilis *et al.* (1989) improve the traditional CSTR train by adding a pre continuous seeder for a conventional stirred tank and choosing a judicious splitting of the monomer and water feeds between the prereactor and the subsequent large reactor.

In their review, Yuan *et al.*, 1991 listed the continuous **suspension** process which suggests the use of CSTR. The authors highlight some issues. The deposition on polymer wall affects the heat transfer and then the product quality. The transfer from a reactor to another in case of CSTR causes some trouble because high viscous monomer-polymer particles could stick on the pipe and pumps. To prevent polymer sticking, the conversion must be of at least 75%. They also reported that there is no commercial plant in continuous mode.

II.2.1.2. Tubular reactor

Tubular reactors benefits are their low cost and simplicity of use and construction. Their implementation in suspension polymerization has been slow because of the reservation on polymer properties and risk of blocking (Yuan *et al.*, 1991)

Few articles refer seriously to the continuous **suspension** polymerization in tubular reactor. Some studies are typical lab scale studies such Yasuda *et al.*, 2010. The authors work with microchannel by using a glass particles packed column to create the dispersion of methylmethacrylate and then the polymerization is performed in a tubular reactor. The monomer and particle sizes remain the same. Dowding *et al.*, 2000 use also millimetric tubular polymerization reactor to prepare large porous polymer beads.

More articles refer to the continuous **emulsion** polymerization in tubular reactor such as packed column or pulsed sieve plate column. Paquet and Ray, 1994 develop pulsation operation to eliminate reactors fouling and plugging (vinyl acetate emulsion polymerization).

In his PhD (1990), Hoedemakers proposed to work in a plug flow mode with turbulent flow in order to avoid coalescence and creaming of the droplet, prevent from fouling and ensure an efficient axial mixing to remove the reaction heat through the wall and avoiding radial temperature profile.

In the two following parts, some polymerizations in such reactors are detailed.

II.2.1.3. Emulsion polymerization in pulsed packed column

The present section describes the work of Hoedemakers. The experiments were realised at lab scale with a pulsed packed column filled with Raschig rings of 6 and 10mm of diameter or with static mixers. The column diameter is of 50mm and the total length 5m. The maximal pulsation frequency is of 3.5Hz and the maximal liquid displacement of 14mm. At the top there is a gas liquid interface and at the bottom of the column the pulsation system is set up. The oscillatory frequency and stroke length could be adjusted and are independent of the feed rate. Consequently, the turbulence can be maintained thanks to the pulsation and independently of the feed flow rate.

The flow is turbulent and the emulsification of monomer operates at low flow rate with a limited axial mixing. These conditions are convenient for the seeding as well as for a high conversion.

In his thesis, Hoedemakers compares the performance of the column packed with Raschig rings or with static mixer SMV8-DN50. For the same conditions, the axial dispersion coefficient is lower with the static mixers than with the Raschig rings which can be related to the organized structure.

Different experiments were conducted and led to the following conclusions:

- The achievement of the process is subjected to pulsation and to the liquid flow rate. A minimum pulsation exists to avoid de-emulsification.
- At high liquid flowrate and for moderate pulsation, the performances are almost the same as in a batch reactor.
- At high residence time, the reaction rate and the particles number decrease slightly in the column, the result is still better than in a CSTR or in a series of CSTR. The Sulzer packing provides the best results.
- The particle size distribution is narrower in the pulsed packed column than in the CSTR.

This process enables to obtain product of great quality.

II.2.1.4. Emulsion polymerization in a pulsed sieve plate column

This section is based on the work of Sayer *et al.*, 2002. The authors study the emulsion polymerization of the vinyl acetate in a pulsed sieve plate column. The dimensions and operating conditions are given Table I- 3.

The different feed streams are the aqueous solution with the emulsifier and the monomer organic phase. The two streams are pre-emulsified in a small pre-mixer before entering the reactor. Both flows upward co-currently from the bottom to the top of the column.

The polymerization has been achieved in half an hour with a high conversion degree. The evolution of the mean particle size as well as the conversion along the reactor is in the expected range and fit very well to their kinetic model.

Characteristics	
Length (m)	5
Length of a section (m)	1
Diameter (mm)	40
Spacing between plate (mm)	50
Oscillation	Piston connected to the bottom of the
Frequency of oscillation (Hz)	0.2-3.5
Stroke length (mm)	5-25
Type of plates	Stainless steel disks

Table I- 3: Pulsed column characteristic and pulsation conditions Sayer et al. (2002)

II.2.2. Suspension polymerization in batch oscillatory reactor

The co-current Oscillatory Baffled Reactor (OBR) consists in a double-jacketed tubular reactor with equally spaced baffles (doughnuts). Table I- 4 reports some polymerization studied with this reactor type. The oscillation technology may also be used batchwise.

The benefits of the oscillatory baffled reactor for suspension polymerization are pointed out. It seems that the oscillation conditions allow the control of the mean droplet size and subsequently of the mean particle size and particle size distribution. Even if the authors underline the suitability of the device for continuous suspension polymerization, they do not provide any example. Moreover, the vinyl chloride monomer presents a totally different characteristic grain morphology compared to MMA, used for their batch tests.

However, these scientific works have demonstrated the interest of pulsed technologies. Particularly, the pulsation seems to limit the fouling issue. All these works have led to the creation of a start-up by Professor Ni (Nitech, http://www.nitechsolutions.co.uk).

References	System	Reactor characteristics	Results
Stephens (1996)	*Organic phase:* MMA (40% mass.) and butylMMA(60%mass.) *Initiator*: dilauroyl peroxide *Aqueous phase*: de-ionized water, sodium sulphate (reduce MMA solubility in water), polyacrilic acid (colloid stabilizer)	*Tubular reactor* (pyrex or stainless steel) D=50mm ; L=300mm 3 Stainless steel Baffles D_B=50mm ; H=37mm; T=12%; Supported by two 3mm stainless steel rods Oscillation conditions Moving of the baffle set up and down the liquid medium at the top of the column f=5Hz ; A=10 mm	Comparison with a stirred tank - oscillatory baffled reactor: similar shear rate radially and all along the reactor leading to narrow particle size distribution - in stirred tank, larger PSD due to wider variation in shear rates and less significant extensional flow component than in OBR
Ni *et al.* (1999)	*Organic phase*: MMA, colloid and surfactant *Initiator:* di-benzoyl peroxide (BPO) *Aqueous phase:* de-ionized water and surfactant 2 T=82°C	Tubular reactor D=50mm ; L=750mm ; Thickness=2mm Stainless steel Baffles D_B=50mm ; e=0.8mm ; H=75mm; T=19%; Supported by two 3mm stainless steel rods Oscillation conditions Fluid oscillation (1.7 times the oscillation bellows) f=3.5-7.5 Hz ; A=4-8 mm (centre to peak)	- d_{32} decreases with the increase of A or f - $d_{v,0.5}$ more influenced by f - $d_{v,0.5} = 3.11 d_{32}$

References	System	Reactor characteristics	Results
Ni *et al.* (2001)	*Organic phase:* Iso-parafinic hydrocarbons steric stabilizer *Monomer phase:* Water and acrylamide	Tubular reactor D=50mm ; L=1000mm ; Thickness=5mm 8 stainless steel baffles D_B=50mm ; e=3mm ; H=75mm; T=23%;	- particle size distribution narrower than in stirred tank - d_{32} affected by both A and f as well as $d_{v,0.5}$

	Initiator:: redox initiator T=50°C	Supported by two 3mm stainless steel rods Oscillation conditions Moving of the baffle set up and down the liquid medium at the top of the column f=1-5 Hz ; A=10-50 mm (peak to peak)	
Ni *et al.* (2002)	Same as the two previous references	Same as the two previous references	- particles with controlled size and morphology in batch or continuous flow thanks to the superimposed oscillation that radially mixes fluids, allows plug flow behaviour (or close to in continuous mode) - High degree of repeatability (>90%) - fines particles inferior to 5% where as 8-10% in stirred tank - narrow Gaussian particle size distribution

Table I- 4 : Suspension polymerization in oscillatory baffled reactor

The last part of this section concerns directly the S-PVC continuous process.

II.2.3. The continuous S-PVC polymerization process in literature

II.2.3.1. Process patent

Few patents describe the continuous polymerization of vinyl chloride and no industrial application is known. The patents remain evasive concerning the employed technologies. In this part, the different patents are presented.

The first noticeable patent dates from 1961 (US 3004013). It proposes a continuous process of vinyl chloride S-PVC with CSTR (continuous stirred tank reactor). The drawing shows two jacketed stirred tank reactors. The monomer and the catalyst are stored together as well as water and suspending agents. The two-phase emulsification is managed by a pump which feeds also the first tank. The mixture circulates in a loop and the dispersion is created by this way. The mixture is then heated to the polymerization temperature and the polymerization starts. The transfer from the first to the second reactor is realized and the polymerization proceeds. The product flows constantly in a flash chamber to recover the unreacted monomer which returns in the monomer storage tank through the vapour return line. The internal pressure of each reactor is monitored and controls the jacketed temperature to set a constant polymerization temperature. The dispersion is admitted to the first reactor in response to the liquid level or pressure in the second reactor. The raw materials are continuously fed in the first reactor at a rate corresponding to the rate of recovery of the PVC product from the second reactor. This first patent suggests then a continuous process with two stirred tank reactors and liquid-liquid dispersion performed in a recycle loop via a pump.

The second major patent is from Hoechst in 1984 (US4424301). The scheme of the continuous process is given in Figure I- 8.

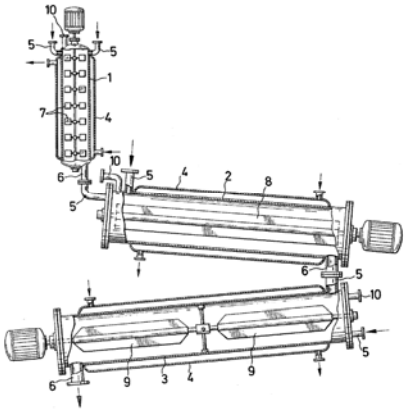

Figure I- 8 : Hoechst process

In this patent, the authors divide the process in three steps corresponding to different conversion depending on the physical behavior of the reactive medium. In a first zone (X<10%), the different components are stirred together to obtain the required mean droplet size. The VCM or a dispersion of VCM in water, demineralized water, granulating-suspending agents, buffer, initiator in solution or in fine dispersion are continuously introduced into a multi stage agitating device. In this step, a low conversion is reached which corresponds to about 10% in weight of conversion. In fact, if the conversion is lower than 3%, the desired particle size will not be reached and if it is higher than 10% in weight, fouling problems and temperature issues are likely. In the second reaction zone, the reaction occurs until 35-45% of conversion. The agitation is moderate. This equipment is designed to avoid fouling problem (special material, no stainless steel). In this range of conversion, the particles are sticky. In the two previous steps, the different reactors used operated in plug flow mode. In the third reaction zone, the reaction proceeds until a conversion ranging from 75-95%. At the end, the mixture is cooled, depressurized and unreacted VCM is removed while the polymer is separated and dried. The different technologies of reactor are not clearly detailed except for the first reactor which looks like a Kühni or Karr column.

This patent was completed with a second one of the same Hoechst Company in 1984. The authors claim that working on the first conversion zone limits the deposit. It is better to create the dispersion at a lower temperature than the polymerization temperature. PVC disposal can be avoided by stabilizing the emulsion at ambient temperature (20°C). Contrary to their previous patent, they suggest a non-reactive liquid-liquid dispersion creation.

Moreover in these patents, some advices of design are given: if the first reactor is 10 liters, the second is 50 to 200 and the third 400 liters. The residence time at constant flow rate in the different reactors fluctuates. On the other hand, to limit the axial mixing, it is advisable to have a reactor length at least 10 times superior to its diameter.

A more recent patent is the Shin-Etsu Chemical (1994, US5282680). It suggests a pre-dispersion step of VCM in water. The polymer slurry tank is connected to the pre-mixer through a polymer passage. This polymer passage is probably a tubular reactor. The flow circulation is ensure thanks to a pump described as follow "a pump comprising a conical hub and an impeller mounted thereon comprised of a single spiral blade". The pump is used for drawing out the aqueous suspension from pre mixer to the polymerization passage and also for discharging the polymer slurry formed in the polymer passage reactor in the slurry tank. The polymerization passage has a sufficient length for allowing the VCM to be polymerized to a predetermined extent.

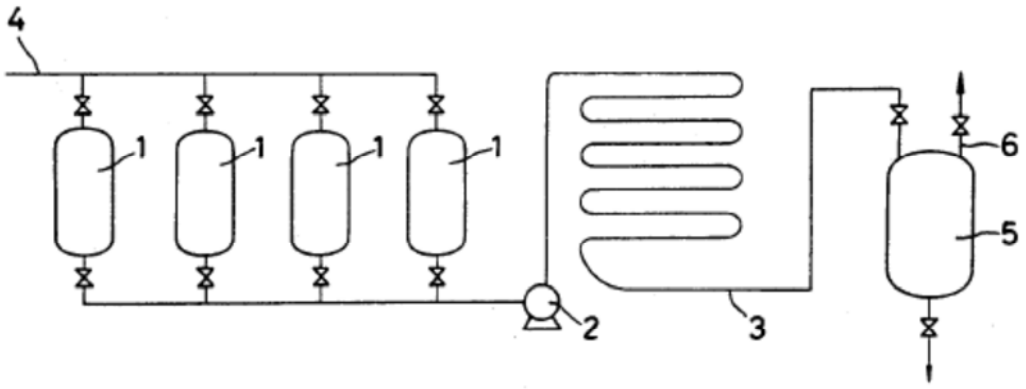

Figure I- 9 : Polymerization apparatus of the Shin Etsu patent 1 tank, 2 pump 3 pre-mixer, 5 slurry tank

Referring to Figure I- 9, one can see that the process is not much described. The first step of pre-mixing can be made in a classical tank or in a static mixer. The goal is to create a uniform suspension. Several reactors in series could be used in order to obtain a continuous process with specific polymerization rate or a given conversion before passing through the polymerization passage. A special pump, hydrostal pump, raises the suspension pressure at the outlet of the pre-mixer and the polymerization starts in the polymerization passage. A plug flow is maintained. The passage polymerization must be equipped with heat exchanger device: double jacket tube or heat exchanger at an intermediate position. The length of the tube is related to the polymerization time. A minimum flow rate of 0.7 $m.s^{-1}$ is required to avoid settling and consequently fouling in the tube.

Other patents are found in the literature among which ones it is proposed to use of a liquid -liquid fluidized bed and a liquid-solid fluidized bed to produce PVC. The residence time of the particles depends on their density evolution (Kanegafuchi Chemical Industry, 1984, US4487898).

Another patent proposes to use a non-cylindrical channel to carry out polymerization (US 6252016B1 (Rohm and Haas Company, 2001). The non-cylindrical walls can have a

common wall or not, but the different channels must be closed enough to ensure a control of the polymerization temperature. A non-cylindrical channel offers a larger surface compared to cylindrical channel for the same length and a more efficient heat transfer. This kind of devices can be heat exchangers such as plate-frame, plate-fin, and spiral-plate heat exchangers. In this patent, the heat exchanger used for the experiment is an Alfa Laval plate frame heat exchanger (Model-Type M6-MGT).

From the analysis of these patents, the liquid-liquid dispersion is often performed apart and another reactor is used to carry out the reaction.

II.2.3.2. Extremely fast initiators

This second series of patents focus more on the recipe and especially on the initiator.

There are two patents of the Akzo Nobel society (2002 WO03054040 and 2007 2007/110350). They present a new type of initiator defined as extremely fast with half-life time ranging from 0.0001 to 0.05 hours. The classical initiator decomposition takes 200 to 400 min. This kind of new initiators improves the polymerization rate control and the final product contains less initiator residual amount. This initiator is quite stable and no secondary reaction occurs. The patent develops the chemicals and there is a concern about continuous process in a tubular reactor. Indeed, decreasing the half-life time of the initiator allow to adapt the technology to the chemistry. The polymerization can be shortened if the devices chosen are not limited by the heat removal capacity. This kind of initiator helps to start the reaction but also to stop it instantaneously by controlling initiator flowrate and concentration.
In their second patent, Akzo Nobel suggests fast initiator used for continuous polymerization process. However, the authors remain evasive concerning the technological choices. They just mention the ideal reactor models: CSTR (continuous stirred tank reactor) and tubular plug-flow reactor or combination of both.

II.2.3.3. Discussion

In conclusion, we can note several points concerning the changeover from batch to continuous:

- As proposed in the Hoechst patent (US4424301,1984), the process is divided according to the physical state of the droplet/particle relative to the conversion. It corresponds to the same stages as identified section I.5. Consequently three steps are identified: the pre-mixing while the droplets are not sticky until a small conversion, the polymerization with coating and high control of the heat removal and polymerization after the sticky stage.
- The liquid-liquid dispersion is often created in equipment specifically designed for emulsification. The importance of creating a stable dispersion to control accurately the particle size distribution is underlined, preferably at ambient temperature.
- The plug flow mode is more suitable to ensure identical properties for all the particles.
- The use of fast initiator allows a better control of the reaction and a decrease of the polymerization reaction time.

II.3. ***Technology identification for the different steps***

The S-PVC process has been divided into different steps based on the particles behaviour and the reaction conversion (Figure I-6).

Regarding the literature concerning S-PVC, this part focuses on the required hydrodynamic conditions and the suitable technology proposed for each step.

II.3.1. Liquid-liquid dispersion step

To perform a liquid-liquid dispersion owning the expected characteristics, the corresponding equipment has to respect the following conditions. All the droplets must experience narrow range of shear rates or energy dissipation rate to obtain a narrow droplet size distribution. Moreover the equipment must ensure a compatibility and industrial flexibility.

According to the literature, this dispersion could be performed in static mixers or in pulsed column. The corresponding energy costs have to be further compared to stirred tank.

We will come back in details on these equipments in **chapter III** (static mixer) and **chapter IV** (pulsed column).

II.3.2. Reaction step

II.3.2.1. Sticky particles

In this step, the reaction starts. The particles are also sticky and the agglomeration must be controlled. It is influenced by some physicochemical parameters such as the PVA-I concentration and the possible introduction of a second one during the polymerization. It is also affected by the stirring speed. Besides, with the reaction, the heat must be released.

To ensure homogeneous properties of the particles, the plug flow behavior of the reactor is more suitable to control the particle size distribution. The final mean particle diameter ranges from 120 to 180 μm. Moreover the equipment must be chosen to avoid fouling and ensure a good heat transfer.

The equipment must also ensure a good homogeneity transport for liquid-liquid dispersion and for liquid-solid suspension. The particles are sticky and can cause encrusting on the reactor wall. This step is very tricky because lots of parameters require attention: agglomeration, heat transfer and encrusting.

The technologies proposed are the continuous stirred tank reactor equipped with heat exchanger and the pulsed column.

The CSTR present the benefit to be available on the industrial site. However, the exothermicity and the conversion are difficult to control. The reasonable number of CSTR to ensure plug flow has to be identified.

II.3.2.2. Reaction

In this step, the suspension particle size distribution does no longer change. The particle structure is then rigid. A narrow particle size distribution must be maintained until 80-90% conversion is reached. So the particle transport must be led with a smooth stirring to avoid crumble.

Consequently the equipment must provide a sufficient stirring, plug flow behavior and a good heat removal.

The same technologies as mentioned above are suitable: CSTR and pulsed column.

III. SCIENTIFIC STRATEGY

In this section, the research orientations of the present work are proposed.

III.1. Continuous S-PVC process research program

Despite the innovative technologies mentioned previously, the stirred tank reactor cannot yet be evicted. Indeed if the bottlenecks previously described cannot be withdrawn, the CSTRs are still an alternative option for continuous S-PVC. The main interrogations concern the sticky step.

Two schemes are then proposed:

- an innovative process in which the liquid-liquid dispersion as well as the reaction are realized in plug-flow reactor: static mixer and/or pulsed column
- a second way is to create the dispersion through static mixer, and to start the polymerization in CSTR until the end of the sticky step in order to have a low internal surface to avoid fouling and complete the reaction in tubular reactor.

The continuous process will be an hybrid process of different technologies. The manuscript will answer some questions particularly concerning the first step. The final process choice depends on the results exposed as well as validation tests at the industrial scale with the VCM and product quality obtained.

III.2. Model phase systems

Due to its dangerousness and to the necessity to work under pressure, the VCM cannot be used at lab scale in large quantity. Consequently, a model system has to be found. In literature the liquid-liquid dispersion in presence of PVA (polyvinyl acetate partially hydrolyzed) has been well studied. The most investigated solvents in literature are the vinyl acetate, the trichloroethylene, the chlorobutane, the benzene, the kerosene and a mixture of solvents such as dichloroethane/ethyl benzene (Shvarev *et al.*, 1996; Shiraishi *et al.*, 1973,; Chung and Wasan, 1988; Padovan and Woods, 1986; Chatzi and Kaparissides, 1994).

Table I- 5 shows the physical properties of the different solvents.

Prior to these similitude properties, the choice of the liquid model is also discussed in term of cost and safety.

Kerosene is not suitable because it corresponds to a crude oil part and a constant composition is not ensured.

The vinyl acetate monomer offers the advantage to allow the suspension polymerization study. However, it can auto-polymerize such as the VCM in presence of oxygen and requires drastic safety conditions (Gustin, 2005). For the liquid-liquid step, it can lead to important constraints. Moreover it possesses a low flash point which is very hazardous for the transfer operation. It can be selected only for the continuous suspension polymerization. (Chapter VI).

The chlorobutane is evicted for two reasons: its cost and the presence of chlorinate. Finally, toluene represents the better compromise for the liquid-liquid dispersion studies. It presents a low cost and the solubility and liquid-liquid parameters are close to VCM ones.

In conclusion, the model phases for each step will be toluene/PVA/water for the liquid-liquid study, PVC/PVA/Water for the suspension transport and VAM (vinyl acetate) for polymerization.

	VCM	ClBu	Kerosene	VAM	Toluene
Boiling temperature (°C)	-13,4	78	200-260	72.7	110.6
total solubility parameter $(J.cm^{-3})^{0.5}$	17,4	17,0			18.2
Density of 20°C $(g.cm_{-3})$	0,911	0,886	0.8 (15°C)	0.934	0.867
Molecular weight $(g.mol^{-1})$	62,5	92,6		86.09	92.1
Refraction index at 20°C	1,37	1,402		1.3955	1.494
Viscosity (mPa.s)	0,23 à 0°C	0,51 à	1.2 à 20°C	0.43	0.59 à 20°C
Solubility in water $(mg.kg^{-1})$	1100	370	Non soluble	23000	530
Superficial tension $(mN.m^{-1})$	20 à 0°C	23,3 à 25°C	23-32 à 20°C	23.8à 25°C	28.5 à 20°C
Interfacial tension with water at 20°C $(mN.m^{-1})$	32	36,1	47-49	30	35

Table I- 5: Characteristics of potential model liquid compared to the VCM

*III.3. **Methodology***

Figure I- 10 represents the methodology followed in the manuscript.

The liquid-liquid dispersion step is studied with two different technologies: static mixer and pulsed equipments. These technologies will be presented and described in the corresponding chapters: static mixer is detailed in **chapter III** and pulsed technologies in **chapter IV**.

The pulsed column being considered as a potential polymerization reactor, the transport of solid-liquid suspension is also studied in **chapter V**.

Finally, the suspension polymerization of the vinyl acetate is discussed to model the S-PVC in **chapter VI**.

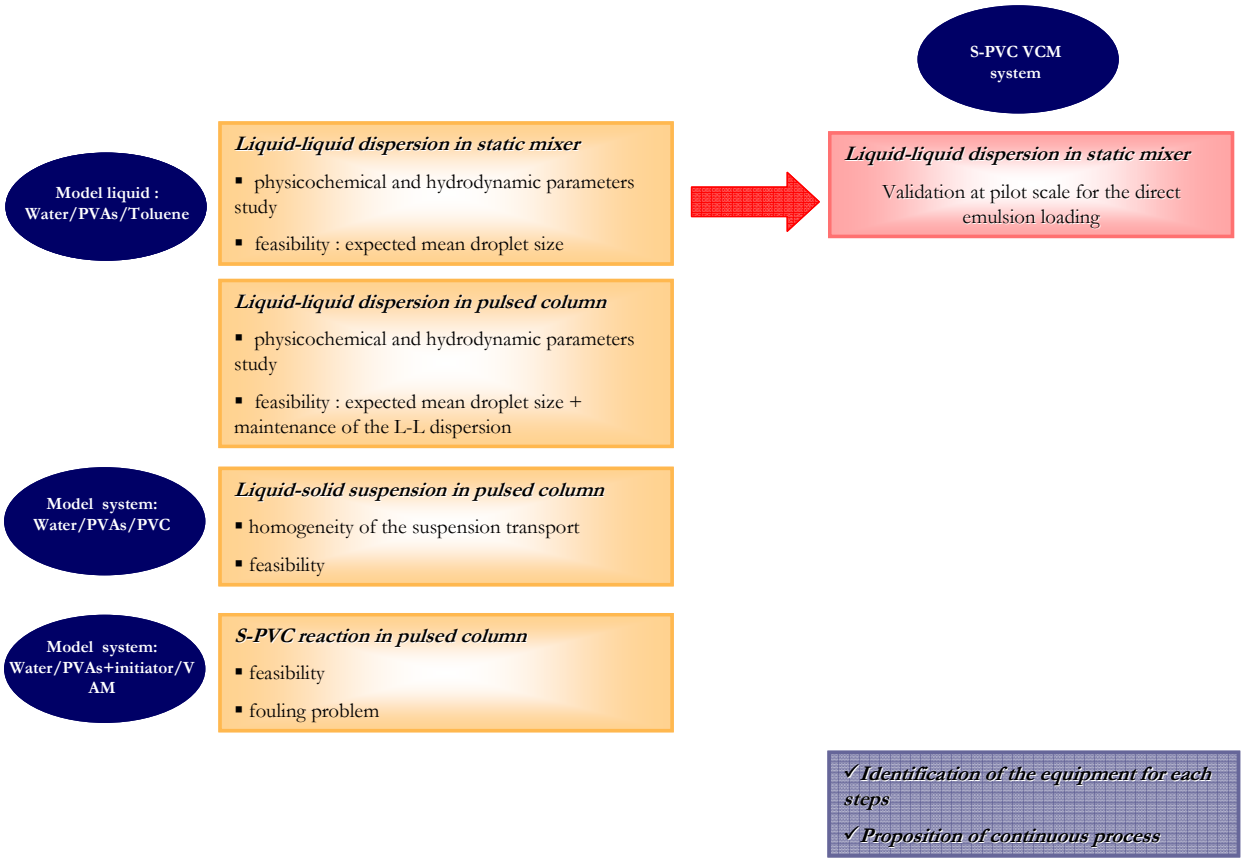

Figure I- 10: Methodology for the S-PVC continuous polymerization process study

CHAPTER II: MATERIALS AND ANALYTICAL ASPECTS

In this chapter, the different systems studied for each of the steps described in chapter I are presented. The analysis techniques employed to characterize the liquid-liquid dispersion, liquid-solid suspension and the reaction product are also detailed.

The liquid-liquid model system (chapter I-part III-2) is characterized as well as the other systems used throughout this work. A special attention is paid to the interfacial tension measurement. The methods to acquire data at equilibrium and at different characteristic times of the involved equipments are presented.

This chapter includes also the techniques developed to characterize the droplet size distribution and the mean droplet size during the liquid-liquid dispersion studies. Three involved techniques will be described. The measurement methods used are either off-line or on-line or allow the visualization of the liquid-liquid dispersion.

The characterization of the particle size distribution is carried out with the same measurement techniques. The principle of the disposal remains the same but the experimental protocol is different.

Finally, some analytical techniques applied to analyze the product of the PVAc (polyvinyl acetate) polymerization reaction are presented.

I. PRESENTATION OF THE STUDIED SYSTEMS

I.1. ***Liquid-liquid systems***

The different systems studied are presented in the following tables.

I.1.1. Liquid-liquid dispersion in SMV static mixer (chapter III)

The different systems properties are summed-up in Table II- 1.

The systems corresponding to our lab model system is printed in blue all along this manuscript. Cyclohexane was purchased from Acros Organics (purity 99%), Tween80 from Panreac, Glycerol (95%) and Toluene from Gaches Chimie (purity 95%). The Tween 80 is a non-ionic surfactant that provides oil-in-water dispersion. It is very soluble in water and its formula is given Figure II-1.

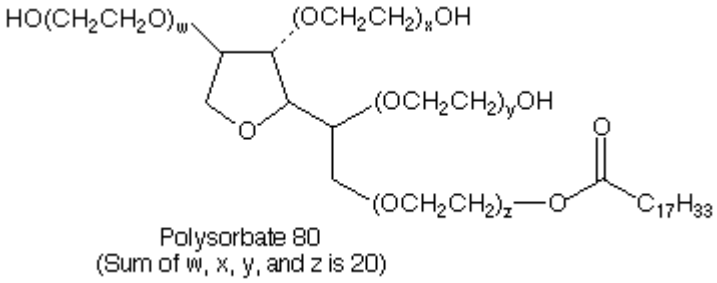

Figure II- 1: Tween80

System	S_1 : Water / Tween 80 / Cyclohexane	S_2 : Water / Tween 80 / Toluene	S_3 : Water / PVA / Toluene	S_4: Water-Glycerol 25%m. / PVA / Toluene
ϱ_c (kg.m^{-3})	995	995	997	1051
ϱ_d (kg.m^{-3})	770	870	870	870
ϱ_e (kg.m^{-3})	939	964	965	1006
ϱ_d/ϱ_c	0.77	0.87	0.87	0.83
μ_c (Pa.s)	0.001	0.001	0.001	0.0021
μ_d (Pa.s)	0.00094	0.0059	0.00059	0.00059
μ_d/μ_c	0.94	0.59	0.59	0.28
Surfactant concentration	1.5% in vol. of the continuous phase	1.5% in vol. of the continuous phase	0.07% in mass. of the dispersed phase	0.07% in mass. of the dispersed phase

Table II- 1: physico-chemical parameters of the four systems investigated where ϱ_c and ϱ_d the continuous and dispersed phase density, ϱ_e the equivalent density, μ_c and μ_d the continuous and dispersed phase viscosity

Two different poly(vinyl acetate) PVA partially hydrolyzed are used in systems S_3 and S_4. The primary suspending agent, PVAI, is the more hydrophilic and contains 88% of OH bounds. It appears as a white powder soluble in water. The secondary suspending agent, PVAII has a hydrolysis degree DH of 45%. It is a yellow viscous liquid and it is diluted at 40% in mass in ethanol and ethyl acetate. Figure II-2 represents their absorption at droplet interface.

The acetate groups are hydrophobic and present more affinity with the droplet phase groups whereas the hydroxyl groups are hydrophilic segments which stabilize the interface on the water side.

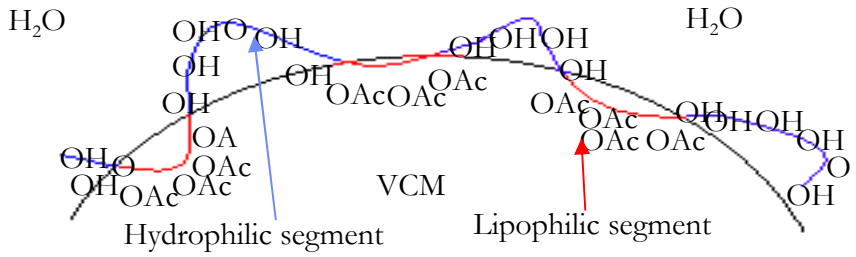

Figure II- 2 : Absorption of the PVA at the water/VCM interface

The equivalent density of each system for a 0.25 dispersed phase concentration in volume is also reported Table II- 1. The equivalent density is calculated as follows:

$$\rho_e = \phi \rho_d + (1-\phi)\rho_c \qquad \textbf{(II- 1)}$$

The amounts of surfactant are always higher than the critical micellar concentration (CMC see part II.3).

Viscosity measurements are carried out using an AR 2000 rheometer (TA Instruments).

I.1.2. Liquid-liquid dispersion in pulsed column and OBR (chapter IV)

In this study, two water/oil/surfactant systems are used. The model lab system and a system involving the same phases with another surfactant are studied. The sodium dodecyl sulfate (SDS) was provided by Panreac and is an anionic surfactant. It is a fine white powder easily soluble in water. PVA is a non-ionic amphiphilic polymeric surfactant. The liquid-liquid dispersion created consists in oil in water dispersion.

The properties of the different systems are summed up in Table II- 2.

	Water/PVA/Toluene	Water/SDS/Toluene
ϱ_c (kg.m^{-3})	997	998
ϱ_d (kg.m^{-3})	870	870
μ_c (Pa.s)	0.0059	0.0059
μ_d (Pa.s)	0.001	0.001
Surfactant concentration	0.07% mass/kg toluene	2.3% mass/kg toluene
σ_e (mN.m^{-1})	3.5	3.5

Table II- 2 : Physicochemical properties of the two systems

I.2. ***Solid-liquid suspension (chapter V)***

In this chapter, the transport of PVC particle is studied. The PVC particles studied are provided by the Mazingarbe plant of Société Artésienne de Vinyle (Tessenderlo, now Ineos ChlorVinyls). The particles correspond to the M5702 grade and their batch number is S5702M/RB12041206.

The continuous water phase is composed of demineralized water and PVA as surfactant.

I.3. ***Vinyl acetate polymerization (chapter VI)***

The products used are the primary suspending agent PVAI (DH 88%), the initiator is the Peroxan BCC (bis(4tert-butyl-cyclohexyl)-peroxidicarbonate)) supplied by Pergan and the monomer is purchased from Sigma Aldrich. The vinyl acetate monomer VAM is inhibited and contained 10-23ppm of hydroquinone.

For safety reasons, hydroquinone from Sigma Aldrich is purchased to inhibit the polymerization for the collected sample.

The continuous phase is composed of demineralized water.

The initiator concentration is set to 0.1% molar based on the VAM concentration. The surfactant concentration is fixed at 2000 ppm. The dispersed phase concentration of the initial VAM is of 16% mass.

The initiator consists of white powder non soluble in water. A premix is realized composed by demineralized water, PVA surfactant and the initiator. An ultraturrax allows to homogenize the mixture.

The different phases are degassed thanks to nitrogen flux to avoid oxygen introduction which is a polymerization inhibitor.

II. INTERFACIAL TENSION MEASUREMENT

The different liquid-liquid systems are characterized in term of interfacial tension measurement. Our systems are composed of an aqueous phase containing the surfactant and an organic phase (solvent). The systems are normally formulated to achieve oil-in-water emulsion.

The surfactant molecule first diffuses from the aqueous medium to the droplet and then absorbs at the interface.

The diffusion and absorption are related to kinetics depending on the nature of the surfactant and the systems. It is obvious that the presence of surfactant leads to the interfacial tension decrease. The interfacial tension value decreases then versus time.

On the other hand, at the outlet of a continuous process, the residence times are really different from one equipment to another. So to access to the transient interfacial tension value, the different interfacial tensions of the systems are measured through a dynamic measurement method. The method employed is the pendant drop method.

II.1. *Principle*

The pendant drop method is an optical method based on the shape analysis of a droplet created at a tip of a needle. To be reliable, the physical systems must handle the following conditions:

- The difference between the density must be high enough to allow the creation of a drop
- The refractive index of the two phases must be rather different to enable the visualization and the droplet shape analysis
- The liquid are supposed to be non-volatile.

The droplet shape is governed by the balance between gravity and capillary forces. The method consists in comparing the droplet profile to the numerical obtained profile thanks to the Laplace-Young equation (II-2). It provides the curvature at each M point.

$$C(M) = \frac{2}{R_0} - \frac{\Delta\rho g h}{\sigma} \qquad \textbf{(II- 2)}$$

C is the curvature, R_0 the radius of curvature at the apex (origin O). h is the height between the M and O points. $\Delta\varrho$ is the density difference of the two phases.

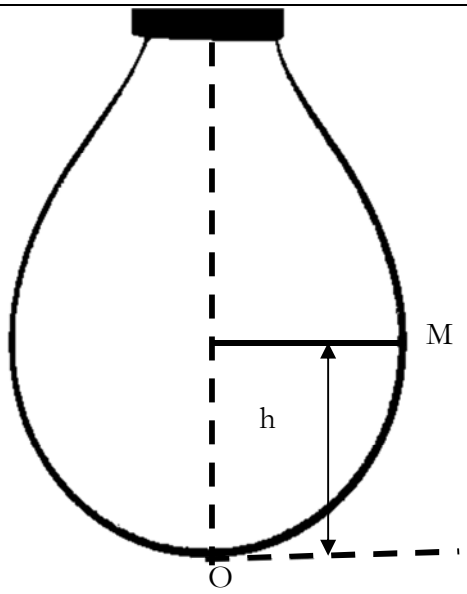

Figure II- 3 : Pendant drop geometry

The relation (II-2) can be expressed through dimensionless number thanks to the expression (II-3).

$$C^* = \frac{2}{R_0} - \frac{\Delta\rho g R_0^2}{\sigma} h^* \qquad \textbf{(II- 3)}$$

With $C^* = R_0 C$ and $h^* = \frac{h}{R_0}$. R_0 is used as the length scale of reference.

Bo is the dimensionless Bond number:

$$Bo = \frac{\Delta\rho g R_0^2}{\sigma} \qquad \textbf{(II- 4)}$$

The droplet shape is described by C*(h*). It depends only on the Bond number established thanks to the radius of curvature at the apex R_0. Figure II- 3 describes this notation.

To validate the Young-Laplace equation, the lone forces acting on the droplet must be related to the gravity and the surface forces (interfacial tension). Moreover, the profile must be axisymmetric.

The method consists in identifying the interfacial tension by analyzing the drop profile and fitting the Young-Laplace model.
The computation method is often automated and the discrepancy between theory and measurement can be evaluated.

II.2. *Experimental facilities and protocol*

A scheme of the disposal is shown in Figure II- 4. The device used to perform the measurement is the DSA 100 (Krüss). The disposal is composed of an automatic syringe pump which allows to fix the droplet volume and its creation velocity (3). The droplet is created at a tip of a stainless steel needle of 1.83 mm of external diameter. Measurements were made by creating a drop of aqueous phase immerged in a square dish of organic phase (4). A source light (2) is available and the set is recorded thanks to a CCD camera (5) with a maximum frequency of one frame per 0.02 second. The threshold is regulated to optimize the profile extraction. The pictures are then treated thanks to the DSA100 software which allows the determination of the interfacial tension. The software provides the discrepancy between the model and the droplet profile extracted from the picture.

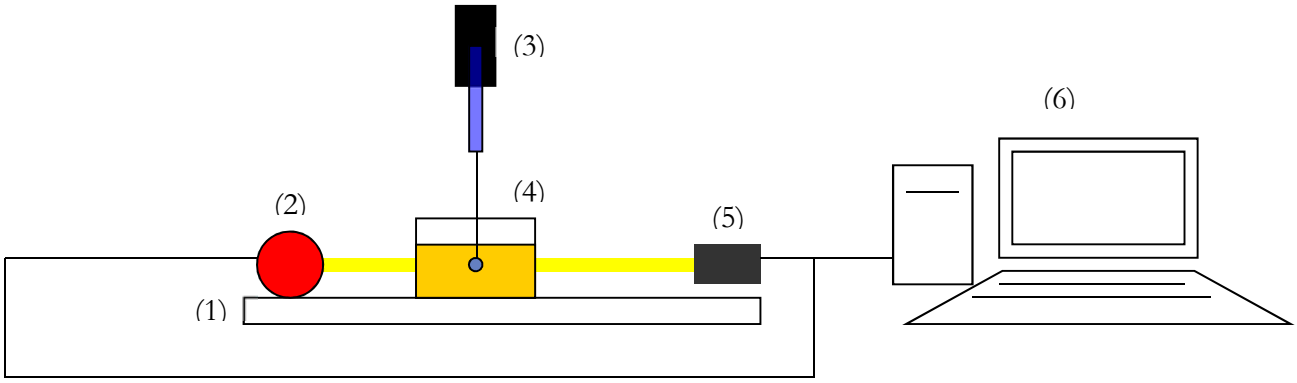

Figure II- 4:Test bench of the interfacial tension apparatus: (1) Optical bench, (2) Light source, (3) automatic syringe pump of the device containing the aqueous phase, (4) square dish filled with the organic phase, (5) CCD camera, (6) computer

This method is used to determine the interfacial tension evolution versus time for all the oil/surfactant/water systems studied and to characterize the model system.

Methods can be defined to automate the procedure. The following parameters must be known:

- The density of the two phases
- The needle dimension for calibration
- The droplet volume
- The syringe pump flowrate

Each measurement is at least performed three times to ensure the reproducibility.

The measurement procedure consists in starting the video recording, creating the drop of controlled volume and at a given creation rate. Each record is then retreated frame by frame

to extract the drop profile and calculate the interfacial tension thanks to the software. Each resulting file contains the droplet age, the interfacial tension value, the droplet volume, the Bond number value and the comparison error factor between theory and measurement.

II.3. ***Measurement results***

II.3.1. Example of the lab system Water/PVA/Toluene

To validate the measurement, the interfacial tension evolutions of the systems without surfactant are estimated. It allows also to check the product purity. The interfacial tension value is constant on all the measurement period. For the water/toluene system, the interfacial tension is estimated to 36.2 ± 0.2 $mN.m^{-1}$. The literature value is of 36.1 $mN.m^{-1}$.

Then, the water/surfactant/oil systems are studied. The critical micellar concentration is estimated. The complete study is presented for our lab model system: the water/PVA/toluene.

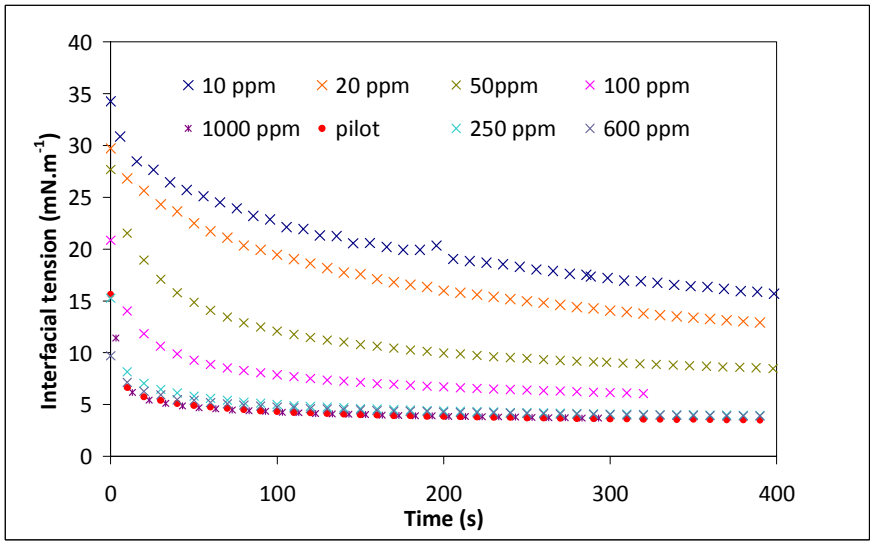

Figure II- 5: Evolution of the interfacial tension measurement for water/PVA/toluene systems- effect of the PVA concentration

In Figure II- 5 the interfacial tension evolution depending on the droplet age is presented for different surfactant concentrations in the water phase. First the interfacial tension decreases quickly corresponding to the diffusion and the adsorption of the PVA molecule at the interface. It is gradually decreasing, but the phenomenon is slower at the end. It corresponds to a rearrangement of the adsorbed molecules at the droplet interface: the contact between the hydrophobic acetate groups and the organic phase is enhanced. This behavior has been

observed in literature for amphiphilic polymers (Rotureau *et al.*, 2004; Nahringbauer, 1995; Babak *et al.*, 2005). Figure II- 6 allows to understand these different steps.

The measurement time is in fact of 1200 s but the results presented here stop at 400 s. This 400 s measurement time corresponds to the adsorption time estimated by Boscher in her PhD (2009).

The subsequent decrease is due to the molecule rearrangement. Moreover for surfactant concentration up to 100 ppm, pseudo equilibrium is established as soon as the droplet age reaches 100 seconds.

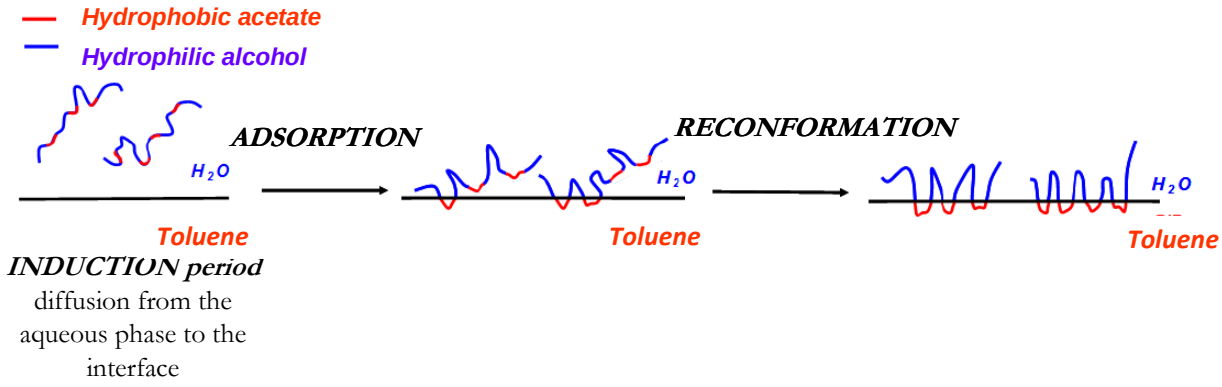

Figure II- 6 : distribution of the PVA surfactant at the droplet interface

From these results, the interface saturation concentration can be estimated. The interfacial tension values for the different concentrations are taken equal to the value at 400 seconds.

For macromolecular surfactants, this concentration is lower than the one for low molecule weight surfactant and it is called critical concentration.

At this value, the interface is saturated and above, the interfacial tension does not evolve in a significant way.

The critical concentration and its corresponding interfacial tension value are evaluated at the intersection of both straight lines. For low molecular weight surfactant, the interfacial tension remains constant after the critical concentration. However in presence of PVA as surfactant, the interfacial tension keeps decreasing slightly after the critical concentration (see Figure II-7Figure II- 7).

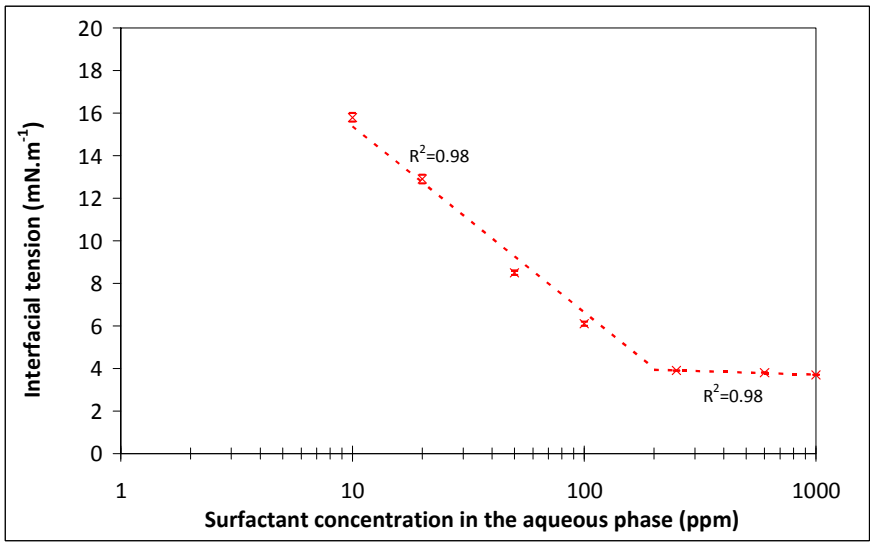

Figure II- 7 : evolution of the interfacial tension with the concentration logarithm

Nahringbauer (1995) develop some assumptions to explain the phenomenon. At low PVA surfactant concentration, the molecule is fully developed and recovers a large part of the interface (Figure II-8 (a)). At the critical concentration, the interface is entirely covered with macromolecule fully developed (Figure II-8 (b)). Then, at higher concentrations, the macromolecules withdraw in order to raise their number at the interface (Figure II- 8 (c)). They form a thick layer which leads to an interfacial tension decrease and to the stabilization of the interface.

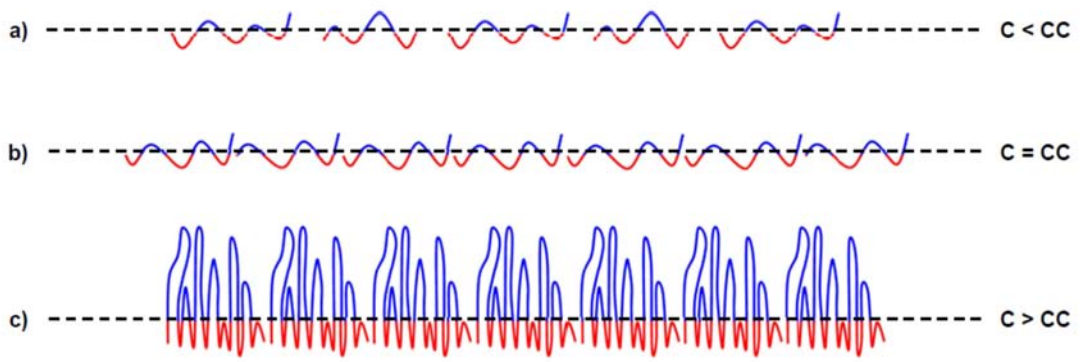

Figure II- 8: PVA conformation at the droplet interface for different concentration (Nahringbauer, 1995)

This preliminary study enables us to identify the critical concentration for the system and to understand the PVA behavior at the droplet interface. The previous results of Boscher (2009) are confirmed concerning the interfacial tension evolution and the adsorption modeling (not described here).

II.3.2. Evolution of the interfacial tension for the different liquid-liquid studied systems

This section summarizes the results relative to the interfacial tension evolution for all the liquid-liquid systems studied.

For the four systems of the Table II-1, considered in chapter III, the interfacial tension decreases strongly at the first seconds and then tends to stabilize. The decreasing is faster in case of Tween 80 because it is a smaller molecule. It happens in the first ten seconds as suggested in Figure II-9.

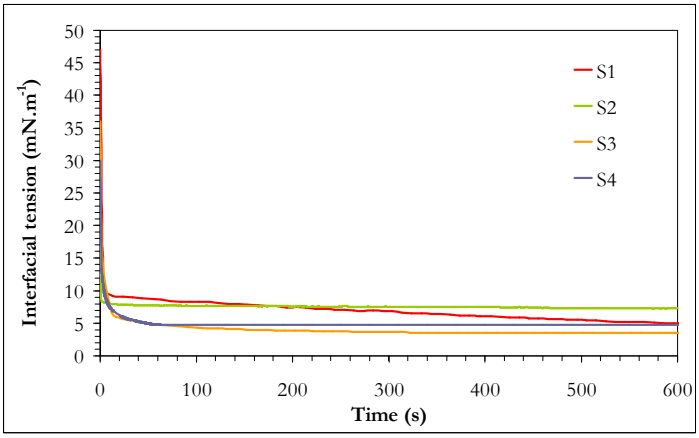

Figure II- 9 : Interfacial tension evolution of the four systems

Besides, Figure II-10 represents the evolution of the interfacial tension for both systems of Table II- 2 in the residence time range and until the equilibrium value.

The equilibrium value for both systems is equal to 3.5 $mN.m^{-1}$. However, the surfactant adsorbed faster in the case of the SDS than in the case of the PVA. Indeed, the global kinetics of surfactant adsorption consists of three steps: the diffusion of the molecule at the interface, the adsorption of this molecule and finally the conformation arrangement of these molecules. Depending on the concentration and on the chemical nature of surfactants, each one of these steps can control the global kinetics adsorption of the surfactant.

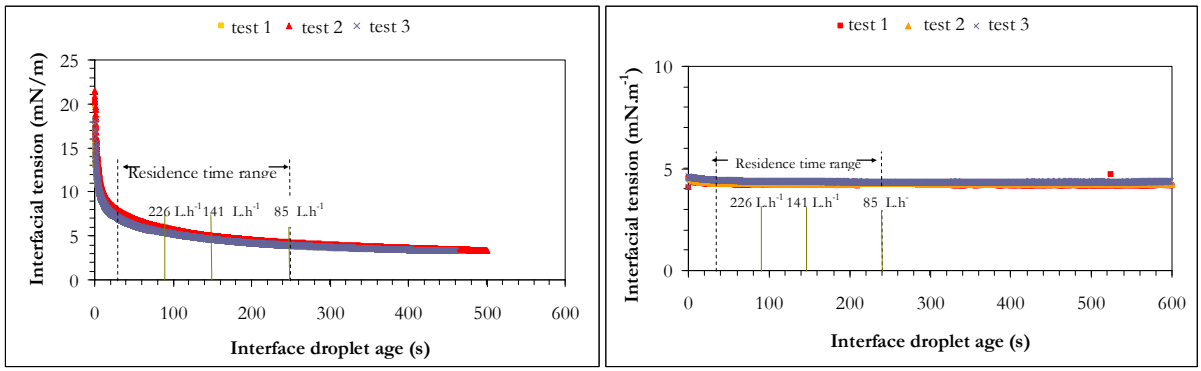

Figure II- 10 : Interfacial tension evolution for the water/PVA/ system (left) and the water/SDS/ system (right)

Concerning the PVA, two different evolution zones can be identified: first, the interfacial tension decreases faster. This step corresponds to the diffusion and adsorption of the PVA at the interface. Then the decreasing slows down. It refers to a rearrangement of the adsorbed molecules at the interface (He *et al.*, 2004; Lankveld and Lyklema, 1972; Nillson *et al.*, 1985). Regarding to SDS surfactant, the adsorption is extremely fast and the stabilization of the interface is almost instantaneously reached.

The residence time range of our experiments is indicated. The global adsorption kinetics of both surfactants is quite different: in case of SDS, the interfacial tension does not evolve significantly on our range studied and the value is close to the equilibrium value σ_e. Yet, with experiments involving PVA, the interfacial tension still decreases and the value is almost divided by an order of two all along the column.

It seems obvious that aiming to explain liquid-liquid dispersion results, the physical properties must be known in relation to the residence time in the equipment. Section II.4 is dedicated to the description of a method allowing to access to the transient interfacial tension values (i.e. interfacial tension at time lower than 0.5s).

II.4. ***Short time measurement method***

II.4.1. Experimental protocol

The previous method allows to access to the interfacial tension from 0.4 second until equilibrium.

In the different equipments in the present work, the residence time ranges from millisecond to several minutes. The shorter residence time ranges from 0.04 to 0.1 second which is really short (static mixers in Chapter III).

The classical Krüss DSA100 is not suitable to carry out this short-time measurement. Lots of techniques have been developed since the 1990s. In their review, Eastoe and Dalton (2000) give a time window of the various dynamic surface tension techniques (i.e.Figure II-11). This figure represents the classical methods commercially available for gas-liquid surface tension measurement.

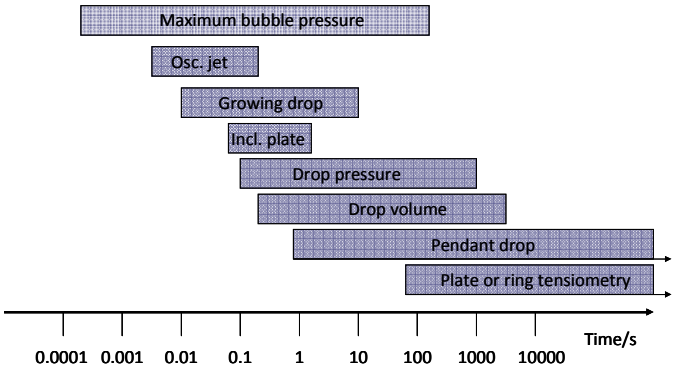

Figure II- 11 Classical methods used for gas-liquid surface tension measurement

To carry out these measurements, we have decided to adapt the pendant drop method using the classical Krüss DSA 100 device available in our lab. Classically, one droplet of aqueous phase with a fresh interface is created at the tip of needle of external diameter of 0.5mm in a quartz dish containing the organic solution. This usual method allows the droplet creation within an interval of 0.40 seconds. The standard apparatus has been modified to reduce this creation time and obtain the first measurements within a time range of 0.04 to 0.08 second. The principle consists in forming a jet thanks to a syringe connected to a stopcock. A syringe pump equipped with a syringe filled with the aqueous phase is located upstream the stopcock (Figure II- 12).

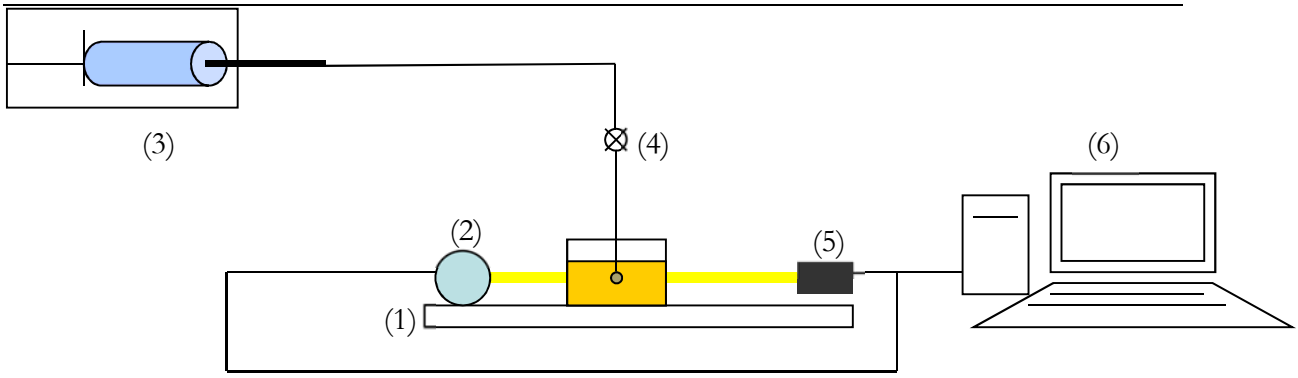

Figure II- 12 Test bench of the interfacial tension apparatus: (1) Optical bench, (2) Light source, (3) Syringe pump and aqueous phase syringe, (4) Stopcock, (5) CCD camera, (6) Computer

The DSA 100 measurement is based on the profile detection of the drop and then all the experiments are recorded with the highest frequency i.e. one frame every 0.02 second. When the stopcock is open, a 300 $mL.min^{-1}$ flowrate is imposed. The stopcock is suddenly closed and the syringe pump stopped. The jet stops and a residual droplet is created at the tip of the needle. Thanks to the recording, the creation time is evaluated to 0.04 s (i.e.Figure II-13). This method provides a droplet creation time ten times lower than the classical method. The pictures are then analyzed thanks to the supplier drop shape analyzer software.

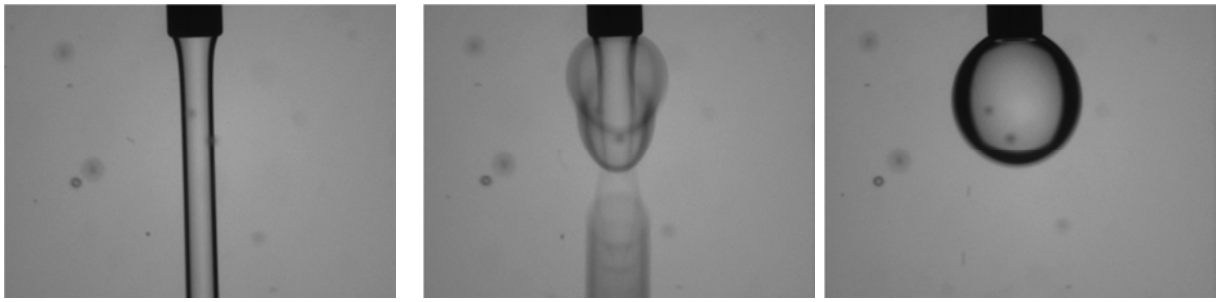

Figure II- 13: Drop creation for the system S_1: Water/Tween80/Cyclohexane

The reliability of the measurement is confirmed by the study of the air/water system. For this system the same procedure is followed and the interfacial tension is evaluated to 71.9 ± 0.3 $mN.m^{-1}$, in total accordance with the literature value. The baseline is placed in order to minimize the difference between the drop profile and the calculation. The measure is considered reliable for a magnification error inferior to 1 μm.

II.4.2. Measurement and treatment of the results

The values which require our interest range over the first 0.1 second. Few data are available in this range. Applying the principle presented in Figure II-13, only five measurements points can be obtained in this range (0.1 second of measurement corresponds to 5 frames considering the camera speed recording). Consequently the different measurements are performed on larger intervals and the raw data are treated and modeled on the first 0.5 second measurement range. The raw data obtained must be retreated to model the evolution of the interfacial tension with the droplet age. For each system the model is established from at least four measurements. Each single measurement is filtered in order to avoid the measurement fluctuation problem. Then the modeling of the interfacial tension value is determined by averaging.

The model used is a phenomenological equation proposed by Hua and Rosen (1988), which is used in different publications (Eastoe *et al.*, 2000; Meyer *et al.*, 2010):

$$\frac{\sigma_{ini} - \sigma(t)}{\sigma(t) - \sigma_E} = \left(\frac{t}{t^*}\right)^n \qquad \textbf{(II- 5)}$$

where σ_E corresponds to the interfacial tension at equilibrium. σ_{ini} is taken equal to the interfacial tension value without surfactant.

t^* (s) and n are both characteristic parameters of the studied system. The parameter t^* depends on the process adsorption rate. The parameter n is function of the surfactant molecule transfer mechanism. If the phenomenon is controlled by the adsorption kinetics, it leads to n higher or equal to 1 whereas if it is controlled by diffusion it provides n equal to 0.5 (Fillipov, 1994a, 1994b).

For each system the parameters n and t^* have been determined in order to fit the average of the measurements data. Figure II- 14 represents the evolution of the interfacial tension versus time and the corresponding model for the S_3 system. Figure II- 15 represents the modeling of the interfacial tension for the four systems.

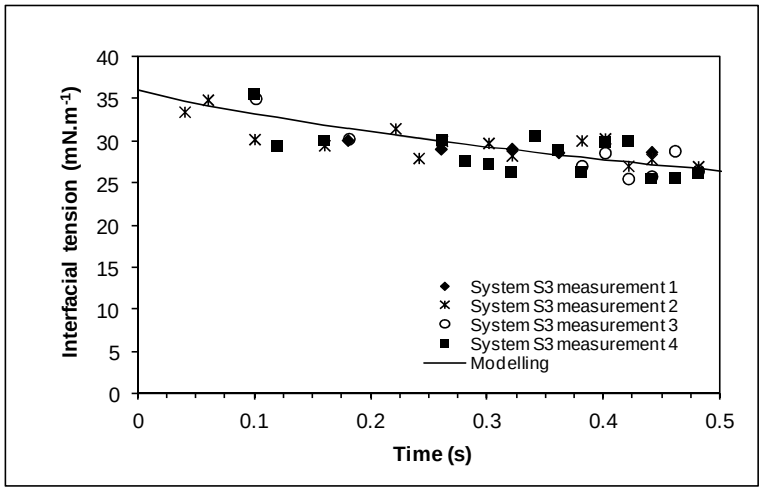

Figure II- 14: Interfacial tension evolution for the system S_3: measurement and modeling

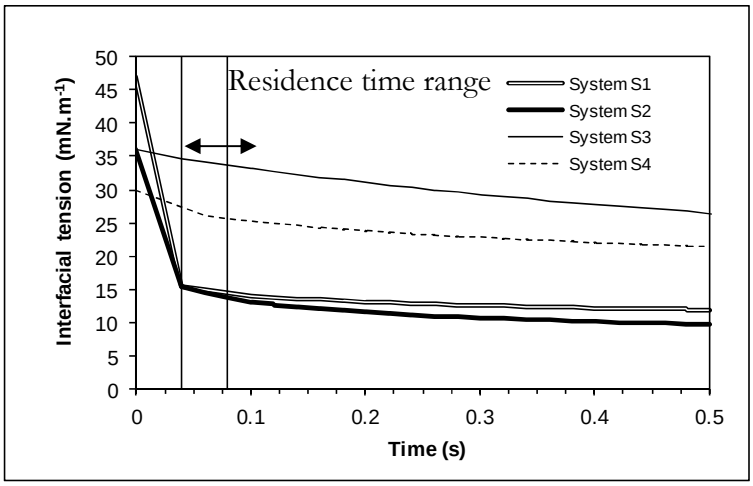

Figure II- 15: Modeling of the interfacial tension for the four systems

The systems S_3 and S_4 present a higher value of interfacial tension than the systems S_1 and S_2 in the measured time range (from 0.04 to 0.5 second). However at the equilibrium, that is to say after several minutes, the four systems have rather close interfacial tension values (i.e. Table II-3). The rupture in the modeling curve is due to the lack of measurement in this range.

The fitting parameters n and t* for the four systems are given in Table II-3. For the four systems the n value is lower than 1. It suggests that for both surfactants used in this work the adsorption kinetics is mainly controlled by diffusion (Fillipov 1994a, 1994b).

t^* allows to compare the different systems quantitatively. Thus for a same dispersed phase (systems S_2 and S_3 with toluene as dispersed phase) t^* is smaller for the surfactant of lower molecular weight, i.e. Tween 80. It confirms that the molecules of small molecular weight diffuses faster and then the interfacial tension drops more quickly.

System	S_1: Water / Tween 80 / Cyclohexane	S_2: Water / Tween 80 / Toluene	S_3: Water / PVA / Toluene	S_4: Water – glycerol / PVA / Toluene
$\sigma_{without\ surfactant}$ ($mN.m^{-1}$)	47	36	36	30
σ_E ($mN.m^{-1}$)	3.0	7.0	3.5	4.7
n	0.18	0.36	0.92	0.50
t^* (s)	0.0002	0.0091	1.3039	1.9318

Table II- 3: Summary of the different values used for the modeling and value of the different parameters of the model

This measurement principle and the modeling will enable us to evaluate the interfacial tension value at time inferior to 0.5s.

III. CHARACTERIZATION OF THE LIQUID-LIQUID DISPERSIONS

Three measurements techniques have been carried out: the off-line laser diffraction, the on-line backscattering measurement and the microscopy visualization of the emulsion. They are complementary because they respectively allow the total droplet/particle size distribution characterization, an on-line measurement of a characteristic diameter of the dispersion/suspension and the visualization of the drops/particles obtained.
These techniques are detailed in the following section.

III.1. ***Laser diffraction measurement***

III.1.1. Principle

The principle of the mean droplet size measurement through laser diffraction depends on the diffraction angle measurement generated when a laser beam focused on the sample. The measurement principle is described in Figure II-16.

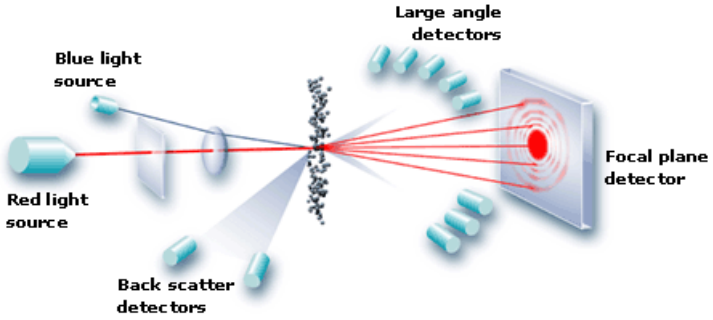

Figure II- 16 : Laser diffraction principle

Figure II- 17 represents the light intensity distribution shared out among the different detectors for a particular sample measurement.

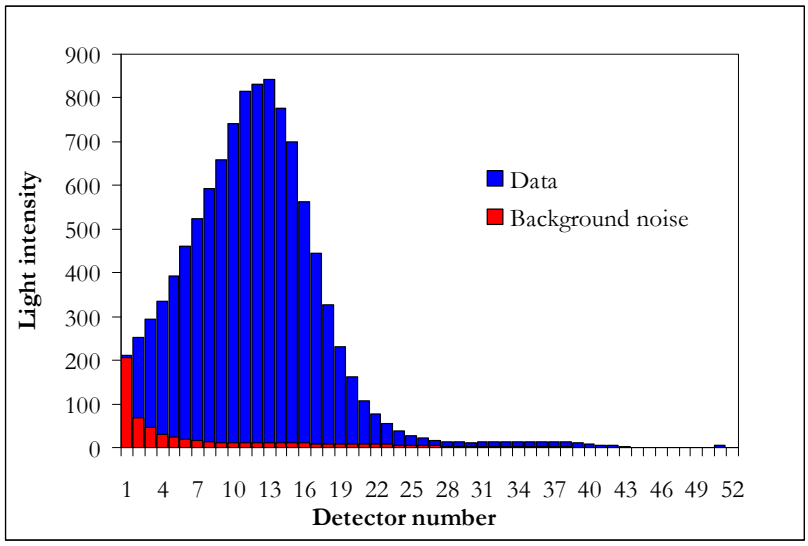

Figure II- 17: Raw data – SMV, 400 L.h^{-1}, 40%, S_3

The detector numbers are related to the diffraction angle spectrum. The generated diffraction angle spectrum by the population is then converted to droplet size distribution. It is calculated by comparing the diffraction angle spectrum to an optical model via an inversion mathematical process. Two optical models are currently used: the Fraunhofer approximation and the Mie theory. The Fraunhofer theory is the easiest model to set-up in contrast to the Mie theory. The user does not have to provide any optical property observation. However it is not accurate to determine fine particle and it leads to over or under estimation of their sizes.

The Mie Theory provides a rigorous solution for the calculation of particle size distributions from light scattering data and is based on Maxwell's electromagnetic field equations. At low diffusion angle, the scattered intensity is important in case of large particles. The scattered light angle variation evolves in a non-monotonous way for non-absorbent particles and it decreases with the scattered angle because of backward destructive interferences. The angular dependency of the scattered light is less pronounced for small particles and allows to derive

information about the particle size. The scattered light intensity depends also on the refractive indices of the particles and of the medium as well as the incident light wavelength.

The Mie theory predicts scattering intensities for all particles, small or large, transparent or opaque within the following assumptions:

- The particles or droplets are well spherical
- The suspension or dispersion is diluted in such a way that the diffracted light by a drop or a particle is not re-diffracted by another one
- The optical properties of the continuous and the dispersed phase are well-known
- The particles or droplets are homogeneous.

In our case, the optical properties of both phases are well-known whatever the systems. Moreover the measurement droplets sizes range from micron to some dozens of microns. Consequently, the Mie theory may be applied.

The droplet size distributions obtained are expressed in volume percentage. The entire population is described thanks to the determination of the frequency corresponding to the volume fraction of particle in each size class.

Distributions are characterized through the mean diameters d_{32} which is called the Sauter mean diameter defined by expression (II-6) and through the span which quantifies the width of the distribution (II-7).

$$d_{32} = \frac{\sum_{i=1}^{n} n_i d_i^3}{\sum_{i=1}^{n} n_i d_i^2} \qquad \textbf{(II- 6)}$$

where n_i is the number of droplets which sizes range from d_i to d_{i+1}.

The span values are calculated as follows:

$$\text{span} = \frac{d_{90} - d_{10}}{d_{50}} \qquad \textbf{(II- 7)}$$

Some authors refer to the d_{43} which is the mean diameter in mass-volume and is expressed as:

$$d_{43} = \frac{\sum_{i=1}^{n} n_i d_i^4}{\sum_{i=1}^{n} n_i d_i^3} \qquad \textbf{(II- 8)}$$

The d_{50} is the median diameter: 50% of the droplets total volume corresponds to the droplets volume of diameter inferior to d_{50}. d_{90} means that 90% of the droplets (in volume) have a diameter inferior to d_{90}. Respectively, the d_{10} mean that 10% of the droplets total volume is occupied by particle having a diameter inferior to d_{10}.

III.1.2. Experimental facilities

The device used is the Mastersizer 2000 (Malvern Instruments). It allows to measure droplets or particles ranging from 0.02 to 2000 μm.

Different disposals are supplied to transport the sample until the measurement cell.

In case of liquid-liquid dispersion, the phase system can be considered as unstable and sensitive to the shear stress. For that reason, a particular disposal has been implemented. It consists of a funnel connected to the measurement cell. A peristaltic pump is then installed at the outlet of the measurement cell and the diluted sample is pumped and the sampling transport is ensured without affecting the droplet size distribution, since the pump is located downstream of the measurement cell.

III.1.3. Experimental protocol

Before each analysis, the following parameters are required to put into practice the Mie theory and are inserted in the software:

- Continuous and dispersed phase constituents
- Absorption and refractive index of these phases

To carry out the analyses, the medium must be diluted. The samples are diluted in their continuous phase. A measurement sequence consists in 5 measurements. To study the reproducibility, several sequences can be done with the same sample.

The software allows to compare the different results between themselves. The characteristic diameters are then provided.

III.2. ***On-line measurement: light multiple diffraction***

III.2.1. Principle

In diluted dispersion, each particle diffuses the light independently from the others. In concentrated dispersion, the light scattered by a particle may correspond to the incident light for one or several particles contained in the volume.

A part of the incident beam is transmitted whereas another part is scattered. The scattered light is a complex function of the observation angle θ, the wavelength of the incident beam Λ, the mean particle size d and the refractive index of both phases. Incident photons undergo

multiple scattering events before absorption, backscattering or transmission through the sample.

If d is superior to the wavelength the scattering is no longer isotropic or quasi isotropic and Mie's model has to be used. The scattered light intensity tends to decrease when the drop size increases but depends on the observation angle in a complex way.

To give a clear cut interpretation of the data to calculate the size of the particle, most laser light scattering equipment requires the dilution of the dispersed system: the photons are then scattered only once.

The on-line Turbiscan allows to measure the backscattered light which is the light reflected backwards and which comes from the multiple scattering. The photons bounce several times on different droplets. In multiple scattering, the light diffused by one droplet becomes the incident light of the next one and so on with a certain amount of light coming out backward. Figure II- 18 illustrates this principle.

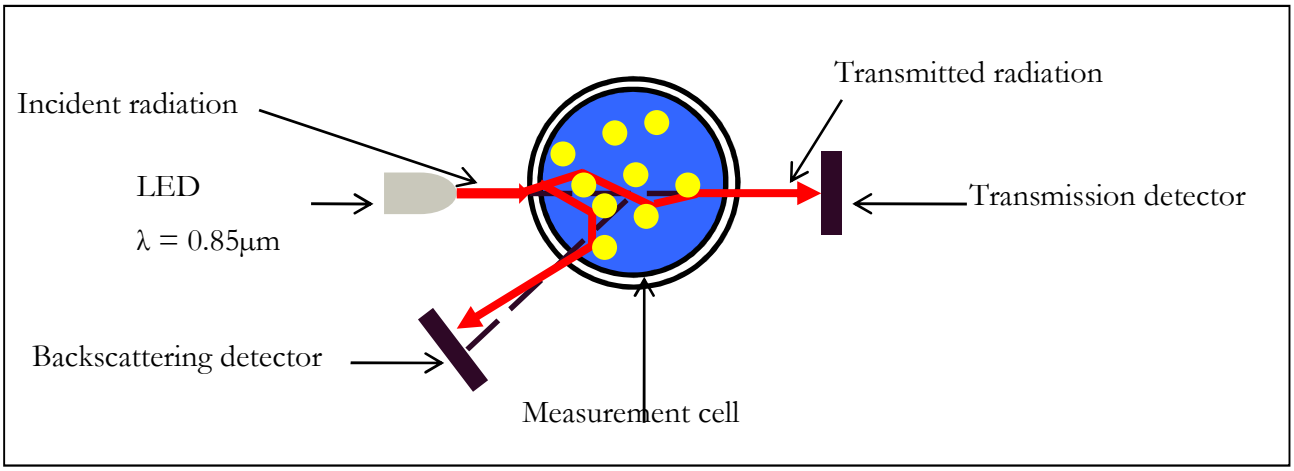

Figure II- 18 : On-line Turbiscan measurement cell principle

The On-line Turbiscan is composed of a cylindrical measurement glass cell, a light source (pulsed near infrared laser beam of wavelength Λ = 850 nm) and two photoelectric synchronous detectors. The transmission detector receives the light which goes through the sample (0° from the incident beam) while the backscattered detector receives the light scattered by the sample at 135°C from the incident beam.

The two detectors have been calibrated by the manufacturer by using a latex suspension of 3 µm of diameter dispersed in a silicon oil medium at Φ_0=10% in volume.

Thanks to this calibration, the backscattered light intensity and the transmission light intensity are known in the reference medium. The software provides then the diffuse reflectance R and the transmission T resulting from the incident light.

Generally, a large transmission signal for transparent to turbid dispersions is obtained while for opaque dispersion, a large backscattered signal and zero transmission is achieved.

In a transparent medium of low optical width, a part of the incident light crosses the dispersion and is received by the transmission detector. The detector catches a light flux f_T transmitted through the dispersion with an incidence θ=135°C. The transmission level or diffuse transmittance T is defined as the light intensity f_T to the fluid reference transmitted intensity f_{0T}.

$$T = \frac{f_T}{f_{0T}} \qquad \textbf{(II- 9)}$$

It can be expressed through the Lambert-Beer law:

$$T(\lambda, r_i) = \exp\left(-\frac{2r_i}{\lambda(\phi, d)}\right) \qquad \textbf{(II- 10)}$$

where r_i corresponds to the internal measurement cell radius and $\lambda(\Phi, d)$ the photon mean path length.

The photon mean path length is the average distance between two scattering events in the medium and is expressed as:

$$\lambda(\Phi, d) = \frac{1}{n\pi\frac{d^2}{4}Q_s} = \frac{2d}{3\Phi Q_s} \qquad \textbf{(II- 11)}$$

$$\phi = \frac{n\pi d^3}{6}$$

n is the particle density, d the particle mean diameter, Φ the particle volume fraction and Q_s is the extinction efficiency factor for scattering and absorption media. In our case this factor corresponds to the scattering efficiency factor.

For higher concentrated dispersion, the photons follow complex diffusion paths before backscattering and reaching the dectector. The light intensity is received with an incidence of θ=45°C. The diffuse reflectance is defined as the ratio between the received light intensity on the light intensity detected for the reference medium:

$$R = \frac{f_R}{f_{0R}} \qquad \textbf{(II- 12)}$$

R is related to the photon mean free path length λ^* which represents the decorrelation length above which the photon "forgets" both the direction of the incident beam and the scattering pattern of single particles:

$$\lambda^*(d, \phi) = \frac{2d}{3\phi(1-g)Q_s} = \frac{\lambda}{1-g} \qquad \textbf{(II- 13)}$$

where λ is the photon mean path length, $g(d, \lambda_{IR}, n_p, n_f)$ is the optical asymmetric factor and $Q_s(d, \lambda_{IR}, n_p, n_f)$ the diffusion efficiency factor. g and Q_s are given by the Mie theory. d is the particle average diameter and Φ the droplet volume fraction.

The measurement of both the transmission and the backscattering allows to derive the mean path length and the photon mean free path in the diffusive medium. Thanks to the Mie theory and assuming rigid spheres, an inverse method provides the mean particle diameter.
In case of rigid monodispersed sphere, it is pretty easy to define a mean diameter but the concept is much more difficult to comprehend in case of polydispersed particles. However, in polydispersed medium, the droplet size distribution affects the dispersion optical properties. If a significant volume of the dispersion is explored by the photons, the inverses of the mean path length and the mean free path length describe the light scattered phenomenon in a polydispersed dispersion.
In case of large particle, with diameter superior to five times the wavelength, the mean diameter obtained corresponds to the mean Sauter diameter d_{32}. For particles of the same size of the wavelength, the value of the mean diameter obtained is located between the d_{32} and the volumetric diameter d_{43}.

III.2.2. Experimental facilities

The On-line Turbiscan measures droplets or particles of size ranging from 100nm to 1mm. The dispersion can be highly concentrated. The supplier claims that the device is suitable up to 95% of dispersed phase concentration but in fact it depends on the system.
The dispersion flows upward through the cell and the measurement cell is directly connected to the process. The supplier recommends flowrate from 40 to 400 $L.h^{-1}$ to have reliable measurement. The maximal acquisition frequency is 0.5 second.
The transmittance, backscattering, photon mean path length and photon mean free patch length can then be followed all along the experiment.

III.2.3. Experimental protocol

Before each analysis, the following parameters required are entered into the software:

- Continuous and dispersed phase constituents
- refractive indices of these phases
- measurement sequence

The analysis cell is directly installed on the pipe. During the data recording, the user can read the backscattered and transmitted percentage intensity as well as the photon transport mean free path and photon mean path length.

After acquiring the data, this signal can be transformed into d_{32} value. Indeed, in our tests, the dispersed phase concentration in volume is always known and the d_{32} is then deduced.

III.3. ***Microscopy***

The liquid-liquid dispersions have been also analysed with an optical microscope in order to identify the shape of the droplet and the nature of the emulsion (oil-in water, water-in-oil, multiple emulsion).

A droplet of the emulsion is simply deposed on a microscope slide, after dilution of the sampling. Different microscopes have been used throughout the manuscript. In Chapter III and IV the microscope is the Zeiss Axioscope and chapter VI the Zeiss AXIO observer A1m.

IV. CHARACTERIZATION OF THE SOLID-LIQUID SUSPENSION OR SOLID PARTICLES

IV.1. ***Laser diffraction measurement (Chapter V)***

The solid-liquid suspension is analyzed thanks to laser diffraction by using the Mastersizer 2000 (Malvern).

On contrary to the liquid-liquid dispersion, the system is not sensitive to the shear stress.

The suspensions are analyzed by using the two modules of the device: the hydro S (humid suspension) and the Scirroco (particles after drying at 45°C).

In the case of the hydro S, the medium must be diluted and the standard operating procedure includes the stirring velocity set at 1600 rpm. To choose the most convenient stirring velocity, different ones have been tested before in order to analyze if there is an impact on the particle size distribution.

For the Scirroco, the solid particles are dried. They are put in the tray. The flow is controlled by using a feed-rate vibrating tray and the dispersion is achieved by accelerating particles within a compressed air stream. The set of parameters is chosen by evaluating the effect of the pressure on the mean particle size. If the mean diameter evolved, it means that the particle can break or agglomerate. The intensity of the vibrating tray is chosen to have a proper obscuration rate.

No effect of the air pressure is noticed in our case. The parameters are then fixed to 1 bar and 60% of feed-rate vibration tray.

IV.2. ***Scanning electronic microscopy SEM (Chapter VI)***

The optical microscopy allows us to evaluate the droplets size of the created liquid-liquid dispersion. The SEM technique gives access to the surface and the shape of the poly (vinyl acetate) particles obtained.

For the batch study, the pictures were analyzed thanks to the Leo 435 VP. The particles were previously dried and then posed on a stub with a carbon scotch. To ensure a continuity of the current and evacuate the charge due to the electron beam (10kV), the sample is metalized with gold via cold cathodic sputtering.

Concerning the sample obtained by continuous process (COBR), the sample are analyzed thanks to the SEM Hitachi TM3000. The only sample preparation providing satisfying results consists in deposing a droplet of the obtained medium, that is too say a sample of VAM/PVAc particles in their aqueous phase on an appropriate stub. The different samples are then placed in a desiccator under ambient temperature during 24h. Unfortunately, the reactive mixture interacts with the carbon scotch and the, after metallization, the sample is not analyzable because of the scotch distortion. Consequently, the samples were not metalized despite the difficulties to evacuate the charge and the risk of obtaining a saturated picture.

V. CONTACT ANGLE MEASUREMENT

The contact angles are classically used to evaluate the wettability of various internals materials. In the case of liquid-liquid dispersion, three phases are in contact. A first interface is composed by the two liquid phases: the dispersed phase and the continuous phase containing the surfactant. The packing of the equipments represent the third phase. Depending on whether the packing is made of stainless steel or PTFE, it interacts differently and leads to different results for the liquid dispersion

To analyze the interaction, the contact angle is measured via the Krüss DSA100 by using the captive bubble method.

A piece of the packing is maintained in the aqueous phase and thanks to a curved needle, a droplet of organic phase (ie, toluene) is posed on the surface. The complementary part of the contact angle is then measured. The packing sample used presented the same story as the packing in the column. As for the interfacial tension, the contact angle measurement is based on the visualization. The needle external diameter is of 0.5 mm (Figure II- 19).

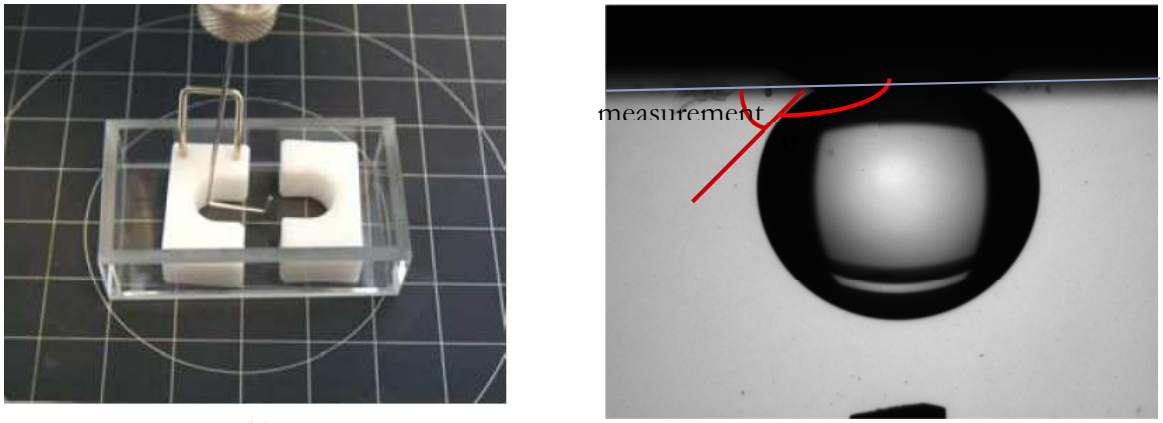

(a) *(b)*

Figure II- 19 : (a) experimental rig of the measurement method and (b) picture obtained by the CCD camera

Table II-4 reports the values of the different contact angles measured.

	PTFE	Stainless steel
Contact angle between solid/toluene droplet in aqueous phase (PVA+water) (°)	55.2	121.8
Contact angle between aqueous phase and solid in air (°)	92.1	43.5
Contact angle between solid/toluene droplet in aqueous phase (SDS+water) (°)	79.1	

Table II- 4 : contact angle measurement via the Krüss DSA100

It appears that the stainless steel surface is more hydrophilic than the PTFE packing. It seems that the PTFE is not preferentially wetted by the aqueous phase. The behavior of our stainless steel can be characterized as partially hydrophilic.
The contact angle measurement will be interesting to be considered in order to emphasize the packing effect on the liquid-liquid dispersion obtained.

VI. CONVERSION MEASUREMENT BY GRAVIMETRIC METHOD

As mentioned in chapter I, the manuscript will conclude with the realization of a suspension polymerization in a pulsed device. The conversion of polymerization has to be evaluated. The initial mass fraction of monomer is known. The sample is collected in a trial balloon. The solvent is evaporated under vacuum thanks to the rotavapor. Knowing the balloon weight before and after the evaporation process, the mass conversion can be deduced.

In conclusion, at the end of this chapter, the whole analytical aspects used during this work have been now presented. In the following chapters, the measurement method will be no longer detailed. The reader has to refer to the respective methods detailed in this chapter.

We have to focus now on the different steps of the polymerization process and first on the liquid-liquid dispersion step (chapter III and chapter IV), and further on the solid suspension step (chapters V and VI).

CHAPTER 3: LIQUID-LIQUID DISPERSION IN STATIC MIXERS

The liquid-liquid dispersion corresponds to the first step of the process (cf chapter I). Indeed, in suspension polymerization, the monomer is first dispersed into the aqueous phase. The granulometry of the final product is strongly affected by the initial droplet size. That is why it is important to accurately control this step and to know how to predict the mean droplet size depending on the operating parameters.

As discussed in the chapter I, this step can be performed in static mixers. They allow the creation of controlled liquid-liquid dispersion in a very fast way. This equipment can be part either of the classical batch process in order to improve it or to a continuous process in the future.

In the first part of this chapter, static mixers and its applications in turbulent liquid-liquid dispersions are presented. The study focuses on the physico-chemical parameters effect on the mean droplet size and droplet size distribution. In suspension polymerization it is important to work at high dispersed phase concentration to have a profitable process. Moreover the need to define a transient interfacial tension value to describe this fast process is highlighted through the comparison of four different systems involving two different surfactants. The results are presented in term of mean energy dissipation rate and the static mixer SMV is compared to the classical batch reactor and to other designs. To predict the mean droplet size, a correlation based on Middleman (1974) is proposed.

Finally, some tests performed at pilot scale at the Mazingarbe plant will be presented. These ones are feasibility tests concerning the direct liquid-liquid dispersion loading.

I. LITERATURE

This part briefly presents the concern of turbulent liquid-liquid dispersion and focuses on the current knowledge on static mixers.

I.1. ***Emulsification in turbulent flows***

Two opposite effects are responsible for the resulting mean droplet size and droplet size distribution during any emulsification process: breakage and coalescence mechanisms.

These different mechanisms are related to the local hydrodynamic conditions at the drop scale, to the physico-chemical parameters of the system and to the dispersed phase concentration.

Before a droplet of size d (m) is breaking, the normal and tangential stresses deform the droplet. The interfacial tension σ ($N.m^{-1}$) is responsible for the spherical shape of the droplet

and allows to withstand any external stress. The pressure difference at the interface is well known and called the Laplace pressure P_L defined by:

$$P_L = \frac{4\sigma}{d} \qquad \textbf{(III- 1)}$$

I.1.1. Break-up in turbulent flow field

In turbulent flow field, the inertial effects dominate over viscous effects. The droplet breakage is induced by the pressure fluctuations associated with the velocity fluctuation on the droplet surface. These velocity fluctuations occur at various length scales, and those responsible for break-up are expected to be in the same order as the droplet diameter (d).

The Kolmogorov-Hinze theory (1955, 1959 and Davies 1989) describes the energy cascade concept and is a universal model for droplet break-up in turbulent flow field. The energy contained in the large structures of the flow is transferred without dissipation to the smallest ones, called the dissipative scale. At this specific scale, the kinetic energy is dissipated by viscous effects into heat. This scale corresponds to the Kolmogorov length scale and is given by:

$$\lambda_k = \frac{\nu_c^{3/4}}{\varepsilon_m^{1/4}} \qquad \textbf{(III- 2)}$$

where υ_c is the kinematic viscosity of the continuous phase ($m^2.s^{-1}$) and ε_m the turbulent energy dissipation per mass unit ($W.kg^{-1}$).

In inertial flows, the mean fluctuation velocity u' (root mean square value) relative to eddies of size λ_K is related to the local energy dissipation rate per unit mass fluid ε_m via the relationship III-3, in the case of homogeneous and isotropic turbulence:

$$u' = K(\varepsilon_m \quad \lambda_K)^{1/3} \qquad \textbf{(III- 3)}$$

K is a constant of order unity (Walstra, 1993).

If a drop interacts with an eddy whose size is larger than the size of the drop, the drop is merely advected by the eddy. On the opposite, the eddies, whose length scales are either equal or smaller than the drop size d, are responsible for the drop deformation till break-up. According to this simple rule and applying the relationship (III- 3), it is expected that the turbulent fluctuations, responsible of drop break-up, will be characterized by the next turbulent velocity:

$$u' = K(\varepsilon_m \cdot d)^{1/3} \qquad \textbf{(III- 4)}$$

The size of the largest stable droplet is fixed by the energy balance between the turbulent energy which tends to deform and break the droplet and the interfacial energy which counteracts this deformation and tries to maintain the drop spherical. The ratio of both

energies allows to introduce the dimensionless droplet Weber number expressed in turbulent flow by:

$$We_d = \frac{\rho_c u'^2 d}{\sigma} \qquad \textbf{(III- 5)}$$

where ϱ_c is the continuous phase density (kg.m^{-3}) and d the droplet diameter and where u' is defined by (III- 4) so that:

$$We_d = \frac{\rho_c (\varepsilon d)^{2/3} d}{\sigma} = \frac{\rho_c (\varepsilon)^{2/3} d^{5/3}}{\sigma} \qquad \textbf{(III- 6)}$$

The maximum size of the droplet that does not break is classically called the maximum stable drop diameter, d_{max}. At this value corresponds a critical value of the Weber number, We_{dcrit}. By this way and according to (III-6) it is usual to estimate d_{max} as follows:

$$d_{\max} = (We_{dcrit})^{3/5} \left(\frac{\sigma}{\rho_c}\right)^{3/5} \varepsilon_m^{2/5} = K \left(\frac{\sigma}{\rho_c}\right)^{0.6} \varepsilon_m^{0.4} \qquad \textbf{(III- 7)}$$

In equation III-7, We_{dcrit} or K have to be experimentally determined. This kind of model was checked to predict the maximum droplet diameter over a wide range of emulsification processes: stirred tank, ultrasound emulsifiers and homogenizers (Lemenand *et al.* 2003).

Thanks to a dimensionless analysis on the energy dissipation per unit mass fluid, it has been established that in any stirred tank (Cutter, 1966; Coulaloglou and Tavlarides, 1977):

$$\varepsilon_m \approx N^3 D^2 \qquad \textbf{(III- 8)}$$

where N is the impeller rotation speed (rpm), and D the impeller diameter. Consequently, the corresponding Weber number may be defined by:

$$We = \frac{\rho_c (ND)^2 D}{\sigma} = \frac{\rho_c N^2 D^3}{\sigma} \qquad \textbf{(III- 9)}$$

(ND) represents the characteristic velocity at the tip of the impeller. Obviously, there is no confusion possible with the previous Weber number, We_d, relative to the droplet.

According to III-7 and accounting with III-8 and III-9, it is easy to establish the following correlation (Shinnar, 1961):

$$\frac{d_{\max}}{D} = K' We^{\,0.6} \qquad \textbf{(III- 10)}$$

Furthermore, this relationship has been extended to any turbulent flow provided that the appropriate Weber number has to be introduced according to the type of agitation involved.

In the previous relations, the viscosity is not taken into account. Davis (1985) assumes it can be neglected for low viscosity liquid but it can play a role for viscous fluid dispersion.

Models reported in literature preferably use the Sauter diameter (expression II-6 chapter II, see table III-2) instead of the maximum stable diameter of the droplet. These two characteristic diameters are experimentally related through a relation of proportionality, such

as d_{max} = K" d_{32}. This relationship has been found by many authors (for instance by Sprow, 1967), K" being of the order of 2.

I.1.2. Coalescence

In most of the dispersions, coalescence also occurs. In the case of dilute dispersions, this mechanism may be neglected. But in the other cases, it has to be taken into consideration, particularly in ours.

A detailed discussion of coalescence is given by Chesters (1991) or more recently by Liu and Li (1999) or Liao and Lucas (2010).

The probability of coalescence occurring is the product of the interdrop collision frequency and of the coalescence efficiency which is the probability that the drop will coalesce once the collision has occurred.

The frequency of drop colliding depends on the external flow field and on the size of the drops. Larger drops are expected more likely to collide. In a turbulent dispersion, drops are randomly moving around and colliding.

For a coalescence event to occur during a collision, the continuous film between the colliding droplets has to drain down to a critical thickness at which it spontaneously ruptures due to the growth of perturbation (Kumar *et al.*, 1993). The film drainage time depends on the interaction force F of the droplets' approach to each other, the degree of flattening of the interface (the film drains faster if the interface is unflattened) and the mobility of the interface (drainage is promoted in the case of mobile interface). Not every collision leads to a coalescence; the external flow brought the two droplets into contact but it can also move them away. The concept of coalescence efficiency arises from this statement.

Coalescence efficiency depends on many parameters. First, the dispersed phase viscosity. An increase of the drop viscosity leads to a decrease of the mobility of its interface. The film between two coalescing drops drains faster if the interface is mobile. An increase of the viscosity provides then a longer film drainage time and a greater chance for the two droplets being separated before the coalescence process is complete. Subsequently, an increase of the dispersed phase viscosity reduces the coalescence efficiency in turbulent systems (Kumar *et al.*, 1993). Secondly, coalescence efficiency depends also on the droplet size. Smaller droplets coalesce more easily. Indeed, there is less liquid to be drained from the intervening film during coalescence. In a particular flow regime, a particular droplet size d_{min} can be defined corresponding to the minimum stable droplet size above which droplets will not coalesce, in a similar way than d_{max} relative to the break-up mechanism. If the minimum stable droplet size d_{min} is inferior to the maximum stable droplet size d_{max}, there is theoretically

a range of drop sizes comprised between these two limits, which can be considered as insensitive either to coalescence or to breakage.

Finally, coalescence is very sensitive to the interfacial properties and to any disturbances (impurities, temperature or composition gradients leading to Marangoni effects …). Particularly, the presence of surfactants affects considerably the coalescence efficiency. In general, the surface active agents are located at the droplets interface that increases the steric repulsion between droplets. It also increases the strength of the liquid film trapped between the two droplets and then the time required for film drainage. Surfactants hinder the coalescence.

I.2. ***Generalities on static mixers***

Static mixers consist of a series of identical elements inserted in pipe, column or reactor. They redistribute the fluid in directions transverse to the main flow. The only energy cost depends on the power required for pumping. The main advantage arises from the fact that the larger the flowrate is, the better the mixing efficiency is. Generally, static mixers offer small space requirement, low equipment cost, short residence time and few maintenance constraints compared to other equipments. Even if they can be incorporated in pump-around loops in batch or semi batch processes, this kind of device is naturally well adapted for continuous processes.

There is a wide variety of static mixers which are optimized for specific applications. Different designs are proposed depending on the flow regime and the applications. In their review, Thakur *et al.* (2003) listed the principal commercial static mixer designs and their different industrial applications including mixing of miscible fluids, the thermal transfer and homogenization, and the interface generation between two immiscible phases.

In our case, we will focus on the use of SMV static mixers to perform turbulent liquid-liquid dispersion. The SMV^{TM} static mixer has been created in 1970 by the Sulzer Company. It consists of a stack of corrugated plate with a "V" shape. This design is preferentially devoted to gas-liquid and liquid-liquid dispersion, reaction or mixing and homogenization of gas or liquid of low viscosity. Curiously there is still a lack of available information about liquid-liquid dispersion in Sulzer SMV static mixer. The only authors who reported emulsification's experiments in this type of mixers are Streiff *et al.* (1977, 1997).

I.3. ***Emulsification in turbulent flow with static mixers***

I.3.1. Pressure drop

Static mixers produce sizeable pressure drops compared to those in empty pipe of same diameter. These ones are directly related to the design of the static mixer. They have to be determined with accuracy to equip the pilot with appropriate pumps.

The pressure drop generated by single-phase flow in static mixers has been widely studied and modeled. But it is not as well as documented concerning two-phase flows. In fact physical properties of such complex systems are not easily assessable, especially the viscosity and the interfacial properties. Numerous references can be found concerning the pressure drop generated by gas-liquid dispersions in static mixers: Shah and Kale (1991, 1992[a], 1992[b]), Chandra and Kale (1995) for the Kenics, Sulzer SMX and Komax static mixers, Streiff (1977) for Sulzer static mixers, Turunen (1994) for SMV static mixer, and Heyouni *et al.* (2002) for the Lightnin mixer. However liquid-liquid dispersions are not so much examined.

For liquid-liquid flows, "mixing" physical properties (density and viscosity) of the system must be defined. Legrand *et al.* (2001) have studied pressure drops in SMX static mixer by assuming the static mixer as a porous media. They use the "mixing" density as follows:

$$\rho_e = \phi\rho_d + (1-\phi)\rho_c \qquad \textbf{(III- 11)}$$

and choose a viscosity model (Taylor, 1932) to calculate an apparent viscosity.

$$\mu_e = \mu_c\left[1 + 2.5\phi\left(\frac{\mu_d + \frac{2}{5}\mu_c}{\mu_d + \mu_c}\right)\right] \qquad \textbf{(III- 12)}$$

Different dimensionless numbers can be encountered to represent the pressure drop generated by static mixers in the literature. Lemenand *et al.* (2005) who have investigated the HEV static mixer define a Z factor corresponding to the pressure drop ratio between the emulsion flow in static mixer (HEV) and a single phase flow in a simple duct:

$$Z = \frac{\Delta P_{\text{liq-liq,SM}}}{\Delta P_{\text{mono,EP}}} \qquad \textbf{(III- 13)}$$

where the $\Delta P_{\text{mono,EP}}$ value is calculated thanks to the Blasius correlation. This expression is valid for turbulent flow field in empty and circular pipe. The Z factor approach concern only Newtonian fluids. They obtained Z factors ranging from 2 to 8 for dispersed phase concentration ranging from 0 to 0.15 in volume, with a decreasing tendency when increasing the dispersed phase concentration.

In the same way as turbulent flow field in empty pipe, the pressure drop in static mixer can be calculated thanks to the Fanning friction factor f or the Newton number Ne only valid for Newtonian fluids (Shah and Kale, 1991, 1992[a], 1992[b]; Streiff *et al.*, 1999). This friction factor or Newton number is correlated to the Reynolds number. The pressure drop is expressed in terms of friction factor f taking into account the geometric parameters of the system, that is to say the porosity of the mixer ε and the hydraulic diameter of the static mixer D_h:

$$f_h = \frac{\Delta P \varepsilon^2}{2\rho V_0^2} \frac{D_h}{L} \qquad \textbf{(III- 14)}$$

In III-15, V_0 is the flow velocity. The ratio V_0/ε is generally called "interstitial velocity", and is used to characterise velocity in porous media. This friction factor is related to the hydraulic Reynolds number:

$$Re_h = \frac{\rho_e V_0 D_h}{\varepsilon \mu} \qquad \textbf{(III- 15)}$$

where the density is the equivalent density defined previously (i.e.III-11) and the viscosity μ is the continuous phase viscosity.

The use of these geometrical parameters allow to take into account the type of the mixer involved.

Bohnet *et al.* (1990) and Li *et al.* (1997) have proposed the correlation (III-16) to model the pressure drop. The -0.25 value of the Reynolds number exponent corresponds to the value found in the Blasius correlation established for turbulent flow in empty pipe (Bird *et al.*, 1924)

$$f = \frac{0.0791}{Re^{0.25}} \qquad \textbf{(III- 16)}$$

I.3.2. Liquid-liquid dispersion

In the literature, liquid-liquid dispersion in turbulent flows has been studied by many authors according to different static mixer designs. The designs mainly investigated are the Kenics mixer (Middleman, 1974; Berkman and Calabrese, 1988; Lemenand *et al.*, 2001, 2003, 2005 and Yamamoto *et al.*, 2007) and the SMX^{TM} Sulzer mixer (Streiff, 1977; Streiff *et al.*, 1997; Hirschberg *et al.,* 2009; Theron *et al.*, 2010; and Theron and Le Sauze, 2011). There are other designs but their use remains rare and they are less documented.

I.3.2.1. Study of different parameters affecting the mean droplet size

Several parameters have a key-role on the mean droplet size.

Three categories are distinguished:

- The physicochemical parameters: the continuous and dispersed phase densities, respectively ϱ_c and ϱ_d, the continuous and dispersed phase densities, respectively μ_c and μ_d, the interfacial tension σ and the dispersed phase hold-up, Φ
- The hydrodynamic parameters: the velocity of the flow V_0
- The geometric parameters: the mixer diameter D, the hydraulic diameter of the mixer D_h, the number of element n_e, the void fraction of the mixer ε, the type of mixer…

I.3.2.1.1. Physico-chemical parameters

Usually, the densities, viscosities and interfacial tension are imposed by the formulation step. Otherwise, the dispersed phase fraction can act on the mean droplet size. Indeed, it is profitable to work with concentrated system. However an increase in the dispersed phase concentration Φ can modify the rheology and subsequently the global behavior of the system. This part introduces the main physicochemical factors studied in literature.

Viscosity ratio

The viscosity ratio μ_d/μ_c tested by the different authors ranges from 0.6 (Middleman, 1974) to 204 (Berkman and Calabrese, 1988). The different authors show that the mean droplet size increases as the μ_d/μ_c ratio increases. Presumably, as already mentioned, it is due to the fact that an increasing droplet viscosity is not favorable to break-up.

Dispersed phase volume fraction Φ

Most of publications deal with dispersed phase concentrations lower than 25% (Middleman, 1974; Streiff, 1977; Matsumura *et al.*, 1981; Al Taweel and Walker, 1983; Berkman and Calabrese, 1988; Al Taweel and Chen, 1996; Streiff *et al.*, 1997; Legrand *et al.,* 2001; Lemenand *et al.*, 2001, 2003, 2005; Hirschberg *et al.*, 2009; and Theron *et al.*, 2010). The effect of the dispersed phase ratio is never clearly studied except by Yamamoto *et al.* (2007) who worked on water-in-oil emulsions and at dispersed phase volume fraction ranging from

2% to 74%, and did not pointed out any clear effect of the dispersed phase concentration on the resulting droplets size distribution.

Table III-1 summarizes the design and the corresponding dispersed phase fraction studied in literature.

Authors	Design	Φ (%)
Middleman (1974)	Kenics	0.5-1.0
Streiff (1977)	SMV	0.25
Matsumura et al. (1981)	Hi Mixer	20
Al Taweel and Walker (1983)	Lightin	1
Berkman and Calabrese (1988)	Kenics	<10
Al Taweel and Chen (1996)	Woven screen	1-4
Streiff et al. (1997)	SMX, SMXL, SMV	0.1
Legrand et al. (2001)	SMX	5-25
Lemenand et al. (2001, 2003, 2005)	HEV	2.5-15
Yamamoto et al.(2007)	NMJ, Kenics, RSM	2-74
Hirshberg et al. (2009)	SMX plus	5
Theron et al.(2010)	SMX	25

Table III- 1: Dispersed phase volume fraction range studied in different static mixers

Interfacial tension

Few results are available in literature concerning the effect of the interfacial tension. It is quite paradoxical because this parameter is often taken into account in correlations used to predict the mean droplet size evolution. Only Berkman and Calabrese (1988) underline that a decreasing of the interfacial tension value leads to a diminution of the mean droplet size. As expected, a lower interfacial tension enhances the emulsification process.

I.3.2.1.2. Geometrical parameters

Geometrical parameters are little studied in literature. However, the design of the static mixer is responsible for the mean droplet size obtained. Thus, an open design like the HEV static mixer provides larger drop than a multi layers design like the SMX static mixer. The different designs are described in the review of Thakur *et al.* (2003).

Not only the design, it seems also important to take into account the number of elements. Indeed, if an increase of the number of element n_e leads to a higher pressure drop, it is important to check if it affects also the mean droplet size. It allows to identify the number of elements required to ensure a given droplet size. Theron (2010) shows that after ten elements (n_e=10), the mean droplet size does not significantly decrease.

Finally to compare the different designs, it is interesting to express the different correlations by taking into account the hydraulic diameter D_h of the static mixer as well as its porosity.

I.3.2.2. Correlation to predict the mean droplet size in static mixer

If there are many correlations in the literature that predict mean diameters resulting from emulsification in static mixers, only few of them have been established for the SMV mixer (cf. Table III-2).

Most of these correlations are based on Kolmogorov's theory of turbulence. The prediction of the Sauter diameter obtained in Kenics mixers was first proposed by Middleman (1974):

$$\frac{d_{32}}{D} = K\ We^{-0.6}\ f^{-0.4} \qquad \textbf{(III- 17)}$$

where We is the Weber number defined as follows:

$$We = \frac{\rho\ V_0\ D}{\sigma} \qquad \textbf{(III- 18)}$$

Assuming a Blasius-like dependency of the friction factor towards the Reynolds number (i.e. part I.3.1), equation (III-19) can be expressed in terms of Weber and Reynolds numbers:

$$\frac{d_{32}}{D} = K\ We^{-0.6}\ Re^{0.1} \qquad \textbf{(III- 19)}$$

After Middleman (1974), many authors proposed correlations based on the Kolmogorov's turbulence theory to predict mean diameters.

Authors	Static mixer	Characteristic diameter	Correlation	Flow regime
Middleman (1974)	Kenics	D	$\frac{d_{32}}{D} = KWe^{-0.6}Re^{0.1}$	Turbulent
Streiff (1977)	SMV	D_h	$\frac{d_{32}}{D_h} = 0.21We_h^{-0.5}Re_h^{0.15}$	Transient, turbulent
Chen and Libby	Kenics	D	$\frac{d_{32}}{D} = 1.14\,We^{-0.75}\left(\frac{\mu_d}{\mu_c}\right)^{0.18}$	Turbulent
Matsumura et *al.*	Hi-mixer	D	$\frac{d_{32}}{D} = KWe_c^{-n}$ $n = 0{,}56 - 0{,}67$	Turbulent
Al Taweel and Walker	Lightnin	D_h	$\frac{d_{32}}{D_h} = K\,We^{-0.6}f^{-0.4}$	Turbulent
Haas (1987)	Kenics	D	$\frac{d_{43}}{D} = 1.2We^{-0.65}Re^{-0.2}\left(\frac{\mu_d}{\mu_c}\right)^{0.5}$	Laminar
Berkman and Calabrese	Kenics	D	$\frac{d_{32}}{D} = 0.49We^{-0.6}\left(1+1.38Vi\left(\frac{d_{32}}{D}\right)^{0.33}\right)^{0.6}$	Turbulent
Al Taweel and Chen (1996)	Woven screen		$d_{32} = 0.682\left(We_{jet}^{-0.859}\varphi^{0.875}\right)\left(\frac{b}{M}\right)^{0.833}$	Turbulent
Streiff *et al.* (1997)	SMV, SMX,		$d = C_n(1+K\varphi)\left(\frac{(1+BVi)We_c}{2}\right)^{0.6}\left(\frac{\sigma}{\rho_c}\right)^{0.6}\left(\frac{\rho_c}{\rho_d}\right)^{0.1}\varepsilon^{-0.4}$	Turbulent
Legrand *et al.*	SMX	d_p	$\frac{d_{32}}{d_p} = 0.29We_p^{-0.2}Re_p^{-0.16}$	Laminar, transient
Lemenand *et al.* (2001,	HEV	D	$\frac{d_{32}}{D} = 0.57We^{-0.6}$	Turbulent
Das *et al.* (2005)	SMX	d_p	$\frac{d_{max}}{d_p} = CWe_p^{-0.33}$	Laminar, transient
Rama Rao *et al.* (2007)	SMX	D	$\frac{d_{43}}{D} = K\left(1.5\varphi\left(1+\frac{\mu_d}{\mu_c}\right)\right)^{0.5}$	Laminar
Hirschberg *et al.* (2009)	SMX plus		$d = C_n(1+K\varphi)\left(\frac{(1+BVi)We_c}{2}\right)^{0.6}\left(\frac{\sigma}{\rho_c}\right)^{0.6}\left(\frac{\rho_c}{\rho_d}\right)^{0.1}\varepsilon^{-0.4}$	Turbulent

Table III- 2: Models found in the literature to correlate the mean droplet diameter to different parameters (hydrodynamic, physical and dimensionless parameters). D is the pipe diameter, d_p the pore diameter and d_h the hydraulic diameter

Correlations recapitulated in Table III-2 show that the Weber number is the main parameter involved in the break-up phenomenon in static mixers. Some authors (Chen and Libby, 1978; Haas, 1987; Streiff, 1997; Rama Rao *et al.*, 2007; and Hirschberg *et al.*, 2009) also reported the influence of some physico-chemical parameters, such as densities or viscosities ratio.

If most of correlations enable to predict d_{32} values, some authors established expressions to estimate d_{43} (II-8) or d_{max} values. For liquid-liquid dispersions, the d_{32} values are preferred as they are easier to determine experimentally and they are usually employed for example for mass transfer issues. In fact it is possible from d_{32} values to calculate the interfacial area A ($m^2.m^{-3}$) developed by the dispersed phase as follows:

$$d_{32} = \frac{6\phi}{A} \qquad \textbf{(III- 20)}$$

II. LAB SCALE EXPERIMENT

These tests are carried out at lab scale with SMV static mixer. It leads to identify the conditions required to create a dispersion of a controlled mean droplet size ranging from 30 to 50 μm. A correlation to predict the mean droplet size is established.

II.1. ***Material and method***

II.1.1. Fluids

The fluids used are the model ones presented in chapter II (section I-1-1). The characteristics have been already presented in the Table II-1 in Chapter II.

II.1.2. Experimental rig

II.1.2.1. Design presentation

The Figure III-1 shows pictures of one Sulzer SMV element. Each element is made of 5 corrugated plates. The diameter D and height H of each element is about 10 mm, which results in an aspect ratio H/D ≈ 1. Table III-3 notices the different geometrical characteristics of a SMV element. The porosity ε is defined thanks to expression III-21:

$$\varepsilon = \frac{V_{free\ for\ liquid\ \ flow}}{V_{apparent\ of\ the\ mixer}} \qquad \textbf{(III- 21)}$$

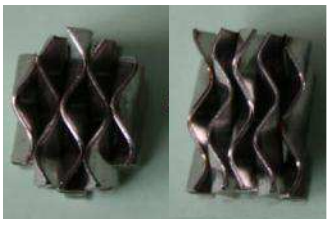

Figure III- 1: Picture of one SMV static mixer element used

Characteristics	
Material	Stainless steel 1.4404
Fabrication mode	Pressed/welded
Diameter D mm	9.45
Height H mm	9.97
Bar width mm	0.14
D_h mm	3.5
ε	0.83

Table III- 3: Static mixer characteristics (D_h hydraulic diameter, ε the porosity)

II.1.2.2. Experimental rig presentation

The schematic diagram presented in Figure III-2 illustrates the experimental rig used for emulsification experiments. It includes two feed tanks of 30L for the two phases involved in each system. The continuous phase feed tank is equipped with a mechanical stirrer in order to dissolve the surfactant in water and to homogenize the aqueous phase. Both phases are conveyed to the mixer thanks to gear pumps. Their characteristics are detailed in Table III-4. The two phases enter the vertical stainless steel pipe containing the mixers through coaxial tubes (Figure III-3). The dimensions are given in Table III-5. The mixer is made of 10 elements packed in the vertical steel pipe with a 90° angle between each element.

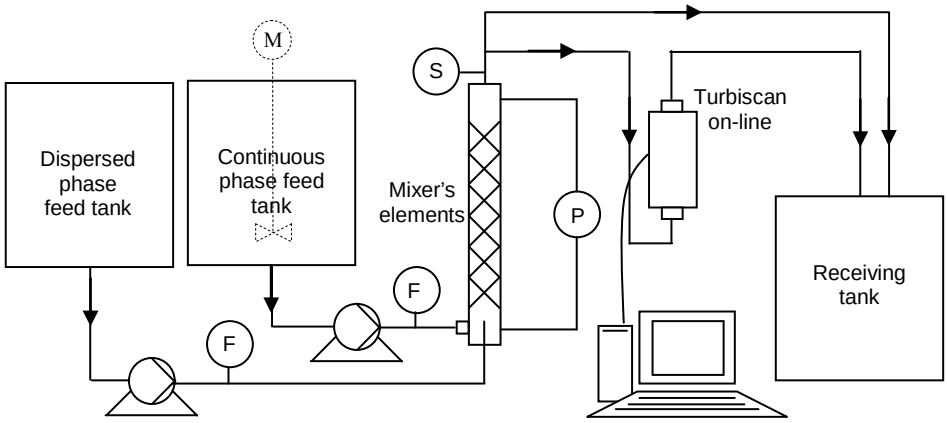

Figure III- 2 : Schematic diagram of the experimental rig: F: flowmeter; P: differential pressure sensor; S: Sampling valve

Pump	Technical characteristics
Aqueous phase pump	Gear pump Verder scale : 80 – 800 $L.h^{-1}$
Dispersed phase pump	Geat pump Verder scale : 40 – 400 $L.h^{-1}$

Table III- 4: Pumps characteristics

Main Tube	
D_{int}	10 mm
D_{ext}	12 mm
L	220 mm
Secondary Tube	
D_{int}	4 mm
D_{ext}	6 mm

Table III- 5: geometrical characteristic of the feeding tubes

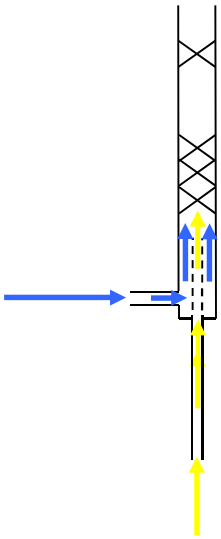

Figure III- 3: schematic representation of the fluid flow distribution in the tube packed with SMV static mixers

The continuous phase is introduced perpendicularly compared to the total flow direction in the coaxial tube.

All experiments are carried out at room temperature, i.e. between 20 and 23°C.

The pressure drop generated by the flow through the mixer is measured with a differential pressure sensor (Rosemount 0-10 bar). The measurement cells of the On-Line Turbiscan (Chapter II) is located downstream the static mixer. A sampling valve is also located at the mixers outlet to characterize the dispersion off-line.

The dispersed phase concentration in volume Φ is fixed thanks to respective phases flowrates as follows:

$$\phi = \frac{Q_d}{Q_d + Q_c} = \frac{Q_d}{Q_{tot}} \qquad \textbf{(III- 22)}$$

where Q_d, Q_c and Q_{tot} are respectively the dispersed phase, the continuous phase and the total volumic flowrates.

II.1.3. Liquid-liquid dispersion analysis

The different techniques are detailed chapter II (section III). The Mastersizer 2000 raises the issue of the analysis representativeness and of the sampling issue. Moreover, the obtained dispersions are highly concentrated and dilution is required to have an opalescent dispersion. The liquid-liquid dispersion is then diluted in the corresponding continuous phase in order to not disturb the physico-chemical conditions of the system. The Mastersizer 2000 provides more information about the distribution characteristics such as the whole different characteristic diameters and the distribution width, whereas the On-line Turbiscan only provides the d_{32} value. They both give d_{32} values, which enables to compare themselves.

The microscopic observation of the emulsion and the comparison between the on-line Turbiscan results and the classical Mastersizer method provide some confidence in the results obtained.

II.1.3.1. Reproducibility studies

The four tested Water/Surfactant/Oil systems exhibit a creaming phenomenon. Indeed the samples collected are composed of two phases: aqueous phase at the bottom and a white opaque phase, the liquid-liquid dispersion. This phenomenon starts only few minutes after emulsification. If creaming is a reversible phenomenon, it may also be followed by some irreversible behavior such as coalescence (Tadros and Vincent, 1983) or Ostwald ripening (Kalbanov *et al.*, 1990; Yarranton and Masliyah, 1997).

According to the procedure defined for the Mastersizer 2000 diffraction analysis (i.e. chapter II-section III), an average of the different measurements of the same sample corresponds to an analysis results (5 measurements according to the volume and the dilution

rate of the sampling). 4 shows the droplet size distributions obtained for a sequence of analysis of 5 measurements. Table III-6 gives the mean Sauter diameter d_{32} corresponding to these measurements. A good reproducibility is observed for the droplet size distribution as well as for the mean Sauter diameter.

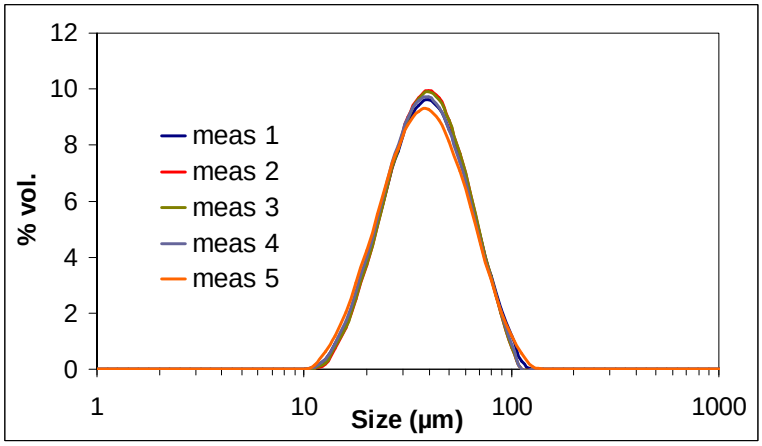

Figure III- 4 : Sequence of 5 consecutive measurements for the analysis of a sample corresponding to S_3, Q_{tot}=450 L.h^{-1} and Φ=0.40

Measurement	Meas 1	Meas 2	Meas 3	Meas 4	Meas 5
d_{32} (µm)	38.2	37.5	37.4	36.7	36.1

Table III- 6 : Mean Sauter diameter d_{32} corresponding to the five measurements of Figure III-4

II.1.3.2. Characterization of the liquid-liquid dispersion obtained

Figure III- 5 is an optical microscopy picture of an emulsion sample obtained during an experiment involving the Water / PVA / Toluene system (S_3). Droplets are well spherical and the diameters measured on the picture range from 10 to 120 µm.

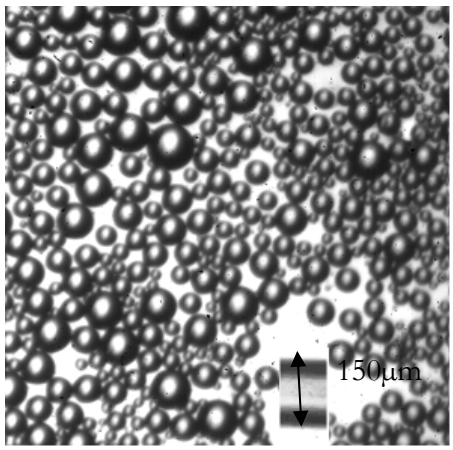

Figure III- 5: Visualization of droplets with the Nikon camera for the experiment carried out with the Water/PVA/Toluene system (S_3) at Q_{tot} = 300 L.h^{-1} and Φ = 0.50, $d_{32,\ Malvern}$ = 59.0 µm

Every laser diffraction analysis for the whole systems lead to similar droplet size distribution as the distribution presented in Figure III-4, which is monomodal in log-normal representation. Distributions are characterized through the mean diameters d_{32} (chapter II, II-6) and through the span which quantifies the width of the distribution (chapter II, II-7).
For all the experimental results, the mean Sauter diameter corresponds to the average on the d_{32} obtained after a sequence except the first measurement. The error bars are determined by taking the maximum and minimum value of the mean d_{32}.
The same procedure is applied to determine the mean value of the whole characteristic diameters and of the mean droplet size distribution.

Figure III- 6 compares d_{32} obtained with both analysis techniques for a total flowrate of 400 Lh^{-1} and a dispersed phase concentration of 0.25 for all systems studied. The two different d_{32} values are in quite good agreement for each system. In fact the discrepancy between both values ranges from 3 to 15% whatever the system. The d_{32} obtained from the On-line Turbiscan is either slightly higher or lower than the d_{32} obtained by the off-line technique. Consequently, no special tendency can be highlighted.

Thus the use of the On-line Turbiscan allows to validate results obtained with the Mastersizer 2000 after sampling, dilution and latency time before analysis.

Both techniques are also compared for the Water/PVA/Toluene system at 400L.h^{-1} and three different dispersed phase concentrations (Figure III- 7). Once again the values are in the same range with a discrepancy ranging from 5 to 15%.

Whatever the system and the dispersed phase concentration Φ, the d_{32} calculated thanks to the On-line Turbiscan measurement are in good agreement with the values obtained from the laser diffraction technique. The main advantage of the Turbiscan is the ability to

work directly on-line with high concentrated systems. The maximum dispersed phase ratio depends on the studied system and generally cannot exceed 0.70 (above this value, phase inversion is expected).

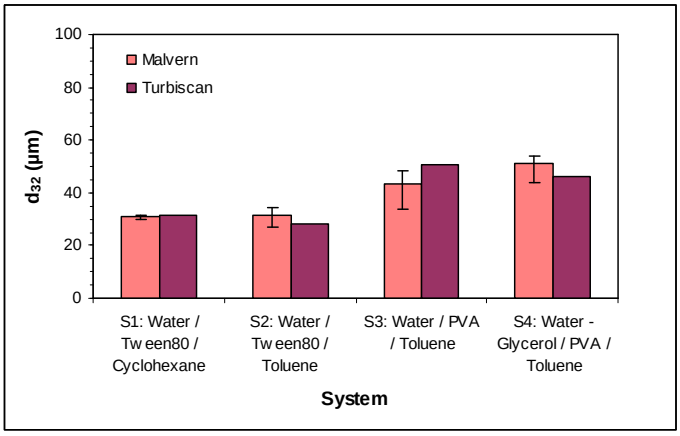

Figure III- 6: Comparison between d_{32} obtained with both Malvern and On-line Turbiscan for the four systems with Q_{tot} = 400 L.h^{-1} and Φ = 0.25

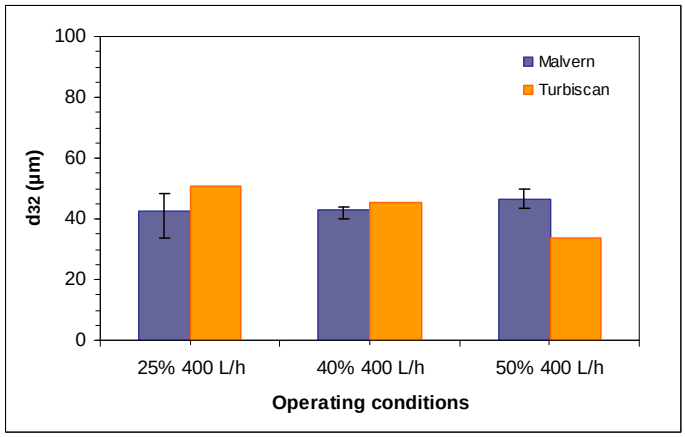

Figure III- 7 : Comparison between d_{32} obtained with both Malvern and On-line Turbiscan for the Water/PVA/Toluene system (S_3) for Q_{tot}=400L.h^{-1} and different dispersed phase concentration Φ

II.1.3.3. Stability of the emulsion

Figure III- 8 illustrates the comparison between droplet size distributions obtained through laser diffraction analysis several minutes after the beginning of the experiment and after nearly 24 hours for the Water/Tween80/Cyclohexane system (S_1) at Φ = 0.25 and the Water/PVA/Toluene system (S_3) at Φ = 0.50. These distributions are almost superimposed, what reveals that whatever the dispersed phase concentration no irreversible phenomenon occurs until Φ = 0.50. The same results are obtained for the two other systems at Φ = 0.25. As a conclusion the four systems investigated here are quite stable during at least 24 hours.

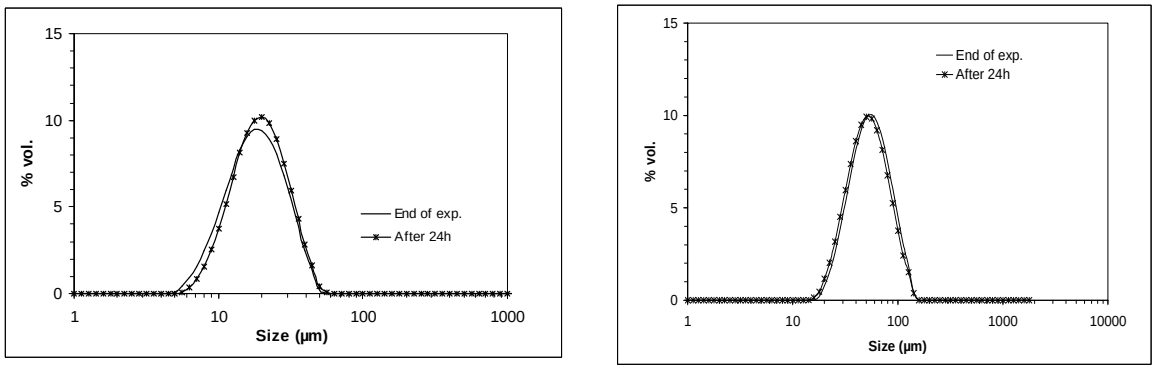

(a) (b)

Figure III- 8 : Comparison between droplets distributions obtained for the experiment carried out with a) the Water/Tween80/Cyclohexane system (S_1) at Q_{tot} = 500 L.h^{-1} and Φ = 0.25 and with b) the Water/PVA/Toluene system (S_3) at Q_{tot} = 450 L.h^{-1} and Φ = 0.50 just after the experiment and about 24 hours after the experiment

II.1.3.4. Process reproducibility

To ensure the repeatability of the obtained emulsion thanks to static mixer, some experiments are carried out at least twice.

Some results are summarized in Table III-7.

System	Operating conditions	$d_{32,1}$ (µm)	$d_{32,2}$ (µm)	Discrepancy (%)
S_1 : Water / Tween 80 / Cyclohexane	Q_{tot}=402 L.h^{-1}, Φ=0.25	30	30.9	2.9
S_3 : Water / PVA / Toluene	Q_{tot}=448 L.h^{-1}, Φ=0.25	38.3	38	0.8
	Q_{tot}=550 L.h^{-1}, Φ=0.40	36.8	35.7	3
	Q_{tot}=400 L.h^{-1}, Φ=0.50	46.5	50.8	8.5
S_4: Water-Glycerol 25%m. / PVA / Toluene	Q_{tot}=300 L.h^{-1}, Φ=0.25	65.6	72.1	9

Table III- 7 : Measurement reproducibility under some operating conditions

The results are in quite good agreement. Nevertheless we can notice that higher discrepancies are obtained at lower flowrate (300 L.h^{-1}) but also at higher dispersed phase concentration. The discrepancies are in a reasonable range.

II.2. ***Effect of the different parameters***

This part presents all the experimental study performed in static mixer. The results are obtained in term of granulometry characterization. The reliability of our results has been previously demonstrated in section II.

The liquid-liquid flow is characterized in term of pressure drop and a modeling of the two-phase flow pressure drop is presented.

The effects of the different studied parameters (hydrodynamic and physicochemical parameters) are then highlighted.

II.2.1. The operating conditions

We remind that in suspension polymerization, the monomer concentration ranges from 0.10 to 0.50 (Zerfa and Brooks, 1996a and 1996b ; Hashim and Brooks, 2002 and 2004). Some studies performed with vinyl chloride/PVA/water systems demonstrate the effect of the dispersed phase concentration on the liquid-liquid dispersion characteristic (Zerfa and Brooks (1996)). All the current studies refer to stirred tanks. In stirred tank reactor, the dispersed phase concentration affects the mean droplet size: it damps down the overall level of turbulence and then results in the production of larger droplet size. This parameter is a major parameter for our study and few studies refer to its effect in static mixer.

Consequently, in this section, the studied parameters are:

- An hydraulic parameter: the total flowrate in the mixer Q_{tot}, which is responsible for the breakage in static mixer and represents the lone energy cost
- The physico-chemical parameters: the density and viscosity ratio, the nature of the surfactant and the dispersed phase volume fraction Φ.

The tested operating conditions and the residence time ranges in the static mixer t_R are reported in Table III- 8. The residence time t_R is calculated thanks to the following equation:

$$t_R = \frac{V_{\text{free for liquid flow}}}{Q_{tot}} = \frac{\varepsilon\, V_{\text{apparent of the mixer}}}{Q_{tot}} \qquad \textbf{(III- 23)}$$

The residence time is calculated taking into account the free volume offered by the mixer to the flow, i.e. the void fraction of the mixer (ε = 0.83).

System	Dispersed phase concentration Φ	Total flowrate Q_{tot} ($L.h^{-1}$)	Residence time (s)
S_1: Water / Tween 80 / Cyclohexane	0.25	274-550	0.04 – 0.08
S_2: Water / Tween 80 / Toluene	0.25	274-552	0.05 – 0.08
S_3: Water / PVA / Toluene	0.10	273-553	0.04 – 0.08
	0.25	197-552	0.04 – 0.11
	0.40	202-550	0.04 – 0.10
	0.50	203-399	0.05 – 0.10
	0.60	278-452	0.04 – 0.08
S_4: Water-Glycerol 25%m. / PVA / Toluene	0.25	274-553	0.04 – 0.08

Table III- 8: Investigated operating conditions

The effect of the dispersed phase concentration Φ on droplets size is studied in the range of 0.10 to 0.60 in volume for the Water/PVA/Toluene system (S_3), our model system.

The four systems are compared each other at a fixed dispersed phase concentration Φ equal to 0.25 in volume. The systems (S_1) and (S_2), and the systems (S_3) and (S_4) respectively enable to evaluate the influence of the dispersed phase density and viscosity either by changing the dispersed phase species or by modifying the continuous phase physical properties. From the obtained results with the systems (S_2) and (S_3), the effect of the surfactant can be highlighted.

II.2.2. Pressure drop generated by the liquid-liquid dispersion

The two calculation methods described part I.3.1 are presented in this section.

First, the pressure drop generated by the liquid-liquid flow in the SMV mixer used in our experiment $\Delta P_{liq\text{-}liq,SM}$ is compared to the pressure drop generated in single phase flow by the continuous phase in an empty pipe $\Delta P_{mono,EP}$ through the Z factor

The Z values obtained respectively for the system S_3 at different Φ values and for the four systems at Φ = 0.25 are recapitulated in Table III- 9 and Table III- 10. The values are much higher than the values reported by Lemenand *et al.* (2005) (Z from 2 to 8). This may be due to the more open design of the HEV mixer.

Φ	0.10	0.20	0.25	0.40	0.50	0.60
Z	122	120	118	117	113	132

Table III- 9: Estimation of the Z factor for S_3

System	S1 : Water / Tween 80 /	S2 : Water / Tween 80 /	S3 : Water / PVA / Toluene	S4: Water-Glycerol 25%m. / PVA /
Z	107	115	118	132

Table III- 10 : Estimation of the Z factor for the four system at Φ = 0.25

Figure III- 9 illustrates respectively the variation of the hydraulic Fanning friction factor f_h (III-14) with the hydraulic Reynolds number Re_h (III-15) in the case of the Water/PVA/Toluene system (S_3) with different dispersed phase ratio and for the four systems at Φ=0.25.

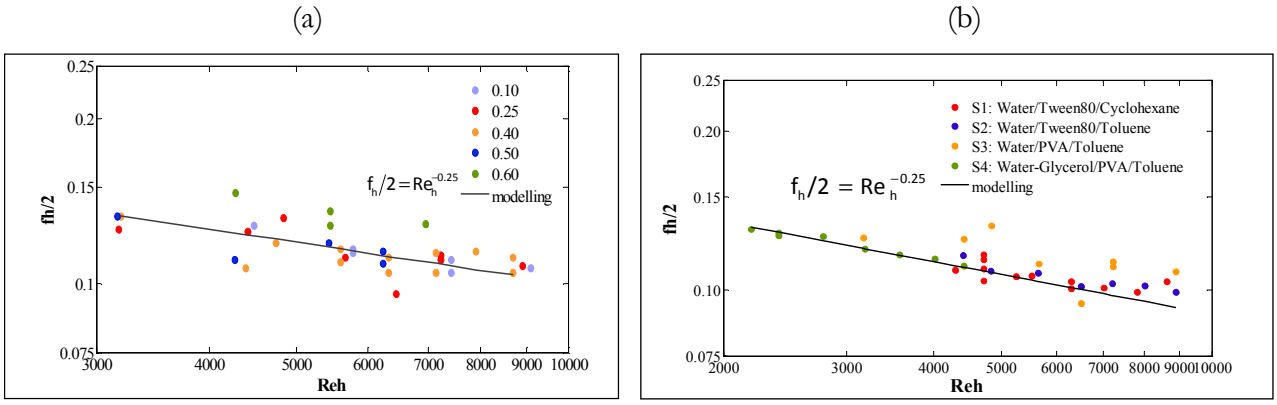

Figure III- 9 : Correlation of experimental results for(a) the Water/PVA/Toluene system (S_3) at different dispersed phase concentration Φ in volume and (b) the four systems tested at Φ = 0.25

The Fanning friction factors f_h is well represented towards the hydraulic Reynolds number by a power law except at Φ=0.60. The obtained result is similar to the result exhibited in single phase flow by Bohnet *et al.* (1990) and Li *et al.* (1997). The -0.25 value of the Reynolds number exponent corresponds to the value found in the Blasius correlation established for turbulent flow in empty pipe.

This result indicates that the obtained emulsions apparent viscosity can fairly be represented by the continuous phase one, even if the rheological behaviors of the systems investigated are more complex.

II.2.3. Effect of the total flowrate

Figure III-10 represents the droplet size distributions obtained for different total flowrate for the system S_3 at a dispersed phase fraction of 40% in volume. It shows that smaller drops are obtained at higher flowrates, since the turbulent energy is higher and enhances the breakage mechanism.

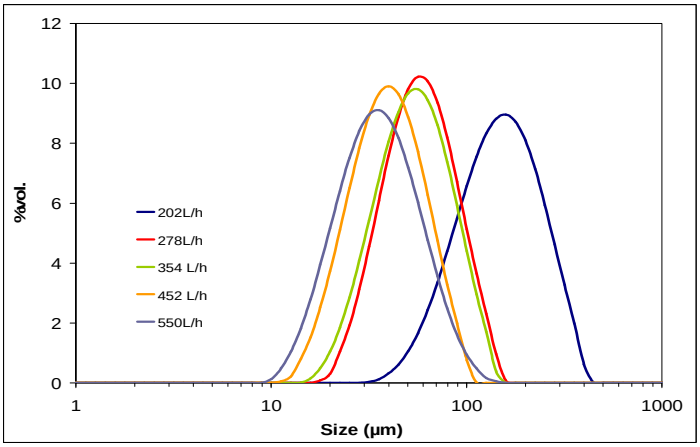

Figure III- 10: Evolution of the droplet size distribution with the total flowrate at a dispersed phase concentration Φ=0.40 for the Water/PVA/Toluene system (S_3)

II.2.4. Effect of the dispersed phase concentration

II.2.4.1. On the pressure drop

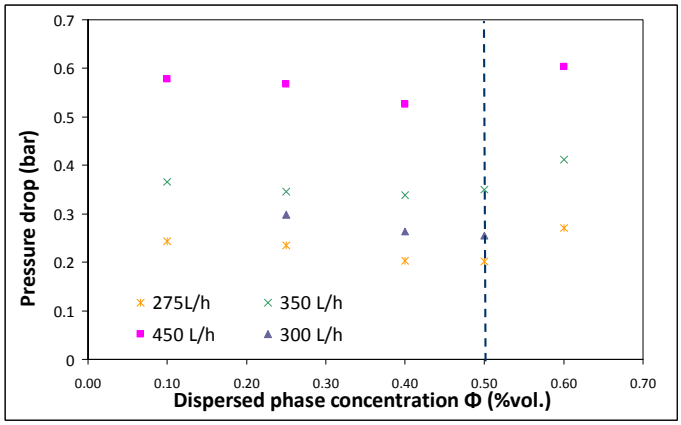

Figure III-11 Evolution of the pressure drop with the dispersed phase concentration Φ at different flowrates for the Water/PVA/Toluene system (S_3)

Figure III-11 represents the evolution of the pressure drop versus the dispersed phase concentration for the Water/PVA/Toluene system (S_3) at four different flowrates. Whatever the flowrate, the pressure drop exhibits the same behavior: it decreases from Φ = 0.10 to Φ = 0.50 and raises suddenly at a concentration close to 0.50-0.60. Moreover, the observation of the sampling after creaming allows the identification of three phases for the emulsion obtained at 0.60: some aqueous phase at the bottom, some emulsion in the middle and some toluene at the top. Thus we assume that the obtained system is not the expected oil-in-water emulsion and tends to be more complex, like perhaps multiple emulsions.

The pressure drop increase between Φ = 0.50 and Φ = 0.60 may thus be due to a phase inversion phenomenon. The same pressure drop evolution has already been reported in the literature in empty pipe for two phases flow without surfactant (Ioannou *et al.*, 2005; and De *et al.*, 2009). The authors studied the phase inversion phenomenon by acting on the dispersed phase ratio at constant flowrate. In the same way as observed here, the pressure drop decreases slightly when increasing the oil fraction (Φ = 0.20-0.50), and then increases significantly over a small range of dispersed phase concentration (Φ = 0.50-0.65). This sudden increase of the pressure drop appears just before the phase inversion phenomenon. Then the pressure drop decreases suddenly when the phase inversion phenomenon occurs. Finally the pressure drop increases gradually up to the single phase oil value.

Phase inversion in static mixers has been studied by Tidhar *et al.* (1986) in stainless steel or Teflon SMV mixers, made of four elements. They worked with water/kerosene, water/carbon tetrachloride (CCl_4) and water/kerosene+ CCl_4 systems, without surfactant. They noticed that whatever the mixer material, phase inversion at high flowrate occurs around Φ = 0.50.

According to our observations and literature comparisons, it can be assumed that at Φ = 0.60, the phase inversion point is almost reached. However, if we have a look on the configuration of the inlet tubes, with an increase of the dispersed phase flowrate, the velocity in the internal tube of 4mm increases a lot. In Table III-11, an example is provided for a total flowrate of 400 $L.h^{-1}$. The ratio of the dispersed to continuous phase velocity ranges from 0.11 to 1.5 in the feeding section of the static mixer (i.e. Figure III- 3). Given this high dispersed phase velocity, a jet effect occurs probably in the mixer, avoiding the emulsification to be properly performed. It may be the reason why at Φ = 0.60 a system of three phases has been obtained.

Φ (vol.)	V_d ($m.s^{-1}$)	V_c ($m.s^{-1}$)	V_d/V_c
0.10	0.88	7.96	0.11
0.60	5.3	3.54	1.5

Table III- 11: Velocity of continuous and dispersed phase in the inlet tubes for different dispersed phase concentration at a flowrate Q_{tot}=400 $L.h^{-1}$

II.2.4.2. On the droplet size distribution

Droplets size distributions obtained at different dispersed phase concentrations, for two flowrates, are presented in Figure III- 12. Table III-12 and Table III-13 give the d_{32} and the span values characterizing these distributions for the system (S_3).

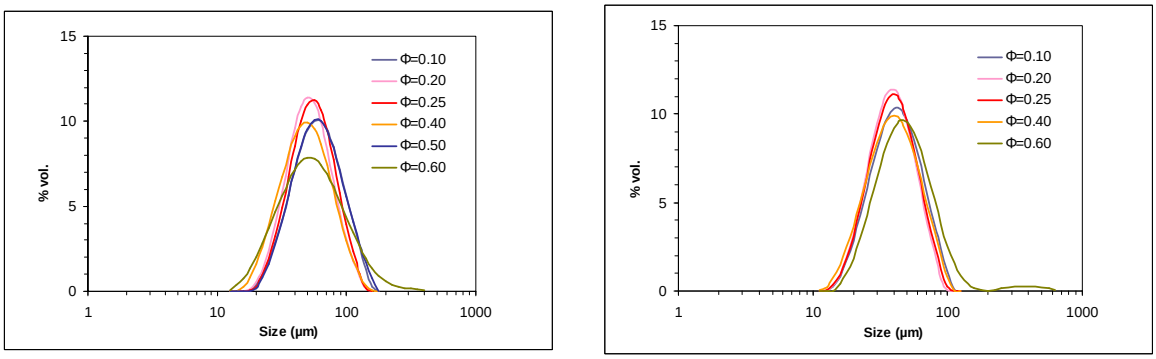

(a) (b)

Figure III- 12: Comparison between droplets size distributions obtained with different dispersed phase concentration Φ for the Water/PVA/Toluene (S_3) system for (a) Q_{tot}=350L.h^{-1} (see Table III-12) and (b) Q_{tot}=450L.h^{-1} (see Table III-13)

Φ	0.10	0.20	0.25	0.40	0.50	0.60
d_{32} µm	61.8	52.3	54.4	46.7	59.6	55.5
span	1.1	1.2	1.1	1.2	1.2	1.9

Table III- 12: d_{32} and span obtained for the different dispersed phase ratio for the Water/PVA/Toluene system (S_3) for Q_{tot}=350 L.h^{-1}

Φ	0.10	0.20	0.25	0.40	0.60
d_{32} µm	38.9	37.1	38.3	37.12	40.1
span	1.1	1.1	1.2	1.2	2.1

Table III- 13: d_{32} and span obtained for the different dispersed phase ratio for the Water/PVA/Toluene system (S_3) for Q_{tot}=450 L.h^{-1}

The droplet size distributions are totally superimposed whatever the dispersed phase ratio, except for Φ = 0.60. The same result is obtained whatever the total flowrate Q_{tot}. For given operating conditions, the d_{32} are in the same range whatever Φ (cf. Table III-12 and Table III-13). Only the span exhibits a significant increase at Φ = 0.60. The dispersed phase concentration seems thus to have a little influence on the distribution obtained, except at a 0.60 dispersed phase ratio. It is interesting to notice that the droplet size distribution change tendency is observed for Φ equal to 0.60, as well as the pressure drop increase described in part II.2.4.1. These results are totally different from the results generally observed in stirred tank, in which the increasing dispersed phase volume fraction leads to larger droplet size (Desnoyer *et al.*, 2003; Angle *et al.*, 2006; Angle and Hamza, 2006), even in presence of surfactants.

It seems that no coalescence occurs and that liquid-liquid dispersion in static mixers is only controlled by the breakage mechanism. In order to justify this hypothesis, we have tried to

compare the characteristic times of the process, i.e. the residence time and the coalescence time. The calculation details are provided in Chapter IV and in ANNEX 1 Table III- 14 summarizes the different ranges of the characteristic times and of the coalescence efficiency for each system.

System	Residence time (s)	Characteristic time t_{ch} (s)	Contact time $t_{contact}$(s)	Drainage time $t_{drainage}$ (s)	$\frac{t_{drainage}}{t_{contact}}$	P
S_1: Water/Tween80/ Cyclohexane	0.04-0.08	$1.8.10^{-4}$ - 3.10^{-4}	$4.9.10^{-5}$ - $2.3.10^{-4}$	$1.2.10^{-3}$ - $2.2.10^{-3}$	9.7 - 23.9	$4.3.10^{-11}$ - $6.2.10^{-5}$
S_2: Water/Tween80/ Toluene	0.04-0.08	$1.7.10^{-4}$ - $3.2.10^{-4}$	5.10^{-5} - $2.1.10^{-4}$	$1.2.10^{-3}$ - $2.3.10^{-3}$	11.2 - 23.8	$4.5.10^{-11}$ - $1.4.10^{-5}$
S_3: Water/PVA/ Toluene	0.04-0.11	$1.1.10^{-4}$ - $3.1.10^{-4}$	$7.5.10^{-5}$ - $5.1.10^{-4}$	$8.0.10^{-4}$ - $2.5.10^{-3}$	4.9 - 10.6	$2.4.10^{-5}$ - $7.9.10^{-3}$
S_4: Water-Glycerol (25%m.)/PVA/ Toluene	0.04-0.08	$9.6\text{-}10^{-5}$ - $2.2.10^{-4}$	8.10^{-5} - $2.5.10^{-4}$	$6.9.10^{-4}$ - $1.7.10^{-3}$	6.1 – 8.6	$4.5.10^{-11}$ - $1.4.10^{-5}$

Table III- 14: Comparison of different characteristic time of the liquid-liquid dispersion

The drainage time is always higher than the contact time. Consequently, the coalescence probability is very low.

The dispersed phase concentration seems to have no influence as long as the oil phase is totally dispersed as droplets in the continuous phase.

II.2.5. Effect of the density and viscosity ratios and of the surfactant

Figure III- 13 illustrates the influence of surfactant, viscosity and density ratios through the four different investigated systems on droplets size distributions obtained at similar dispersed concentration (Φ = 0.25) and total flowrate (Q_{tot} = 300 $L.h^{-1}$). Sauter mean diameters as well as span characterizing these distributions are recapitulated in Table III- 15.

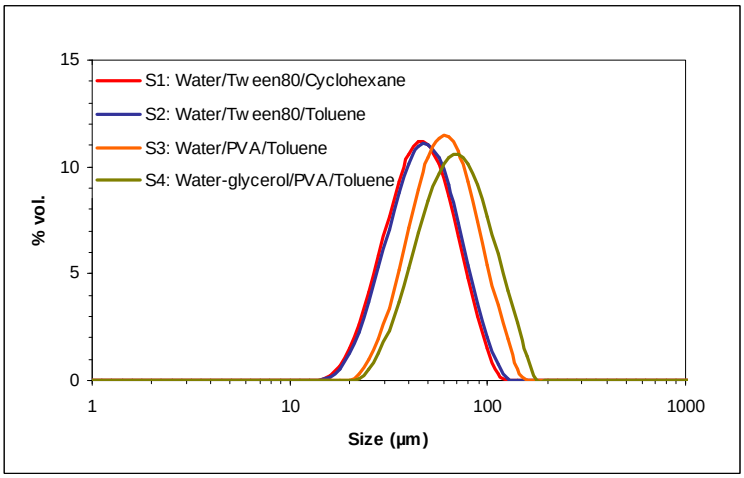

Figure III- 13: Comparison between droplets size distributions obtained with the four systems tested at Φ = 0.25 and Q_{tot} = 300 L.h^{-1} (see Table 10)

System	S_1 : Water/Tween80/ Cyclohexane	S_2: Water/Tween80/ Toluene	S_3: Water/PVA/ Toluene	S_4: Water-Glycerol (25%m.)/PVA/Toluene
d_{32} (µm)	45.0	46.9	59.8	72.1
span	1.1	1.1	1.0	1.2

Table III- 15: d_{32} and SPAN obtained for the four systems from experiments carried out at Q_{tot} = 300 L.h^{-1} and Φ = 0.25

Figure III- 13 shows that whatever the continuous phase and dispersed phase, droplet sizes are smaller when the Tween80 surfactant is involved. Distributions obtained with PVA as surfactant present higher minimum and maximum diameters than distributions obtained with Tween80. The distribution obtained with Water-Glycerol (25% mass.) as continuous phase is slightly shifted to larger sizes compared to the distribution obtained without glycerol. The only difference between systems S_2 and S_3 is the surfactant. This result indicates that the interfacial tension plays obviously an important role in the break up phenomenon. The two systems can be compared in term of interfacial tension. In Table III-16, different interfacial tension values are provided for the different systems. They correspond to the value without surfactant, at equilibrium and to two transient values at a time of the order of the residence time and half residence time in the mixer. These values are calculated thanks to relation II-5 proposed in chapter II.

As already discussed in chapter II, the interfacial tension value in the correlations is the equilibrium interfacial tension value σ_E. The discrepancy between interfacial tension values at equilibrium of systems S_2 and S_3 is too low to explain the discrepancy between the

distributions obtained for these systems. For both systems the surfactant concentration is higher than the Critical Micellar Concentration (CMC). The break-up phenomenon in static mixer occurs during a very short time (t_R = 0.04 – 0.11 s). The equilibrium interfacial tension value between both phases after the emulsification is probably not reached. It depends here on the short time surfactant adsorption kinetics, which depends on the surfactant properties. The interfacial tension values at half the residence time in the mixer $\sigma(t_R/2)$, i.e. transient interfacial tension values for the operation considered, are reported in Table III-16 for each system at Q_{tot} = 300 L.h^{-1}. The transient interfacial tension value in the mixer is lower for the Water/Tween80/Toluene system (S_2) than for the Water/PVA/Toluene system (S_3). This may be explained by the higher molecular weight of the PVA that results in slower diffusion times, whereas lower interfacial tension values at equilibrium due to higher sterical crowding are reached with PVA.

System	S_1: Water / Tween 80 / Cyclohexane	S_2: Water / Tween 80 / Toluene	S_3: Water / PVA / Toluene	S_4: Water – glycerol / PVA / Toluene
$\sigma_{without\ surfactant}$ (mN.m^{-1})	47	36	36	30
σ_E (mN.m^{-1})	3.0	7.0	3.5	4.7
$\sigma(t_R$=0.06s) (mN.m^{-1})	14.91	14.49	34.19	26.18
$\sigma(t_R/2)$ (mN.m^{-1})	17.13	18.33	35.47	27.93

Table III- 16: Interfacial tension values without surfactant, at equilibrium, and at half the residence time in the mixer for Q_{tot} = 300 L.h^{-1} ($t_r/2$ = 0.03 s) for the four systems

In Figure III- 13, the slight discrepancy between both distributions obtained with Tween80 (systems S_1 and S_2) may be explained by the measurement accuracy. For the two systems involving PVA (systems S_3 and S_4), the discrepancy is more important, and may thus be explained by the difference between viscosity and density ratio. In fact, a decrease of both the ϱ_d/ϱ_c μ_d/μ_c ratio results in an increase of the maximum diameter, and thus in an increase of the d_{32} and the span values.

II.3. ***Correlations of the results***

The effects of the different parameters on the mean droplet size have been pointed out. The results can then be modeled as a function of these parameters. The Middleman's approach (1974) is finally applied to propose a modified correlation which takes into account the physical properties and the transient interfacial tension value.

II.3.1. Validation of the Sprow law

The proportionality relationship between the Sauter mean diameter d_{32} and the maximum diameter is often assumed. This relationship is very important to use the Kolmogorov's turbulence theory that relates the maximum diameter to the mean energy dissipation rate.

In order to check this relationship the d_{90} is used instead of the d_{max} because it is measured with more confidence by the laser diffraction used here.

Figure III- 14 (a) represents d_{90} versus d_{32} for the Water/PVA/Toluene (S_3) system at different flowrates and for a dispersed phase concentration Φ ranging from 0.10 to 0.50 and (b) represents the evolution of d_{90} as a function of d_{32} for the four systems at Φ=0.25. In every case, the d_{90}/d_{32} ratio is nearly constant and equal to 2. As a conclusion d_{90} are well proportional to d_{32} for the four systems tested. So even if the proportionality is not strictly checked between d_{max} and d_{32}, these results allow to propose correlations predicting Sauter mean diameters as characteristic diameters. Moreover, the ratio d_{90}/d_{32} allows the quantification of the width of the dispersion on the larger diameter size. Indeed, a high ratio means that the d_{90} value is far from the d_{32}. This width seems to be independent from all the physico-chemical parameters and be only related to the mixer geometry.

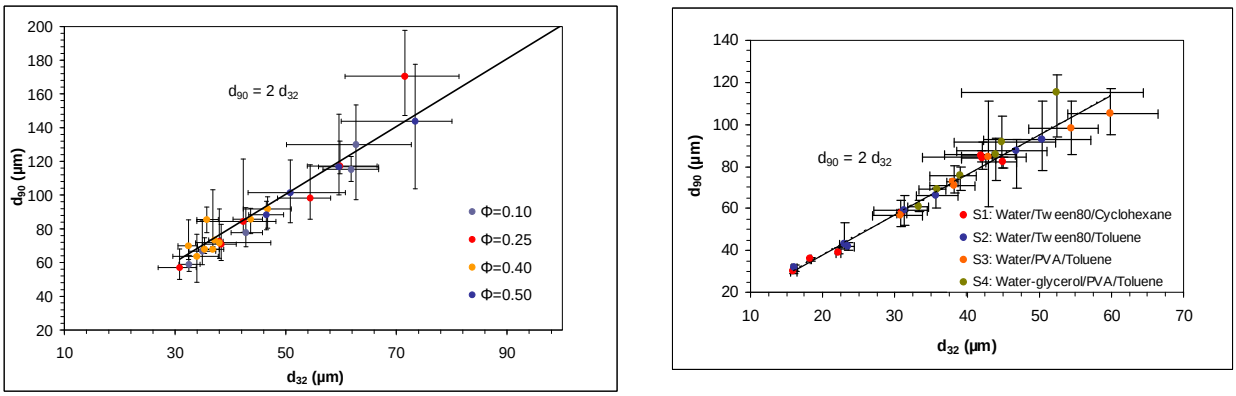

(a) (b)

Figure III- 14: d_{90} as a function of d_{32} for (a) the Water/PVA/Toluene system (S_3) and (b) the four systems at Φ=0.25

II.3.2. Validation of the results thanks to the Kolmogorov turbulence theory

The energy cost of the operation only depends on the power required for pumping. To evaluate this parameter, the pressure drop is measured as noticed in the section (III.2). The pressure drop measurement allows the calculation of the mean energy dissipation rate ε_m per fluid mass unit as follows:

$$\varepsilon_m = \frac{Q\,\Delta P}{V_{\text{free for liquid flow}}\,\rho_c} = \frac{Q\,\Delta P}{L\frac{\pi D^2}{4}\varepsilon\,\rho_c} \qquad \textbf{(III- 24)}$$

The relationship between experimental d_{32} and corresponding mean energy dissipation rates per fluid mass unit ε_m is evaluated in order to check the applicability of the Kolmogorov's theory of turbulence. Experimental data obtained with the Water/PVA/Toluene system (S_3) at different dispersed phase concentrations are plotted on Figure III- 15 (a), and experimental data obtained with the four systems at $\Phi = 0.25$ are reported Figure III- 15 (b).

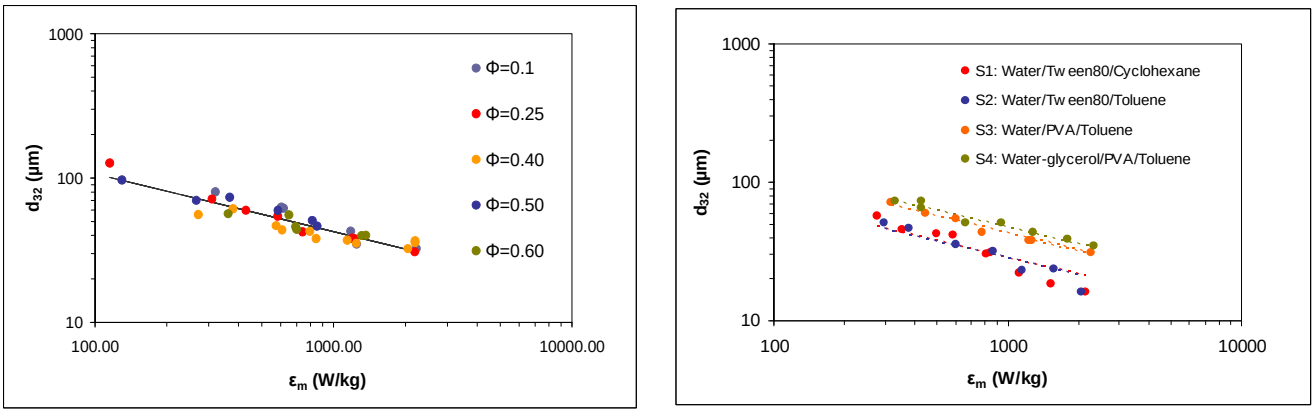

(a) (b)

Figure III- 15: Sauter mean diameters as a function of mean energy dissipation rate per fluid mass unit for (a) the Water/PVA/Toluene system (S_3) at different dispersed phase concentration Φ and (b) the four systems tested with $\Phi = 0.25$

For each data series, d_{32} are well linearly related to $\varepsilon_m^{-0.4}$ in logarithmic representation. These values show that the experimental data fit rather well with the Kolmogorov's theory of turbulence, whatever the dispersed phase concentration until 0.60. So this indicates that the turbulence flow field generated by the SMV mixer is rather homogeneous and isotropic even if some slight discrepancies can be noticed, especially for the systems S_1 and S_2. It can be assumed that the break up conditions are not completely of "Kolmogorov's type" i.e. governed by smallest eddies size. It is also possible that a "jet effect" due to the dispersed

phase introduction through the center of the mixer influences a little the breakage mechanism, and especially at the highest dispersed phase concentration.

Figure III- 15 also enables to compare the influence of surfactant as well as viscosity and density ratios on d_{32}. This comparison is more relevant than this proposed in part II.2.5. It takes into account the energy consumption of the operation. Figure III- 15 shows that mean droplets size are lower when the Tween80 is involved. Moreover, for the two systems involving PVA, d_{32} are lower when ϱ_d/ϱ_c as well as μ_d/μ_c increase. Thus, as highlighted in part II.2.5., the interfacial tension between both phases is the most important physico-chemical parameter on the break-up phenomenon. Moreover, the density and viscosity ratios influence a little the result of the operation.

II.3.3. Correlation to predict the mean droplet size and effect of the transient interfacial tension value

The correlations proposed to predict the mean droplet size are often presented via a dimensionless relationship.

Assuming the Kolmogorov's theory of turbulence and the Blasius type dependence of the Fanning friction factor towards the Reynolds number, the experimental Sauter diameters of the present study are correlated as a function of hydraulic Weber and Reynolds numbers as proposed by Middleman (1974):

$$\frac{d_{32}}{d_h} = K\ We_h^{-0.6}\ Re_h^{0.1} \qquad \textbf{(III- 25)}$$

Where the hydraulic Weber number We_h is calculated as follows:

$$We_h = \frac{\varrho\ V^2{}_0\ D_h}{\varepsilon^2\ \sigma} \qquad \textbf{(III- 26)}$$

The results will be presented by taking into account four different evaluations of the interfacial tension values:

- The equilibrium interfacial tension
- The interfacial tension value without surfactant
- The transient interfacial tension value at a time corresponding to the residence time in the mixer
- The transient interfacial tension value at a time equal to the half and to the residence time t_R in the mixer

To take into account the density and viscosity ratio, the correlation is modified as follows:

$$\frac{d_{32}}{D_h} = K\ We_h^{-0.6} Re_h^{0.1} \left(\frac{\mu_d}{\mu_c}\right)^{-0.1} \left(\frac{\rho_c}{\rho_d}\right)^{0.1} \qquad \textbf{(III- 27)}$$

In this relationship, one has to notice that the exponents relative to the Reynolds number and to the phase characteristics, such as viscosities and densities, are low, equal to 0.1. Clearly, the influence of these parameters is not expected to be predominant.

II.3.3.1. Modeling by using the classical interfacial tension value:

For the four systems the interfacial tension values at equilibrium are mentioned in Table III- 16. The system S_2 exhibits the highest value (7 $mN.m^{-1}$) and the system S_1 the smallest value (3 $mN.m^{-1}$). The interfacial tension values for the systems S_3 and S_4 are respectively 3.5 and 4.7 $mN.m^{-1}$.

Figure III-16 shows that according to this representation at a given dimensionless numbers product the Tween80 surfactant provides the smallest d_{32}/Dh ratio. And then, at constant hydraulic diameter, the Tween80 surfactant allows to reach the smallest mean droplet size. And smaller mean droplets sizes are reached for the system S2 which exhibits the highest interfacial tension at equilibrium. Thus for this surfactant the Sauter mean diameters values as well as the slopes representing the mean droplets size evolution seem to depend on other parameters. In the correlation (III-27) the physico-chemical parameters as well as the hydrodynamic parameters are already taken into account, but, as already mentioned, without any major influence. Subsequently, no relevant parameters seem to explain the discrepancy except the interfacial tension.

Moreover the systems S_2 and S_3 involve the same dispersed phase, density and viscosity ratios. The slopes are similar despite they exhibit different interfacial tension values. Consequently it is very difficult to explain the difference between the slopes of these four systems.

As the break up phenomenon in continuous apparatuses like static mixers occurs at times much lower than the surfactant adsorption/diffusion kinetics another approach could be developed to calculate the Weber number with the interfacial tension without surfactant. Such approach is presented in Figure III-17. If the four systems present equilibrium interfacial tension of the same order (Table III-16), the interfacial tension value without surfactant σ_0 for the four systems studied in this study ranges from 30 $mN.m^{-1}$ (system S_4) to 47 $mN.m^{-1}$ (system S_1).

Figure III-17 shows that at a given dimensionless numbers product the d_{32}/D_h are higher for the system S_4 and smaller for the system S_1. In the present case D_h is constant so the mean droplet sizes are higher for the system S_4 and smaller for the system S_1. While the systems S_2 and S_3 have the same interfacial tension value and the same density and viscosity ratio, the system S_3 leads to higher mean droplets sizes. No physic-chemical or hydrodynamic parameter seems to be relevant to explain this difference.

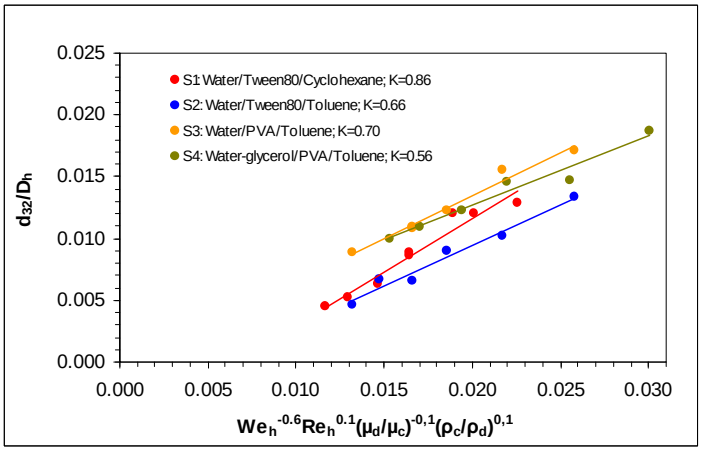

Figure III- 16: Middleman's correlation with the interfacial tension corresponding to the equilibrium value

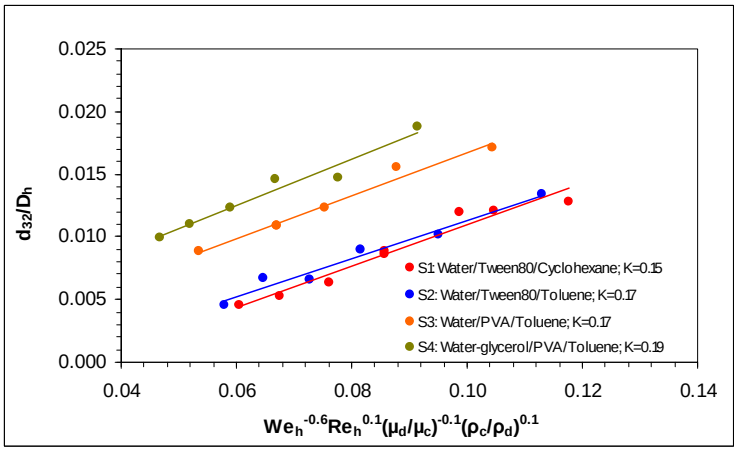

Figure III- 17: Middleman's correlation with the interfacial tension corresponding to the value without surfactant

From Figure III-16 and Figure III-17 it can be concluded that the use of an inappropriate interfacial tension value leads to a misunderstanding of the physical phenomenon. Moreover the interfacial tension value is an extremely sensitive parameter which explains the different evolutions of the mean droplet size to hydraulic diameter ratio. The interfacial tension value must thus be estimated at a time that better represent the state of the system.

II.3.3.2. Modeling by taking into account the transient interfacial tension value at a time of the order of the residence time in the mixer

The approach proposed consists in calculating the interfacial tension at a time of the same order of the residence time in the mixer. The different interfacial tension values are calculated thanks to the modeling of the analysis exposed in chapter II. Two representations are proposed: firstly calculating the interfacial tension at the residence time in the mixer (Figure III-18), and secondly calculating the interfacial tension at half the residence time in the mixer (Figure III-19). The different values are given at t_R = 0.06 second in Table III-16.

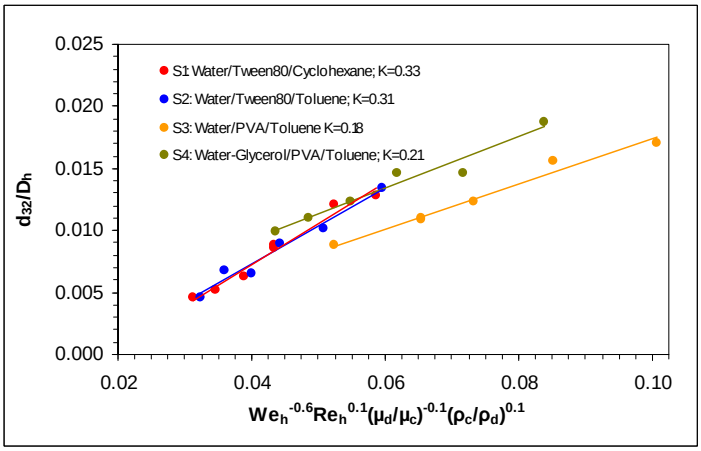

Figure III- 18: Middleman's correlation with the interfacial tension corresponding to the residence time value

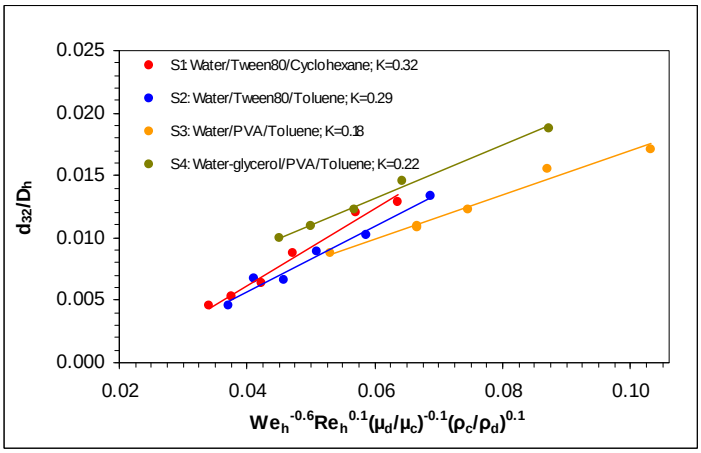

Figure III- 19: Middleman's correlation with the interfacial tension corresponding to the half residence time value

For both representations the mean droplet size to hydraulic diameter ratio d_{32}/D_h follows the same evolution with almost the same slopes for the two systems involving Tween80 (systems S_1 and S_2) and for the two systems involving PVA (systems S_3 and S_4). It thus appears that the break up phenomenon in static mixers is ruled by the surfactant

properties. These two last representations show that taking the interfacial tension value at a time of the order of magnitude compared to the process characteristic times leads to a better understanding of the different physico-chemical parameters which affect the system. The method used in the present study to access such interfacial tension value can easily be used for engineering approaches.

Moreover based on Theron *et al.* (2010, 2011) results it seems that the breakup phenomenon mostly occurs in the first five static mixer elements. Then the droplet size keeps on decreasing but less significantly. The coalescence phenomenon is neglected given that its probability is very low (Lobry *et al.* 2011). The droplets interface is constantly regenerated and new surfactant molecules are absorbed. Consequently the approach that is retained is to calculate an apparent value of the interfacial tension at half the residence time in the mixer (Figure III-19).

Despite the discrepancy observed between the four systems the slopes are closer and a general correlation is proposed:

$$\frac{d_{32}}{D_h} = 0.20\ We_h^{-0.6} Re_h^{0.1} \left(\frac{\mu_d}{\mu_c}\right)^{-0.1} \left(\frac{\varrho_c}{\varrho_d}\right)^{0.1} \qquad \textbf{(III- 28)}$$

Figure III- 20 represents the calculated d_{32}/D_h ratio as a function of experimental values. The regression coefficient is rather suitable given that the measurement uncertainty on the d_{32}. The K value (0.20) depends on the parameters which are not taken into account in our correlation such as the diffusion of the surfactant which is included in the fitting parameters of the interfacial tension model.

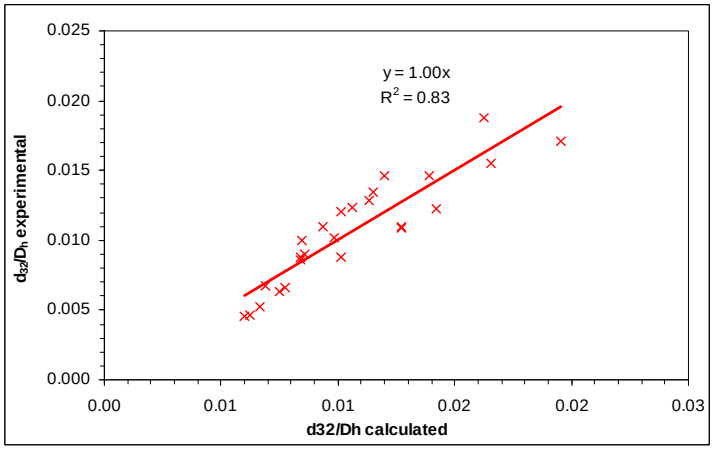

Figure III- 20: Comparison between experimental and modelled d32/Dh ratio when using the correlation

The correlation is suitable for the S_3 systems for all the dispersed phase concentration studied (Figure III- 21).

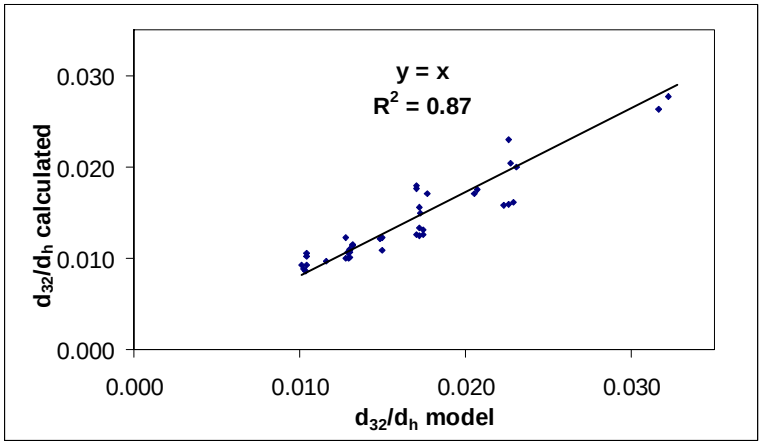

Figure III- 21 Comparison between experimental and modelled d32/Dh ratio when using the correlation for the Water/PVA/Toluene system under different dispersed phase concentration

II.4. ***Conclusion***

The static mixer provides promising results to perform the emulsification step of our S-PVC process. The required specifications on the liquid-liquid dispersion are satisfactory:

- To ensure a mean droplet size of 30-50µm, the corresponding flowrate for this equipment size is of 400 to 550 $L.h^{-1}$. For extrapolation at same design characteristic, the pressure drop must be preserved;
- The droplet size distribution are narrow;
- The creation is faster than in batch.

Moreover, these lab scale tests allow to establish a correlation that will take into account the physico-chemical parameters of the systems.

III. PILOT SCALE EXPERIMENT

The goal of these tests is to perform the direct emulsification loading in a batch and to carry on the polymerization. It is expected to decrease the loading time in batch and the time to obtain the dispersion. Currently, the different products are introduced in 15 min and it takes 65 min more to heat the reactants at the polymerization temperature and create the VCM droplets.

This step can be easily improved with few investments. The use of static mixers allows the creation of the dispersion in few milliseconds and the loading time can be controlled thanks to the flowrate.

The tests presented in this section were performed with a minimum investment: only the static mixers were purchased. They correspond to the first tests achieved at pilot scale to check the feasibility and the improvement of the process.

The expectations of these tests are exposed below:

- To confirm the feasibility of the loading process;
- To study the effect of the flowrate, the stirring and the hot charging on the final quality products;
- To evaluate the benefits compared to the classical process.

However, it is obvious that our working conditions are not optimal.

The static mixer has been designed in cooperation with the Sulzer Company. Knowing our mean droplet size expectation and the loading time and flowrate, Sulzer proposed a design at a given diameter. Our lab experiments were used to help to the design choice and to check their correlation. Keeping the pressure drop as invariant allows to access to the same droplet size.

In the following section, the pilot and the procedure are detailed. For each test performed, a reference batch test is also carried out in order to compare the results and identify clearly the benefits or drawbacks of our loading procedure.

III.1. **Fluids and recipe**

The tests are performed at the pilot scale at the Mazingarbe plant. Among the different grades produced by the Ineos Company, the recipe tested is: the M7102. The quantities are provided to fill the 100L pilot stirred tank.

The recipe is based on the same monomer quantity. All the additives are calculated as a function of this initial quantity. (Table III-17)

Product	Quantity
VCM (kg)	29.1
Demineralized Water in the reactor (kg)	18
Demineralized Water (kg)	24.1
Primary PVA (ppm)	563
Secondary PVA (ppm)	43
Peroxidicarbornate (ppm)	407
P3 LTIS+20min ppm	86
Primary PVA LTIS+85min ppm	134
Radical scavenger ΔP = 1.5 bar or 500	3
Temperature (°C)	55

Table III- 17 : M7102 recipe, LTIS(polymerization temperature reached)

In case of hot charging or use of hot water, the quantity of initiator is increased up to 600ppm.

Another recipe is used (M5702). The same constituents are involved. The additives concentrations are different concerning the PVA (given that this recipe provide PVC particle of different morphology. The initiator concentration is four time higher than in the classical recipe to carry out the polymerization in one hour. More details are provided section IV-4-4.

Three steps are involved in the process:

- The dispersed phase composed by the VCM: the VCM is stored in two tanks at pilot;
- The water is directly provided by the internal network (17bar);
- 750mL of premix is prepared at the pilot lab: a solution of surfactants and initiator is prepared and mixed to create an emulsion. The solution is stored in a graduated test tube of 1 L. This "premix" will be directly pumped into it. 500mL are introduced.

III.2. ***Material and method***

III.2.1. Experimental rig- the stirred tank reactors

The pilot plant contains four stirred tanks. Practically, only three of them will be used in this study. The characteristics of the different reactors are detailed in Table III-18.

Reactor	Material	V_R (L)	Connection with the SM
R103	Enamel	100	Direct
R101	Stainless steel	100	2m of annulated pipe
R104	enamel	100	2m of annulated pipe

Table III- 18 : characteristics of the pilot stirred tank used in the loading study (V_R: reactor volume)

Before each experiment, the reactors are coated in order to avoid the encrusting and misbatch. The process parameters are followed in the control room. The jacketed temperature, the product temperature and the pressure inside the tank are recorded.

Besides, before the loading, the pre-added water is stirred at the proper stirring velocity and heated at the polymerization temperature. The jacketed temperature is regulated to maintain a product temperature of 55°C.

III.2.2. Experimental rig – the loading part

The reactors are filled thanks to the static mixer. The static mixers provided by the Sulzer Company are the SMV static mixers, previously studied at lab scale and the SMX static mixer.

A picture of the SMV static mixers is provided in Figure III- 22 and the characteristics are given in Table III-19.

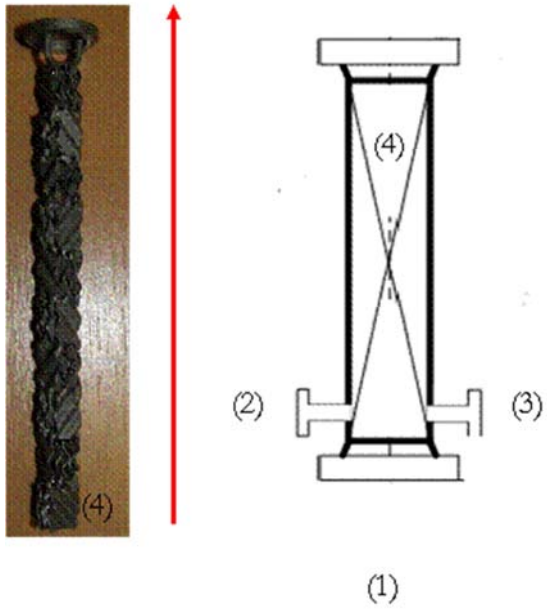

Figure III- 22 : Sulzer SMV static mixer at pilot (1) VCM introduction, (2) and (3) peripheral inlet (4) packing: SMV

Characteristics	SMV static mixer	SMX static mixer
D mm	10	10
D_h mm	3.5	2.45
ε	0.83	0.67
Material	Stainless steel 316L	Stainless steel 316L

Table III- 19 : static mixers specifications (D total diameter of the mixer, D_h: hydraulic diameter and ε void fraction)

The SMX is usually used to perform liquid-liquid dispersion in laminar flow with viscous fluids. Our goal is to obtain a mean droplet size between 30-50 µm. The calculation completed by the Sulzer company propose to use the SMV but also this closest design (SMX) to succeed in achieving small droplet size (30µm).

Two different configurations were tested:

- Two inlet flows: the VCM enters through the central tube and the water phase flow, in which the premix is introduced, enters via a secondary inlet. (Figure III- 23 (a))
- Three inlet flows: the VCM (dispersed phase) enters through the central tube and the two secondary inlets are dedicated to the water and to the premix (Figure III- 23(b)). This configuration was used to avoid the direct contact of the peroxide with the hot water in the case of hot charging tests.

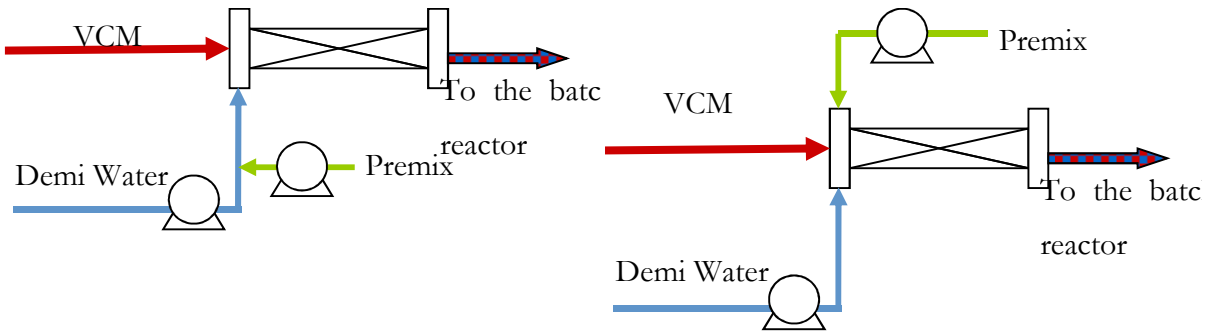

(a) Two inlets flows configuration (b) Three inlets flows configuration

Figure III- 23 : tested configurations (a) with two inlets and (b) with three inlets

It is hard to accurately control the flowrate because no additional pump was available.

- The VCM flowrate is function of the pressure imposed in the VCM storage tank of the pilot by the nitrogen. To measure the flowrate, the introduction time is measured and thanks to the Coriolis flow meter which controls the introduced amount of VCM, the flowrate is estimated. The flowrate can also be read on the control room. However, it is not registered. There are lots of fluctuations on the VCM flowrate.
- The flowrate of the demineralized water is ensured by the OBL pumps (piston pumps). Five pumps are connected in series: two pumps of 90 $L.h^{-1}$ with an admissible pressure of 12 bar and three pumps with an admissible pressure of 40 bar of different maximum flowrates: 40, 35 and 11 $L.h^{-1}$. A Coriolis flowmeter allows checking the amount of water. The flowrate is estimated thanks to the loading time of the total amount of water and can also be read at the control room.
- The flowrate of the premix is ensured by the same kind of pump with a maximum flowrate of 4 Lh^{-1} and 40 bar of pressure. The introduced volume is read on the test tube and the flowrate is estimated thanks to the loading time.

The static mixer pilot can be easily connected to the different reactors thanks to different pipes. The length of pipe to connect the static mixer is not the same for all the reactors. Initially, it has been constructed to be implemented on the R103 reactor. The static mixer pilot is connected to the other reactor thanks to a 2m long annulated tube. So the liquid-liquid dispersion is not directly introduced in the reactor but flow through the annulated tube before entering.

III.2.3. Loading procedure

The global procedure is not detailed but the main points are:

- The pre-loading of the reactor with a small amount of water to start the stirring and the heating of the reactive mixture;
- The vacuum is made on the entire circuit to avoid the presence of oxygen which can affect the polymerization reaction kinetics;
- The VCM and premix flowrate are stopped before the water flowrate in order to clean the equipment and remove the residual amount of initiators and surfactants.

The liquid-liquid dispersion created in the static mixers is composed of about 60% mass of dispersed phase. The dispersion is then diluted to 40% mass. in the reactor due to the water already introduced.

III.2.4. Analyses

The classical analysis performed to analyse the final products characteristics is performed. For each batch, 5 L of slurry are collected and the following analyses are carried out:

- The particle size distribution is analysed through laser diffraction (Mastersizer 2000, Malvern Instrument) in suspension and after drying. The particles are also observed by SEM (scanning electron microscope);
- The porosity of the grain CPA and the bulk density (o-BD and m-BD) are also analysed: these characteristics are important for the shaping step of the PVC grains and its application;
- The fisheyes quantifies the number of particles grains that have not gelified after a standard friction and heating time;
- The NGP (non gelified particles) list the particles with a gelification time inferior to the average. It is estimated at a shorter time than the standard time of a resin (i.e. 5 min for the KV71);
- The K-Wert which corresponds to the polymerization degree;
- The residual PVA concentration in the slurry water.

These tests are classically performed in PVC industry to check the product quality. So the different analytic procedures are not detailed here.

The results obtained for the SM loading tests will be compared to the reference batch test. The discrepancy with the usual specifications and the noticeable results will be pointed out and detailed if necessary.

III.3. ***Operating conditions***

To check the reliability of our process, the following parameters are studied:

- Hydrodynamics effect on the final product of
  - ✓ The global flowrate of the direct liquid-liquid dispersion loading
  - ✓ The stirring velocity of the reactor

- Process parameters :
  - ✓ The temperature of the loading
  - ✓ The comparison between the classical batch and the loading thanks to the static mixer.

The global flowrate is estimated by adding the different flowrates. This value is approximately indicated given that there is some uncertainty on the VCM and water flowrates (which fluctuate a lot referring to the control room registrations).

Table III-20 sums up the different tests performed. The tests performed without static mixer are printed in orange.

Test number	Reactor Stirring	SM+inlet configuration	Total flowrate ($kg.h^{-1}$)	VCM loading time (min)	Water loading time (min)	Premix loading time (min)	Recipe and remarks
1033619	R103 275 Rpm	SMV;2inlets		NOT MEASURED			M7102
1033620	R103 275 Rpm	SMV;2inlets	354	11	8	8	M7102
1033624	R103 275 Rpm						M7102
1033621	R103 200 Rpm	SMV;2inlets	449	8	6.83	7.33	M7102
1033623	R103 200 Rpm	SMV;2inlets	350	10.75	9.5	10.75	M7102
1033625	R103 200 Rpm						
1033622	R103 275 Rpm	SMV;3inlets	318	11.67	10.75	10.80	M7102 Hot charging
1033627	R103 275 Rpm						M7102 Hot water
1042811	R104 225 Rpm	SMV;3inlets	376	10	7.83	8	M7102
1042813	R104 225 Rpm						M7102
1013619	R101 275 Rpm	SMV;3inlets	202	15.78	14.73	14.25	M7102 Hot charging
1013620	R101 275 Rpm	SMX;3inlets	283	14.83	10.92	10.92	M7102 Hot charging
1013621	R101 275 Rpm						M7102 Hot water
1042812	R104 225 Rpm	SMV;2inlets	356	9.82	5.42	6.17	M5702 Polymerization in one
1042814	R104 225 Rpm						M5702 Polymerization in one

Table III- 20 : Description of the different SM loading tests performed

The flowrate fluctuations are due to the pressure fluctuation on the network. The effect of the flowrate can be shown by comparing 1033621 and 1033623 at the same stirring velocity effect.

Unfortunately, we did not succeed in keeping a constant flowrate for the different tests where as other parameters were changed. Some trends can nevertheless been highlighted. Thanks to the reference tests performed, the benefits and drawbacks of this type of loading can be pointed out. So the economical and practical interest of the process can be demonstrated.

III.4. ***Results***

III.4.1. Effect of the different parameters on the particle properties

The recipe used is always the M7102 except for the tests 1042812 and 1042814.

The tests performed in the reactor 101 are dedicated to the hot charging.

The different analysis results on the powder are presented on the Table III- 21, Table III-22 and Table III- 23.

The different samples are also analysed through SEM to compare the grain aspects obtained with the classical batch and with the direct liquid-liquid dispersion loading. Figure III- 24 is an example of the pictures obtained.

Test number	Reactor Stirring	SM+inlet configuration	Total flowrate ($kg.h^{-1}$)	d_{50} (µm)	d_{10} (µm)	d_{90} (µm)	Span	CPA	o-BD ($kg.m^{-3}$)	m-BD ($kg.m^{-3}$)	NGP 4 min	FE
1033620	R103 275 Rpm	SMV;2inlets	354	134	90	195	0.78	34.8	479	497	86	24
1033624	R103 275 Rpm			131	87	193	0.81	36.2	463	494	73	50
1033621	R103 200 Rpm	SMV;2inlets	449	146	107	201	0.69	35.4	461	487	78	18
1033623	R103 200 Rpm	SMV;2inlets	350	176	129	250	0.68	34.3	485	515	6	7
1033625	R103 200 Rpm			185	136	216	0.59	35.6	468	499	19	9
1033622	R103 275 Rpm	SMV;3 inlets	318	240				MISBATCH (Hot charging)				
1033627	R103 275 Rpm			157	106	231	0.80	36.5	462	482	70	52

Table III- 21 : PVC particles characteristics under the different investigated conditions in R103 (M7102 recipe)– effect of the hydrodynamic parameters

Test number	Reactor Stirring	SM+inlet configuration	Total flowrate $kg.h^{-1}$	d_{50} (µm)	d_{10} (µm)	d_{90} (µm)	Span	CPA	o-BD ($kg.m^{-3}$)	m-BD ($kg.m^{-3}$)	NGP 4 min	FE
1042811	R104 225 Rpm	SMV;3inlets	376	107	76	151	0.70	32.2	490	507	5	
1042813	R104 225 Rpm			120	82	172	0.72	35.6	475	500	17	
1042812 M5702 fast	R104 225 Rpm	SMV;2inlets	356	214	154	294	0.65		558	589		
1042814 M5702 fast	R104 225 Rpm					BALLS						

Table III- 22 : PVC particles characteristics under the different investigated conditions in R104

Test number	Reactor Stirring	SM+inlet configuration	Total flowrate $kg.h^{-1}$	d_{50} (µm)	d_{10} (µm)	d_{90} (µm)	Span	CPA	o-BD ($kg.m^{-3}$)	m-BD ($kg.m^{-3}$)	NGP	FE
1013619	R101 275 Rpm	SMV;3inlets	202	154	113	207	0.61	35	462	489	8	2
1013620	R101 275 Rpm	SMX;3inlets	283	171	124	238	0.67	32.5	498	525	7	4
1013621	R101 275 Rpm			159	113	226	0.71	35.7	472	498	45	23

Table III- 23 : PVC particles characteristics under the different investigated conditions in R101

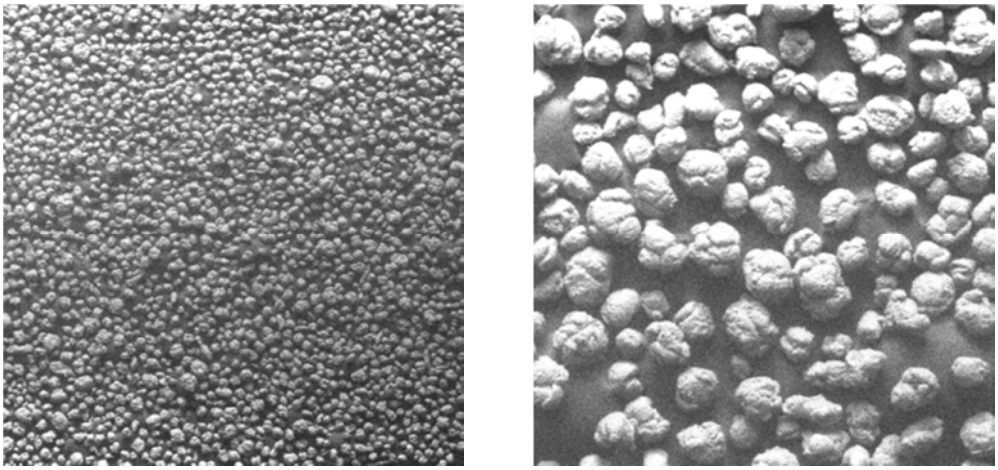

(a) SEM pictures for the 1033620 tests: SM loading – 275Rpm

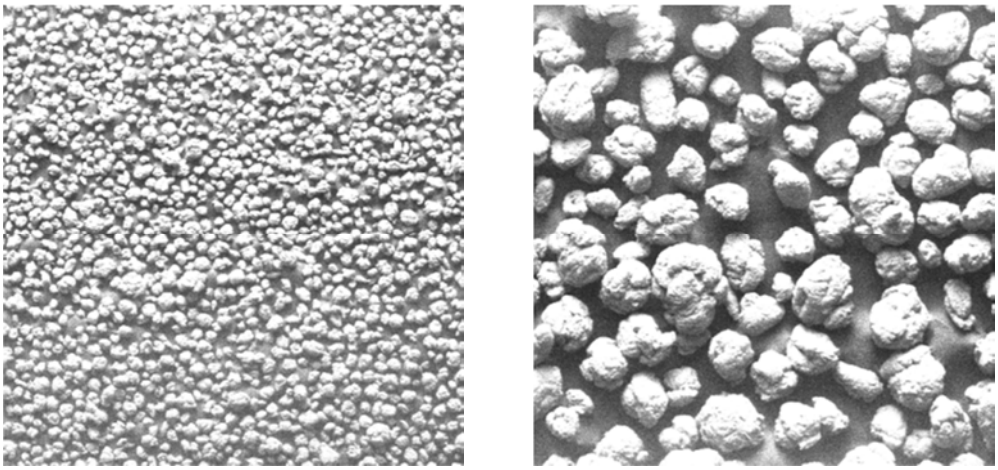

(b) SEM pictures for the 1033624 test –classical batch(same conditions as 1033620)

Figure III- 24 : Some example of the visualisation of the PVC grains obtained: comparison between a classical batch and a loading of a created liquid-liquid distribution by SMV static mixer

The particle sizes obtained are in the expected range. Moreover, from the SEM pictures, the particles have a shape which correspond to which is obtained in batch.

III.4.1.1. Effect of the hydrodynamic parameters

Effect of the flowrate

Test 1033621 and 1033623 allow to emphasize the effect of the flowrate. The expected trend is observed: a higher flowrate leads to smaller particles. It suggests that the liquid-liquid dispersion is well created thanks to the static mixers, and controls the resulting grain granulometry.

Effect of the stirring

Tests 1033620 and 1033623 show that, a decrease of the stirring velocity leads to larger particle size. In the classical process, the stirring velocity controls the properties of the liquid-liquid dispersion and the agglomeration of the particle during the polymerization reaction. In these two tests, the liquid-liquid dispersion is created thanks to the static mixers. The tests were performed under the same other operating conditions. The mean droplet size and droplet size distribution obtained for the two tests present then the same characteristics. As a consequence, the droplet size evolution is due to the agglomeration process which tends to be more important in case of lower stirring velocity. However, additional tests with an appropriate control of the flowrate would be necessary to control the mean droplet size of the liquid-liquid dispersion and clearly identified if larger sizes results in agglomeration.

III.4.1.2. Effect of the process parameters on the final powder characteristics

Comparison between the classical batch process and the loading of the dispersion through static mixer

From Table III- 21, Table III- 22 and Table III- 23 , the difference and similitude between the two processes can be pointed out.

All the tests provide a good specification concerning the mean particle size and particle size distribution. Either in the classical batch process or in static mixer loading batch process, the size characteristics are in the same range. The span which characterized the width of the distribution tends yet to be shorter in case of static mixers. It suggests that static mixers allow the creation of a narrower droplet size distribution and clearly affects the final particle size distribution.

The physical characteristic of the powder such as the CPA and the o- and m-BD values present no significant evolution from classical to static mixer loading process. It is important to notice because it suggests that the properties of PVC grains are not affected by this new loading process. These properties are responsible for the future applications of the powder. However, the NGP and FE (non gelified particle and fisheye) numbers are considerably reduced. It suggests a better homogenization of the additives (initiator and surfactants) in the droplet and at the droplet interface.

Hot charging experiments

The hot charging tests are performed on the reactor R101. The corresponding results can then be found on Table III-23. The experiment conducted with static mixer leads to considerably less fisheyes and non gelified particles. Moreover, the dispersion arrived in the reactor almost at polymerization temperature. This result is then encouraging to improve the current process. On top of reducing the loading time, the heating time is shortened too.

III.4.2. Effect of the loading process on the slurry water

Table III-24 presents the different analysis performed on the slurry water. The tests are not described. The reader can report on Table III-20 for extended information.

Test number	Residual PVA $mg.L^{-1}$
1033620	0.4
1033624	8.1
1033621	2.6
1033623	3.5
1033625	9.3
1033622	3.7
1033627	8.3
1042811	3.4
1042813	12.1
1042812	7.5
1042814	52
1013619	3.8
1013620	1.6
1013621	11.6

Table III- 24 : Summary of the analysis on the slurry water for all the tests performed

The residual PVA concentration in the slurry water is always lower in the case of the static mixer tests. It suggests a better absorption and distribution of the surfactants. This assumption could be validated by adding an additional analysis: the surface tension measurement of the slurry water.

III.4.3. Effect of the loading process on the kinetics of the reaction

Figure III-25 provides an example of the data recorded at the control room: the pressure in the reactor, the product temperature, the jacket temperature and the stirring.

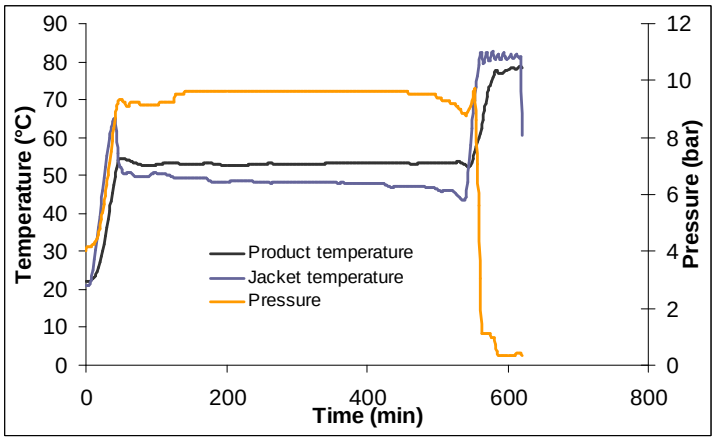

Figure III- 25 : example of data recorded – test 1033620

In Table III-25, the polymerization reaction time and the conversion obtained are summed up for all the tests.

For all the tests, it appears that the reaction time is longer in the case of the loading with static mixer. This result is not surprising given that in the case of static mixer loading; the water introduced was not completely degassed. Only the water pre-added at the beginning to ensure the stirring and the heating in the reactor during the introduction was treated. On the contrary, for the classical batch tests, all the oxygen was totally removed from the water. This difference can explain a longer polymerization time due to the induction period. Besides, the premix is not stirred during the loading in static mixer. Further tests will be conducted by stirring this emulsion.

Concerning the conversion, the same rate is obtained.

Test number	Reaction polymerization time (min)	Conversion (%)
1033620	510	76.4
1033624	468	89.1
1033621	510	82.1
1033623	510	84.6
1033625	457	82.1
1033622	505	
1033627		
1042811	479	76.4
1042813	422	84.3
1042812	75	87.6
1042814	80	
1013619	363	85.8
1013620	430	85.9
1013621	375	82.1

Table III- 25: Reaction data for all the tests (classical batch and static mixer loading)

III.4.4. Preliminary tests for the loading of a CSTR

Our final goal is obviously to carry out the Suspension Polymerization of the vinyl chloride by using continuous equipments. Among the two foreseen strategies, the stirred tank reactor in series is an alternative which could be easily implemented in the current plant, even if it is not the most innovative.

In this objective, the tests 1042812 and 1042813 (classical batch references) were performed to have a total polymerization reaction time of one hour. The amount of VCM is of 15 kg and the initiator is four times more concentrated as usual. The goal of this test is clearly not economical but consists in checking the ability of the static mixer loading process to obtain a polymer with acceptable properties in critical conditions and also to produce it very fast in case of the application in CSTR if the current flowrate is maintained (i.e. 355 $kg.h^{-1}$).

Regarding Table III-22, it appears that the PVC grains obtained are larger than usual. However the other specifications concerning the powder characteristics (Table III-22) or the slurry water (Table III-24) are in the expected range. Unfortunately the fisheyes and the NGP were not measured.

However, the reference batch test provides a PVC powder of very bad quality: the particles obtained were balls and the additives were clearly bad mixed given the high residual PVA concentration in the slurry water.

III.5. ***Discussion and perspectives***

Regarding all the previous parts, it is clear now that static mixer loading reveals itself as an interesting improvement of the classical S-PVC batch process.

These preliminary tests were conducted in non-favourable conditions: the lack of control of the flowrates, the bad homogeneity of the premix and the non-degassed demineralized water. However, in spite of these difficulties, the process has proved its efficiency to obtain PVC grain with properties in the expected range. Indeed, the particle size distributions as well as the bulk density are clearly controlled. It seems that the fisheye and NGP are also decreased, suggesting a better distribution of the additives also proved by the decrease of the residual PVA concentration in the slurry water.

The research on this field must carry on and the pilot is now equipped of pumps to regulate the flow of the different fluids. These pumps will allow us to work at a sufficient flowrate to obtain the expected droplet size of 30μm. Some tests will be performed to study the effect of

the inlet conditions (no studied despite the use of 3 inlets for the hot charging tests), the reproducibility of the test and different configuration as proposed Figure III-23.

In this scheme, we propose to first prepare the organic phase by mixing the VCM, the initiator and the secondary PVA and then to perform the liquid-liquid dispersion with hot water. Eventually, a third static mixer could be inserted to the pilot to prepare water at a sufficient temperature to ensure that the dispersion entered in the stirred tank at polymerization temperature.

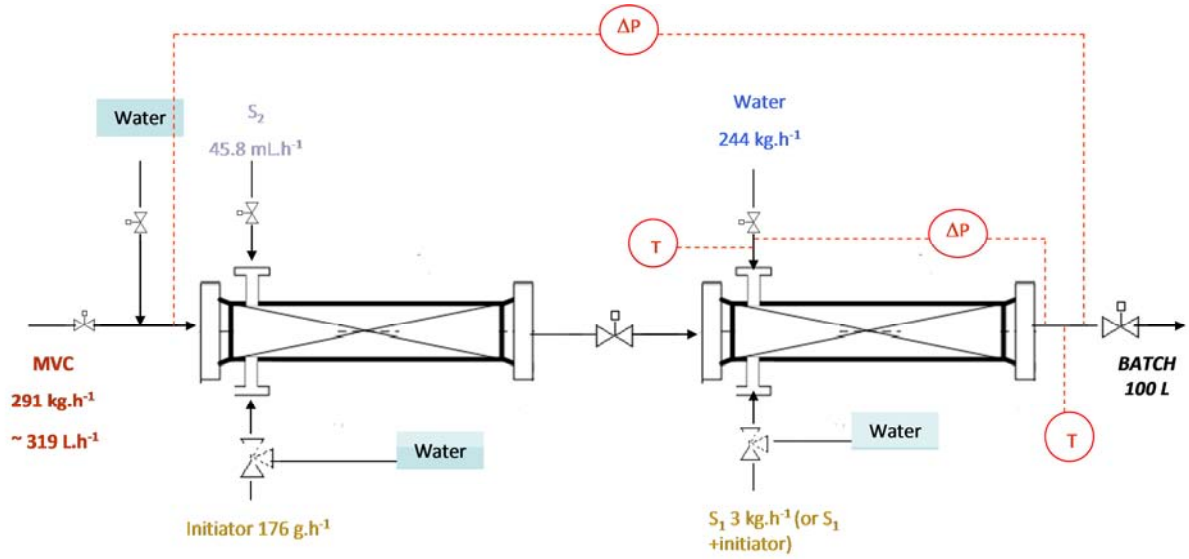

Figure III- 26 : Scheme of the loading process comprising a homogenization of the dispersed phase unit and an emulsification unit

All the different configurations have to be studied in order to define the most efficient and the easiest one to implement at the industrial scale depending on the available utility flow.

IV. CONCLUSION

The liquid-liquid dispersion in static mixer has been studied at lab-scale and implemented at pilot scale to improve the current suspension polymerization batch process but also in the point of view of developing a continuous batch process.

For a given system, the droplet size obtained is strongly affected by the flowrate. At lab-scale, the parameters studies consist mainly in physicochemical parameters. The obtained results were successfully correlated through a Middleman-kind correlation (1974) by taking into account the dispersed phase to continuous phase density and viscosity ratio and the dimensionless Reynolds and Weber number. Given the short residence time of the flows in the static mixer, a special attention is paid to the interfacial tension value and to the role of the surfactant. For a set of hydrodynamics and physicochemical parameters, the mean droplet size can then be estimated.

The system was applied at pilot scale to perform the direct liquid-liquid dispersion loading. It has provided very promising results for the improvement of the current process. The main properties of the grains are preserved which suggest the conservation of the global applications for a K-Wert given. Besides, the static mixers seem to ensure a better homogeneity and distribution of the additives by increasing the quality (less FE and NGP) and decreasing the residual quantity of PVA. Moreover, the first tests of hot charging deliver product of good quality. As a result, the current process could be easily improved with reasonable investments. The occupation time of the batch could be easily decreased and the productivity could be then increased

.

CHAPTER IV: Liquid-liquid dispersion in pulsed columns

In this chapter the liquid-liquid dispersion in pulsed column is studied. Contrary to the liquid-liquid dispersion performed in static mixer, not only the creation but also the maintaining of the dispersion will be investigated.

First a short literature survey presents the pulsation devices and their characteristics. In the second part, the results obtained in a discs and doughnuts co-current pulsed column with an upflow are introduced and commented. In a third part, the liquid-liquid dispersion is performed in a COBR (Continuous Oscillated Baffle Reactor from Nitech Co.), which is a horizontal pulsed column packed with doughnuts only. Finally the results are compared in term of energy.

I. LITERATURE

Among the available continuous process, the pulsed column has already been largely studied in the past, mainly for counter-current liquid-liquid extraction processes. It consists in a column packed with discs and doughnuts equally spaced or perforated sieve plates. Nowadays it may also be potentially considered as a tubular plug flow reactor for continuous crystallization, for polymerization (Ni et al. 1999, Carvalho et al. 2006) or for the biodiesel production (Stamenkovic et al., 2010), but with a co-current flow. Different designs have been studied in literature and some studies confirm its ability to perform a good mixing (Mackley and Ni, 1991 and 1993) and transport of liquid-liquid dispersion and liquid-solid suspension (Mackley et al., 1993) . A special design composed of rings equally spaced is particularly studied. It corresponds to the continuous oscillatory baffled reactor for which heat transfer (Stephens and Mackley,2002), mixing performance (Ni et al.,1998;Fitch et al.,2003), liquid-liquid dispersion (Ni et al., 1999;Hounslow and Ni,2004; Pereira and Ni,2002) are particularly detailed.

I.1. ***Background on the pulsed columns***

The first patent relative to a pulsed column was published by Van Dijck in 1935. The main claim concerns the movement of the liquid thanks to a vertical oscillation of the perforated sieve plate or thanks to an external mechanism with immobile internals. This second configuration is the most popular. This process was initially created for counter-current liquid-liquid extraction. The role of the mixing imposed by the oscillation and the insert is to create and to maintain a liquid liquid dispersion in order to improve the interfacial area between phases and then to promote and control the mass transfer kinetics.

During the 1960s, pioneering works inside the nuclear industry show that the fluid oscillation generated in a sieve plate column could produce effective liquid-liquid dispersion and columns were successfully used to enhance solvent extraction (Logsdail *et al.* (1957), Lo and Baird (1987)). It has been demonstrated that by combining oscillations with periodically spaced baffles in a tube, vigorous eddy mixing can be achieved between baffles leading to an excellent mixing (Brunold *et al.*, 1989) radially homogeneous (from the central axis of the column to the wall).

Different designs are described in literature and two kinds of column can be distinguished. In the first group, the pulsation is guaranteed by an external means and the flow passes through plates of different designs. This group corresponds to the "pulsed plate column". The second group is composed of perforated plates set which moves up and down. It is the reciprocating plate column.

In the Table IV- 1, H represents the distance between two plates, D the column diameter, T the transparency (the open free area of the baffles), f the oscillation frequency and A the amplitude peak to peak, D_0 the hole diameter.

There are also some columns with a huge variety of insert (from Raschig ring to more structured insert such as static mixer) but it is not the concern of this part.

Lot of work is available in literature concerning pulsed column and oscillatory flow mixing. In the following part, an insight on the different studies parameters is proposed.

Reference	Type of column	Plate	Characteristics	Applications
Karr(1959)	Reciprocating pulsed column	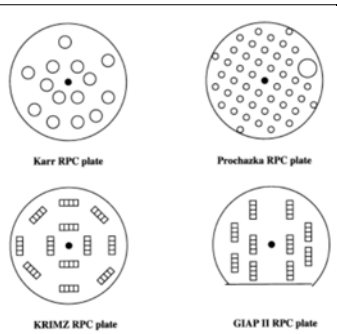	D up to 150mm (1.7m in industry (Lo et al. 1991)) H=25 to 100m	Nuclear industry
Tojo et al. (1957,1980) Miyanami et al. 1973,1975	Multistage vibrating disc contactor	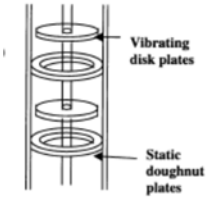	D_D/D=0.75-0.8 D_O/D=0.5-0.7 H/D=1	Gas-liquid contactor Liquid-liquid dispersion
Yadav and Patwardhan (2008)	Pulsed sieve plate column	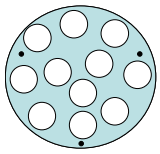	Table I of the publication provides all the details	Liquid-liquid extraction
Gourdon (1989) Brunet *et al.* (2005)	Disc and doughnut pulsed column	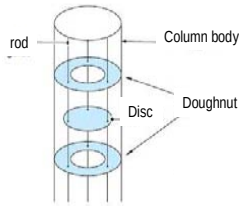	The discs promotes the radial mixing	nuclear
Nitech company	Baffled tube	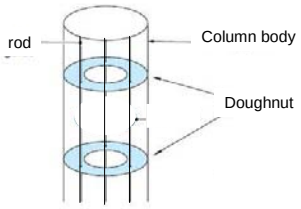	H/D=1.8	crystallization

Table IV- 1 : Kind of column

I.2. ***What is a pulsed or oscillatory flow mixing?***

The terms "unsteady", "pulsatile" or "oscillatory" are commonly used in the literature to describe flows in which velocity or pressure depends on time. Oscillatory flow is a periodic flow that oscillates around a zero value. Pulsatile flow is a periodic flow that oscillates around a mean value not equal to zero: it is a steady flow on which is superimposed an oscillatory flow.

In this manuscript, the kind of flow studied is the pulsatile flow mentioned as pulsed flow sometimes.

Pulsatile flow may be laminar, transitional or turbulent. However due to the parameters characterizing the oscillation (mainly oscillation frequency, *f*, and oscillating velocity amplitude A) in addition to the time dependence of the flow as a whole, the flow patterns of each regime and the transition from one to another are rather complex.

Aiming to work under plug-flow conditions, the mixing has to be as efficient as possible, radially. Among the different references available in literature, Mackley and Ni (1993) provide some visualisation of flow profiles with and without baffle under various hydrodynamic conditions. The presence of baffle allows to decrease the backmixing (the axial dispersion). When oscillations are superimposed to the net flow, particles are uniformly mixed and the chaotic advected flow generates a good mixing. Figure IV- 1 explains the vortices creation. The periodic motion of the flow accelerates and decelerates. At each acceleration, vortices are formed downstream of the baffles. When the flow decelerates, those vortices are swept into the bulk and subsequently unravelled with the bulk flow acceleration in the opposite axial direction. This vortices cycle formation is repeated and then the strong radial velocities provide an uniform mixing in each inter-baffle zone and cumulatively along the length of the column (Brunold et al., 1989; Mackley and Ni, 1991, 1993).

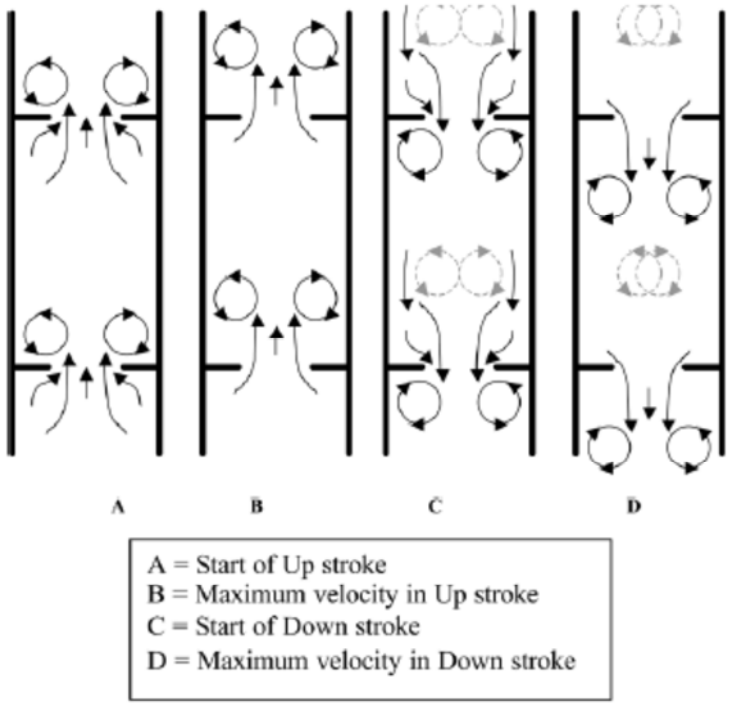

Figure IV- 1 : Movement of the flow in oscillatory baffle reactor (Mackley and Ni 1993)

The pulsatile flow is composed of a steady component and a superimposed periodical time varying component called oscillation. Consequently, the instantaneous velocity of the liquid U(t) in the column has two components: a permanent part due to the flowrate U_0 and a pulsed part due to the pulsation $U_p(t)$.

$$U(t) = U_0 + U_p(t) \qquad \textbf{(IV- 1)}$$

There are different definitions for the pulsation velocity which are discussed in part I.3.2.

The pulsation velocity averaged over a period T is called U_{pm}, the mean pulsation velocity:

$$U_{pm} = \frac{1}{T}\int_0^T U(t)dt \qquad \textbf{(IV- 2)}$$

In the operating conditions described in this paper, the U_{pm}/U_0 ratio ranges from 2 to 13. It corresponds to a pulsed flow (Legarrec, 1993). In the Nitech COBR, the optimal ratio is located between 2 and 12 (Stonestreet, 1995). In this type of flow, an inversion of the flow occurs at every half period if $U_{pm}/U_0 > 1$.

I.3. ***Parameters governing the oscillatory flow***

The oscillatory flow may be presently characterized by a few fundamental dimensionless groups:

- The classical net flow Reynolds number Re_n
- The oscillatory Reynolds number Re_o
- The Strouhal number: St

I.3.1. Net flow Reynolds number Re_n

In flow pipe, the Reynolds number Re_n is the dimensionless number used as the indicator type of flow in question and depends on the pipe diameter D, the net flow velocity U_0 and the fluids properties, υ being the kinematic viscosity:

$$Re_n = \frac{U_0 D}{\nu} \qquad \textbf{(IV- 3)}$$

I.3.2. Oscillatory Reynolds number

When an oscillatory motion is superimposed on the net flow, the oscillatory Reynolds number is defined to characterize this motion.

The pure oscillatory flow was defined in the 1940s. The pulsating Reynolds number is defined as:

$$Re_p = \frac{U_p D}{\nu} \qquad \textbf{(IV- 4)}$$

where U_p is the pulsating velocity.

Different expressions of U_p are listed in literature. It is often defined as $x_0\omega$ where x_0 is the oscillation amplitude measured centre-to-peak and ω is the angular piston velocity.

Sarpkaya (1966) defines it as the amplitude of the periodic component of the cross-sectional mean velocity.

$$U_p = \frac{\pi x_0 A_{piston}}{A_{pipe}} \qquad \textbf{(IV- 5)}$$

where A_{piston} and A_{pipe} are the cross sectional areas of the piston and tube.

For disc and doughnut pulsed column, the instantaneous pulsation velocity created by a piston mechanical device is classically given by:

$$U_p(t) = \pi A f \cos(2\pi f t) \qquad \textbf{(IV- 6)}$$

where A and f are respectively the oscillation amplitude of the fluid in the column and the oscillation frequency.

The mean flow velocity U_m is the sum of permanent flow velocity U_0 and mean pulsation velocity U_{pm}. Over a period T of oscillation, one can easily find:

$$U_{pm} = \frac{1}{T}\int_0^T U(t)dt = 2Af \qquad \textbf{(IV- 7)}$$

The pulsation Reynolds number is then written:

$$Re_p = \frac{2AfD}{\nu} \qquad \textbf{(IV- 8)}$$

Besides, Re_p may be further expressed as the product of some dimensionless characteristics, like the shape factor of the insert and the amplitude and frequency parameters, as follows:

$$Re_p = 2\ \frac{H}{D}\quad\frac{A}{H}\quad\frac{fD^2}{\nu} \qquad \textbf{(IV- 9)}$$

The pulsed flows are a superposition of the previous one and are described by the three parameters: Re, A/H or A/D and fD^2/υ. Here, A is the amplitude defined peak-to-peak. A is then equal to $2x_0$.

I.3.3. The Strouhal number

The Strouhal number St is defined as

$$St = \frac{fD}{u} \qquad \textbf{(IV- 10)}$$

u is the fluid velocity, f the frequency of the phenomenon and D is a characteristic diameter.

The Strouhal number can be important when analysing unsteady oscillating flow problems. It represents a measure of the ratio of inertial forces due to the unsteadiness of the flow or local acceleration to the inertial forces due to changes in velocity from one point to another in the flow field.

*I.4. **Energy dissipation rate***

Jealous and Johnson (1955) first evaluated the power dissipation in pulsed column using a quasi-steady state model. The model assumed that the flow is fully developed at any moment within the fluid oscillation. These authors related the instantaneous power consumption to the static pressure, to the inertia force to accelerate the liquid and to the hydrodynamic frictional force imposed by the baffle and other fittings. The power dissipation rate ε is expressed as:

$$\varepsilon = \frac{P}{\varrho V} = \frac{16\pi^2 N}{3C_d^2}\frac{\left(1 - T^2\right)}{T^2}\left(x_0 f\right)^3 \quad \textbf{(IV- 11)}$$

$(W.kg^{-1})$

where N is the number of baffled cells per unit length (m^{-1}), T fractional free area defined as $\left(\frac{D_0}{D}\right)^2$ where D_0 and D are the orifice and tube diameter (m) respectively and C_d the orifice coefficient for the flow through the baffle hole and is assumed to be 0.6 for fully developed conditions.

Baird and Stonestreet (1995) noticed that the previous law fits well at large amplitudes A and low frequency f.

For the lower amplitudes (5mm) and higher frequencies (3 to 14Hz), they proposed a new flow model based on acoustic principles and eddy viscosity:

$$\varepsilon = 1.5\frac{\omega^3 x_o^2 l}{HT} \quad \textbf{(IV- 12)}$$

$(W.kg^{-1})$

l is the mixing length (m) which is an adjustable parameter of the same order of the pipe diameter and H the baffle spacing (m)

In his PhD, Aoun Nabli (1995) establishes a correlation of the mean energy dissipation for oscillating flow in disc and doughnut columns (no net flowrate in the column). The velocity is defined as $U_p(t) = \pi A f \cos(2\pi t)$.

$$\frac{\langle\varepsilon\rangle D}{(2Af)^3} = 1.4\times 10^{3}\left(\frac{1}{h^*}\right)^{1.29}\left(\frac{1}{T^*}\right)^{1.34}\left(\frac{1}{A^*}\right)^{0.37}\left(f^*\right)^{0.62} \quad \textbf{(IV- 13)}$$

for h^*=0.156-0.406, T^*=17-40%; A^*=0.057-0.200 ; f^*=55406-124582

The different ratios are defined below:

Insert shape ratio: $h^* = \frac{H}{D}$ **(IV- 14)**

Frequency and amplitude parameters:

$$f^* = \frac{fD^2}{\nu} \quad \textbf{(IV- 15)}$$

$$A^* = \frac{A}{D} \quad \textbf{(IV- 16)}$$

I.5. ***Axial dispersion***

To ensure plug-flow condition, the axial dispersion must be minimized. Lot of work is still available in literature and it is summarized in Table IV- 2.

It provides some description of the research concerning axial dispersion in continuous pulsed column found in literature.

This list is obviously non exhaustive.

More recently, Charton *et al.* (2011) proposed an unified law for single phase axial dispersion in disc and doughnut pulsed column:

$$\frac{Af}{u} > 0.5 \text{ then } Sc = Re_p^{1.011} A'^{0.205} \max(1; h*)^{3.306} \quad \textbf{(IV- 17)}$$

$$\frac{Af}{u} < 0.5 \text{ then } Sc = 7.488.10^{-4} Re_p^{0.495}$$

Af is the oscillation velocity, u represents the inlet velocity, A' is the ratio between A*(IV-16) and h* (IV-14), Sc is the Schmidt dimensionless number defined as the ratio between the kinematic viscosity to the axial dispersion coefficient.

Re_p is a modified oscillatory Reynolds number which takes into account the aspect ratio of the column and the characteristic length is equal to H (baffle spacing) instead of the column diameter.

The discrepancy between their correlations and previous results is given in the last line of Table IV- 2.

In oscillatory baffled reactor, other studies refer to the plug flow behaviour which can be achieved. Stonestreet and Van der Veeken (1999) recommend a ratio between the pulsation velocity and the net flow velocity ranging from 2 to 6. Some authors enlarge this range up to 12.

In oscillatory baffled reactor, Mackley and Ni (1991 and 1993) and Pereira demonstrate that the amplitude oscillation presents a higher influence on the axial dispersion than the oscillation frequency.

	Disc and dougnuts pulsed column			Continuous oscillatory baffled	
	Buratti (1988)	Lanoë (2002)	Borda (1992)	Pereira (2002)	Palma and Giudici
Geometry	Cylindrical column	Cylindrical column	Annular column	Cylindrical column	Cylindrical column
RTD method	Conductimetry, radioactive tracers	Calorimetry	Conductimetry	Conductimetry	Colorimetry
D(mm)	25 to 300	15	92.5-99.5	40	39.6
H(mm)	12.5 to 50	20	28 to 33	72	25 to 100
T (%)	0.125 to 0.25	0.2	0.25 to 0.33	0.21	0.223
A*f ($cm.s^{-1}$)	0 to 7.5	1.5 to 4.8	0 to 3	0 to 72	0.1 to 11.25
SFR ($m^3.h^-$	1.5 to 53.5	5 to 25	10 to 30	24 to 91	3.2 to 9.7
h* (IV-14)	0.25 to 1.1	1.33	0.28 to 0.32	1.8	0.63 to 2.53
A*(IV-16)	0 to 1.6	0 to 6.2	0 to 1	0 to 0.6	0.126 to
f*(IV-15)	0 to 74970	33 to 225	0 to 6600	0 to 4800	313-7056
Correlations	$D_{ax} = 0.71A^{1.13}f^{0.8}H^{0.74}$	$D_{ax} = 1.129\times10^{-4}\left(\frac{A}{100}\right)^{0.83}f^{1}DST^{0.1}$		vertical $D_{ax} = 0.072(x_0 f)^{0.6}u^{0.4}$ horizontal $D_{ax} = 0.0658(x_0 f)^{0.66}u^{0.34}$	Linear relation between $D_{ax}/(uH)$ and Af/u
$\left\|\frac{D_{ax,corr} - D_{ax,exp}}{D_{ax,exp}}\right\|$	11%	21%	27%	20%	20%

Table IV- 2 : Axial dispersion correlations in literature, D is the column diameter, H the plate spacing, T the transparency factor, SFR the feed flowrate Charton et al. (2012)

I.6. ***Liquid-liquid dispersion***

As previously mentioned, the pulsed column is seen as a potential reactor, able to create but also to maintain the liquid-liquid dispersion.

In any pulsed column the drop breakage is ensured by the pulsation and also by the interactions with the different kinds of plates or packing.

As already mentioned in chapter III, the liquid-liquid dispersion is affected by:

- The physicochemical parameters: the interfacial tension σ, the dispersed and continuous phase density and viscosity, the nature of the surfactant, the dispersed phase concentration Φ
- The hydrodynamic parameters: the pulsation conditions (frequency and amplitude), the flowrate
- The geometric parameters: the kind of baffle, the baffle thickness δ, the baffle spacing H, the effect of the column diameter D…
- The material of the column

The effects of these parameters have been studied in literature and are reported in the following parts.

I.6.1. Effect of the physico-chemical parameters

Effect of the interfacial tension

In batch oscillatory baffle reactor, Ni *et al.* (1998) refers to the effect of the surfactant concentration on the liquid-liquid dispersion of the MMA monomer in the aqueous phase (for suspension polymerization). They demonstrate that whatever the surfactant concentration (i.e. a magnitude 2 in the different interfacial tension) the minimum oscillation time to obtain a stable dispersion remains the same. However, as expected, and similarly to the static mixer study in Chapter III, a lower interfacial tension leads to a narrower droplet size distribution and then to a smaller mean droplet size.

The same effect is noticed in disc and doughnut pulsed column (Torab-Mostaedi *et al.*, 2011; Jahya *et al.* 2009). Indeed, high interfacial tension systems (such as toluene/water) create larger mean droplet size than low or medium interfacial tension systems because break-up of droplets into smaller ones is limited.

Effect of the dispersed phase concentration

In pulsed column, the effect of this parameter has not been clearly exhibited. Generally for investigating this parameter in a counter-current mode, the continuous phase flowrate is kept constant whereas the dispersed phase flowrate is increased. Consequently the global flowrate increases too.

An increase of the dispersed phase flowrate and then of the dispersed phase concentration (without surfactant) lead generally to larger mean droplet size. This increase in size is emphasized for high interfacial tension systems. The mean droplet size increase is mainly due to the coalescence mechanism, and partly to the interaction with the continuous flow patterns. This result is confirmed in the work of Torab-Mostaedi *et al.* (2011).

In the COBR, the dispersed phase concentration has not been also clearly investigated. In the Pereira PhD dealing with liquid-liquid dispersion in COBR, Φ ranges from 2 to 10% in volume. The dispersed phase concentration is then defined as follows:

$$\Phi = \frac{Q_d}{Q_d + Q_c} \qquad \textbf{(IV- 18)}$$

It is a perspective of its work to evaluate the mean droplet size at higher dispersed phase ratios. Zhang *et al.*, 1999, study the effect of the dispersed phase concentration on the complete dispersion in batch oscillatory baffled reactor (Batch OBR). The oil-phase fraction ranges from 10 to 70% in volume. The same oscillation conditions for complete dispersion are found. They do not mention the mean droplet size.

I.6.2. Effect of the hydrodynamic parameters

I.6.2.1. Effect of the oscillation velocity

The mean droplet size is highly affected by the oscillation amplitude and the oscillation frequency. Depending on the authors, the amplitude and frequency do not have exactly the same role in the breakage phenomenon.

Generally, an increase of the frequency and/or the amplitude leads to smaller mean droplet size and narrower droplet size distribution. Table IV- 3 sums-up some dependency for different pulsed columns.

References	Column	System	A effect	f effect
Pereira and Ni (2000) and Pereira, PhD	Continuous OBR	Water Silicon oil	vertical $d_{32} \propto (x_0)^{-0.89}$ horizontal $d_{32} \propto (x_0)^{-0.76}$	vertical $d_{32} \propto (f)^{-0.53}$ horizontal $d_{32} \propto (x_0)^{-0.85}$
Ni *et al.* (1998)	Batch OBR	MMA Surfactant Water (recipe b)	Equal part $d_{32} \propto (x_0 f)^{-1.2}$	
Torab-Moestadi *et al.* (2011)	Disc and doughnut pulsed column	Water/toluene Water/n-Buylacetate Water/n-butanol	Investigated together D_{32} decreases with the (Af) product	

Table IV- 3: Mean droplet size evolution depending on the oscillations conditions for different pulsed column

I.6.2.2. Effect of the net flow rate

In liquid-liquid pulsed column, the continuous net flow seems to have no significant effect on the mean droplet size d_{32}. This result is largely admitted in literature (Sreenivasulu *et al.,*1997; Van Delden *et al.*, 2006; Jahya *et al.*,2009; Torab Mostaedi *et al.*,2011; Pereira PhD, 2002).

I.6.3. Effect of the geometrical parameters

Concerning oscillatory baffle reactor, lot of research allows to define the convenient geometry:

- The baffle spacing has been optimized and for this kind of reactor h* which represents the ratio between the baffle spacing and the column diameter is assumed to be 1.5 to 1.8 (Brunold *et al.* 1989). However, in their work concerning liquid-liquid dispersion, Zhang *et al.*, 1999, do not point out any effect of the baffle spacing. It is quite surprising given that baffle spacing controls the development of eddies within each baffled cavity, and then the spacing could affect the mechanism of moving fluids

from wall to the center for this type of reactor. If baffles are too close each other, the generation of vortices is subject to a strong effect of suppression. This effectively restrains the growth of the vortices, and reduces the required radial motion within each baffled cell. On the contrary, if baffle spacing are too far each other, the opposite effect occurs and vortices formed behind baffles could not effectively cover the entire inter-baffle regions. In this case, it is most likely that stagnant 'plugs' would be created, into which the vortices disperse and diminish.

- The transparency factor: A decrease of the ratio of the effective baffle orifice area to the tube area leads to smaller mean droplet size. It is related to the power input of the system.
- The baffle thickness: Ni *et al.*, 1997, and Ni *et al.* 1998, identify an optimal baffle thickness of 3mm for mixing time and dispersion stabilization in the oscillatory baffle reactor.

In disc and doughnut pulsed column, the same studies are available. Aoun Nabli (1995) studies the oscillating flow in disc and doughnut pulsed column. Depending on the baffle spacing H/D different eddy regimes are distinguished. Instable eddy regime is characterized by eddy with life time inferior to the oscillation period. They appear and disappear along the time. When an eddy is contained in each compartment and its position and size evaluate without disappearing, the regime is stable. Oh (1983) and Legarrec (1993) observed experimentally and numerically the transition regime in column with relatively low H/D ratio (0.156 and 0.234) by changing the oscillation conditions.
Aoun Nabli observed only the instable regime at low H/D ratio and the stable regime at high H/D ratio.

I.6.4. Effect of the material

The optimum baffle material depends on the phases nature. Collisions of drops against internal walls and discs or doughnuts play an important role in the evolution of the hydrodynamic properties. The measurement of the adhesion work could be helpful in order to study the removal of a drop from a plate (Mate *et al.* 2000).
It relies on the Young equation $\gamma_{LV} \cos\theta = \gamma_{SV} - \gamma_{LS}$ where θ is the contact angle between the droplet and the surface, γ_{LV} is the surface tension between the liquid and vapor ($N.m^{-1}$), γ_{LS} is the surface tension between the liquid and the solid ($N.m^{-1}$) and γ_{SV} the surface tension between the vapor and the solid ($N.m^{-1}$).

The Young Dupré equation allows the calculation of the adhesion work plate or free surface energy W_{LS} ($N.m^{-1}$)(Hüttinger *et al.* 1992).

$$W_{LS} = \gamma_{LV}(1 + cos\,\theta) \quad \textbf{(IV- 19)}$$

Ousmane *et al.* (2011) take into account the adhesion work in the mean droplet size correlation and hold-up and extraction efficiency.

I.7. ***Modeling of the mean droplet size d_{32} in pulsed column***

Lots of correlations are available in literature to predict the mean droplet size in pulsed columns. Most of them deal with counter-current flow. Some others correspond to the continuous oscillatory baffle reactor (Nitech).

Some of the most important correlations are listed in Table IV- 4. Different dimensionless numbers are taken into account depending on the hydrodynamics, the physico-chemical parameters (interfacial tension, viscosity and density) and the packing geometry.

References	System	Flow	Correlations
Kumar and Hartland 1986 and 1996		Counter current pulsed sieve plate column	$\frac{d_{32}}{\sqrt{\sigma/\Delta\rho g}} = 1.35\varepsilon^{0.4}\left(h_c\frac{\sqrt{\rho_* g}}{\sigma_*}\right)^{0.18}\left(\frac{\mu_d g^{1/4}}{\rho_*^{1/4}\sigma_*^{3/4}}\right)^{0.14}\left(\frac{\sigma}{\sigma_*}\right)^{0.06}\times\left[0.23+exp\left(-26.66\frac{Af^2}{g\varepsilon}\right)\right]$ $\varepsilon = \frac{2\pi^2\left(1-e^2\right)}{3e^2C_0^2h_C}(Af)^3$ $\frac{d_{32}}{H} = \frac{C_\Psi e^n}{\frac{1}{C_\Omega\left(\frac{\sigma}{\Delta\rho g H^2}\right)^{0.5}} + \frac{1}{C_\Pi\left[\left(\frac{\varepsilon}{g}\right)\left(\frac{\Delta\rho}{g\sigma}\right)^{0.25}\right]^{n_1}\left[H\left(\frac{\Delta\rho g}{\sigma}\right)^{0.5}\right]^{n_2}}}$
Van Delden et al. (2006)		Counter current disc and doughnut pulsed column	$\frac{d_{32}}{\sqrt{\sigma/\Delta\rho g}} = C_1 e^{n_1}\left(h_c\frac{\sqrt{\rho_* g}}{\sigma_*}\right)^{n_2}\left(\frac{\mu_d g^{1/4}}{\rho_*^{1/4}\sigma_*^{3/4}}\right)^{n_3}\left(\frac{\sigma}{\sigma_*}\right)^{n_4}\times\left[C_2+exp\left(C_3\frac{Af}{e(\sigma_* g/\rho_*)^{1/4}}\right)\right]$ C_1, C_2, C_3, n_1, n_2, n_3 and n_4 are respectively 2.84, 0.16, -2.59, 0.30, 0.18, 0.14, 0.06 ϱ_* and σ_* : density and surface tension of water at 20°C
Torab-Mostaedi,M., 2011	Without mass transfer	Counter current Disc and doughnut pulsed column	$\frac{d_{32}}{\sqrt{\sigma/\Delta\rho g}} = 33.53\times10^{-3}\left(\frac{Af^4}{g\sigma}\right)^{-0.283}\left(\frac{d_a\rho_c\sigma}{\mu_c^2}\right)^{0.29}\left(\frac{\rho_c\sigma^4}{\psi\mu_c}\right)^{-0.13}\left(\frac{\Delta\rho}{\rho_c}\right)^{2.86}\left(\frac{\mu_d}{\mu_c}\right)^{0.085}\left(\frac{h_c}{d_a}\right)^{-0.734}(1+R)^{0.34}$ $\psi = \frac{2\pi^2\left(1-e^2\right)}{3e^2C_0^2h_C}(Af)^3$ H_c : compartment height ; e: fractional free area; C_0 orifice coefficient;D_a doughnut aperture diameter; R: flow ratio

Pereira and Ni 2001	Without surfactant	Co current continuous oscillatory baffled reactor	$d_{32} = 1.72\times10^{-2}\ Re_0^{-0.91}\ Re_n^{-0.42}$ (m) $d_{32} = 3.7\times10^{-5}\varepsilon^{-0.3}\varepsilon_n^{-0.14}$, $3.18 \le \varepsilon \le 25$ W.kg^{-1} ε energy dissipation due to power input;ε_n energy dissipation due to the net flow
Pereira , PhD, 2002	Without surfactant		Vertical COBR - Riser $\frac{d_{32}}{D} = 0.40(\pm 54\%)\ Re_0^{-0.57(\pm 17.72\%)}\ Re_n^{0.31(\pm 12.25\%)}$ (R_2=0.744) - downcomer : $\frac{d_{32}}{D} = 1.24(\pm 41.88\%)\ Re_0^{-0.66(\pm 10.9\%)}\ Re_n^{0.29(\pm 15.65\%)}$ (R_2=0.867) Horizontal COBR $\frac{d_{32}}{D} = 107\ Re_0^{-0.90}\ Re_n^{0.13}$

Table IV- 4 : mean droplet size expression in different pulsed column

Other papers are available in literature based on the use of the population balance equation, able to predict the drop size distribution, provided that break-up and coalescence models are provided (Gourdon and Casamatta, in Liquid-liquid extraction equipment, ed. by Godfrey and Slater, 1994).

The originality of the work proposed in the following section concerns the study of liquid-liquid dispersion in disc and doughnut pulsed column. The literature is relatively extended concerning oscillatory baffled reactor (OBR) even if it is often limited to batch or liquid-liquid system without surfactant. As for discs and doughnuts pulsed column, few studies concern upward co-current flow.

Two configurations are studied: the first concerns the disc and doughnut vertical pulsed column and the second is related to the horizontal oscillatory baffled reactor. The two equipments will be obviously compared in term of mean energy dissipation rate.

II. LIQUID-LIQUID DISPERSION IN UP-FLOW DISCS AND DOUGHNUTS PULSED COLUMN

This section is divided into three parts. First, the experimental rig and preliminary studies are presented. Then, the operating conditions are described as well as the different results. The effect of hydrodynamics, physico-chemical and insert material parameters are pointed out and finally discussed.

II.1. ***Material and method***

II.1.1. Experimental rig

The experimental set-up consists of a 3 m long column of 50mm internal diameter D_c packed with immobile discs and doughnuts equally alternated and spaced (H=24mm) made of stainless steel or PTFE. Whatever the insert materials, the open free area T (transparency factor) is of 26%. The internals are mounted horizontally and centered with respect to the column axis. A stage consists of two rings and a disc between them. The outer edge of the rings is extended to the column wall. The flow follows two passages: a central passage through the ring aperture and a peripheral passage between the disc edge and the column wall.

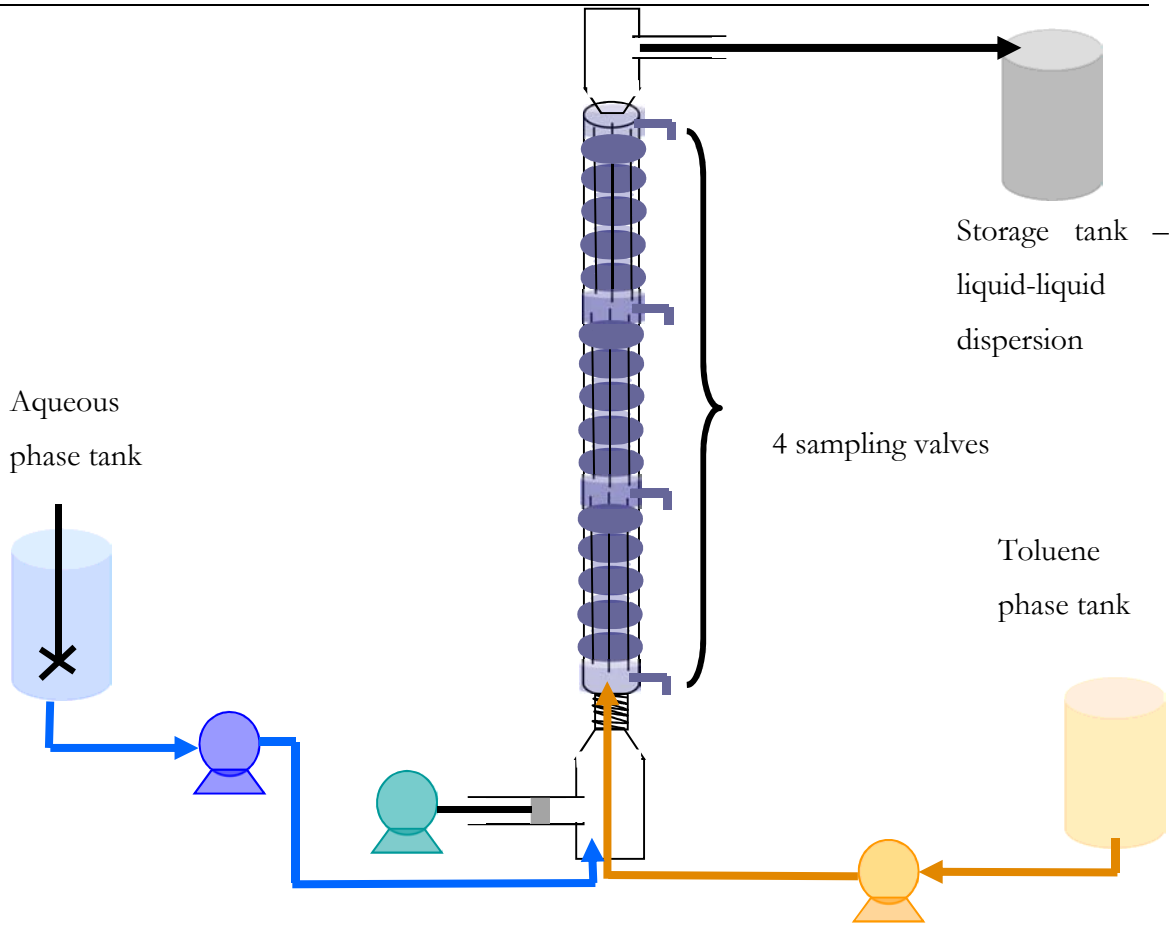

Figure IV- 2: Experimental rig of the disc and doughnut pulsed column

The aqueous phase is prepared in a 220L tank and consists in mixing the water and the surfactant. The toluene is stored in a tank of 200L. Each tank is put on a balance in order to control the flowrates for each test. The two flows are pumped thanks to membrane pumps at the bottom of the column. The feed lines are equipped with anti-pulsatory balloons which absorb the pulsation due to the volumetric pumps and then ensure a constant flowrate. The two liquids are flowing upwards co-currently. The pulsation is imposed via a pump without check valves allowing the control of the oscillation amplitude, A, via the pump vernier and of the oscillation frequency,f , thanks to the variable frequency regulator. This system provokes reciprocal up and down movements of the fluids. Different samples are collected all along the column: at the basis (generation of the dispersion at the first doughnuts) and after every meter. The different samples will be characterized in term of droplet size distribution.

The amplitude A corresponds to the total displacement of the flow. In our case, the minimum amplitude corresponds to the length between a disc and a doughnut H_{min} and the maximum amplitude correspond to the distance between 2 successive discs $D_{di\text{-}di}$ or a doughnut-doughnut distance $D_{do\text{-}do}$, H_{max}.

D_a is the inner diameter of the ring aperture, D_d is the disc diameter. The disc diameter is larger than the ring aperture in order to hamper a direct flow along the axial direction.

The characteristics of the different internals (disc and doughnut) are summed-up in Table IV-5

D_c (mm)	50
D_d (mm)	43
D_a (mm)	25
H_{min} (mm)	24
H_{max} (mm)	52

Table IV- 5: discs and doughnuts insert characteristics

The dispersed phase concentration in volume, Φ, is fixed thanks to the respective phases flowrates as follows:

$$\phi = \frac{Q_d}{Q_d + Q_c} = \frac{Q_d}{Q_{tot}} \quad \textbf{(IV- 20)}$$

where Q_d, Q_c and Q_{tot} are respectively the dispersed phase, continuous phase and total volume flowrates. In the co-current up-flow, this relationship assumes that there is no relevant slip velocity.

II.1.2. Stability of the emulsion

The two tested Water/Surfactant/Toluene systems (chapter II) may exhibit a creaming phenomenon. This phenomenon can start a few minutes after emulsification. If creaming is a reversible phenomenon, it may also be followed by some irreversible behavior such as coalescence or Ostwald ripening.

Figure IV- 3 illustrates the comparison between droplets size distributions obtained through laser diffraction analysis several minutes after the experiment and nearly 24 hours after for the Water/PVA/Toluene system with PTFE insert. These distributions are almost superimposed, what reveals that no irreversible phenomenon occurred. The same results are obtained for the other systems. The two systems investigated here are quite stable during at least 24 hours.

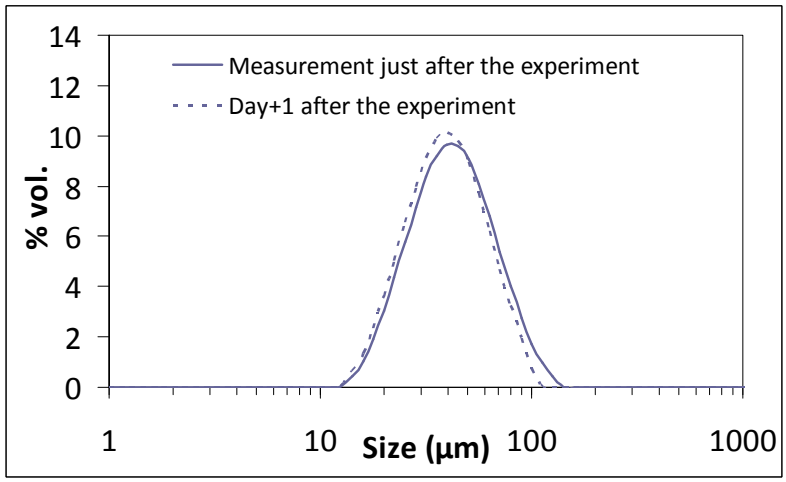

Figure IV- 3: Comparison of two droplet size distribution after the experiment and 24h after. Q_{tot}=85 L.h^{-1}, A=52mm, f=1.56Hz, H=1m, Φ=25%, 3m of PTFE insert

Besides, it is clearly exhibited that it is possible in the pulsed column to obtain droplet sizes right in the range expected for the process, i.e. 10 to 100 µm.

The liquid-liquid dispersions have also been observed through microscopy to control the type of dispersion obtained (Figure IV- 4 and Figure IV- 5).

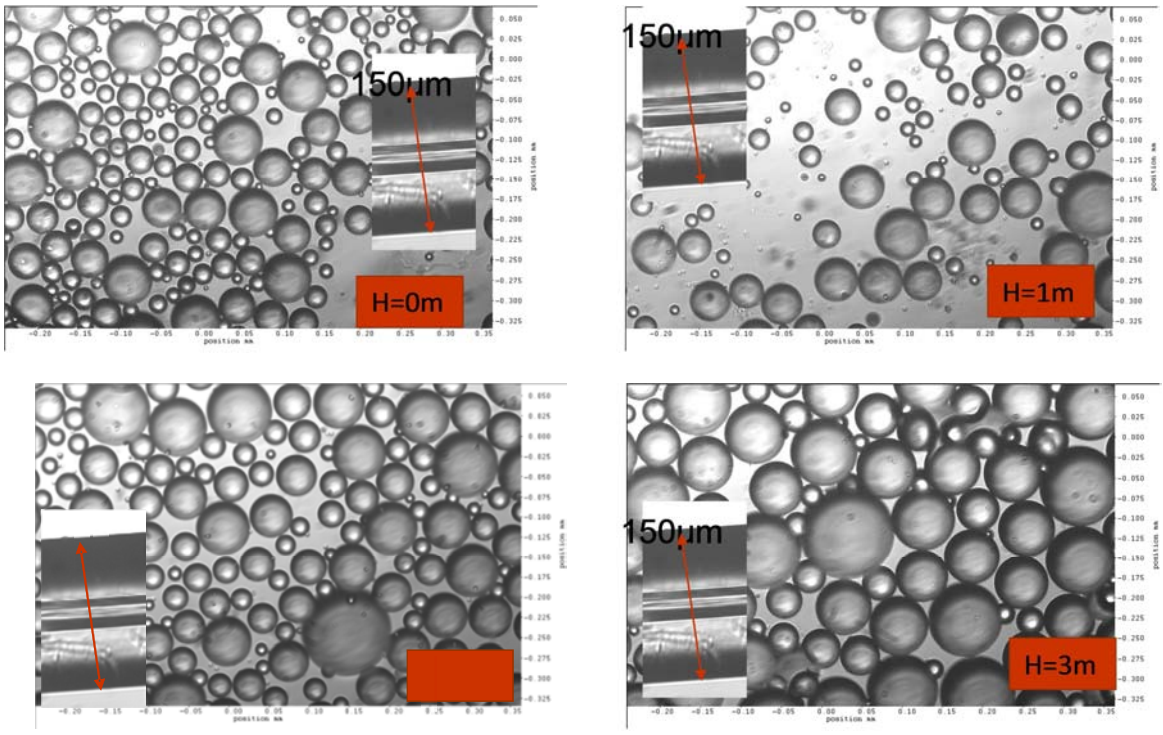

Figure IV- 4 : Water/PVA/toluene sytem, Φ=25%, Q_{tot}=85 L.h^{-1}, A=52mm, f=1.56 Hz, PTFE insert, diluted sample

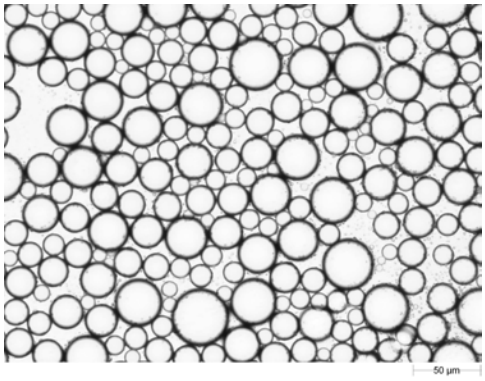

Figure IV- 5 : Water/SDS/toluene system, Φ=40%, Q_{tot}=141L.h^{-1}, H=1, A=38mm, f=1.56Hz, PTFE insert, diluted sample

The droplets are well spherical and the dispersions obtained are of the oil in water type.

II.1.3. Repeatability studies

Table IV- 6 sums-up the characteristic diameters d_{32} and d_{90} obtained for three tests performed in pulsed column with the water/SDS/toluene system under the same operating conditions. The mean characteristic diameters variation is satisfactory.

	Axial position	**Test SDS-Rep1**	**Test SDS-Rep2**	**Test SDS-Rep3**	**Error to the mean value %**
d_{32} (µm)	0	18.5	19.8	19.4	3.8
	1	18.8	18.1	20.3	1.4
	2	25.7	22	24.6	6.6
	3	51.9	46	46.1	8.1
d_{90} (µm)	0	39.4	43.6	45.2	8
	1	39.1	37	41.3	0.1
	2	55.5	45.2	50.4	10.2
	3	90.8	82.6	82.4	6.5

Table IV- 6 : Repeatability Q_{tot}=85 L.h^{-1}, A=52mm, f=1.56Hz, Φ=25%, PTFE insert

In the same way, the Figure IV- 6 presents the droplet size distribution evolution for the water/PVA/toluene system with stainless steel inserts for different operating conditions.

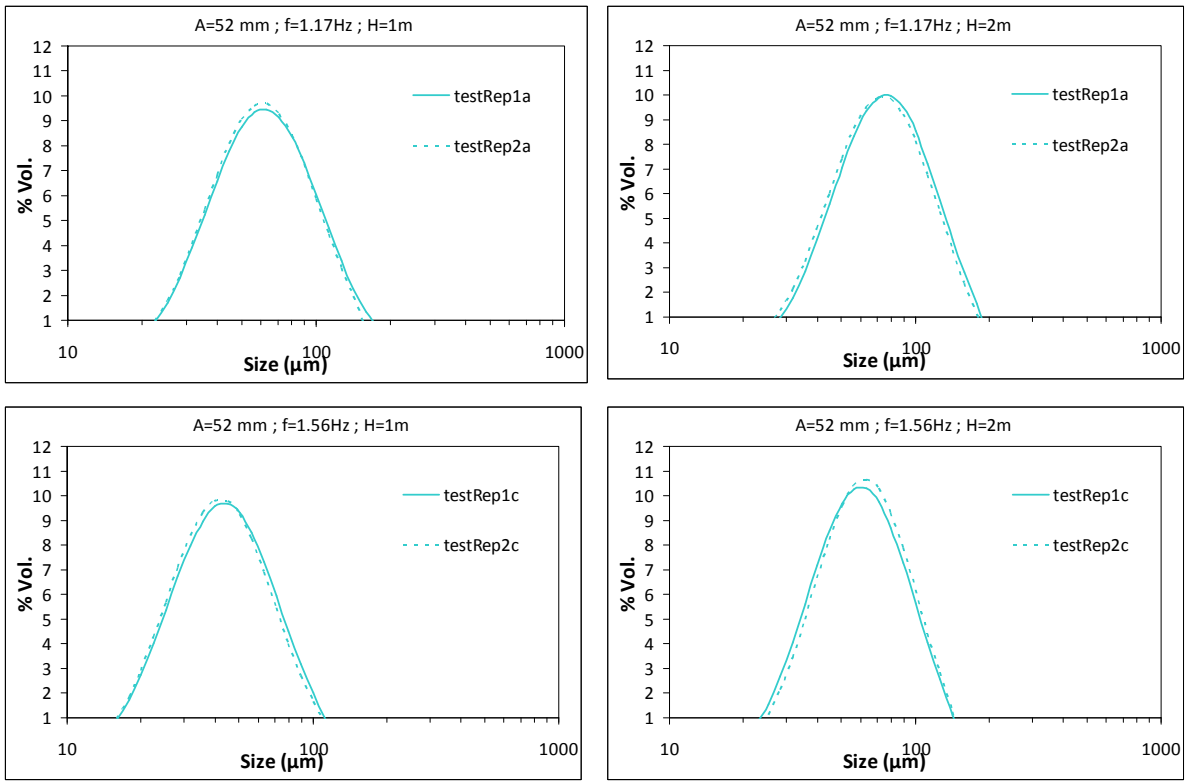

Figure IV- 6 : Water/PVA/Toluene system, Φ=25%, stainless steel insert, Q=85L.h^{-1}, different oscillation conditions and sample positions

The droplet size distributions overlap each other. No significant difference is observed.

II.2. *Operating conditions*

The operating conditions tested for the two systems are summarized in Table IV- 7.

Systems	Material	Height of inserts	Dispersed phase inlet	Φ(% vol.)	Q_{tot} ($L.h^{-1}$)	A (mm)	f (Hz)
Water/PVA/Toluene	Stainless steel	3 m	Bottom	25	85-141-226	24-38-56	1.17-1.56-
				8	141	24-38-52	1.56
		1 m		25	85-141-226	24-38-52	1.17-1.56
	Without insert	0 m			85-141-226	38-52	1.17-1.56
	PTFE	1 m			85-141-226	24-38-52	1.17-.56
		3 m			85-141-226	24-38-52	1.17-1.56
					300-350-375	0	0
				40	85-141-226	24-38-52	1.17-1.56
			After 1m	25	85-141	24-38-52	1.56
			After 2m		85	24-38-52	1.56
Water/SDS/Toluene			Bottom		85-141-226	24-38-52	1.17-1.56
				40	85	24-38-52	1.17-1.56
					141	38	1.56

Table IV- 7 : Operating conditions

The flowrate is chosen to avoid settling of a 150µm PVC particle. The flow velocity has to be much larger than the terminal velocity of a single particle calculated by applying Stockes' law.

II.3. Effects of the different parameters

II.3.1. Effect of the inlet conditions

The inlet of the toluene phase is placed at different positions all along the column. It is introduced at the bottom of the column (H=0m), after 1 or 2 meter of insert (H=1m and H=2m). The insert is made of PTFE.

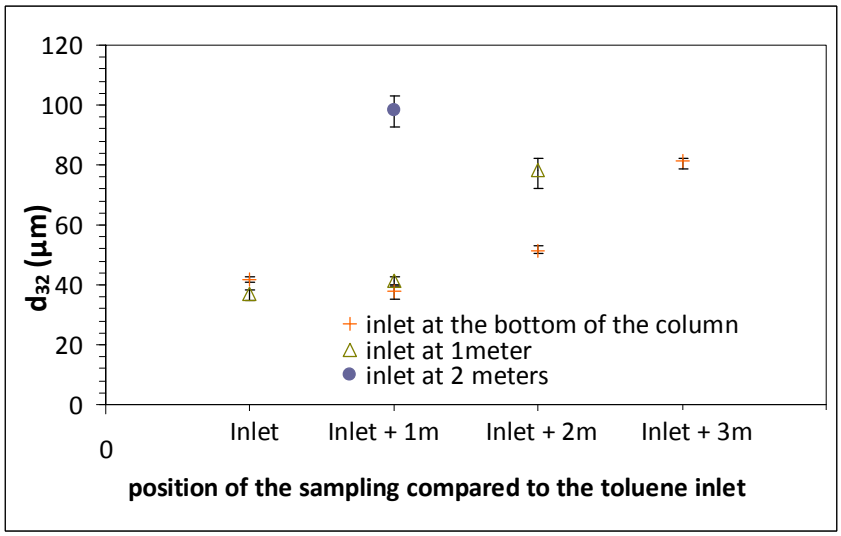

Figure IV- 7: Evolution of the Sauter mean diameter along the column for different toluene inlet positions, Water/PVA/Toluene system at Φ=25% and 3m height of PTFE insert, Q_{tot}=85L.h^{-1}, A=52mm, f=1.56Hz

In the Figure IV- 7, the mean diameter evolution is presented as a function of the corresponding position of the sample If the inlet intervenes at the bottom of the column, there are four sample positions: at the inlet (H=0m), after 1 meter (H=1m), two meters after the inlet (H=2m) and three meters after the inlet (H=3m). In the same way, if the inlet is located after 1 meter of insert, the sampling are located at H=1m (inlet), H=2m (one meter after the inlet) and at H=3m (two meter after the inlet). The mean droplet sizes obtained are the same at the inlet and at the inlet + 1m for the plus and empty triangle series. As can be seen, for an inlet after 2 meters of insert (full black circle), the measurement performed at inlet +1 m corresponds to a sampling at the top of the column and the results doesn't fit at all with the other measurements. The same discrepancy is observed at inlet+2m which corresponds to the sample at H=2m for the plus series and H=3m for the empty triangle one. It seems obvious that this sampling caused some trouble in the interpretation of the results obtained. Indeed, the third meter sampling is located close to the disengagement part of the column, where the velocity decreases (due to the larger section of the settler) compared with the

velocity inside the column section. Consequently for the end of this chapter, this sampling will be considered as unreliable.

II.3.2. Effect of the hydrodynamic parameters

For this part, the results refer to the water/PVA/toluene system.

II.3.2.1. Effect of the oscillation parameters

The oscillations are due to the product of the amplitude and of the frequency. Figure IV- 8 represents the droplet size distribution for different oscillation velocities under the same other operating conditions at a sampling position after one meter of insert. The oscillation velocity is simply defined here as the Af product.

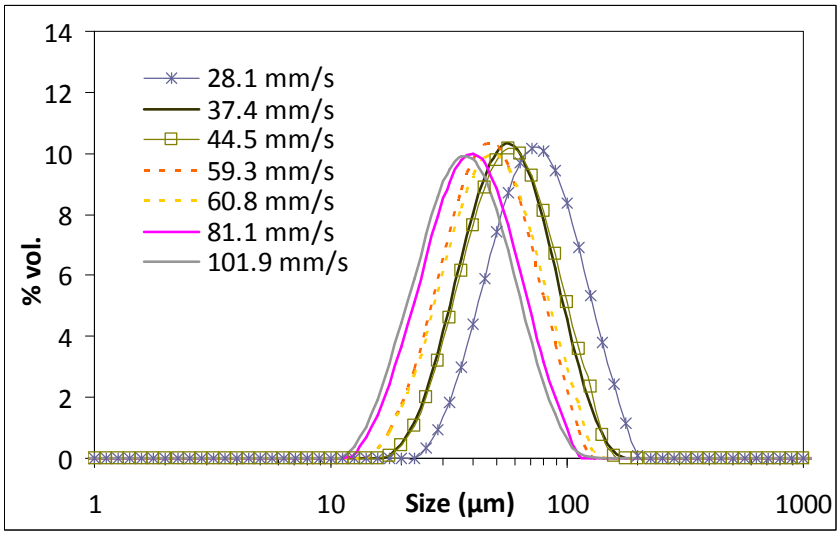

Figure IV- 8 : droplet size distributions evolution with the Af product (system water/PVA/toluene, Q_{tot}=85 $L.h^{-1}$, Φ=0.25, H=1m, bottom introduction, 3m of PTFE insert)

Increasing the oscillation rate leads to a smaller mean droplet size d_{32} and to the shifting to the left of the droplets size distribution because of the breakage predominance. This result is in agreement with all the results presented in literature (see part I.6.2.1).

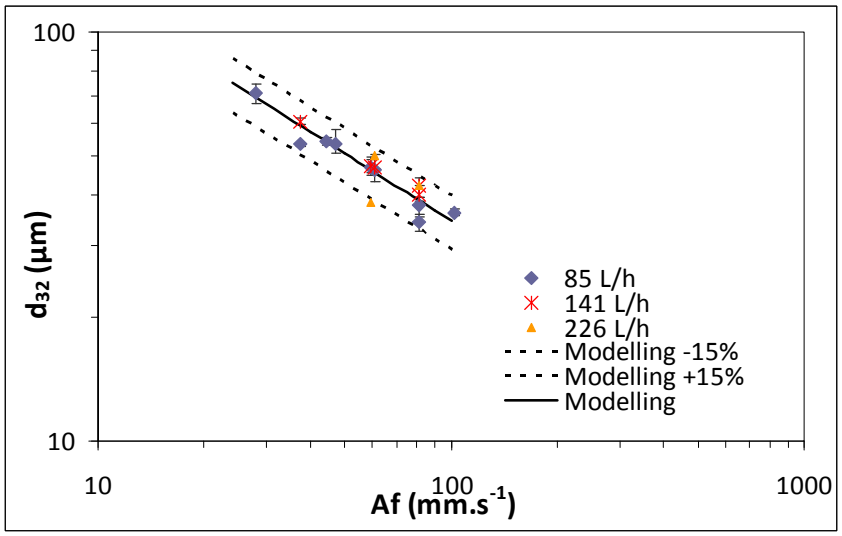

Figure IV- 9: evolution of the mean droplet diameter with the Af product (system water/PVA/toluene, Φ=0.25, H=1m, bottom introduction, 3m of PTFE insert)

In Figure IV- 9, the resulting Sauter diameters after one meter of insert are represented versus the Af product. The mean droplet size evolution follows a decreasing power law with an exponent of -0.54 whereas the Kolmogorov theory predicts a decreasing power law with a -1.2 exponent.

The modeling is checked at more or less 15% which is really good in our conditions.

Consequently, it is confirmed that the Af product plays a major role in the breakup phenomenon.

II.3.2.2. Effect of the total flowrate

Without pulsation

At a flowrate inferior to 300 $L.h^{-1}$, that is to say a net flow Reynolds number of 2190, the droplet created are too coarse and no sampling was taken to analyse the droplet size distribution due to the instability of the dispersion. By increasing the flowrate from 300 to 375 $L.h^{-1}$ (Re_n=2675), no influence of the flowrate is noticed (Figure IV- 10).

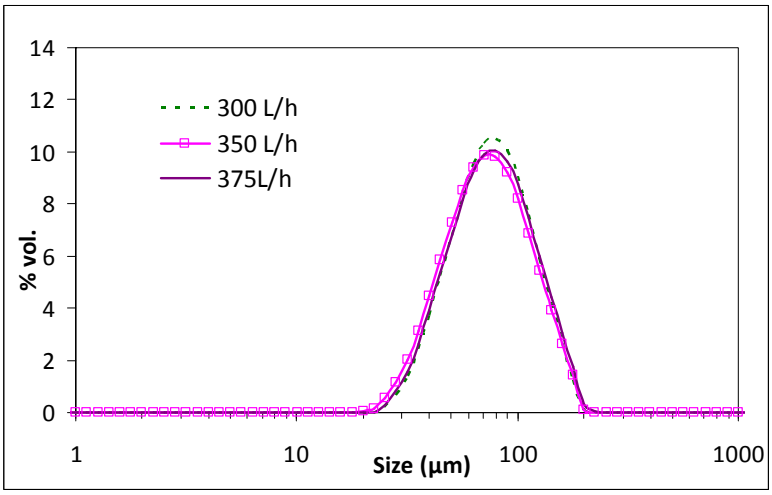

Figure IV- 10 : droplet size distributions evolution with the total flowrate Q_{tot} (system water/PVA/toluene, without pulsation, Φ=0.25, H=1m, bottom introduction, 3m of PTFE insert)

On the first meter, the droplet size is imposed by the droplet generation conditions and the physico-chemical parameters of the system.

Regarding the mean droplet size evolution along the column, no relevant difference according to the flowrate is noticed in Figure IV- 11.

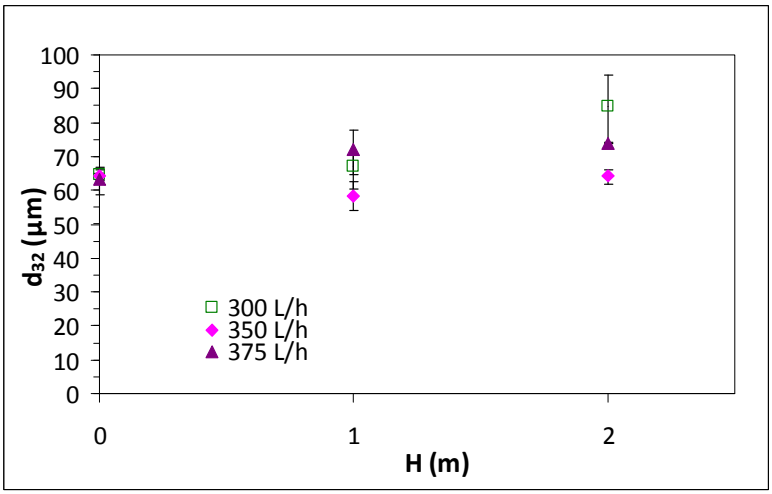

Figure IV- 11: evolution of the mean droplet size all along the column, without pulsation, (system water/PVA/toluene, without pulsation, Φ=0.25, H=1m, bottom introduction, 3m of PTFE insert)

With pulsation

Under pulsed conditions, three different flowrates are tested corresponding to 3, 5 and 8 times the terminal velocity (u_t=4mm.s^{-1}) of a PVC particle of 150µm.

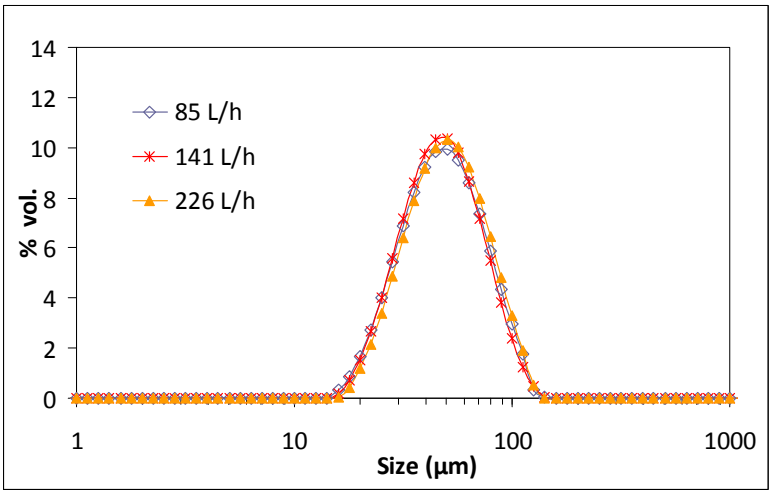

Figure IV- 12 :droplet size distributions evolution with the total flowrate Q_{tot} under the same pulsation conditions (system water/PVA/toluene, A=52mm, f=1.17Hz, Φ=0.25, H=1m, bottom introduction, 3m of PTFE insert)

No effect of the flowrate under pulsation conditions is pointed out in Figure IV- 12. The droplet size distributions are perfectly superimposed. The same results are obtained for the whole pulsed conditions investigated. The results are in accordance with the literature results (part I.6.2.2).

II.3.3. Effect of the physico-chemical parameters

II.3.3.1. Effect of the surfactant

The interfacial tension evaluation and evolution have been presented in chapter II. Even if the two involved surfactants lead to the same equilibrium interfacial tension value (ie. 3.5 $N.m^{-1}$ see table II-2, chapter II), the overall adsorption kinetics of these two molecules are different, as well as their nature (PVA: polymeric and non-ionic, SDS: molecule anionic).
A simple comparison under identical operating conditions is given on Figure IV- 13. The SDS provides the smallest droplet sizes (filled symbols).

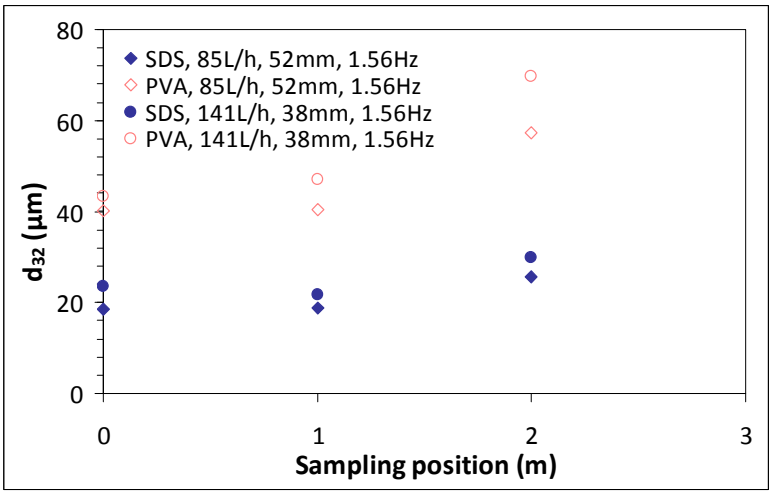

Figure IV- 13: evolution of the mean droplet size under different condition for the both systems (Φ=0.25, bottom introduction, 3m of PTFE insert)

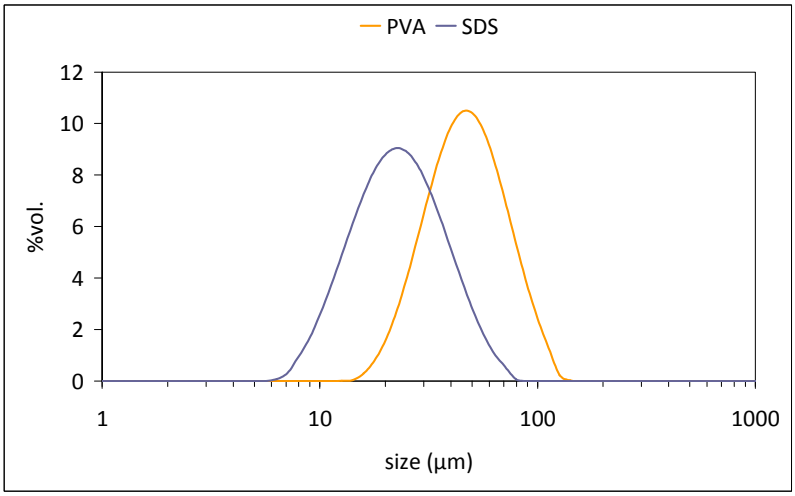

Figure IV- 14: Comparison of the droplet size distribution for the both systems at same other operating conditions (Φ=0.25, bottom introduction, 3m of PTFE insert, Q_{tot}=141 L.h^{-1}, A=38mm, f=1.56 Hz)

Regarding Figure II-10 (chapter II) which represent the evolution of the interfacial tension along the column, the PVA interfacial tension is higher than the SDS interfacial tension value in the residence time range. The droplet size difference between the two systems is related to this different evolution of the interfacial tensions.

Provided that the surfactant concentration is above the CMC, the superficial excess concentration and interfacial molecular area are given in Table IV- 8.

The excess concentration is defined by the Gibbs equation:

$$\Gamma = -\frac{1}{RT}\frac{d\sigma}{d\ln c} \qquad \textbf{(IV- 21)}$$

For polymeric compounds, the Gibbs equation can be applied to polymer with the following formula (Nahringbauer, 1995):

$$\Gamma = -\frac{\overline{M_{sequence}}}{RT}\frac{d\sigma}{d\ln c} \quad \textbf{(IV- 22)}$$

It corresponds to the concentration of the surfactant at the interface when it is just recovered by the molecules. This concentration is superior in the case of PVA.

	System SDS	System PVA
Excess concentration Γ	0.59	0.87
Interfacial molecular area A (Å^2.molecule^{-1})	80.9	3499

Table IV- 8: calculation of the excess concentration Γ and of the interfacial molecular area A for both systems

A, the area occupied by a surfactant molecule at the liquid-liquid interface, can be deduced from the excess concentration Γ. A PVA molecule required a larger space compared to a SDS molecule.

Consequently, less PVA molecules are required to stabilise the interface. However, given that the sterical cluttering, the droplet sizes obtained are larger with PVA than with SDS. Due to the largest size of the PVA molecule, the surfactant adsorption is followed by a rearrangement of the molecule at the interface.

Finally, all the previous comments confirm the larger droplet size obtained with the PVA surfactant.

II.3.3.2. Effect of the dispersed phase concentration

The dispersed phase concentration can affect the mean droplet size. It is a relevant parameter in batch process.

Figure IV- 15 shows a difference of the droplet size distribution between low dispersed phase (8%) and higher dispersed phase concentrations (25% and 40%). At 8% in vol., a lower coalescence frequency can be assumed. It increases above and in the same range for the two other dispersed phase fractions investigated. Indeed, the number of droplets per unit volume increases as well as the number of collisions. Despite the presence of surfactant, some of them are successful and lead to coalescence. However no relevant difference is noticed between 25 and 40% of dispersed phase concentration.

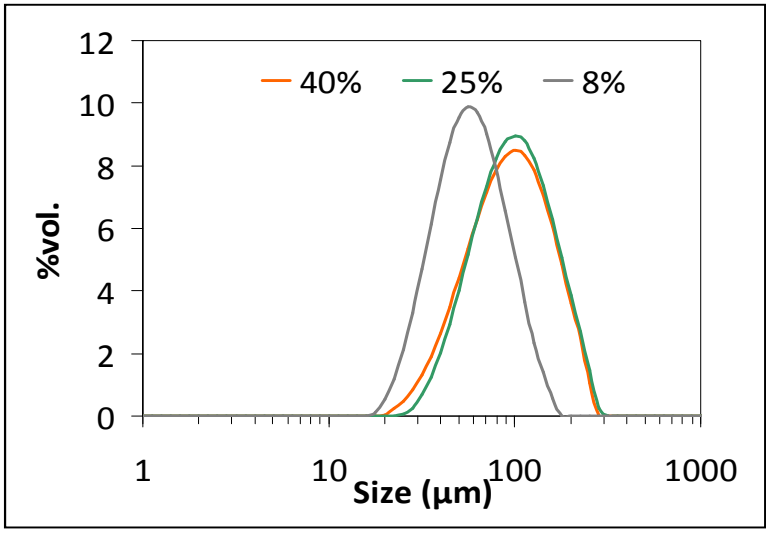

Figure IV- 15 : Droplet size distribution for the three dispersed phase concentration (bottom introduction, 3m of stainless steel insert, Q_{tot}=141 L.h^{-1}, A=24mm, f=1.56Hz, sampling after on meter of insert H=1m)

Figure IV- 16 presents the Sauter diameters at a given flowrate for three meters of stainless steel insert, different pulsation conditions and water/PVA/toluene.

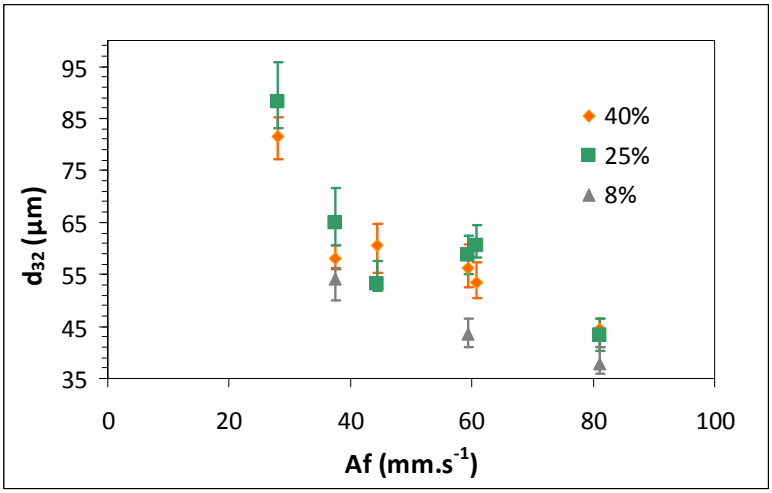

Figure IV- 16: Sauter mean droplet size evolution with the Af product for the three dispersed phase concentrations (bottom introduction, 3m of stainless steel insert, Q_{tot}=141 L.h^{-1}, H=1m)

For a dispersed phase concentration of 8%, the Sauter mean diameter is slightly inferior to the Sauter mean diameter obtained with the other dispersed phase concentration conditions. No significant difference is noticed between the two higher dispersed phase concentrations.

In conclusion, at high concentrations (superior than 25%up to 40%), it is expected to have no major influence on the drop size distribution, provided that it results from an equilibrium between breakage and coalescence. On the opposite, the size distribution seems to be sensitive to coalescence when the dispersed phase fraction is varying from some percent to 25% in volume.

II.3.4. Effect of the insert

These results are reported with the Water/PVA/Toluene system. Two parameters have been studied here: the insert dimension (height) and the nature of the insert (stainless steel or PTFE).

II.3.4.1. Height of the insert

Three configurations have been studied concerning the effect of the height of the insert on the mean droplet size and on the droplet size distribution. The results are presented without insert, with insert on the first meter of the column and with insert all along the column.

The objective is to check whether insert is necessary or not, and if yes, to determine the insert height sufficient to create and maintain the expected size distribution.

Without insert

Figure IV- 17 presents the evolution of the mean droplet size along the column without insert. The oscillation conditions have no effect on the Sauter mean droplet size. It is only controlled by the physico-chemical parameters of the systems and by the inlet phase conditions. The Sauter mean droplet size evolves along the column from 55µm to 80µm.

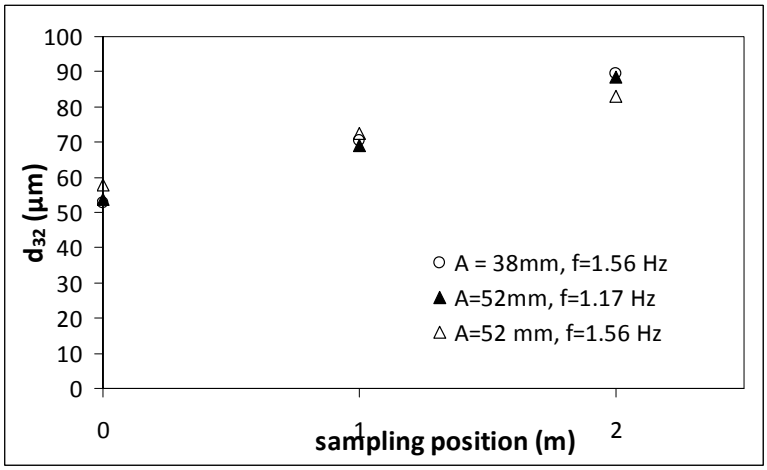

Figure IV- 17: Mean Sauter diameter evolution along the column for different pulsation condition at Φ=0.25, Q_{tot}= 85L.h^{-1} bottom introduction, without insert

With stainless steel insert

Figure IV- 18 and Figure IV- 19 present both evolutions of Sauter diameters and droplet size distribution for a stainless steel 3 m insert. The left graph (a) presents the mean droplet size all along the column for different pulsation conditions. On the right part (b), the graph corresponds to DSD obtained at the first meter sampling.

The insert is made of stainless steel. With insert all along the column (Figure IV- 18), the pulsation is the main parameter which affects the drop breakage.

However, with just one meter of insert (Figure IV- 19), the oscillation conditions seem to have no effect. All the mean droplet size and droplet size distributions are superimposed which suggests a breakage control by the inlet conditions and the physico-chemical parameters of the system.

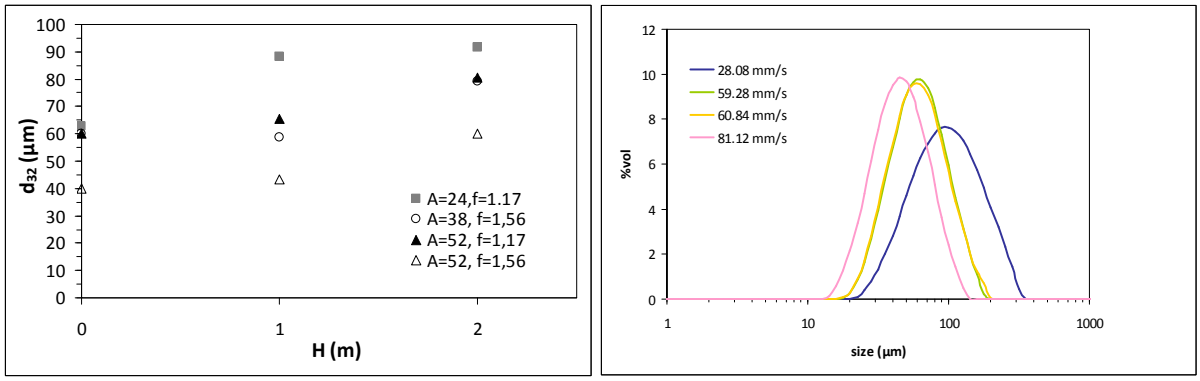

Figure IV- 18: (a) Mean Sauter diameter evolution along the column for different pulsation condition at Φ=0.25, Q_{tot}= 85L.h^{-1} bottom introduction, 3m of stainless steel insert and (b) droplet size distribution for the corresponding Af product at H=1

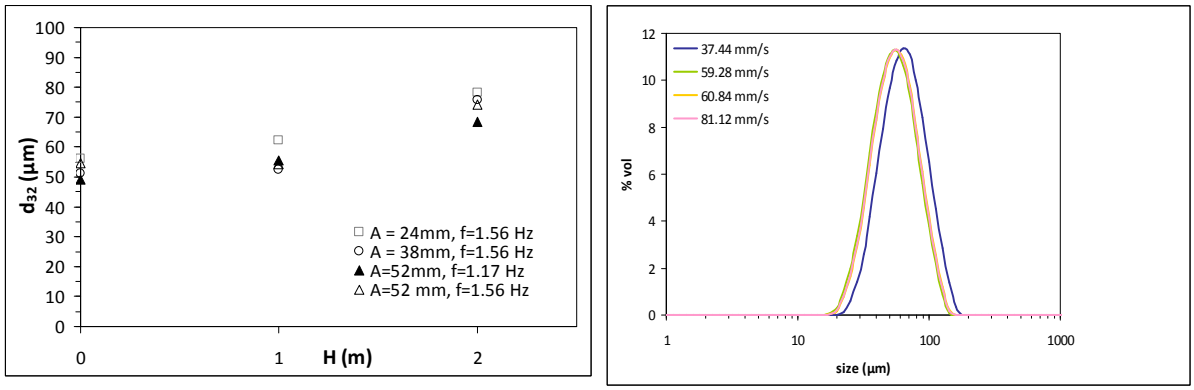

Figure IV- 19: (a) Mean Sauter diameter evolution along the column for different pulsation condition at Φ=0.25, Q_{tot}= 85L.h^{-1} bottom introduction, 1m of stainless steel insert and (b) droplet size distribution for the corresponding Af product at H=1

With PTFE insert

Now, in the case of PTFE insert, both heights of insert and operating conditions control the mean droplet size (Figure IV- 20). Indeed, an increase of the oscillation velocity as well as an increase of the insert height contributes to the decrease of the mean droplet size as observed. (Figure IV- 20 a and b Figure IV- 21). The PTFE is known to be an inert material whereas the stainless steel properties may evolve with the time (from hydrophilic to hydrophobic). Consequently, in case of PTFE insert, the hydrodynamics conditions are expected to control the mean droplet size, much more than in the case of stainless steel.

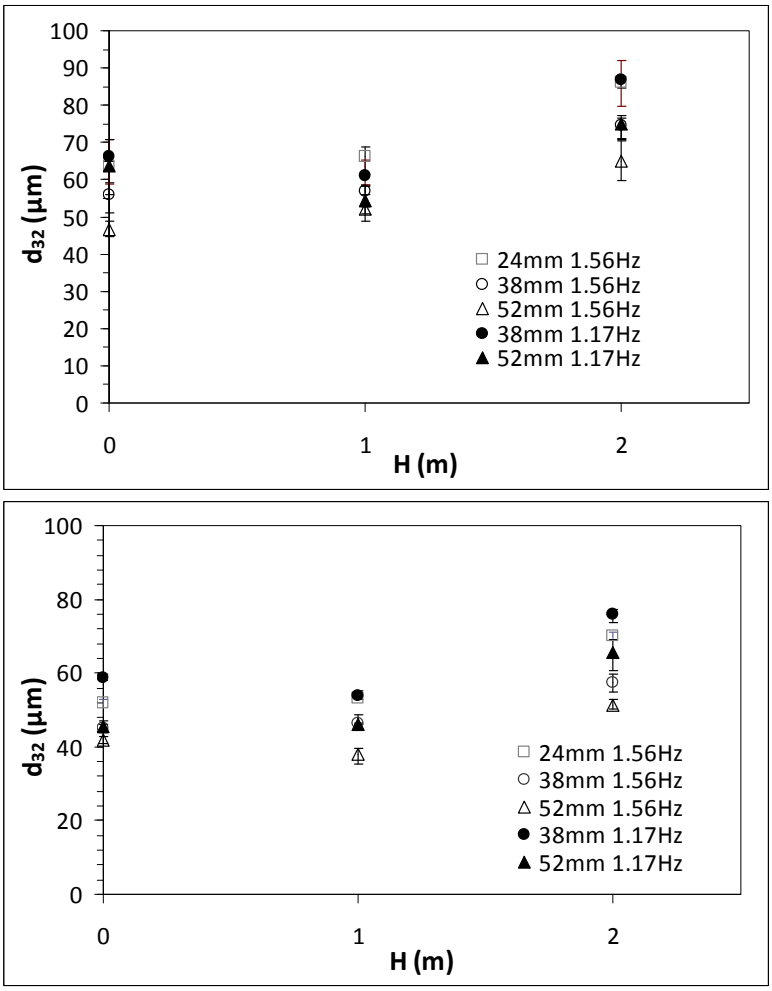

Figure IV- 20 : Mean Sauter diameter evolution along the column for different pulsation condition at Φ=0.25, Q_{tot}= 85L.h^{-1} bottom introduction, with PTFE insert on (a) 1meter height and (b) on three meter height

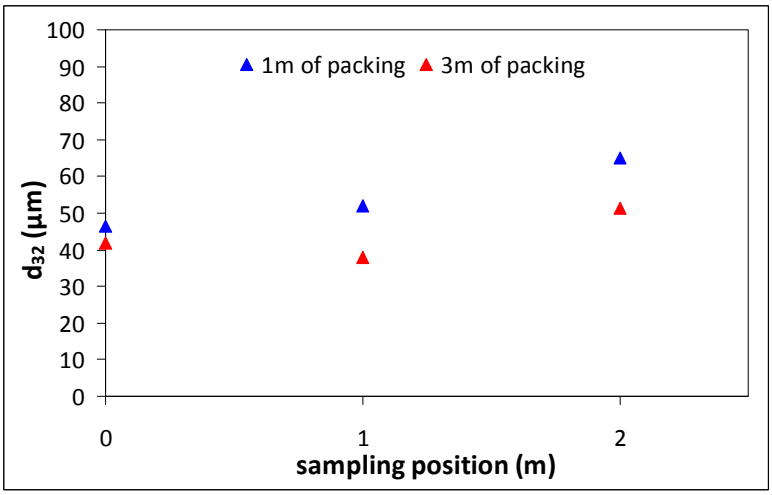

Figure IV- 21: mean Sauter diameter evolution along the column for two different height of PTFE insert Φ=25%, Q_{tot}= 85L.h^{-1} A=52 mm f=1.56Hz bottom introduction

II.3.4.2. Effect of insert materials

Indeed, as already mentioned, both materials present different wettability characteristics (see chapter II- Table II-4).

On the Figure IV- 22, two operating conditions are reported with three meters of insert under two different operating conditions.

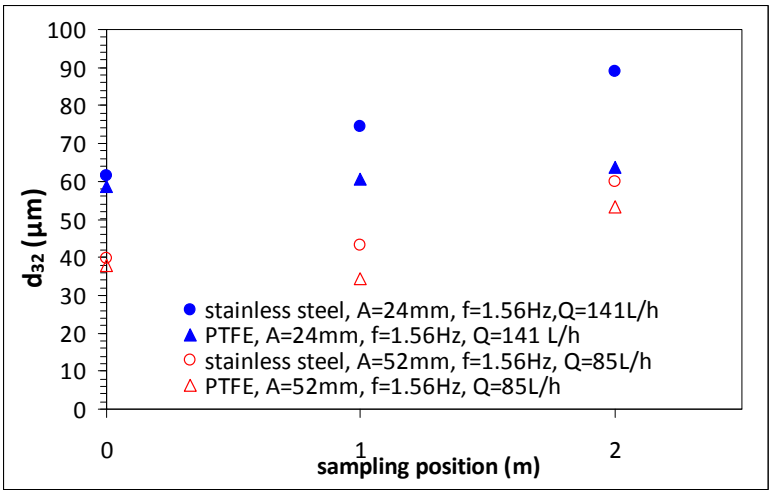

Figure IV- 22: Effect of the insert on the mean Sauter diameter evolution along the column

The same trends mentioned above are observed: there is an increase of the mean droplet size all along the column and an increase of the amplitude leads to smaller droplet sizes. The smallest droplet sizes are obtained with PTFE insert.

Collisions of drops against internal walls and discs or doughnuts play an important role in the evolution of the dispersion properties. Table IV- 9 presents the adhesion work calculation (see expression IV-19)

System	Θ (°)	σ_{LL} (mN.m^{-1})	W_{LS} (mN.m^{-1})
Water/PVA/Toluene PTFE	61.3	3.5	5.2
Water/PVA/Toluene Stainless	124.6	3.5	1.5

Table IV- 9: Adhesion work for the different systems under study

The free surface energy is lower in case of stainless steel than by using PTFE. A decrease of the surface energy corresponds to a decrease of the wettability. The toluene presents more affinity for the PTFE than for the stainless steel.

In the work of Bracou (1995), the effect of the internals wettability has been studied and an increase of the wettability leads generally to an increase of the mean Sauter diameter at a given mean energy dissipation. For a mean energy dissipation rate inferior to this limit, the trend is

the totally reverse. In fact in case of wettability, there is a balance between the rate of drop-film coalescence and rate of redispersion that produces larger drops (Bracou 1995, Mate *et al.* 1996). In our case, the PTFE is the wetting insert relative to the organic phase. Contrary to that should have been expected, the PTFE provides in our case the smallest droplet size and seems to be well adapted for our study.

II.4. Modelling of the mean droplet size

II.4.1. Modelling of the mean droplet size with the energy dissipation rate

The correlation of Jealous and Johnson (1955) has been used to calculate the mean energy dissipation rate (see equation IV-11).

The d_{32} and d_{90} are related with a proportional relationship (d_{90}/d_{32}=1.9). So the mean Sauter diameter evolution can be represented versus the mean energy dissipation rate (see chapter III).

Figure IV- 23 represents the mean Sauter diameter evolution with the energy dissipation rate for the two investigated systems and for the two types of insert. The mean droplet size corresponds to the size obtained after one meter of insert.

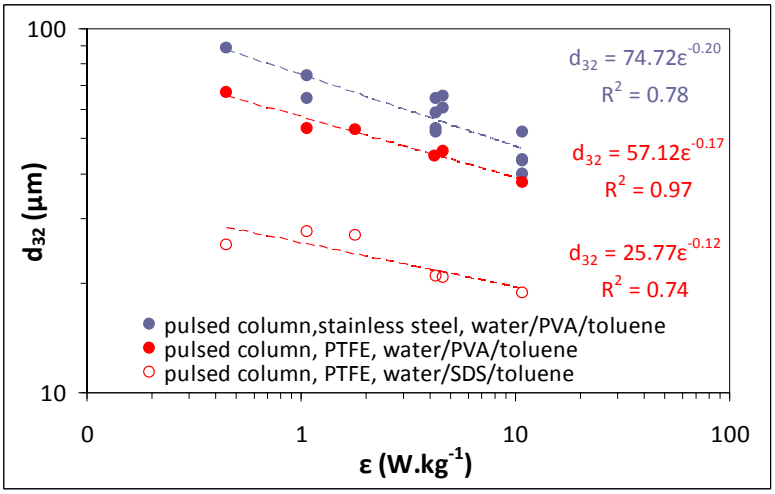

Figure IV- 23: mean droplet size evolution with the energy dissipation for the three systems combination at Φ=25%, h=1m

Theoretically, the Kolmogorov cascade theory assumes a decreasing power law versus the energy dissipation rate at with an exponent equal to -0.40 under the assumption of isotropic homogeneous turbulence.

In our case, the decreasing is less important, the fitting exponents being in the range -0.12 to – 0.20. For the break-up mechanism, it exhibits a weaker dependency on the turbulent flow patterns than on the interactions with the inserts. Obviously, the hydrodynamical parameters play a role in the breakage and coalescence balance as mentioned previously (part 4.3.) but this effect seems to be less important than the insert influence caused especially by the wettability property.

In others works in the past, one can find various values of exponents. For instance, in the work of Gourdon, 1989, the pulsed column and the rotary-agitated Kühni column have been compared. The maximum stable diameter follows a decreasing power law according to the energy dissipation rate with an exponent of -0.25 for the pulsed column and -0.55 for the Kühni column.

More recently, Pereira suggests an evolution close to ours (see Table IV- 10).

References	Correlations
Pereira, PhD 2002	Vertical COBR - Riser $\frac{d_{32}}{D} = 0.018(\pm 9.38\%)\varepsilon^{-0.16(\pm 5.9\%)}$ (R_2=0.37) - Downcomer : $\frac{d_{32}}{D} = 0.022(\pm 5.4\%)\varepsilon^{-0.23(\pm 3.63\%)}$ (R_2=0.72) Horizontal COBR $\frac{d_{32}}{D} = 0.0159\varepsilon^{-0.30}$

Table IV- 10 : mean droplet size evolution with the energy dissipation rate in pulsed column

Most of the time, these different exponent values account for the actual flow conditions that are not perfectly homogeneous and isotropic like in the theory.

Since the dispersed phase fractions investigated in our work are higher than the classically one found in literature, we have tried in the next section to apply the up-to-date breakage and coalescence models to our conditions in order to explain the evolution of our experimental characteristic drop diameters. The aim is just here to detect the respective roles of breakage and coalescence.

II.4.2. Breakage and coalescence frequencies

In this section, we intend to focus on the understanding of the breakage and coalescence phenomena which occur during the pulsating flow. The different models of coalescence and breakage found in literature are presented. Then, coalescence and breakage frequencies are roughly estimated. Our goal is not to propose a new model related to our process and to our phase system, but just to estimate frequencies in order to point out which mechanism should be predominant in our liquid-liquid dispersion system.

There are lots of models available in the literature. The two first parts are devoted to a short explanation of the models chosen in this work. Finally, the respective breakage and coalescence frequencies are evaluated by using our experimental conditions (physico-chemical parameters, energy dissipation…).

II.4.2.1. Coalescence frequency

Recently Lia and Lucas (2010) write an exhaustive review concerning the coalescence frequency models. The following calculations are based on the works of Chesters (1991) and the review of Lia and Lucas (2010).

The interdrop coalescence frequency is represented as the product of the coalescence efficiency, P, with the collision frequency, C, the latter being defined by the following expression:

$$C = kvd^2n^2 \quad \textbf{(IV- 23)}$$

where d represents the characteristic droplet diameter and n the number of droplets by volume unit. This expression is directly derived from the collision theory of Smoluchosvski. The k constant and the relative collision velocity, v, depend on the hydrodynamics conditions which lead to the interdrop collision. These conditions are defined thanks to the comparison of the drop size with some of the characteristic flow scales. Generally, in turbulent flows, there is an usual scale, which represents the limit between the inertial domain and the viscous one. This is the Kolmogorov length scale, calculated via the following relationship:

$$\lambda_K = \left(\frac{\nu^3}{\varepsilon_m}\right)^{1/4} \quad \textbf{(IV- 24)}$$

where ν is the kinematic viscosity and ε_m is the mean energy dissipation rate ($W.kg^{-1}$). It is the scale representative of the viscous dissipation (Kolmogorov energy cascade).

Comparing the droplet size, d, with the Kolmogorov length scale, it is possible to define whether the interdrop collision occurs in the viscous domain or in the turbulent inertial subrange. The respective parameters k and v for the collision rate are classically expressed according to the drop size d versus λ_K (see Table IV-11).

	v	**k**
Inertial subrange: $d > \lambda_K$	$v = (\varepsilon d)^{1/3}$	$\left(\frac{8\pi}{3}\right)^{1/2}$
Viscous turbulent flow : $d < \lambda_K$	$v = \left(\frac{\varepsilon}{\nu}\right)^{1/2} d$	$\left(\frac{2\pi}{15}\right)^{1/2}$

Table IV- 11 : Parameters k and v for the collision rate

In Figure IV- 24, the evolution of both sizes is represented as a function of the mean energy dissipation rate. On this figure, the characteristic drop size corresponds to our experimental Sauter diameters, the Kolmogorov scale being calculated thanks to relation (IV-24).

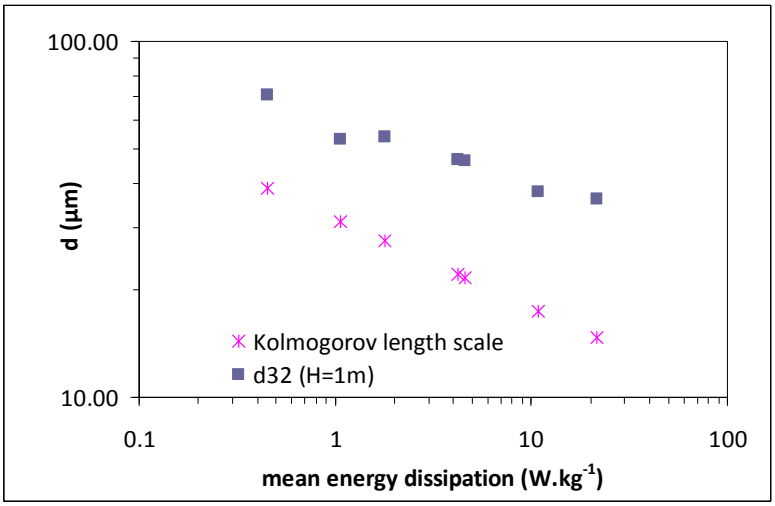

Figure IV- 24 : Evolution of the mean droplet size and the Kolmogorov length scale

As it can be seen, the mean Sauter diameter and the Kolmogorov length scale are pretty close each other, but, within the whole range of dissipation rates, the experimental d_{32} remain larger than the Kolmogorov length scale. It implicitly means that the collisions happen to be governed by the turbulent inertial regime.

The determination of the coalescence efficiency P is not easy and still remains a scientific challenge. Indeed, different models are available in the literature. Generally, it is linked to two characteristic times: the film drainage time and the contact time. The basic principle is as follows: if the collision leads to a contact time between the two colliding drops sufficiently long so that the continuous film separating the two drops could be drained, the collision will be successful in term of coalescence and the coalescence probability will be equal to one. If not, the coalescence probability will decrease. On this basis, most of the coalescence efficiency models are expressed as follows:

$$P = \exp\left(\frac{t_{drainage}}{t_{contact}}\right) \qquad \textbf{(IV- 25)}$$

where $t_{drainage}$ and $t_{contact}$ are respectively the time for the film drainage and the interdrop collision duration, ie the contact time.

The contact time can be estimated by:

$$t_c \approx \frac{d_{32}}{v} \qquad \textbf{(IV- 26)}$$

v being the relative collision velocity,

The drainage time is much more difficult to be predicted. We refer here to the work of Chesters (1991), who proposed the following expression:

$$t_{drainage} = t_{ch} \ln \frac{h_c}{h_0}$$

(IV- 27)

where t_{ch} is a characteristic time defined such as:

$$t_{ch} = \frac{3\pi\mu_c R^2}{2F} \quad \textbf{(IV- 28)}$$

with F an interaction force (R being the drop radius)

$$F = 6\pi\mu_c R^2 \sqrt{\frac{\varepsilon_m}{\nu_c}} \quad \textbf{(IV- 29)}$$

and h_c the critical film thickness corresponding to the continuous film rupture and expressed by: $h_c = \left(\frac{AR}{8\pi\sigma}\right)^{1/3}$ **(IV- 30)**

where A is the Hamaker constant, generally taken equal to 10^{-20} J.

Consequently, as presented in Figure IV- 25 , the coalescence frequency can be evaluated versus the drop diameter for a given energy dissipation rate. It is expected that the coalescence frequency decreases with the mean droplet size.

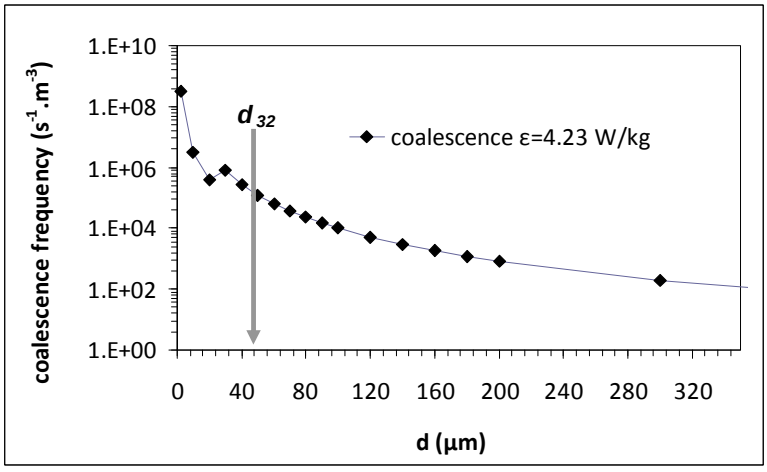

Figure IV- 25 : coalescence frequency evolution versus drop diameter for a given energy dissipation rate

II.4.2.2. Breakage frequency

Recently, a broad and detailed overview of the existing laws is given in the papers of Liao and Lucas (2009) and in the work of Maaß and Kraume (2012).

Two kinds of model are available in literature. In the first class, a mechanistic model for the drop breakage is proposed (Coulaloglou and Tavalarides, 1977), whereas the second class is based on a stochastic process (Narsimham *et al.*, 1979; Ross, 1983; Alopaeus *et al.*,

2002). The first class of model is described below. Regarding the second class of model, it assumes a random breakage of the initial mother drop in various disjointed elements in one or several steps. This assumption is extensively used even if Villermaux (2007) demonstrates experimentally that significant differences exist between experimental data and stochastic distribution.

The mechanistic model for the drop breakage rate proposed by Coulaloglou and Tavlarides (1977) assumes that the breakage frequency is the product of the fraction of the total number of breaking drops and the reciprocal time needed for the drop breakage to occur.

The fraction of breaking drops is assumed to be proportional to the fraction of turbulent eddies colliding with the drops that have a turbulent kinetic energy greater than the drop surface energy. The drop breakage time is the time that is needed to breakup an initially undeformed drop (Stork, 2005).

The resulting expression is:

$$k_{BR} \approx \frac{1}{t_{BR}} \exp\left(-\frac{E_\sigma}{E_{KIN}}\right) \qquad \textbf{(IV- 31)}$$

E_σ refers to the drop surface energy defined as:

$$E_\sigma \approx \pi d^2 \sigma \qquad \textbf{(IV- 32)}$$

E_{KIN}, the mean turbulent eddy kinetic energy can be expressed as:

$$E_{KIN} \approx \pi \varrho_c d^3 \left\langle \bar{u}^2 \right\rangle / 6 \qquad \textbf{(IV- 33)}$$

Where $\left\langle \bar{u}^2 \right\rangle \approx \varepsilon^{2/3} d^{2/3}$

The breakage time is expressed as follows (Coulaloglou and Tavalarides, 1977):

$$t_{BR} = \frac{1}{B_1} \frac{d}{(\varepsilon d)^{1/3}} \qquad \textbf{(IV- 34)}$$

Eddies with size comparable to the droplet size are most efficient causing drop breakage: smaller eddies have much lower energy and larger eddies tend to drag the drop instead of deforming it. Consequently the breakage frequency should be high since the droplet and eddies are in the same size range.

The breakage frequency is then defined by expression (III-35).

$$k_{Br} = B_1 \frac{\varepsilon^{1/3}}{d^{2/3}} \exp\left(-B_2 \frac{\sigma}{\rho_c \varepsilon^{2/3} d^{5/3}}\right) \qquad \textbf{(IV- 35)}$$

B_1,B_2 are fitting constants. Traditionally, each author presents his own set of parameter values based on trial-and-error attempts to reproduce experimental results in liquid-liquid application. The following table presents some values found in literature. It refers to the paper of Maaß and Kraume (2012) and Ribeiro *et al.* (2011).

Reference	Model equation	B1	B2	B3
Model from Coulaloglou and Tavalarides (1977)				
Coulaloglou and	$k_{Br} = B_1 \frac{\varepsilon^{1/3}}{d^{2/3}} \exp\left(-\frac{B_2 \sigma}{\rho_C \varepsilon^{2/3} d^{5/3}}\right)$	3.36 10^{-}	1.06 10^{-}	
Gäbler et al. (2006)		6.16 10^{-}	5.70 10^{-}	
Ribeiro et al. (2011)		4.81 10^{-}	5.58 10^{-}	
Azizi and Al Taweel		8.6 10^{-1}	4.1	
Maas and Kraume		9.1 10^{-1}	3.9 10^{-1}	
Model from Chen et al. (1998)				
Chen et al. (1998)	$k_{Br} = B_1 \frac{\varepsilon^{1/3}}{d^{2/3}} \exp\left(-\frac{B_2 \sigma}{\rho_C \varepsilon^{2/3} d^{5/3}} - \frac{B_3 \eta_D}{\rho_D d^{4/3} \varepsilon^{1/3}}\right)$	6.4 10^{-1}	1.14 10^{-}	7.85 10^{-}
Ruiz and Padilla		4.4 10^{-1}	5 10^{-3}	5 10^{-3}
Maaß and Kraume		295	3.9 10^{-1}	7.85 10^{-}
Model from Alopaeus et al. (2002)				
Alopaeus et al. (2002)	$k_{Br} = B_1 \varepsilon^{1/3} \mathrm{erfc}\left(\sqrt{\frac{B_2 \sigma}{\rho_c d^{5/3} \varepsilon^{2/3}} + \frac{B_3 \eta_D}{\sqrt{\rho_C \rho_D} d^{4/3} \varepsilon^{1/3}}}\right)$	3.68	7.75 10^{-}	2 10^{-1}
Gäbler et al. (2002)		3.63 10^{-}	2.49 10^{-}	7.24 10^{-}
Singh et al. (2009)		7.7	1.5 10^{-2}	1 10^{-2}
Maaß and Kraume		1.6 10^{2}	1.6 10^{-1}	2 10^{-1}

Table IV- 12 : comparison of the fitting parameters obtained for different model in the literature

From the Table IV- 12, it appears that the different fitting parameters whatever the model are varying according to several orders of magnitude. Different value combinations can be used to describe the same set of experiments with one model. Additionally, many physical influent parameters on drop size are still not implemented in the models or described properly. It can explain the broad variety of parameters described in Table IV- 12.

The goal in this section is not to define an umpteenth (B_1,B_2) couple but just to understand their physical meaning.

In addition, in their experimental data, Maaß and Kraume 2012 underline that the breakage rate function evolution versus drop size presents a maximum. This evolution of the breakage rate is not mathematically depicted in the Chen and Alopaeus models but only in the mechanistic model of Coulaloglou and Tavlarides (1977). So the representation proposed by Coulaloglou and Tavlarides (1977) can be used with confidence.

To take into account of the dispersed phase fraction ϕ, the initial Coulaloglou and Tavlarides model (equation IV-31) is corrected as follows:

$$k_{Br} = B_1 \frac{\varepsilon^{1/3}}{(1+\phi) d^{2/3}} \exp\left(-B_2 \frac{\sigma (1+\phi)^2}{\rho_c \varepsilon^{2/3} d^{5/3}}\right) \qquad \textbf{(IV- 36)}$$

By this way, it allows to account with the damping effect on the turbulence level induced by the dispersed phase fraction.

The determination of the breakage constants couple (B_1, B_2) is then a major challenge.

In our case, in order to get the order of magnitude of these (B_1,B_2) parameters, the maximum stable diameter is roughly assimilated to the d_{90} experimentally found, since above this size limit the drops are expected to break-up and to disappear. Consequently, it is assumed that the breakage probability may be considered as quasi null (10^{-5}) at this drop size value.

First, the different values of B_1 taken from the literature (see Table IV-12) have been implemented and by this way, the corresponding B_2 values have been identified (Table IV-13). These values are in the same range of the ones usually found in literature.

ε (W.kg^{-1})	B_1	B_2
0.45-21	0.91	0.42-1.8
	0.86	0.42-1.8
	$6.14\ 10^{-4}$	0.25-1.09
	0.336	0.36-1.7

Table IV- 13 : Values of B_2 for a zero breakage frequency for the different literature B_1 value under our experimental energy dissipation rate

Now B_2 being fixed to an averaged value of 0.79, B_1 is calculated with the same method. B_1 varies of several order of magnitudes.(Table IV-14Table IV- 14).

It is a physical nonsense. Indeed, the breakage time is defined by:

$$t_{Br} = \frac{t_C}{B_1} \qquad \textbf{(IV- 37)}$$

Where t_c is the contact time expressed by (IV-26) which is equivalent to the eddy life time.

In Table IV-14Table IV- 14, the breakage time, and eddy life time are added according to the values of the mean dissipation rate and (B_1,B_2) values.

B2	**B1**	**Breakage time (s)**	**Eddy life time (s)**
0.79	$2.65\ 10^{-5} – 7.7410^{7}$	$22.7\text{-}4.46\ 10^{-11}$	$6.08\ 10^{-4}\text{-}3.45\ 10^{-3}$

Table IV- 14 : B_1 values at a given B_2 and the corresponding characteristic times in the range of our experimental dissipation rate

At this step now, it is important to emphasize that the breakage time has to be lower than the life time of an eddy. Consequently, to our opinion, B_1 must be larger than one and one can forget the values identified as being inferior to 1.

Besides, the breakage time must be also lower than the residence time in the column compartment (a disc and doughnut stage) since breakage occurs during the flow passage. The residence time in our volume is equal to 2 seconds.

To get an idea of the order of magnitude of the breakage time, let's refer to literature. For instance, in pipe flow it is often reported that the breakage time is of the order of a few milliseconds, between 4 (Eastwood *et al.*, 2004) and 100 ms (Hesketh *et al.*, 1991).

For this reason, too high B_1 values cannot be considered.

Finally, it seems that these literature breakage time values are within the range of the contact times (Table IV-14). In conclusion, the B_1 constant is estimated in this work by assuming that the breakage time is at least 1.5 times lower than the contact time. It leads to our proposal to set a B_1 constant equal to 1.5.

II.4.2.3. Comparison in the pulsed column case

These models allow the understanding of the phenomena that happened in the different compartments of our discs and doughnuts column.

At a given investigated operating condition, three characteristics drop diameters can be defined (Figure IV-26):

- the mean Sauter diameter d_{32} obtained experimentally thanks to the Malvern Mastersizer 2000 analysis (H=1m)
- the maximum stable diameter $d_{max,stable}$ which corresponds to the breakage frequency theory and corresponds to the maximum droplet size which is stable. It corresponds to the drop diameter for which the breakage frequency is equal to zero. Experimentally, it could be in a first approximation assimilated to d_{90}.
- the equilibrium diameter d_{eq} defined as the diameter for which the coalescence and breakage frequencies are equal.

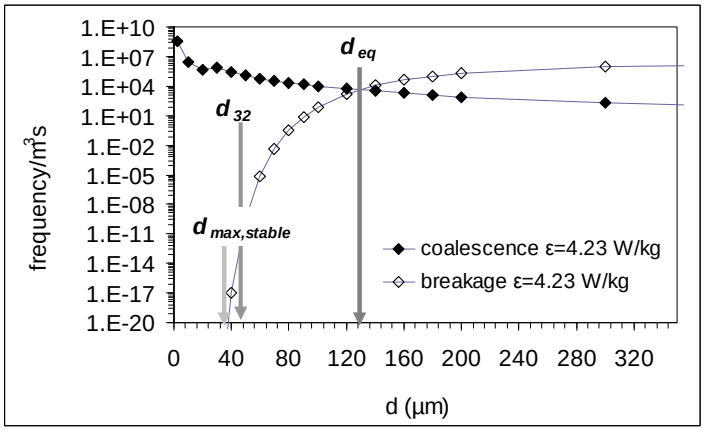

Figure IV- 26: breakage and coalescence frequency evolution with droplet diameter and identification of three characteristics diameter of the dispersion

At a diameter lower than the d_{eq}, the coalescence frequency is superior to the breakage frequency. Consequently, in the breakage and coalescence balance, the coalescence becomes predominant. On the contrary, for a diameter superior to d_{eq}, the breakage frequency is superior to the coalescence frequency. In this case, breakage is prevailing.

To summarize all the results, the Figure IV- 27 represents the evolution of these three characteristic diameters versus the turbulent energy dissipation rate.

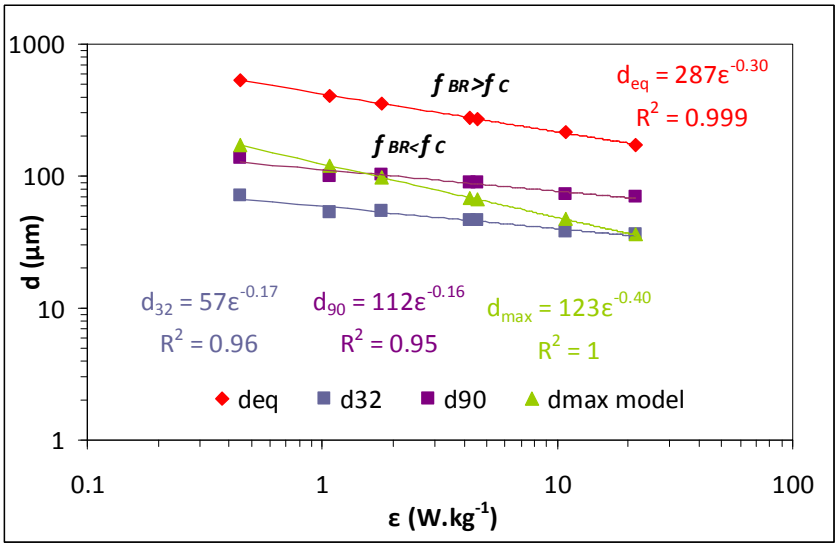

Figure IV- 27: Evolution of the three characteristics diameter with the mean energy dissipation rate for the water/PVA/toluene system at Φ=25%

First of all, in our case the equilibrium diameter d_{eq} is always superior to the maximum stable diameter and consequently to the d_{32}. Therefore, in the balance between breakage and coalescence, the coalescence is expected to be the prevailing mechanism which affects the droplet size and the droplet size distribution.

By taking into account the different dispersed phase concentrations (Figure IV-28), the breakage frequency is modified and consequently, the maximum stable diameter and the equilibrium diameter too.

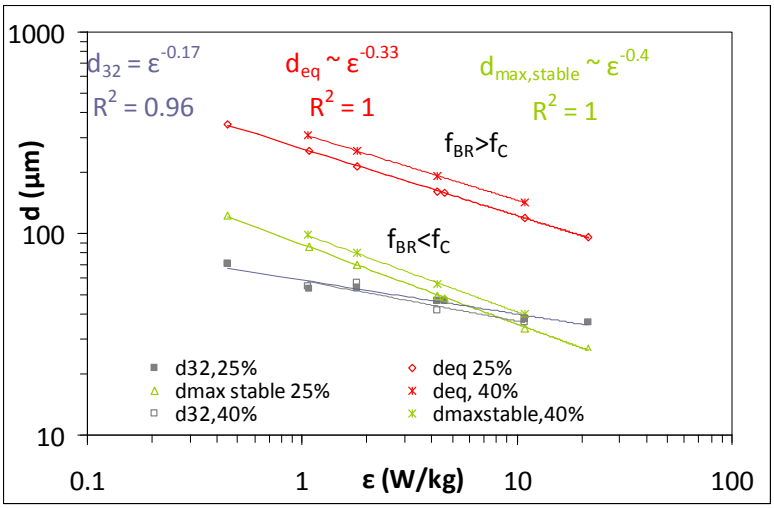

Figure IV- 28 : Evolution of the three characteristics diameter with the mean energy dissipation rate for the water/PVA/toluene system by taking into account the dispersed phase concentration in the calculation of the frequencies.

With an increase of the dispersed phase concentration, the d_{eq} and the $d_{max;stable}$ are larger than those calculated at lower dispersed phase concentration. However, the mean Sauter diameter is not affected by the dispersed phase concentration.

II.4.3. Modeling of the mean droplet size evolution through dimensionless numbers

As presented in part I., the mean diameter evolution can be presented via dimensionless numbers. Accounting with the dependency of the droplet size pointed out previously, the evolution is presented through the oscillatory Reynolds number (equation (IV-8)) to take into account the oscillation effect on the droplet size (Figure IV- 29).

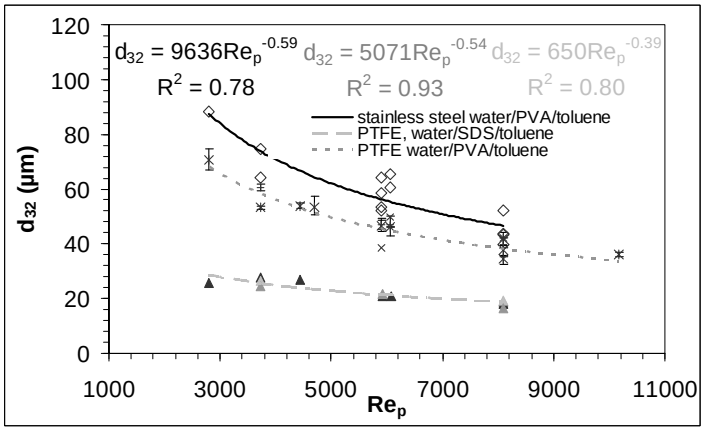

Figure IV- 29: Evolution of the mean Sauter diameter with the pulsation Reynolds number for the three systems at Φ=25% and H=1m

The evolution presents a power law in the same range, whatever the insert material. The only difference can be explained by the surface wettability. So it has to be taken into account in the correlation.

In the case of the PTFE insert, the difference between the Sauter diameter evolutions can be explained thanks to the interfacial tension. Consequently the dimensionless Weber number is also a relevant dimensionless number.

To take into account the adhesion work in which intervenes the interfacial tension, a special Weber number is defined. It corresponds to the ratio between the inertial energy to the interfacial energy. This specific dimensionless Weber We_s is expressed as follows:

$$We_s = \frac{E_{inertial}}{E_{adhesion}} = \frac{\rho_c u^2 d_h^3}{\sigma(1+\cos\theta)d_h^2} = \frac{\rho_c u^2 d_h}{\sigma(1+\cos\theta)} \qquad \textbf{(IV- 38)}$$

U is the velocity related to the fluid displacement. The fluid displacement is due to the pulsation and to the net flow. Consequently, the specific dimensionless Weber number We_s is expressed by:

$$We_s = \frac{\rho_c (u_c + 2Af)^2 d_h}{\sigma(1+\cos\theta)} \qquad \textbf{(IV- 39)}$$

The dimensionless Weber number is calculated by taking the interfacial tension value at a time corresponding to the residence time after one meter of insert in the column.

We are looking for a dimensionless correlation aiming with the prediction of the Sauter diameter relatively to the column diameter, by taking into account, the oscillatory flow Reynolds number Re_o and the specific Weber number We_s.

Consequently, the correlation is expressed as:

$$\frac{d_{32}}{D} = A Re_o^{\alpha} We^{\beta} \qquad \textbf{(IV- 40)}$$

.The different coefficients A, α and β are evaluated by using the excel simulator for each set of experiment by the mean square method. Then, an average of the coefficients provides the value for the correlation.

The fitting correlation is finally given by:

$$\frac{d_{32}}{D} = 5\,Re_o^{0.85}\,We_s^{0.26} \qquad \textbf{(IV- 41)}$$

Figure IV- 30 allows the comparison between experimental and model data.

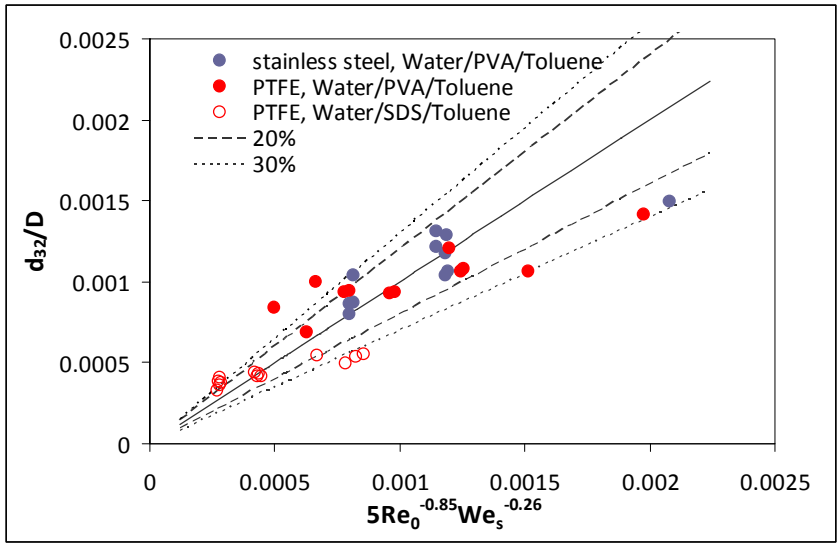

Figure IV- 30 : Comparison between the model and the experimental results

This error range is reasonable given that the measurement uncertainty on the mean droplet size (sampling, measurement method), contact angle, flowrate, oscillation…

This relation IV-41 needs to be confirmed by additional experiments with different phase systems. The geometrical parameters could be studied as additional parameters.

II.5. ***Conclusion***

The disc and doughnut pulsed column is here used co-currently to create a liquid-liquid dispersion. Despite the use of surfactant, it seems that a coalescence phenomenon occurred in the last meter of the column. Different parameters have been investigated and their effect on the mean droplet size has been studied.

The droplet sizes obtained are for the whole conditions investigated generally satisfactory according to the further requirements related to the continuous polymerization process. Concerning the hydrodynamic parameters, it is demonstrated that the net flow rate

has no significant effect. Moreover, the most important hydrodynamic parameter is the oscillation velocity characterised by its oscillation amplitude and frequency product. An increase of the pulsation velocity leads to a smaller mean droplet size. Besides, for a same pulsation condition, the residence time can be modified without effect on the dispersion properties. According to the application, the residence time can then be controlled.

Concerning the physico-chemical parameters, the nature of the surfactant has been investigated. Both surfactants (PVA and SDS) provide the same value of interfacial tension at equilibrium. However, their nature and adsorption mechanism are different. Larger mean droplet sizes are obtained with PVA which are characterized by larger molecules than SDS.
The dispersed phase concentration has been also studied. At high concentration (25% and 40%) no effect is pointed out. However, for more diluted liquid-liquid dispersion, the mean droplet sizes obtained are smaller. So, at higher dispersed phase concentration, the coalescence and breakage frequencies are modified.

Concerning the insert, the nature of insert affects both the mean droplet size and the behaviour of the dispersion according to the height of insert. Without insert, the mean droplet size is not influenced by the hydrodynamics because whatever the operating conditions, the same drop sizes are obtained. It means that the mean droplet size is only governed by the initial conditions. In case of PTFE insert, the hydrodynamics controls the mean droplet size: the droplet size distribution and the mean droplet sizes evolve with the pulsation velocity and the height of the insert. On the contrary, with stainless steel insert, with just one meter of insert, the mean droplet sizes do not evolve with the pulsation conditions. The liquid-liquid dispersion is then influenced by the insert height and by the insert nature. The comparison between both inserts has been performed under the same other operating conditions. It appears that smaller mean droplet sizes are obtained with PTFE insert than with stainless steel insert. This result is unexpected given that the PTFE is preferentially wetted by the dispersed phase. Maybe smaller droplets are detached from the discs or doughnuts and modified the droplet size distribution obtained.

The evolution of the mean Sauter diameter is modelled through different correlations. Regarding the results obtained in term of mean energy dissipation rate, it seems that the turbulence is mainly affected by the insert geometry.
A dimensionless correlation to predict the mean droplet size is proposed. It takes into account the interfacial tension of the system as well as the insert nature. In addition to the classical dimensionless numbers characterizing the pulsed flow (Re_n and Re_p), the Weber number We_S depending on the interfacial tension and the on the adhesion work has been introduced.

The goal of this work was to check whether it was possible to control the emulsification step of the polymerization process thanks to a pulsed flow. Since the preliminary results are very promising, the next step is to perform some feasibility tests with

industrially commercialized equipment like the COBR (Nitech), able to ensure longer residence times compared to the pulsed pilot column.

III. LIQUID-LIQUID DISPERSION IN HORIZONTAL CONTINUOUS OSCILLATORY BAFFLED REACTOR (NITECH LTD.)

The section is dedicated to the liquid-liquid dispersion performed in a continuous oscillatory baffled reactor (COBR).

If lot of literature is available concerning liquid-liquid dispersion in batch oscillatory baffled reactor BOBR (ie section I of this chapter), to our knowledge, the continuous oscillatory baffled reactor applied to liquid-liquid dispersion has been only studied by Pereira (2002). The configurations and the phase system as well are quite different from ours. Especially no surfactant is involved in Pereira's study.

III.1. ***Materials and method***

III.1.1. Experimental rig

The oscillatory baffled reactor is made of borosilicate glass tube. The reactor is horizontally implemented. Two kinds of sections are bond each other. The straight section is a 700mm long section of 15mm internal diameter. The glass baffles are spaced from 26mm (plus or minus 1 mm) and leave an annular opening of 8mm. There are 23 baffles per section. Every four straight sections, a U-shape section is connected. This U-shape section is 250mm long and the glass baffled spacing is of 31mm. The transparency factor is equal to 28% (against 25% in the part II concerning the pulsed pilot column).

Figure IV- 31 is a picture of the experimental rig to show the arrangement of the different sections. The flow direction is presented in Figure IV- 32. On the right size, the U sections are on the same plane whereas on the left side, the U tubes are perpendicular to the horizontal plane and then the flow is upward.

Figure IV- 31 : Continuous oscillatory baffle reactor COBR , general configuration

Consequently, on the first length, section 1, the aqueous phase is introduced. The organic phase is introduced from the first straight section of the second length, quoted "2" on the Figure IV- 32. There is an U tube perpendicular to the horizontal plane and the biphasic flow enters the third section. It is then connected to a storage tank.

Figure IV- 32 : direction of the flow in the COBR

The flowrates of both flows are ensured thanks to two gear pumps with flowrate ranging from 15 to 150 $g.min^{-1}$. The pumps are equipped with check valves to avoid the backward of the flow. The pulsation is performed thanks to a piston connected at the basis of the first section. The stroke length of the piston ranges from 10 to 70 mm and the pulsation frequency from 0.35 to 1.4 Hz. The regulation is made thanks to the command panel. The displacement in the column corresponds to 20 to 140mm.

The sections are jacketed except the U-tube but the liquid-liquid dispersion is achieved at room temperature that is to say between 20 and 23°C.

On each feeding line, a temperature sensor, a flow meter and a densimeter are implemented in order to register their evolution along the time. The set-point flowrate is entered and a PID regulator controls the valve opening for regulating the flowrate.

Due to the oscillation, the flowrate fluctuates but the mean flowrate corresponds to the set-point value with an error inferior to 2%.

Sampling valves are installed all along the reactor in order to measure the droplet size distribution and the mean droplet size all along the reactor. Five valves are located respectively at 0.7 m, 1.40m, 3.05m, 3.75m and 4.45m after the toluene inlet. At the COBR outlet, the on-line Turbiscan measurement cell is set to follow the steady-state flow and to have access to the Sauter diameter.

A global representation scheme of the experimental set up is provided on Figure IV- 33.

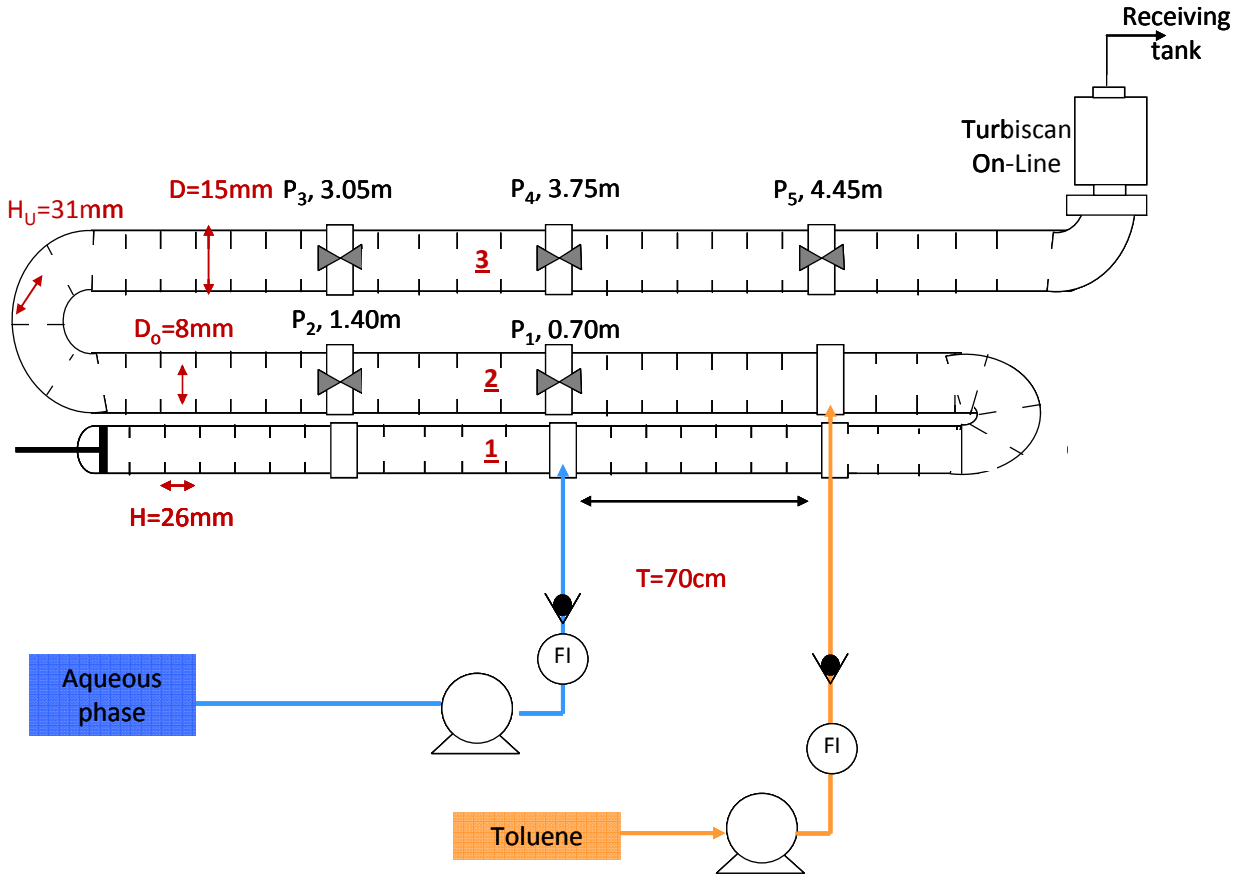

Figure IV- 33 : global presentation of the experimental rig

III.1.2. Repeatability studies

Some experiments were conducted two times to improve the repeatability of the process.

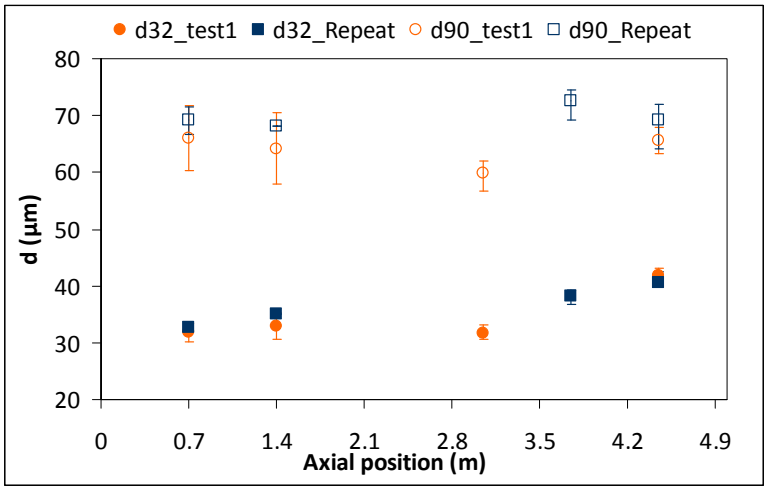

Figure IV- 34 : Evolution of the characteristic diameter along the column axis at Q_{tot}=10.3 L.h^{-1} A=35mm, f=1Hz

The mean droplet size and d_{90} obtained in the two cases are superimposed but for the measurement errors.

III.2. Operating conditions

The different parameters investigated in this section are:

- The total net flowrate: it fixes the residence time in the reactor
- The pulsation conditions: both frequency and stroke length are investigated
- The dispersed phase concentration defined as the dispersed phase flowrate to total flowrate ratio.

The Table IV- 15 summarizes the operating conditions.

The amplitude parameter A* defines by expression (IV-16) ranges from 0.667 to 3.33 and f* defines by expression (IV-15) ranges from 79 to 315.

Φ (%vol.)	**Q_{tot} (L.h^{-}**	**$Q_{toluene}$ (g.min^{-1})**	**$Q_{aqueous\ phase}$ (g.min^{-1})**	**Af (mm.s^{-}**	**A (mm)**	**f (Hz)**
25	7.63	27.70±0.40 g.min^{-1} (±1.43%)	95.10±0.54 g.min^{-1} (±0.6%)	14-50	10-20-30-40-50	0.35-0.50-0.75-1.00-1.25-1.40
	10.18	39.90±0.70 g.min^{-1} (±1.90%)	126.90±1.48 g.min^{-1} (±1.17%)	14-50	10-15-20-25-30-35-40-50	0.50-0.75-1.00-1.25-1.40
40	7.63	44.30±0.26 g.min^{-1} (±0.60%)	76.30±0.60 g.min^{-1} (±078%)	10-50	10-15-20-25-30-35-40-50	0.35-0.75-1.00-1.25-1.40
	10.18	59.04±0.50 g.min^{-1} (±085%)	101.50±1.01 g.min^{-1} (±0.99%)	10-50	10-15-20-25-30-35-40-50	0.35-0.50-0.75-1.00-1.25-1.40
	12.69	73.60±0.30 g.min^{-1} (±0.41%)	126.50±1.37 g.min^{-1} (±1.09%)	15-37.5	15-20-25-30-35-40	0.75-1.00-1.25-1.40

Table IV- 15 : Operating conditions in the continuous oscillatory baffled reactor

III.3. ***Effect of the different parameters***

III.3.1. Evolution of the mean droplet size and droplet size distribution along the COBR

First, the evolutions of the mean droplet sizes and droplet size distributions are represented for different axial positions of samplings.

Figure IV- 35 presents the evolution of the mean droplet size for two different operating conditions.

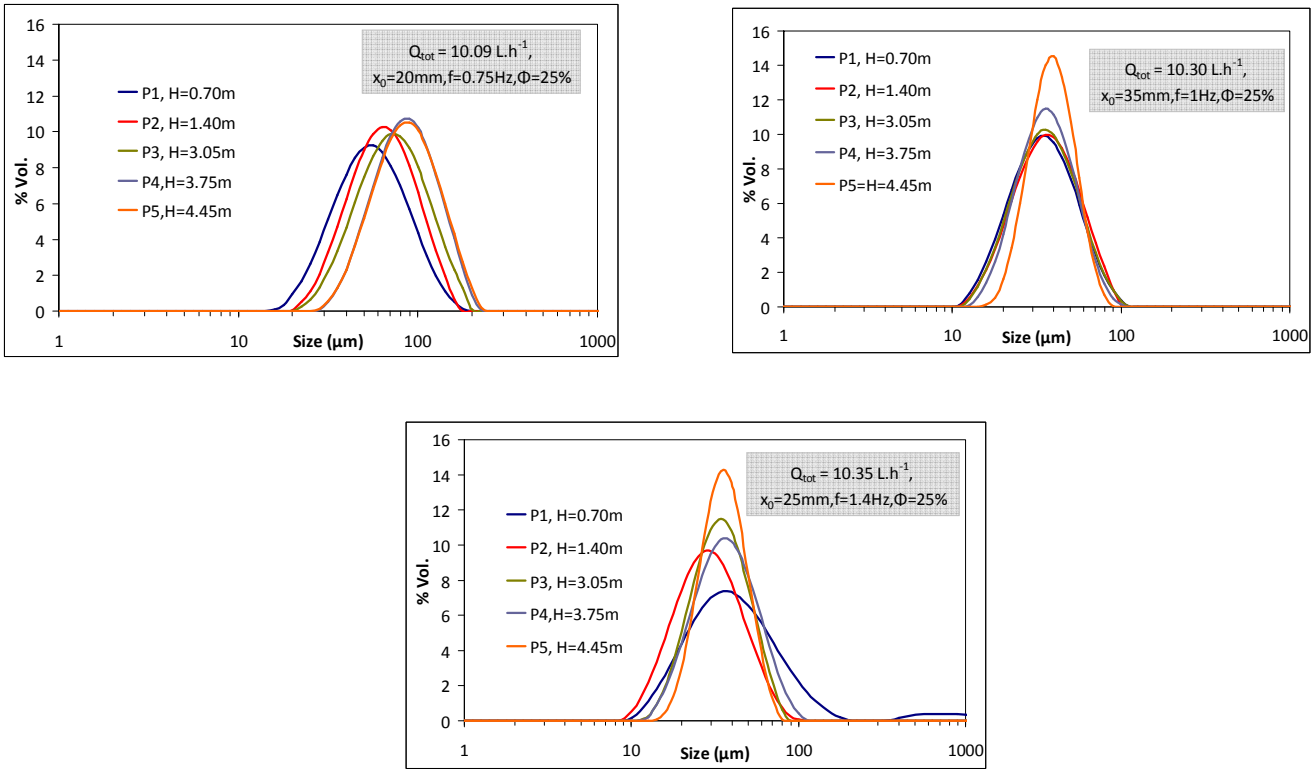

Figure IV- 35 : Droplet size distribution all along the column for different operating conditions

The oscillation conditions seem to affect the droplet size distribution stabilization. Indeed, on the left upper graph, the droplet size distributions are shifted to the larger size along the reactor and then the mean droplet size is larger at the column outlet than at the beginning. On the contrary, on the right graph, the droplet size distributions are almost superimposed and the mean droplet size is maintained all along the column. Besides, it seems that the droplet size distribution is narrower as the sampling is away from the inlet. A halfway case can be noticed. In this case, the droplet size distributions are first become narrower and provide smaller sizes from P3.

Consequently, a mapping of the stability efficiency along the column can be defined. All the investigated conditions are studying studied regarding the evolution of the mean droplet size along the column (Figure IV- 36).

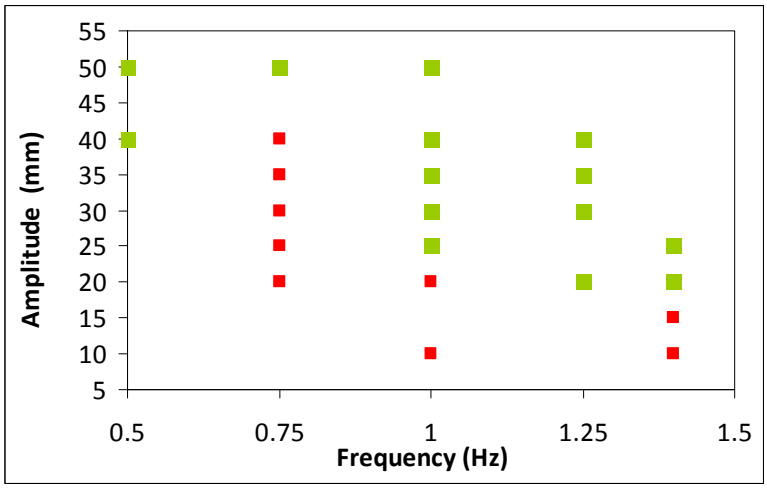

Figure IV- 36 : Mapping of the dispersion stabilization on all the tests performed: in red the DSD are shifted to the larger size and in green the mean droplet size is at least maintained on P3, P4 and P5 with narrower DSD

Figure IV- 36 is interesting for the future polymerization tests presented in the chapter VI and allows to determine the oscillating conditions which are required to obtain a stabilization of the mean droplet size. Indeed, for the tests, we have to stay out of the red zone.

From Figure IV- 35 and Figure IV- 36, under stabilization conditions, the mean droplet size is constant from the third sampling. However, for some cases the droplet size distribution is narrower after this sampling. Unless it is detailed, the mean droplet size evolution and modeling will be performed while considering the value corresponding to the last sampling.

To confirm the stabilization, the Figure IV- 37 presents some mean droplet size evolution along the column and at the column outlet. This last drop size measurement is obtained thanks to the On-line Turbiscan. The On-line Turbiscan cell is installed at the outlet of the COBR.

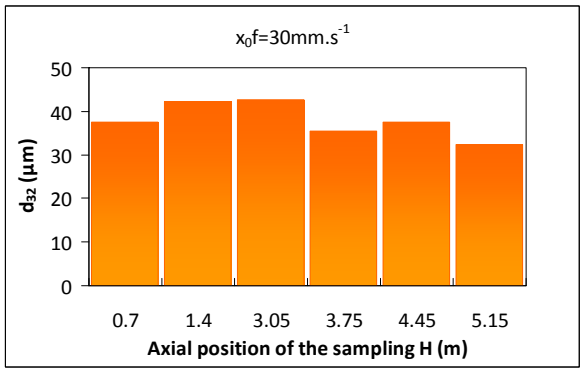

x_0=30mm, f=1Hz, Q_{tot}=7.63 L.h^{-1},Φ=25%

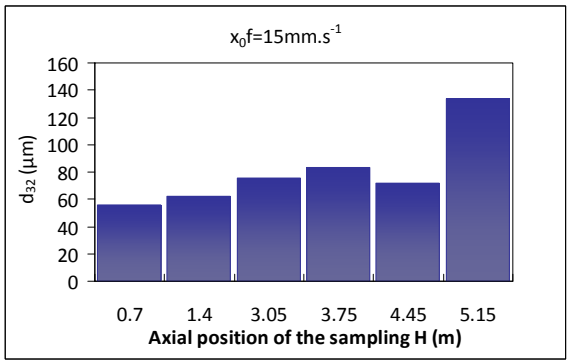

x_0=20mm, f=1.75 Hz, Q_{tot}=7.65 L.h^{-1},Φ=25%

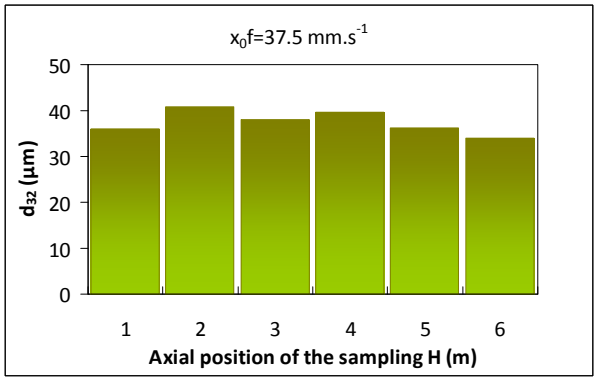

x_0=30mm, f=1.25 Hz, Q_{tot}=7.62 L.h^{-1},Φ=25%

Figure IV- 37 : Evolution of the mean Sauter diameter in different operating conditions all along the column

The mean droplet size is quasi constant in the operating condition considered as stabilized in the Figure IV- 36. The mean droplet size varies again at the column outlet in case of unstabilized condition (x_0f=15 mm.s^{-1}).

III.3.2. Effect of the hydrodynamic parameters

III.3.2.1. Effect of the total net flowrate in the COBR

Due to the limitation range of the pump, only two flowrates were tested for a dispersed phase concentration Φ of 25%: 7.63 L.h^{-1} and 10.18 L.h^{-1} corresponding to three and four times the terminal velocity for a PVC particle of 150 µm. At a higher dispersed phase concentration (ie. Φ=40% in volume) a third flowrate, 12.69 L.h^{-1}, is added corresponding to five times the terminal velocity.

Figure IV- 38 presents the mean droplet size evolution at 25% of dispersed phase concentration under different pulsation conditions (amplitude and frequency) and different total flowrate.

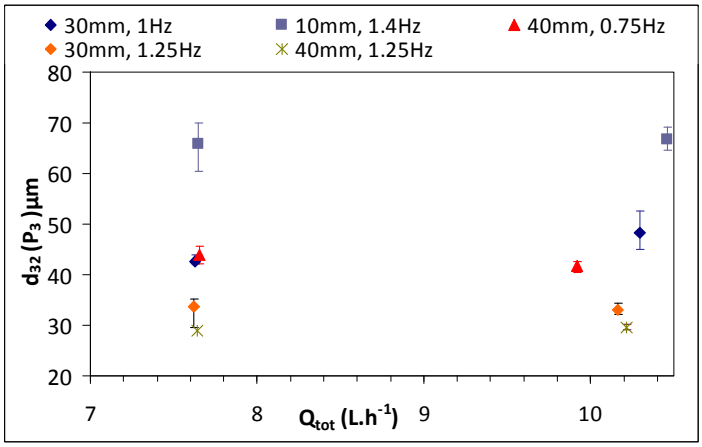

Figure IV- 38 : Mean droplet size evolution with the total flowrate Q_{tot} under different pulsation conditions Φ=25%

Whatever the pulsation conditions, it seems that the evolution of the mean droplet size is insensitive to the net flowrate. Given that only two flowrates were tested, it is more relevant to study the net flowrate effect on the mean droplet size by taking the results obtained at 40% of dispersed phase concentration for which three different flowrates or net flow Reynolds numbers were tested.

Figure IV-39 reports then the mean droplet size evolution with the net flow Reynolds number defined by expression (IV-3) for different pulsation conditions. The pulsation conditions are expressed with the dimensionless oscillatory Reynolds number which is evaluated thanks to the expression (IV-8).

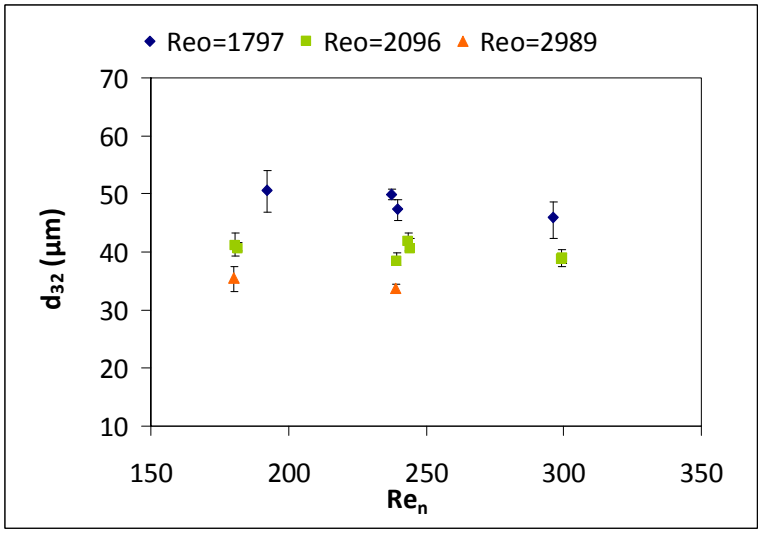

Figure IV- 39 : Effect of the net flowrate under different pulsation condition for a dispersed phase concentration equal to 40%

From this figure, the net flow Reynolds number seems to have a low impact on the mean droplet size value. Our result is consistent with the literature results (see I.6.2.2).

Moreover, on the opposite, the mean droplet size seems to be affected by the oscillation conditions. Indeed, at higher oscillatory Reynolds number Re_o, the mean droplet size obtained are smaller. (Figure IV-9)
The oscillatory parameters effects are described in the following section.

III.3.2.2. Effect of the oscillating conditions

In order to compare our results with those of Pereira, 2002, both effects of the amplitude and of frequency have been evaluated independently.

Effect of the amplitude

The amplitude effect is investigated alone at a constant net flow Reynolds number (241) and at different fixed frequencies.
The trend observed on the Figure IV- 40 is similar to the one suggested by Pereira (2002): an increase of the oscillation amplitude leads to the decrease of the mean Sauter diameter d_{32}. This is an expected result since the amplitude is related to the mean energy dissipation rate and consequently to the turbulent intensity. The exponent is about -0.80. It is the same exponent found by Pereira equal to -0.76.

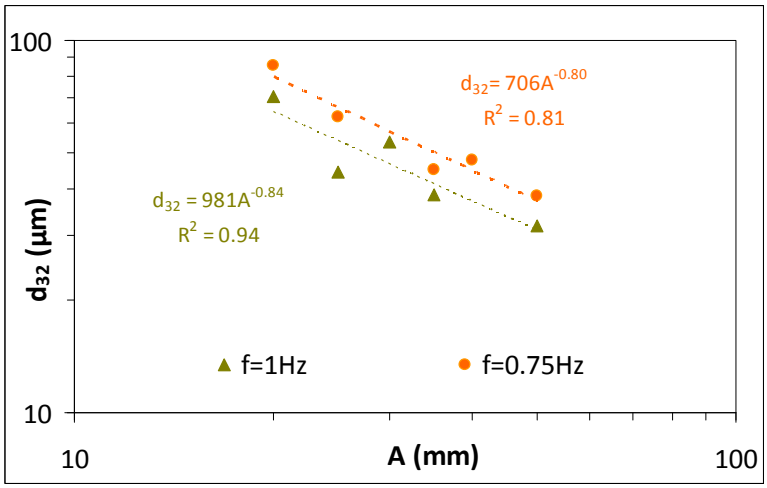

Figure IV- 40 : Effect of the amplitude on the mean droplet size Re_n=241 Φ=25%

The same result can be presented via the droplet size distribution. The droplet size distributions are shifted to the smaller sizes with the increase of the amplitude as it can be seen on Figure IV- 41.

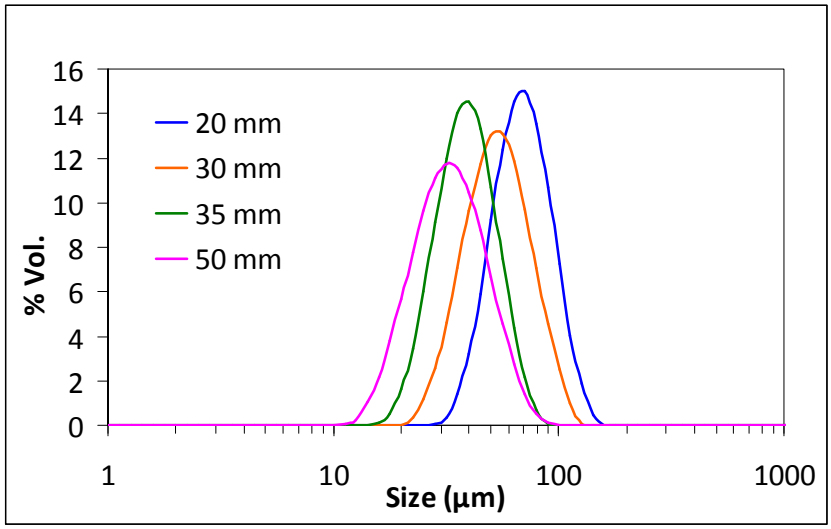

Figure IV- 41 : Mean droplet size evolution Re_n=241, phi=25%, f=1Hz, P5

Effect of the frequency

The effect of the second oscillation parameter, the frequency, is also separately investigated. As observed on Figure IV- 42, the frequency effect leads to the same conclusion than for the amplitude.

However, it seems that the frequency is more responsible of breakage than the amplitude. This result matches with the Pereira observations for horizontal continuous oscillatory baffled

reactor. The power of the law (-0.92) is not far from the value -0.85 found in the Pereira's study.

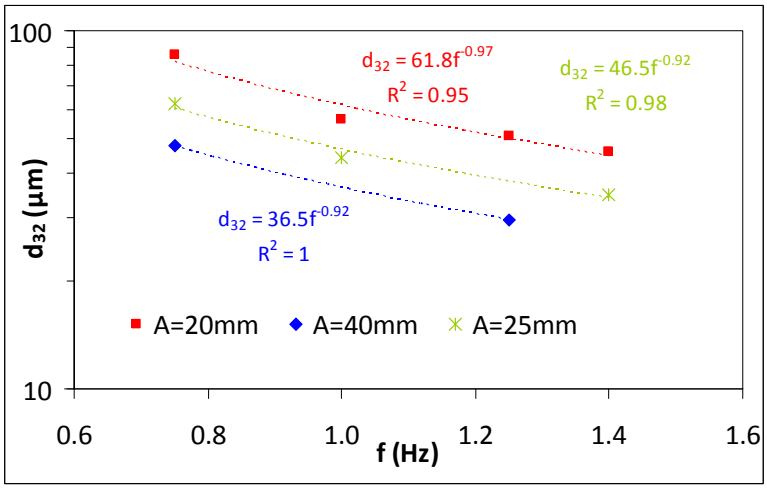

Figure IV- 42 Effect of the frequency on the mean droplet size Re_n= Φ=25%

Effect of the oscillating conditions: Re_o

The results are finally interpreted thanks to the oscillatory Reynolds number. Remind that the oscillatory Reynolds number is defined thanks to the equation IV-8 (part I-3).
Given that it was previously shown that the net flow Reynolds number has no effect on the mean droplet size, the mean Sauter diameter evolution according to the oscillatory Reynolds number is presented on Figure IV- 43 for the two net Reynolds numbers tested and for a dispersed phase fraction of 25%.

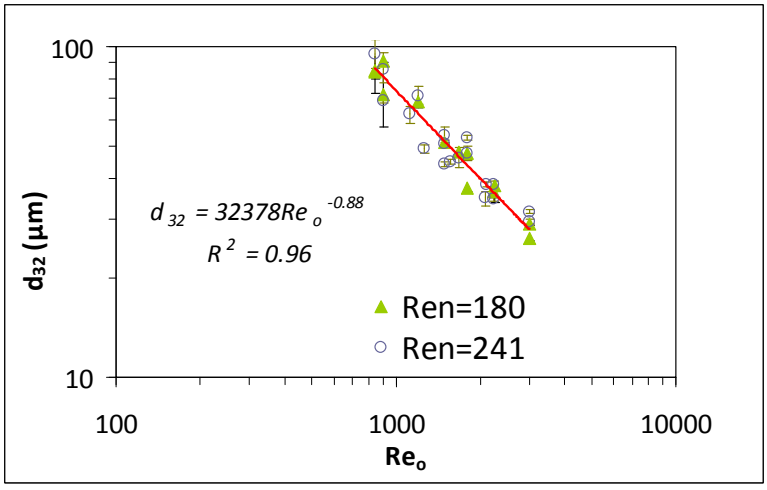

Figure IV- 43 : Evolution of the mean droplet size with the oscillation Reynolds number, Φ=25%

The mean droplet size decreases with Re_O by following a power law with an exponent -0.88. The fitting is in agreement with the model proposed by Pereira in his PhD.

III.3.3. Effect of the dispersed phase fraction

Two dispersed phase fractions have been tested which are respectively equal to 25% and 40% in volume. The other operating conditions (total net flowrate and oscillation conditions) are maintained constant.

The results are presented in term of droplet size distribution (Figure IV- 44) and mean droplet size evolution under different operating conditions (Figure IV- 45).

Under the same operating conditions, the droplet size distributions are totally superimposed whatever the dispersed phase fraction. In the same way, the mean droplet size follows the same evolution in both cases.

Consequently, under the investigated parameters, the dispersed phase fraction has no effect on the characteristic diameter of the liquid-liquid dispersion. We note that whatever the operating conditions investigated to perform the emulsification step, the dispersed phase concentration has no effect in the fraction range studied.

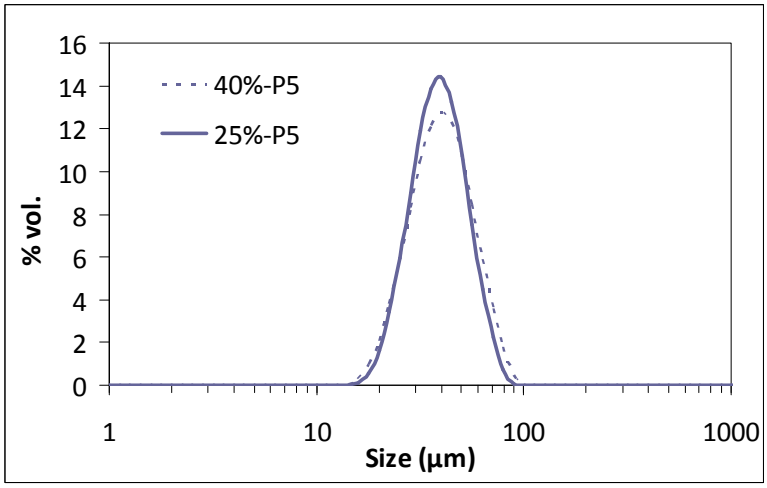

Figure IV- 44 : Droplet size distributions obtained at Re_n= 240, A=50mm, f=0.75 Hz at the final axial position sampling at a dispersed phase fraction equal to 25% and 40%

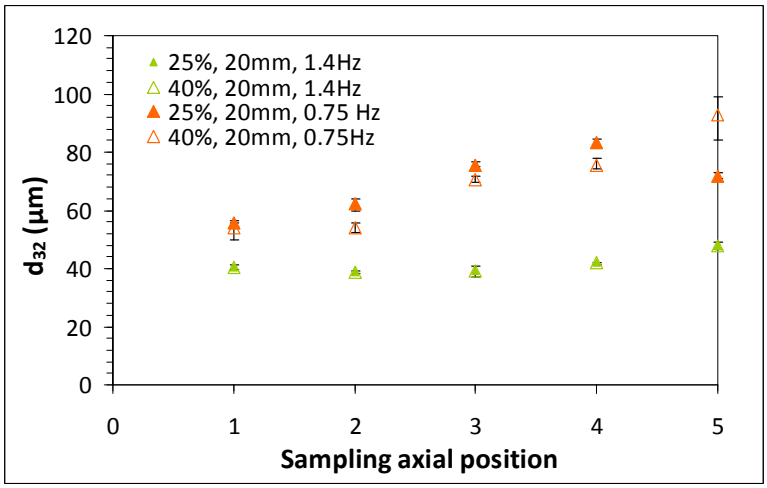

Figure IV- 45 : Evolution of the mean Sauter diameter with the axial position for different dispersed phase fraction, under two different oscillation conditions, Re_n=180

III.3.4. Axial dispersion

The axial dispersion is estimated thanks to the previous correlation established by Ni and Pereira (2000) and Pereira (2002) for an oscillatory baffled reactor of larger size. Table IV-16 reminds the geometrical characteristics of the reactors of this study and in the Pereira's study.

	COBR of this study	**COBR Pereira(2002)**
Column diameter D (mm)	15	40
Baffle hole (mm) Do	8	18
Baffle spacing H (mm)	26	72
Baffle free area %	28%	21%

Table IV- 16: Comparison of the Pereira (2002) COBR and the COBR of this study

Ni *et al.* (2001) compare the axial dispersion coefficient for different pulsed devices (close-fit, loose-fit baffle, Karr plate and multiperforated plate of various scales). They demonstrate that the axial dispersion coefficient is proportional to the mean energy dissipation rate and to the geometrical characteristics of the system, as follows:

$$D_{ax} \propto l^{4/3}\varepsilon^{1/3} \propto (x_o f)D\left(\frac{H}{D}\right)^{1/3}\left(\frac{1-T^2}{T^2}\right)^{1/3} \quad \textbf{(IV- 42)}$$

D_{ax} is the axial dispersion in $m^2.s^{-1}$, D is a characteristic diameter of the column which corresponds to the hydraulic diameter (m), H is the baffle spacing (m) and the transparency factor.

In case of baffled pulsed column, the hydraulic diameter is equal to the baffle hole diameter D_0.

The authors investigate the correlation with different pulsed column and find a proportional relationship between the two equation terms of 1.1.

This correlation is used to have an insight of the axial dispersion in the COBR. The corresponding Peclet numbers range from 30 to 100. The plug flow is ensured from a Peclet number value of 40. The Peclet lower values (ie, higher axial mixing coefficients) are obtained for the higher amplitudes.

III.4. ***Modeling***

III.4.1. Mean energy dissipation rate

The results can be expressed in term of mean energy dissipation rate. It represents the mean energy dissipation rate due to the oscillation. An additional part can be added which corresponds to the mean energy dissipation due to the baffle.

The pressure drop due to net flow through a baffled tube can be expressed as:

$$\Delta P = N_{tot} \frac{\varrho u^2}{2C_D} \frac{1}{T^2} \quad 1 \qquad \textbf{(IV- 43)}$$

With ΔP the pressure drop in Pascal, u the flow velocity ($m.s^{-1}$), ϱ the density of the flow, N_{tot} the total number of baffle in the column and T the fractional open area. C_D is the standard orifice coefficient, usually taken at 0.6.

The mean energy dissipation due to the net flow in the column can then be expressed as:

$$\varepsilon_n = \frac{\Delta P u}{\varrho L} \qquad \textbf{(IV- 44)}$$

The net mean energy dissipation obtained is 2 times in case of very soft pulsation condition to 83 times lower than the mean energy dissipation induced by the oscillatory component of the flow.

Therefore, the net mean energy dissipation is not taken into account.

The evolution of the mean Sauter diameter as a function of the mean energy dissipation is represented on Figure IV- 46.

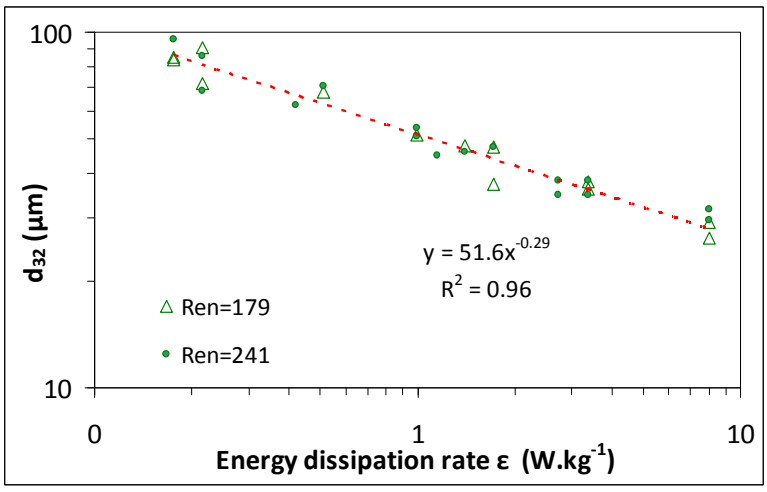

Figure IV- 46 : mean droplet size evolution with the energy dissipation rate

The mean droplet size evolution follows a decreasing power law with the mean energy dissipation with an exponent of -0.29. This result is also in agreement with the Pereira results (Table IV- 4). Again, the Kolmogorov's theory which suggests a -0.40 exponent is not checked. The discrepancy is due to the non-perfect homogeneous and isotropic turbulence and to the role played by the insert on the breakage phenomenon.

III.4.2. Dimensionless number interpretation

In the different publications, the mean droplet size is classically expressed as a power law of the oscillatory Reynolds number and of the net flow Reynolds number. Given that no effect of the net flow Reynolds number was pointed out, the mean Sauter diameter is expressed as a function of the oscillatory Reynolds number only. The mean Sauter diameter is a decreasing power law with a -0.88 exponent. It is the same result within experimental errors than the exponent found in the correlation for horizontal COBR of Pereira (2002) (-0.90 exponent) (Figure IV- 29)

Such correlations do not take into account the fluid properties involving the dimensionless Weber number. It is surprising that the interfacial tension properties are never included in the correlations. Indeed, it is usual to express the mean Sauter diameter as a function of the dimensionless Weber number. The Weber number has been described in chapter III and part II of this chapter. It represents the ratio between the inertial forces and the interfacial forces. It depends on the continuous phase physical properties and on the interfacial tension.

To extend this correlation for different systems, the dimensionless Weber number is defined with the hydraulic diameter:

$$We_h = \frac{\varrho_c \left(x_0 f\right)^2 D_h}{\sigma} \qquad \textbf{(IV- 45)}$$

As a consequence, the oscillatory Reynolds number is defined thanks to the hydraulic diameter D_h. The corresponding hydraulic diameter is in fact the orifice baffle diameter D_0.

Finally, with our system the correlation is:

$$\frac{d_{32}}{D_h} = 3.6\, Re_{oh}^{-0.88}\, We_h^{-0.41} \qquad \textbf{(IV- 46)}$$

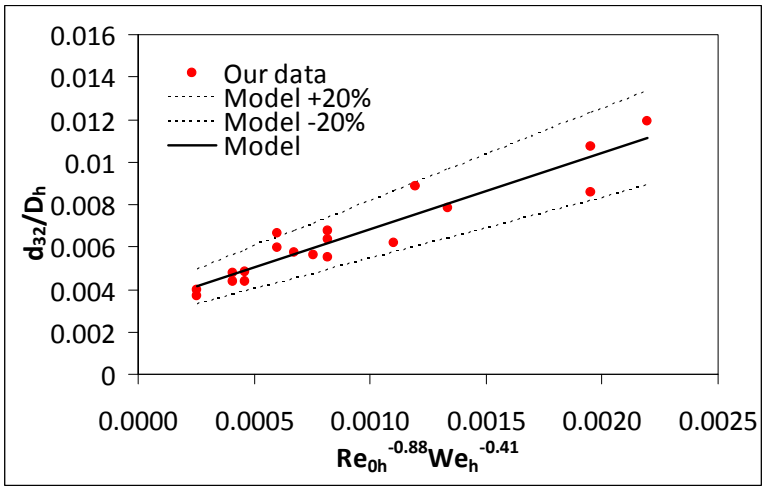

Figure IV- 47 : Correlation of the mean Sauter diameter evolution as function of dimensionless numbers

Some additional experiments with a different systems will be useful to precise the exponent of the hydraulic Weber number.

III.5. ***Conclusion***

The same system as previously used in chapter III and at the second section of this chapter was studied in COBR.

The oscillating conditions needed to obtain a stabilized dispersion have been identified. These date are particularly interesting for choosing the future polymerization conditions (chapter VI).

The droplet sizes obtained are for the whole conditions investigated generally satisfactory according to the further requirements related to the continuous polymerization process.

Concerning the hydrodynamic parameters, it is demonstrated that the net flow rate has no significant effect. Moreover, the most important hydrodynamic parameter is the oscillation velocity characterised by its oscillation amplitude and frequency product. An increase of the pulsation velocity leads to a smaller mean droplet size. Besides, for a same pulsation condition, the residence time can be modified without effect on the dispersion properties. According to the application, the residence time can then be controlled. We find the same trend than the one previously mentioned by Pereira (2002).

Only two dispersed phase concentration value have been studied. No significant effect is noticed on the mean droplet size and droplet size distribution.

The evolution of the mean Sauter diameter is modelled through different correlations. Regarding the results obtained in term of mean energy dissipation rate, it seems that the turbulence is mainly affected by the baffle geometry.

A dimensionless correlation to predict the mean droplet size is proposed. To take into account of the physical properties of the system, the dimensionless Weber number is introduced. A correlation is proposed but knowing that only one system has been studied, additional experiments will be necessary.

The goal of this work was to check whether it was possible to control the liquid-liquid dispersion step of the polymerization process thanks to a pulsed flow. The results are very encouraging.

Three different equipments have been studied in this manuscript to perform this step. In the last part we propose a comparison in term of mean energy dissipation and energy.

IV. COMPARISON BETWEEN THE TWO PULSED COLUMN

Three different equipments were tested in chapter III and IV to perform liquid-liquid dispersion. The three equipments are compared in term of mean energy dissipation in the Figure IV- 48.

As it can be seen, pulsed columns (disc and doughnut and COBR) allow to obtain mean droplet size of the same range of the SMV static mixer but with a lower energy dissipation. At energy dissipation lower than 1 $W.kg^{-1}$, both columns exhibit the same trend but a higher energy dissipation, the COBR provides lower mean Sauter diameter.

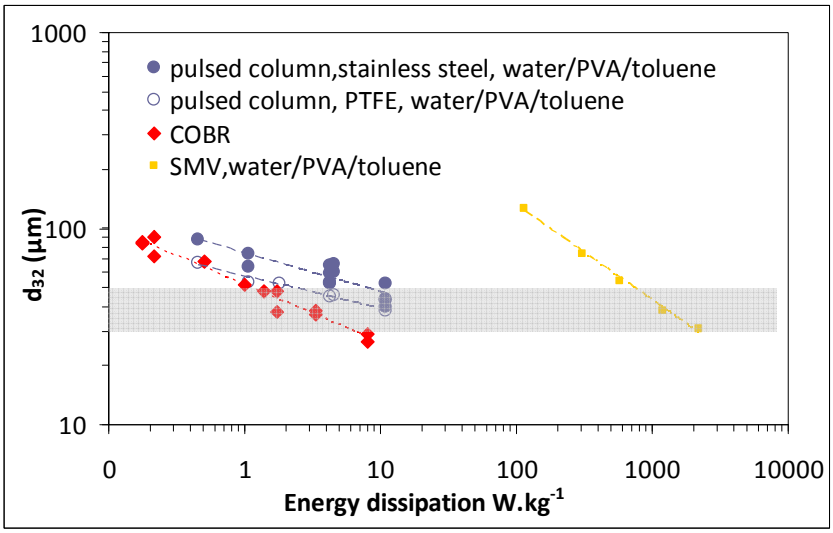

Figure IV- 48 : mean Sauter diameter evolution with the mean energy dissipation for the different liquid-liquid equipment

This representation does not take into account the time truly involved to create the emulsion. It seems interesting to convert the energy dissipation rate into energy by regarding the characteristic time of the emulsification. The energy may be evaluated thanks to the product of the mean energy dissipation by the time to create the emulsion, so that:

$$E = \varepsilon \times t_R \qquad \textbf{(IV- 47)}$$

It represents the energy loss per unit mass fluid.

The time t_R corresponds to the residence time for the static mixer, the residence time in the first meter of the column for the disc and doughnut pulsed column and for the COBR to the residence time after 3 meters (liquid-liquid dispersion stabilized for the largest part of the investigated operating conditions).

Figure IV- 49 shows that the SMV static mixer consumes less energy than the COBR and at least than the pulsed column, in order to reach the expected range of droplet sizes.

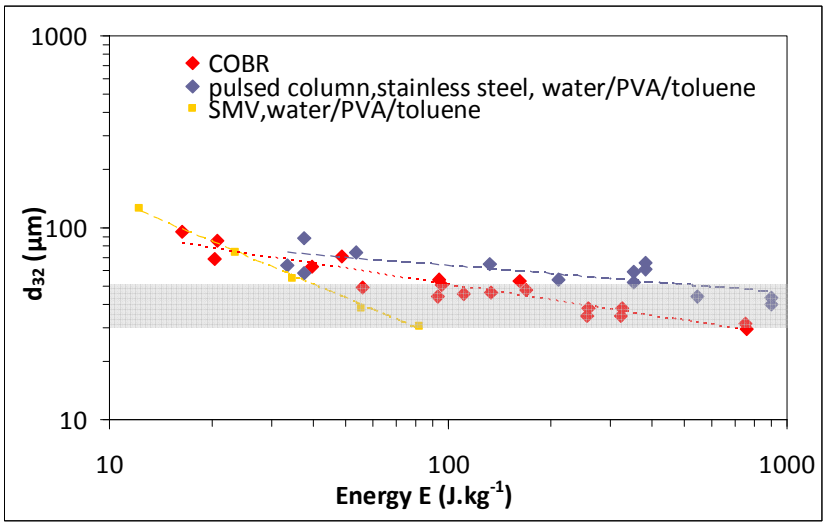

Figure IV- 49 : mean Sauter diameter evolution with the energy for the different liquid-liquid equipment

Besides, these three equipments present large differences in residence times. The static mixer can be used to create dispersion in a very short time.

Both pulsed devices have the same use: to create the dispersion and to maintain it all along. From an energetics point of view the COBR seems to be more interesting than the disc and doughnut pulsed column.

V. CONCLUSION

According to specific oscillation conditions, the pulsed devices studied have demonstrated their abilities to create liquid-liquid dispersion in the expected range. The experimental tests have led to the identification of pulsation conditions which allow also the stabilization of the dispersion.

In both cases, correlations to model the mean droplet size have been proposed. They were established depending on hydrodynamics parameters (oscillation conditions) and on some of the physico-chemical properties of the phases. These models need further improvement to be used for all the liquid-liquid systems and also for accounting with the geometrical conditions (different baffles or baffle spacing) as well as for the scale-up of the device.

Regarding the energy consumption, the static mixers can be considered as the most economical device to obtain a dispersion in the expected range (d_{32} ranges from 30 to 50 μm). However, their use should be exclusively dedicated to the creation of the liquid-liquid dispersion given that the very short residence time imposed by the flowrate to obtain the expected droplet size. The pulsed devices present the advantages of creating and maintaining the dispersion. Besides, thanks to their independency to the net flowrate, the residence time can be piloted. That is why they are foreseen as potential S-PVC reactors. Their use is also now considered to maintain a suspension and to carry out the polymerization reaction

.

CHAPTER V: Solid-Liquid Suspension in pulsed column

Considering the three steps of the polymerization process presented at the end of the chapter I, the third one consists in carrying on the polymerization reaction while the particle size does no longer evolve. Consequently, the corresponding equipment has to ensure the transport of a dense suspension and not to enhance the particle agglomeration in order to maintain the size distribution. Compared to the stirred tank, the plug flow tubular reactor seems to be more appropriate for that purpose. Therefore, this chapter aims with the demonstration of the ability of the pulsed column to transport solid particles without affecting their granulometry and by maintaining the inlet solid phase fraction.

In a first part, a short literature study is presented on the solid particle transport in pulsed column. Then, the modifications brought to the discs and doughnut pulsed column pilot are detailed. The transport particle ability of the device is discussed regarding the previous operating conditions investigated. Remind that the initial VCM droplets present a density of about 911 $kg.m^{-3}$ (at 20°C) whereas the final PVC particles have a density of 1400 $kg.m^{-3}$. Due to some technological limitation, the highest suspension concentration investigated is 8% in mass.

I. SHORT LITERATURE STUDY

This part does not claim to be an exhaustive review relative to solid-liquid suspension flows. It is just focused on the work performed in pulsed column to control the solid flow. In suspension transport, the main problem is to avoid the granulometry dispersion. So the operating conditions must be carefully defined. The main results found in literature refer to counter-current pulsed flows. This short bibliographic section defines the basic concept for solid-liquid flow and presents some relevant work for the control of solid flow in different pulsed columns.

I.1. ***Particle velocity***

The terminal velocity of spherical particles represents the steady-state velocity of a single particle falling (or rising) in a stagnant fluid. It is expressed thanks to the following relationship:

$$u_t = \sqrt{\frac{4}{3} dg \frac{\Delta\rho}{\rho_c} \frac{1}{C_w}} \qquad \textbf{(V- 1)}$$

with d the particle diameter, C_w the drag coefficient, $\Delta\varrho$ the density difference and ϱ_c the continuous liquid phase density.

U_t is the result of the forces balance between gravity forces, drag forces and Archimede force. C_w depends on the hydrodynamic conditions characterised by the particle Reynolds number, Re_p:

$$Re_p = \frac{d u_t \rho_c}{\mu_c} \qquad \textbf{(V- 2)}$$

Kunii and Levenspiel listed the different correlations for C_w and u_t for the different particle Reynolds number range. These ones are reported in Table V- 1.

Reynolds number range	C_w	U_t ($m.s^{-1}$)
$Re_p < 0.4$	$\frac{24}{Re_p}$	$\frac{g\Delta\rho d^2}{18\mu_c}$
$0.4 < Re_p < 500$	$\frac{10}{\sqrt{Re_p}}$	$\left[\frac{4(\Delta\rho)^2 g^2}{225\rho_c\mu_c}\right]^{1/3} d$
$500 < Re_p < 200000$	$C_w = 0.43$	$\left[\frac{3.1\Delta\rho d}{\rho_c}\right]^{0.5}$

Table V- 1 : Correlations for the terminal velocity depending on the particle Reynolds number

In any suspension flow inside a column, there is a simple kinematic relationship between the particle velocity $u_d(h,d)$ and the continuous phase velocity $u_c(h)$ for a d particle diameter and at a given height h in the column:

$$U_d(h,d) = u_c(h) + u_r(h,d) \qquad \textbf{(V- 3)}$$

U_r is the relative velocity of a particle of diameter d at the height h in the column. It is generally expressed by the following expression:

$$U_r(h,d) = (1-\varphi(h))^{\alpha}\, u_r^*(d) \qquad \textbf{(V- 4)}$$

$u_r^*(d)$ is the velocity of a single particle in the column and φ the local dispersed phase holdup in the column. In this relation, Richardson and Zaki (1954) claim that α ranges from 1.4 to 3.6 depending on the Reynolds number related to the particle. It represents the slowing effect on the single particle velocity induced by the presence of other particles

Besides, $u_r^*(d)$ is expressed as:

$$U_r^*(d) = Cr(Af, packing, d).u_t(d) \qquad \textbf{(V- 5)}$$

where Cr is a coefficient depending on the pulsation, packing and particle size which characterized the slowing down.

Only, few studies report on the control of the solid flow. In literature, two main cases are relevant. They concern either the counter current pulsed column with a solid flow in the opposite direction to the liquid flow or the works in oscillatory baffle reactor. Both cases are exposed in the following sections.

I.2. ***Counter-current solid transport in pulsed column***

The first relevant work concerning the transport of particle by means of pulsation is published by Boyadzhiev (1972). An asymmetric pulsation with higher acceleration than deceleration can contribute to the dense particle transport. It is only a numerical work and no experimental contribution was performed.

In all the studies aiming with solid-liquid extraction processes, generally, the solid particles (the heavy phase) are fed into the column at the top and thanks to gravitational effect are flowing down at the bottom. A lot of effort has been performed in the past in order to find technological solutions for the solid phase feeding and sampling at the outlet, in order to avoid any type of flooding. In most cases, the difference density between the solid phase and the solvent is too small, leading to some disturbances of the flow, for instance flooding at the top or solid phase entrainment at the top by the counter-current solvent flow. Whatever, the particle residence time is obviously conditioned by the density difference, and sometimes, it may be considered as a killer for the counter-current process. Consequently, some attempts have been tested in the past in order to decorrelate the residence time of the solid phase and the density difference. Among them, Brunet *et al.* (2007) have developed a new type of pulsed column in order to better control the polydispersed particle flow. This author worked with two kinds of polystyrene powder of 200 and 900 μm in diameter. Contrary to the usual counter-current flow, the solid is obliged to flow from the bottom to the top and the washing solvent from the top to the bottom. The column is composed of stacked compartments which are separated by a filtering cloth and a pneumatic valve. The filtering cloth allows the solvent flow and solid particle retention. The solid suspension is only able to circulate through the pneumatically controlled valve. The column operates in a cycle mode with a mixing step and an impulsion step. The first one is dedicated to the ability to drive the particle and the second to the solid transport from one compartment to another. The step mixing allows to control the solid residence time. The pulsation allows to ensure an homogeneous transport of the solid suspension.

I.3. ***Batch solid homogenization in pulsed column***

In batch oscillatory baffled reactor, some authors (Zhang, 1998 and Stephens, 1996) performed some suspension polymerizations and obtained satisfactory particle size distribution all along the reactor. This result confirmed the previous work of Mackley *et al.* (1993) who demonstrate the control of the particle segregation thanks to the pulsation whatever their size, density and size distribution. Their experiments consisted in creating a solid bed at the bottom of the column and to change the pulsation in amplitude (from 0 to 6 mm) and frequency (from 1 to 20 Hz). The solid phase concentration is of 10% in volume. At low pulsation intensity, the particles settle whereas at sufficient pulsation conditions, the particles are uniformly distributed in the column. An increase of the frequency or of the amplitude leads to a more expanded bed. The authors explain the phenomenon by the entrainment of the solid by the chaotic liquid flow. Highly turbulent zones are created and disappeared between the doughnuts due to the pulsation and the packing. They define a ratio between concentrations corresponding at two different levels in the column γ which is expressed by:

$$\gamma = \left[1 - \exp\left(-R_{Mackley}\,\frac{2\pi A f}{u_t}\right)\right] \qquad \text{(V- 6)}$$

$R_{Mackely}$ is an empirical constant.

When the ratio is equal to 1, the suspension is uniformly distributed along the column packed with doughnut. If the value is less than 1, a concentration gradient is noticed.

Moreover, for different particle populations, with low pulsation, the segregation can be controlled.

I.4. ***Co-current pulsed column or analogous column***

Reis *et al.* (2005) study a continuous flow screening mesoreactor. It consists in a continuous oscillatory baffled reactor. The baffle corresponds in fact to glass restriction. The internal diameter of the column is of 4.4mm and the diameter at the restriction is of 1.6mm. They identify the suitable oscillation conditions for different particles (silica resin, polyamide resin, ion exchange resin) with distinct size and sedimentation velocity. They observe that it is easier to keep particles suspended in the horizontal configuration of the reactor than in the vertical configuration.

Some works concerning crystallization in oscillatory baffled reactor are available in literature. For instance, Lawton *et al.* (2009) perform the crystallization of an active

pharmaceutical ingredient in a COBR for which the configuration is close to the one studied chapter IV section 3. They synthetized a API with a good morphology of the crystals. Uniform crystals sizes are produced. A good control of the shape and the size of the crystal is ensured.

Based on these observations, we are confident concerning the suitability of the pulsed column to ensure the homogeneity of the suspended PVC particles if the operating conditions are properly chosen.

II. MATERIAL AND METHODS

II.1. ***Experimental rig***

The pilot is almost identical to the one presented in chapter IV (part II-1) for the liquid-liquid dispersion: the discs and doughnuts pulsed column. The major difficulty lies in the ability to generate a homogeneous suspension before entering into the column at the bottom.

To create the suspension, a tank is mounted directly on the feed of the pump. It is composed by a PVC cylindrical tank and the suspension is loaded and continuously stirred by means of a gear pump which creates a recirculation loop. The initial PVC granulometry is not affected by this pump (see Figure V-2). This recirculation allows to avoid the settling of the particles and to ensure a homogeneous pumping of the suspension.

The circulation of the suspension is then ensured by a Netzsch pump which is suitable for conveying solid. It is divided in two parts: the first part is composed by the stainless steel tank (above which is located our feeding tank) which contains an endless screw. It ensures the solid-liquid transport to the elastomer endless screw. The second part is composed by the elastomer endless screw which is constituted by a rotor and a stator which is able to convey the suspension to the column by avoiding the leakage of the solid feed (Figure V-1).

Figure V- 1 : NETZCH pump

The engine of the screw is connected to a Leroy Somer frequency variator which allows to range the initial suspension flowrate from 0 to 36 $kg.h^{-1}$.

The liquid flowrate is ensured thanks to a membrane pump and ranges from 0 to 220 $L.h^{-1}$. Both flows meet before entering the column. A sampling valve is located just after to check the particle size distribution and the solid phase fraction.

The initial suspension prepared in the feed tank is 10kg. It is composed by 40% in weight of solid PVC particles and in 60% in weight of demineralized water containing PVA as surfactant.

The liquid flowrate is composed only by demineralized water.

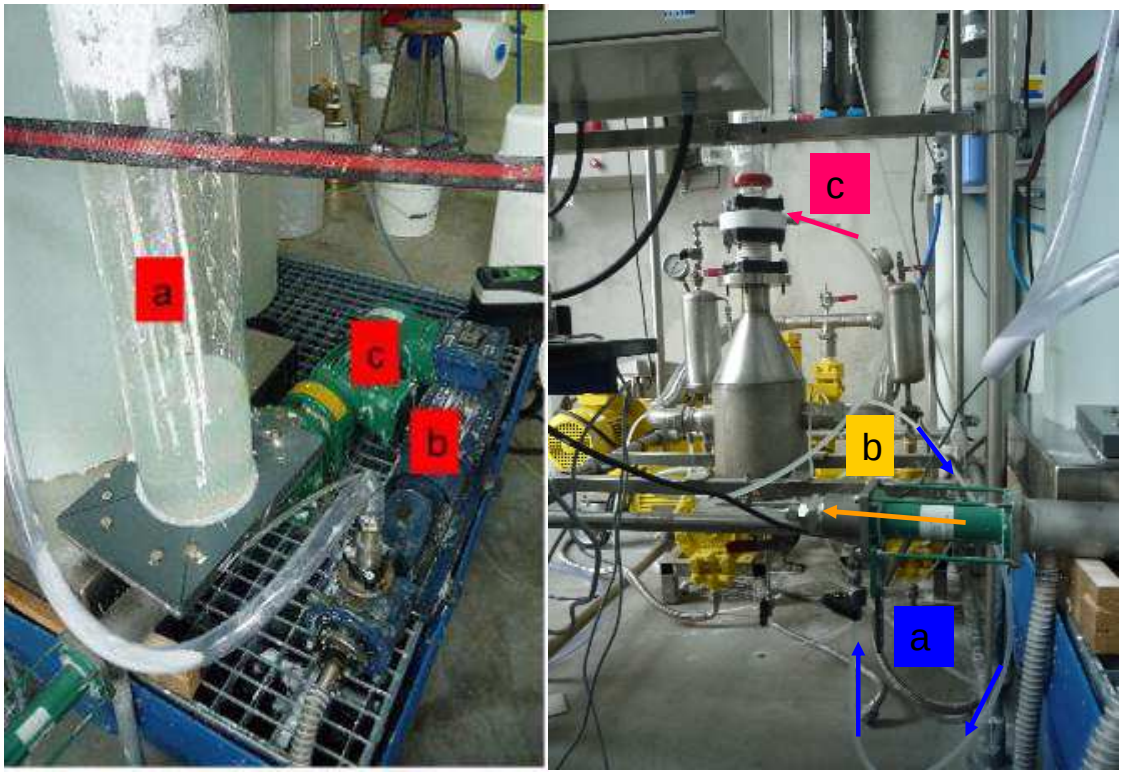

Figure V- 2 : Left: Suspension creation (a) tank (b) gear pump for the recirculation (c) Netzsch pump for the solid liquid transport Right: (a) aqueous phase circulation and introduction at the end of the screw (b) suspension of 40% in weight of PVC particles (c) introduction of the diluted suspension in the column

The column is the same as the one described in chapter IV.

The different samples collected at the bottom and all along the column are analysed thanks to laser diffraction measurement (Mastersizer 2000) in suspension and after drying. The solid mass fraction is evaluated by weighting the sample before and after drying at 45°C.

II.2. *Validation of the feeding process*

First, the homogeneity of the suspension delivered by the Netzsch pump is evaluated by checking the constancy of the solid phase fraction according to time.

In Figure V- 3, the evolution of the solid phase fraction (without drying) is presented. The samples are collected in graduated test tubes at different times and after particle settling, the volumes occupied by each phase are measured. However, the PVC grain particles are porous and some water may be absorbed which explain the high values obtained for the solid phase fractions.

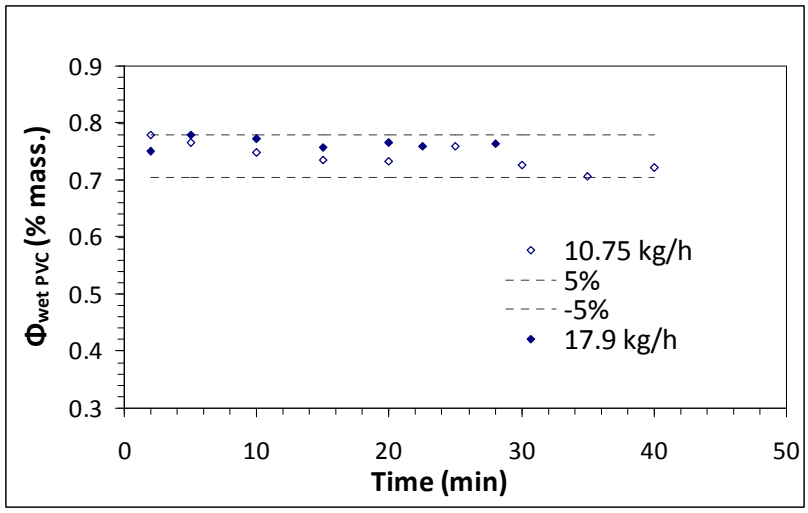

Figure V- 3 : homogeneity of the suspension at the Netzsch pump outlet for a total flowrate of 10.75kg.h^{-1} and 17.92kg.h^{-1}

But, the most important is to check that the solid phase fraction, whatever the value, is constant at more or less 5% all along the experiment. The error is maximal at the lowest flowrate.

III. OPERATING CONDITIONS

The total flowrate conditions were previously defined based on the principle that the flow velocity has to be much larger that the terminal velocity of a single particle, in order to transport the solid phase without any settling. The terminal velocity of a 150µm solid particle is estimated via the Stokes' law. The flow velocity chosen in our study correspond to five times the former terminal velocity, corresponding to a total flowrate of 141 L.h^{-1}. Below this value, the water flowrate is not high enough to transport the suspension from the pump to the column basis. Above this value, the suspension flowrate delivered by the Netzsch pump is too low to ensure a correct solid phase fraction.

The oscillation conditions investigated are exactly the same as in chapter IV. From Table V- 2, in theory, the solid phase fractions are estimated to 5, 8 and 9.8% in mass but some of the solid settled in the tank of the pump and is never dragged away. To be sure of the solid phase fraction entering in the column, a sampling is collected for further analysis.

We note that these mass solid phase fractions are below the dispersed phase concentration investigated in the liquid-liquid dispersion study (chapter IV) due to the technological limitation.

Flowrate of the suspension phase $kg.h^{-1}$	Flowrate of the continuous phase $kg.h^{-1}$	Oscillation conditions
17.9	125	A = 24-38-52 mm
28.7	115	f = 1.17 -1.56 Hz
35.9	110	

Table V- 2 : Operating conditions for the solid-liquid tests in disc and doughnut pulsed column

III.1. ***Reproducibility of the measurement***

The measurement is performed three times for a given operating condition. The measurement leads to perfectly superimposed particle size distribution.

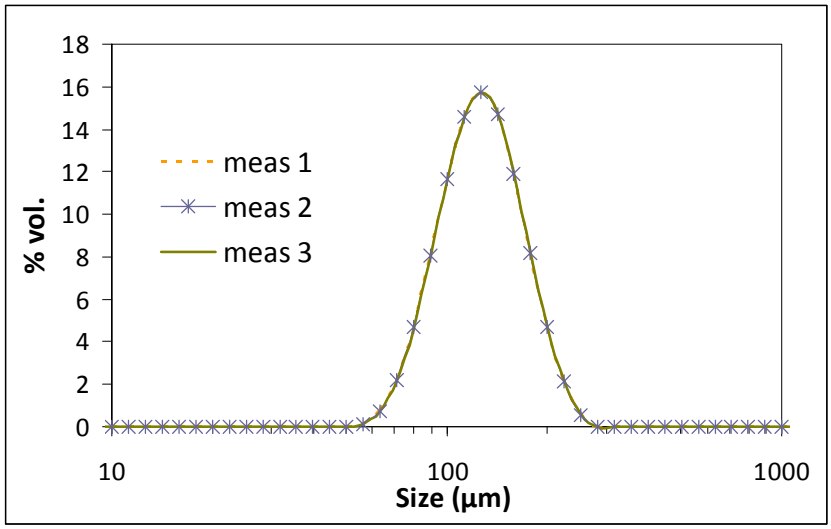

Figure V- 4 : reproducibility of the measurement in the analysis of a sample (A=24mm, f=1.56 Hz, H=0m, Q_{liq}=, Q_{susp}=)

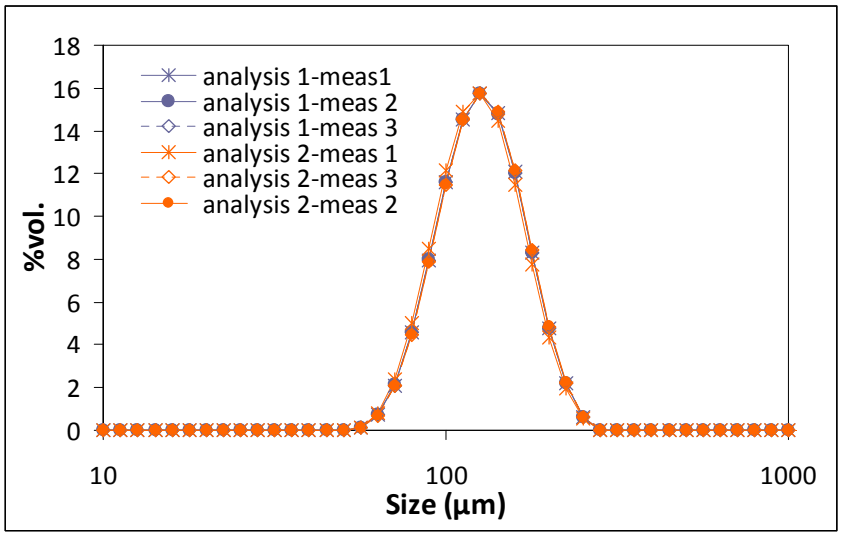

Figure V- 5 A=38 mm f=1.56Hz H=1 (1503)

The measurement is then reproducible as well as the sampling.

The same considerations are noticed for the distribution obtained after drying (ie. Figure V- 6 and Figure V- 7)

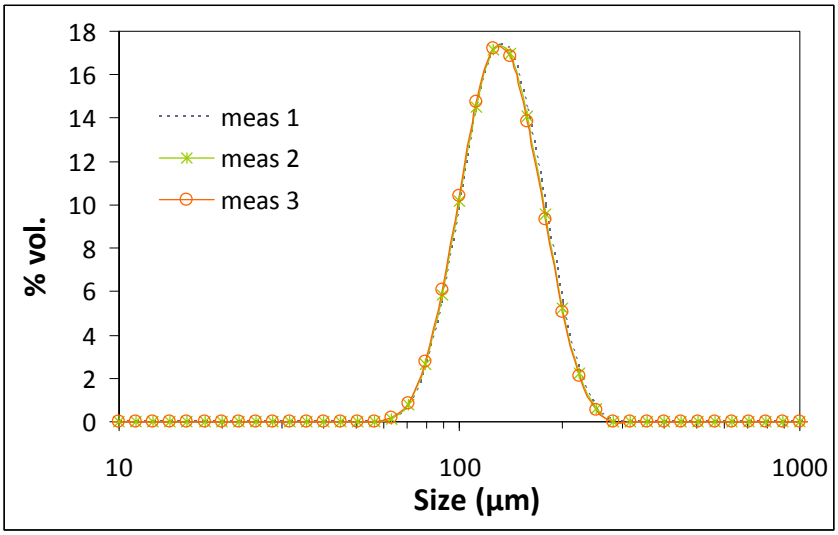

Figure V- 6 : Reproducibility of the measurement on the dry particle for the initial loading of the pump

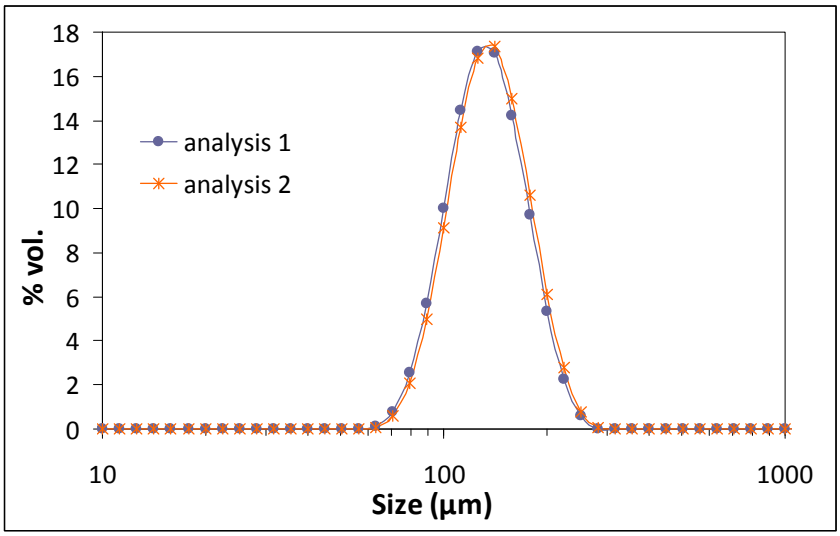

Figure V- 7 : repeatability of the sampling (two sampling of a same experiment)

III.2. ***Reproducibility of the process***

In the same way, some experiments are performed two times to check the reproducibility of the process.

It is evaluated in term of particle size distribution and in term of solid phase fraction evolution.

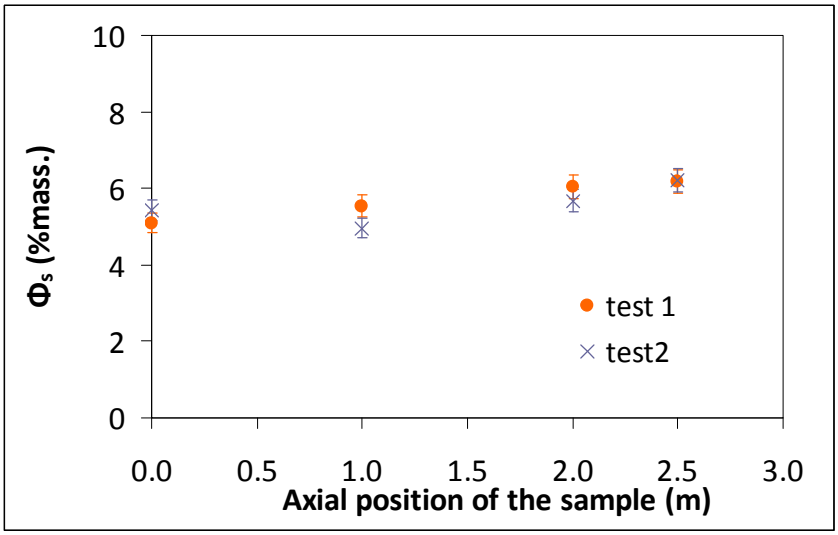

Figure V- 8 : Evolution of the solid phase fraction from the basis to the top of the column at a liquid flowrate of 115L.h^{-1} for pulsation conditions A=24mm and f=1.17Hz

The dispersed phase concentration is constant and the experiments are reproducible.

The same consideration can be made from the particle size distribution (Figure V- 9).

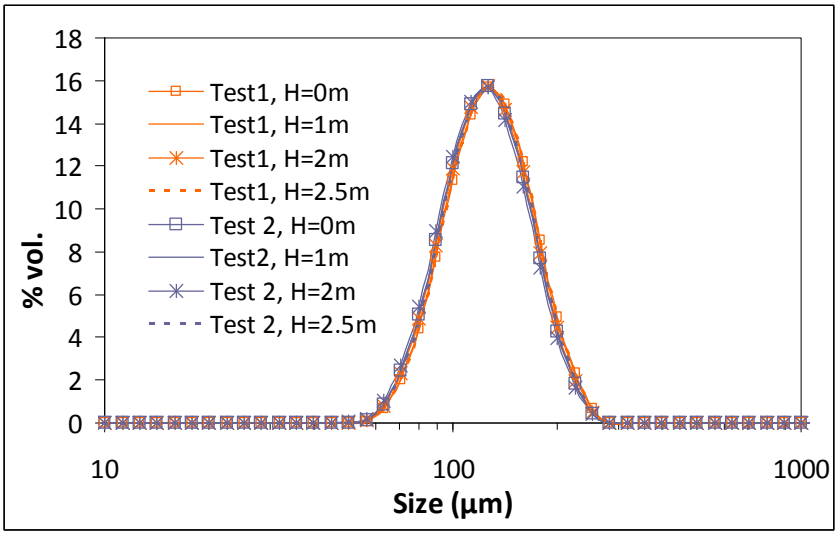

Figure V- 9 : Particle size distribution all along the column, Q_{liquid}=115 kg.h^{-1}, A=24mm, f=1.17Hz (humid way)

Several points must be noticed:

- The sampling at the third meter is not taken into account. Indeed, the particle size distributions obtained are shifted to the larger size at this sampling. The column section becomes larger and then the velocity decreases resulting in a particle settling. This point is then not relevant for our study. We remind that this sampling was evicted too at chapter IV for similar reasons.
- It can be noticed that the solid phase concentrations obtained are lower than expected by the theory. Indeed, the flowrates were initially calculated at 5, 8 and 10% in mass whereas the effective solid phase fractions are respectively close to 4, 6 and 8% in mass. Several explanations can be proposed. First, it was observed that in the feeding tank above the pump, there is a settling phenomenon in the endless crew and some particles are not carried away. Moreover, at the basis of the column, there is the same problem that at the top: the section is larger and due to the backward flow with pulsation, some solid are settling progressively at the column bottom. To avoid the solid accumulation, the column is drained after each series of experiments (composed by two to three tests). This discrepancy between the theoretical phase fraction and the experimental solid phase fraction is completely reproducible as seen in Figure V- 8 and further.

IV. RESULTS

IV.1. *Effect of the pulsation conditions*

For a total flowrate and a solid phase concentration constant, the effects of the pulsation on the particle size distribution and on the solid phase fraction evolution along the column are investigated

From the Figure V-10, it can be seen that whatever the oscillation conditions, the solid is carried uniformly all along the column. This result suggests that the disc and doughnut pulsed column is suitable to ensure a homogeneous transport of the ¨PVC particles.

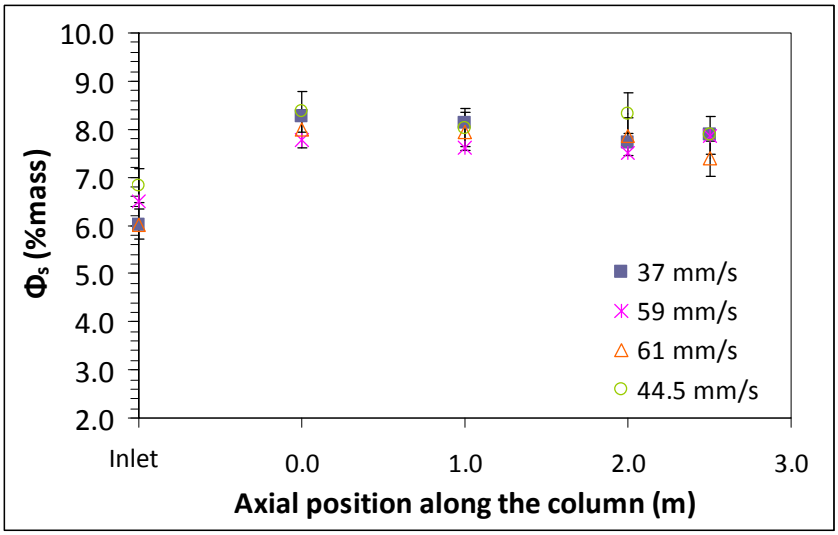

Figure V- 10 : Evolution of the solid phase fraction along the column for different pulsation condition (Q_{liquid}=110 kg.h^{-1})

Now, the particle size distribution must be analysed to check if there is no granulometry dispersion and if the solid particle population is carried at a whole.

From Figure V-11, the effect of the pulsation conditions is noticed on the mean particle size: the particle size distributions are totally superimposed for the different samples collected all along the column. It suggests then a perfect homogeneity of the solid transport. Several particle size distributions corresponding to different oscillation conditions are reported.

Figure V-11 corresponds to the samples collected at different positions along the column. It can be clearly seen that no significant difference among the PSD is observed. Consequently, the entire particle population is carried in a homogeneous way.

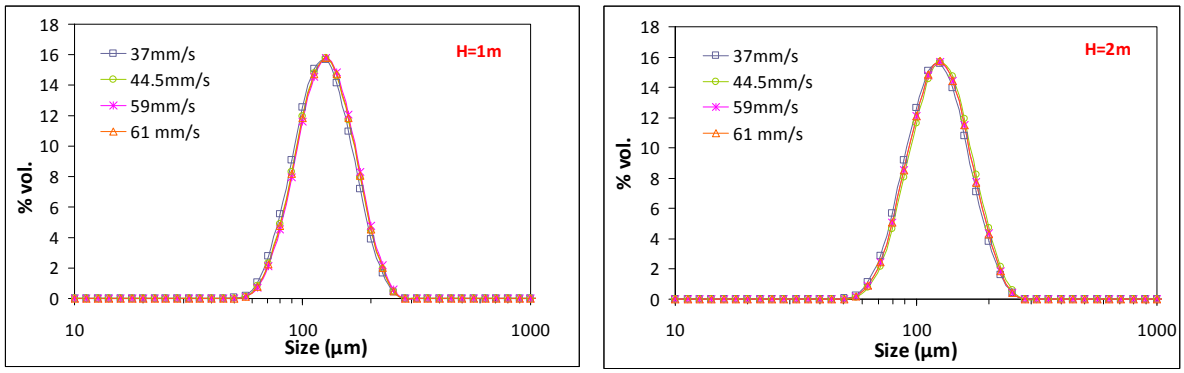

Figure V- 11 : Evolution of the particle size distribution (PSD) for different pulsation conditions at H=1m and H=2m (Q_{liquis}=110 kg.h^{-1}) – wet suspension analysis

To conclude, the oscillation conditions investigated do not allow to point out any effect of the oscillation conditions. The suspension is as homogeneous at the inlet of the column as the outlet of the column. It is satisfactory because it implies that the previous conditions used for liquid-liquid dispersions are suitable to perform the transport of the solid-liquid suspension too.

IV.2. ***Effect of the solid phase fraction***

Given that the total flowrate is maintained constant at more or less five percent, the solid phase fraction ranges from 5 to 10 % in mass approximately. In fact, as already said, it ranges from 4 to 8% in mass.

The same trends described in the previous part for 8% are observed. Figure V-12 represents the evolution of the solid phase fraction in the same oscillating condition. The solid phase fraction is carried out homogeneously from the bottom to the top of the column for all the solid phase fractions studied.

In a same way, the particle size distributions are reported in Figure V-13. The particle size is exactly the same all along the column at given operating conditions. For the three solid phase fractions studied, the particle size distributions are totally superimposed. There is no settling of the particles and no axial distribution of the particle. The same population is encountered from the basis to the top.

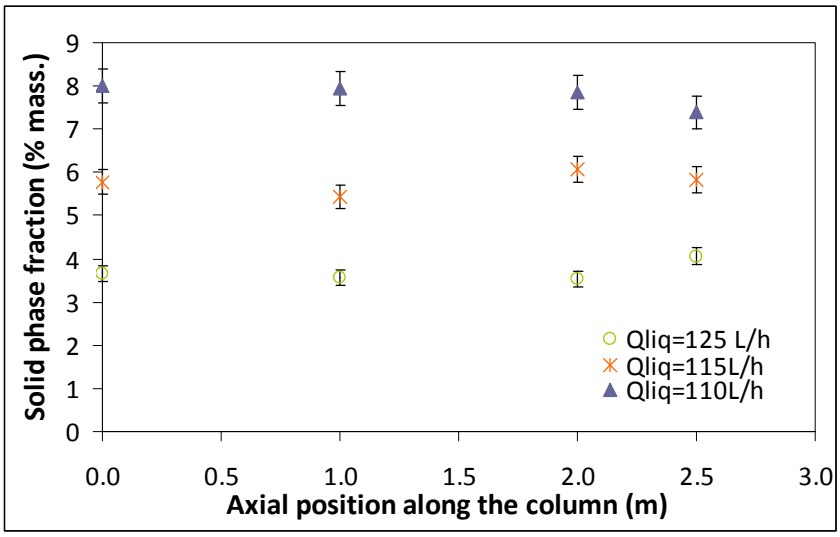

Figure V- 12 : Evolution of the solid phase fraction for A=52mm and f=1.17Hz with a total flowrate of 141 L.h^{-1} along the column for different liquid flowrate

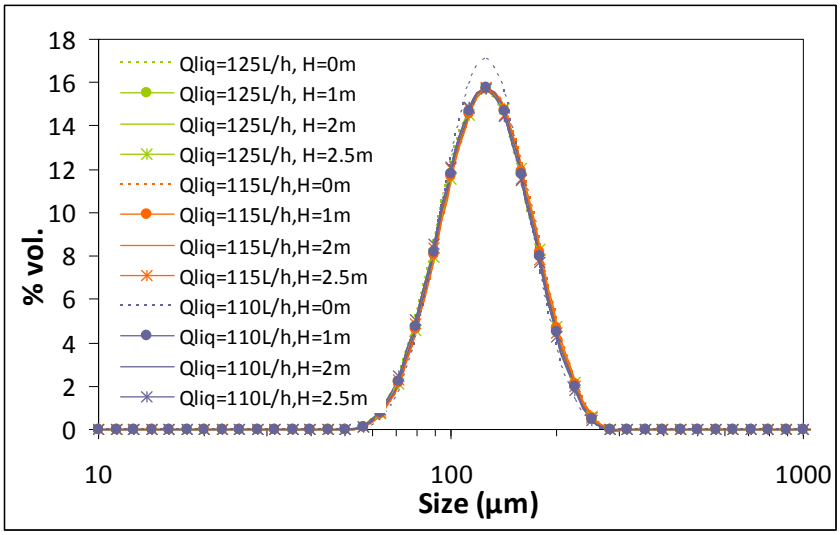

Figure V- 13 : Particle size distribution all along the column A=52mm, f=1.17Hz for three different solid phase fraction

The range of phase fractions studied is unfortunately relatively low, because of practical reasons. However, for the investigated conditions, the disc and doughnut pulsed column reveals itself perfectly suitable to ensure a homogeneous transport of the PVC solid particles and to maintain the particle size distribution.

V. CONCLUSION

In this chapter, some practical problems encountered are not directly linked to the S-PVC process. Some implementation difficulties are simply due to question of the initial suspension creation. This step corresponds to the last step of the process during which the agglomeration process is achieved and the reaction occurs whereas the particle size does no longer vary. In a continuous process, the suspension enters the column, or depending on the chosen process keeps evolving in the column. The co-current disc and doughnut pulsed column has demonstrated its ability to maintain the particle size distribution and the solid phase fraction. Consequently, this process can be interesting at least to lead the polymerization reaction until the expected conversion rate. Of course, once the material of the column chosen (wall and packing), a heat transfer study has to be performed.

To conclude the previous chapters, the disc and doughnut pulsed column may be considered as a potential reactor to create the initial liquid-liquid dispersion and to start the reaction but also as the termination reactor after the agglomeration step. In the last chapter, a suspension polymerization is performed to study its resistance to the fouling.

Given the operating conditions (high pressure) needed for VCM polymerization (as well as the security), a model polymerization system is used (see chapter II and VI). This reaction is detailed in our last chapter.

CHAPTER VI: Continuous suspension polymerization in a pulsed reactor – the case of vinyl acetate

The goal of this study is to identify the equipment suitable to perform the suspension polymerization of vinyl chloride in a continuous way. One of the major bottleneck (see chapter I section I-4-2) identified is the fouling and encrusting. During this step, the particles are sticky. This physical behaviour of the polymerizing droplets occurs during the agglomeration step (see Figure I-4).

The pulsed column or the continuous oscillatory baffled reactor have been considered as potential suspension polymerization reactors. Their abilities to create and to maintain a suitable liquid-liquid dispersion and further the solid-liquid suspension have been demonstrated respectively in chapter IV and in chapter V. The only remaining bottleneck of their use as continuous suspension polymerization reactor is to check their ability to prevent from fouling. So we have decided to perform a feasibility study of a suspension polymerization reaction with the continuous oscillatory baffled reactor (COBR). This reactor is long enough to ensure a total residence time of one hour.

As mentioned in chapter I, the vinyl chloride monomer VCM is a toxic gas and the reaction must be carried out under pressure. Consequently as described in the section III (chapter I), the vinyl acetate suspension polymerization has been chosen as test reaction because the suspension polymerization can be carried out easily at ambient pressure and the vinyl acetate presents physico-chemical properties close to the VCM . Besides, the different stages of polymerization are similar. Particularly, the sticky stage is also observed during the vinyl acetate polymerization. The main difference between both processes is that the vinyl acetate polymer (PVAc) is soluble in vinyl acetate monomer (Ueda *et al.* 1972). The monomer dissolves its polymer: the monomer droplets pass through a viscous syrup state and finally are transformed into solid clear little spheres called beads.

This chapter does not intend to study the vinyl acetate polymerization deep in detail with the effect of the different parameters (pulsation, flowrate, temperature, initiator concentration, primary suspending agent concentration…). It is mainly a feasibility study to check the ability to perform a polymerization in a continuous pulsed reactor and particularly to observe the reactive mixture behaviour during the sticky stage of the process. The system studied as well as the recipe are completely detailed in chapter II, section I-3.

In this chapter, some characteristics of the vinyl acetate suspension are taken from the literature. Then, the different experimental rig and processes are described. Preliminary batch experiments were carried out to better understand the basics of the reaction. Batch and continuous experimental tests provide an insight of the shape and physical appearance of the obtained particles. Finally the last part focuses on the test performed in the continuous oscillatory baffled reactor. The difficulties encountered are highlighted and the preliminary results are presented.

I. VINYL ACETATE MONOMER SUSPENSION POLYMERIZATION IN LITERATURE

The suspension polymerization of the vinyl acetate monomer VAM leads to the poly(vinyl acetate) polymer PVAc, which can be partially hydrolysed by saponification to product the PVA at different hydrolysis degrees and used as suspending agent in polymerization, especially in the case of vinyl chloride suspension polymerization. The PVA is also largely used in medicine, such as for the tumor embolization (Peixoto *et al.*, 2006 and 2009).

The PVAc is mainly produced by emulsion polymerization and few publications concern the suspension polymerization of VAM.

Kalfas *et al.* (1993) published some results concerning the kinetic study. They studied the effect of the monomer to water ratio and the effect of the monomer solubility in water. They used the kinetic constants established by Teymour (1989) which are reproduced in Table VI- 1. The decomposition kinetic constant of our initiator is also indicated.

Decomposition initiator kinetic constant k_d (s^{-1})	$k_d = 7.44\times10^{15}\exp\left(-129.39\times10^{3}/RT\right)$
Propagation kinetic constant k_p ($L.mol^{-1}.s^{-1}$)	$k_p = 3.2\times10^{7}\exp\left(-6300/RT\right)$
Transfer to monomer k_{trM} ($L.mol^{-1}.s^{-1}$)	$k_{trM} = 0.238\times10^{-3}k_p$
Transfer to polymer k_{trP} ($L.mol^{-1}.s^{-1}$)	$k_{trP} = 0.34\times10^{-3}k_p$
Termination kinetic constant k_{td} ($L.mol^{-1}.s^{-1}$)	$k_{td} = 3.7\times10^{9}\exp\left(-3200/RT\right)$

Table VI- 1 : Kinetic constant for the VAM suspension polymerization (T in degree Kelvin, R cal.mol^{-1}.K^{-1} the gas constant except for k_d in J.mol^{-1}.K^{-1})

The solubility of VAM in water is of 2.9% in weight at 50°C (Kalfas *et al.*, 1993). Some authors have reported some noticeable effects on the polymerization rates, composition and molecular weights of suspension polymers (Bahargava *et al.*, 1979; Mino, 1956; Taylor and Reichert, 1985). Kalfas *et al.* (1993) demonstrated the evidence of monomer mass-transfer limitation in vinyl acetate suspension polymerization. They applied a homogeneous polymerization model and their experimental data do not fit well with the model. The model predicts a higher conversion than the experimental one. Consequently, they modified their model by taking into account the dissolved monomer in the aqueous phase and the dilution effect of the water in the organic phase. They reveal then that the dissolved monomer remains in the aqueous phase and does not return to the polymer particle at high conversion.

II. EXPERIMENTAL RIG

II.1. *The batch reactor*

The reaction is first performed in a 2L jacketed glass batch reactor. It is equipped with four baffles and a four inclined blades impeller.

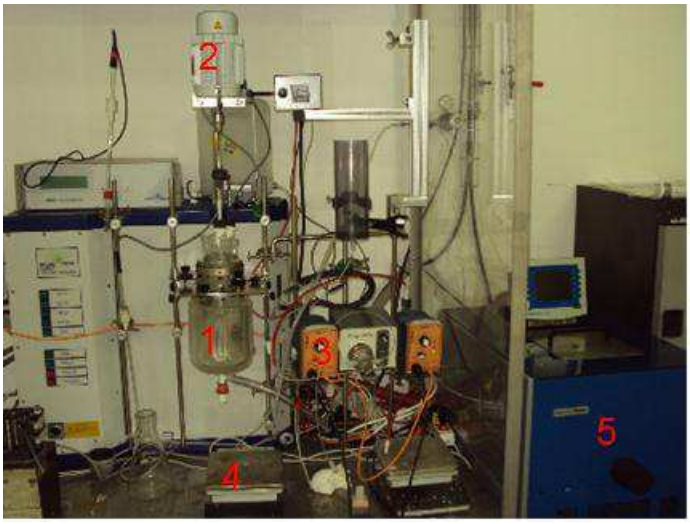

Figure VI- 1 : Experimental rig for the batch test

Figure VI- 2: Batch reactor

The reaction is entirely piloted by the Labmax® software. The pilot allows to measure the main operating parameters: the stirring velocity, the jacketed temperature, the product temperature, the dosing profile…

The aqueous phase and initiator are introduced manually. The vinyl acetate is introduced thanks to a pneumatic pump which is controlled by the software. The vinyl acetate mass

introduction is easily followed thanks to the weight control. The weight evolution is also recorded by the acquisition software.

For the temperature registration, the PT100 probe is immerged in the reactor close to the impeller. It corresponds then to the reactor temperature noted T_r. The jacket temperature T_j is also recorded.

The Labmax® unit is composed by three modules: a thermal regulation unit, a control unit of the instrument, a heat exchanger (thermostat). The jacket of the reactor is filled with silicon oil. It flows in the reactor jacket and through a plate exchanger in which the cryostat fluid circulates too. The silicon oil flowrate is set thanks to the Labmax regulation unit and adjusted thanks to an electrovalve.

The Labmax® unit allows to compute all the reaction steps and then no manual operation is needed. But, contrary to the classical calorimeter reactor, the software does not allow to calculate the reaction polymerization enthalpy.

The aqueous phase is swept by a nitrogen flux and the vinyl acetate bottle as well because the oxygen is responsible for an induction period in the polymerization (Levy and Hinojosa, 1992).

The following steps for the reaction are as follows:

- The reactor is initially filled with water, the primary suspending agent PVAI and the initiator (details chapter II part I-3). The aqueous solution is stirred at N=400 rpm and the reactor temperature T_r is maintained at 20°C. The solution is stirred under nitrogen.
- The reactor temperature is maintained at 20°C. The vinyl acetate is introduced within five minutes. The stirring is fixed at 400 rpm (except of the test Batch01: N=350 rpm). This liquid-liquid dispersion step lasts 30 min according to literature (chapter I part I-2).
- Then the reactor is heated at 60°C. The reactor temperature is kept constant by controlling the jacketed temperature.
- The reaction proceeds until the product temperature and the reaction temperature are equal.
- The reactor is then cooled at 20°C and drained.

The mixture is then filtered on a filter under vacuum and the cake is dried under vacuum at 20°C during 48 hours.

The conversion can then be estimated with the ratio PVAc mass to initial monomer introduced.

II.2. ***The continuous oscillatory baffled reactor***

The oscillatory baffled reactor (COBR, Nitech) already used in chapter IV will be considered now for the continuous suspension polymerization.

However in chapter IV, the total reactor length was not necessary. Indeed, the reactor is composed of 68 circa glass tubes of 70cm and of 32 U-tubes in a vertical position on the left and in a horizontal position on the right. It leads to a nearly 51 m long reactor.

First, the total length was foreseen for the polymerization reaction. But due to some difficulties (mass polymerization due to poor stirring, see section IV), the column length was then reduced. The goal for this feasibility study is just to reach a convenient conversion range corresponding to the sticky behavior of the particles (see chapter I-section I-3).

To estimate the conversion and temperature profile along the column, some sampling valves and temperature probes (PT100) are placed all along. Their positions are indicated relatively to the initial position (H=0m) corresponding to the contact location of the 3 reactive phases.

To have access to the reaction temperature, four PT100 probes are placed along the column:

- section 6 at the first branch at the start of the heating (H=10.8m)
- at the first branch of section 10, H=23m
- at the first branch of section 11, H=27.45m
- at the third branch of section 13, H=32.15m

Similarly, in order to follow the conversion along the column, different sampling valves allow to collect the product.

They are respectively located:

- at the section 4 for the liquid-liquid dispersion, H=4.70m
- at the third branch of the section 7, H=15.25m
- at the first branch of section 10, H=23m
- at the third branch of section 11, H=27.45m
- at the reactor outlet, H=34.25m

Figure VI- 3 describes the whole experimental rig.

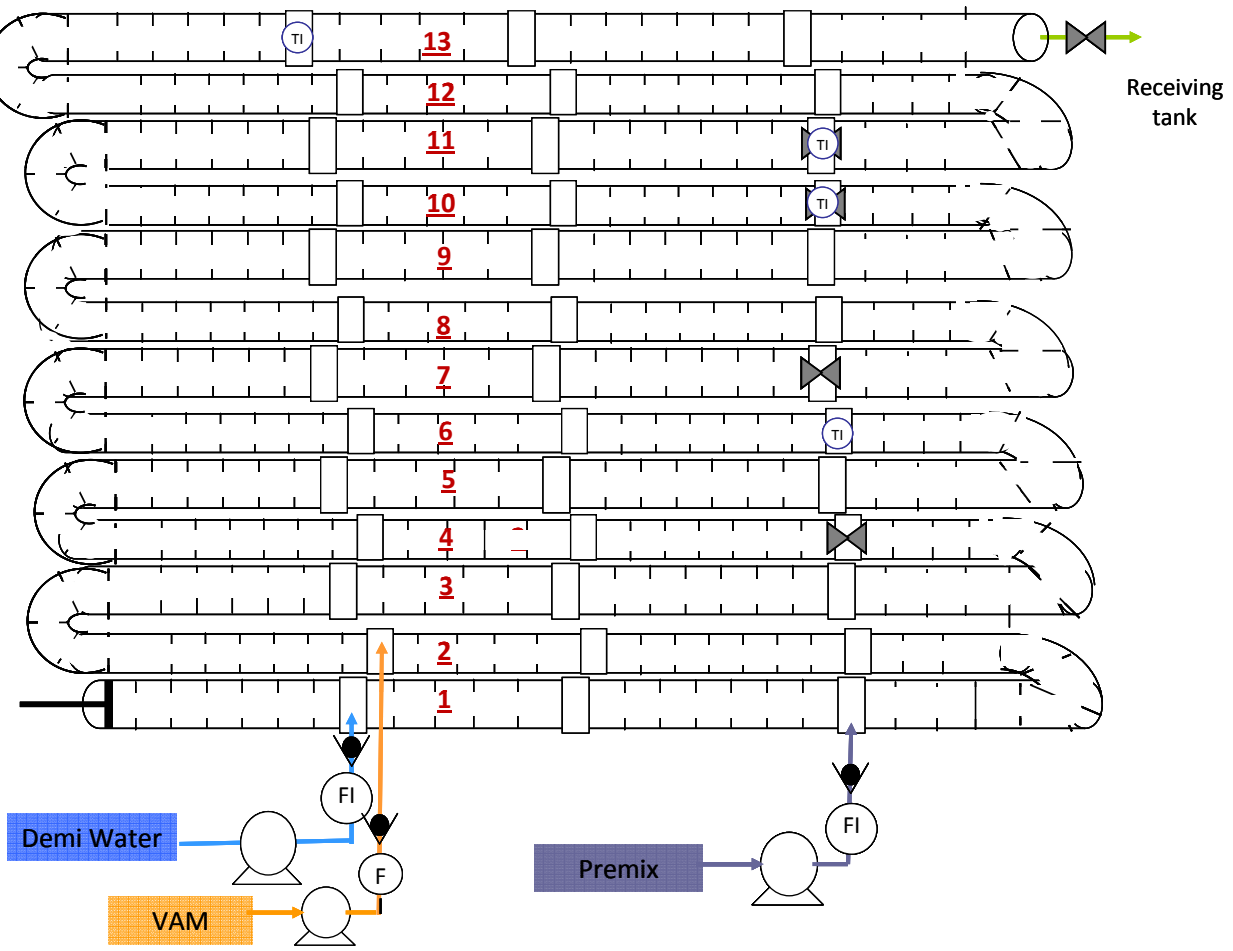

Figure VI- 3 : Schematic representation of the continuous oscillatory baffled reactor, FI corresponds to the flowrate, TI to the PT100 probes

The demineralized water and the vinyl acetate are pumped by a centrifugal pump. The flowrates can range from 0 to 150 g.min^{-1}. The flowrate and the density of both inlet phases are recorded. The premix is fed by a piston HPLC pump (ARMEN). All the feeding lines are equipped with check valves.

The different sections of the column are devoted to different operations:

- the demineralized and degassed water is introduced 70 cm after the piston
- the premix composed by demineralized water, initiator and PVA surfactant under nitrogen and continuous stirring is introduced 1.40m after the first introduction
- the vinyl acetate (17kg barrel surrounded by a nitrogen blanket) is introduced on the last branch of the second section, 5.15m after the piston.
- then sections 3 to 5 are devoted to the liquid-liquid dispersion. The jacket is maintained at 22°C. (total length 9.15m for the liquid-liquid dispersion)
- from sections 6 to 9, the mixture is heated at the polymerization temperature. Initially the polymerization reaction temperature is expected to be 60°C. However, with the oscillation and the subsequent alternate high pressures and low pressures caused by

the piston, the vinyl acetate tends to degas and create bubbles which reduce the pulsation intensity. Consequently, the jacketed temperature is set to 62°C. The length of this section is of 12.2m.

- in the following section (10-12) the polymerization temperature is maintained. The jacketed temperature is set to 55°C. The length of this section is of 9.15m.
- in the last section (13), (length of 3.75m) the mixture is cooled below 20°C for safety reason: the reaction is then stopped (the initiator decomposition begins at 35°C).

The total flowrate is of 145.5 $g.min^{-1}$. The total residence time is around 45min but only 30 min is devoted to the polymerization reaction.

The pulsation conditions are determined thanks to the results obtained in chapter IV (see Figure IV-36). We have chosen a stoke piston length of 30mm (60mm of displacement in the column) and a frequency of 1 Hz. Let's underline that the COBR is also equipped with a pressure sensor for security reason and as soon as 5 bar are reached, the pulsator stops. So the operating conditions must not have to exceed 4 bar (that's why the pulsation are set to fulfill this additional condition)
It is expected that under these conditions the monomer conversion will be not complete.

Lots of problems have been encountered during the preliminary tests. The first tests were conducted by using the whole column length (17 tubes) to reach a total residence time of 1 hour. Tests have been run to evaluate the jacketed temperature in order to reach 60°C inside the reactor. At ambient pressure, the boiling temperature of the vinyl acetate is 72°C. However at 60°C, the vinyl acetate tends to degas in the column sections. This is due to the compression and depression induced by the piston on the flow. This degassing creates lots of bubbles in the column. The bubbles progressively move on with the flow but tend to coalesce in the last sections. The resulting vapor slugs annihilate the pulsation effect and the reactive mixture is no longer mixed. At the beginning, the flowrate is maintained but progressively the polymer fills the cells of the apparatus and then the reactor is completely stuck. The first tests have then led to an encrusting of the reactor. Figure VI- 4 shows some pieces of polymer blocks.

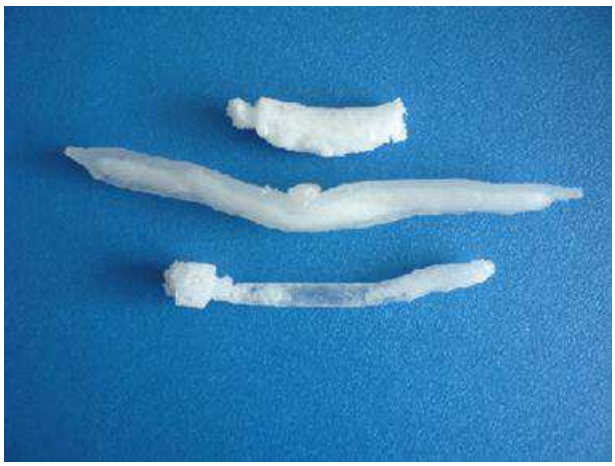

Figure VI- 4: polymer block resulting from the encrusting of the COBR

The degassing could be avoided by decreasing the temperature of the polymerization. Another solution could consist in adding an on-line gas purger at every U-tube. By lack of time, the first solution has been chosen.

A second problem was related to the flowrate. Indeed due to the pulsation, the flowrate is fluctuating a lot. Some counter-pressure elements have been added to limit the pulsation effect. Moreover, it is difficult to ensure a constant flowrate with the ARMEN pump in the presence of solid particles (initiator).

Finally, the piston tends to pump external air. The problem was solved by linking the piston leak to a bottle of demineralized water.

III. PRE-STUDY IN BATCH

III.1. Operating conditions

Figure VI- 5 and Figure VI- 6 depict the operating conditions evolution for the test batch02 and 03. All the monitoring parameters are represented: the reactive mixture temperature and the corresponding set-point (green), the jacketed temperature (purple), the stirring velocity N (orange). The vinyl acetate mass set-point and introduction are also represented. The software calculates also the difference between the reactant and jacket temperatures. The test batch 01 is not described but the same trends are observed. The main difference is the evolution of the stirring velocity from 350 to 400 rpm during the polymerization.

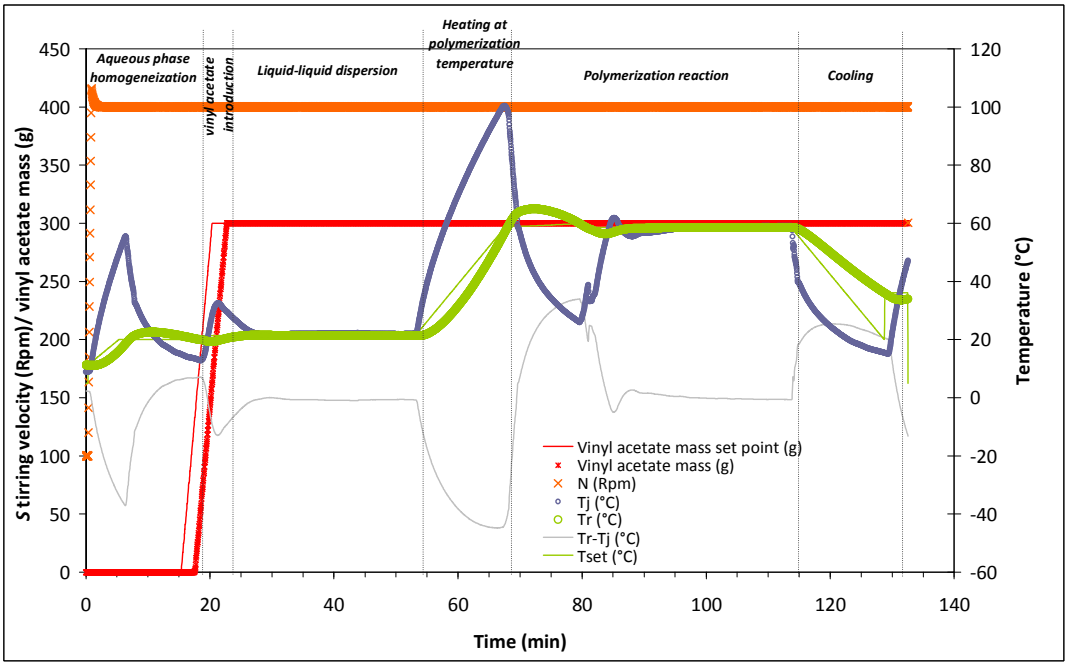

Figure VI- 5 : Batch polymerization process monitoring-batch02 test

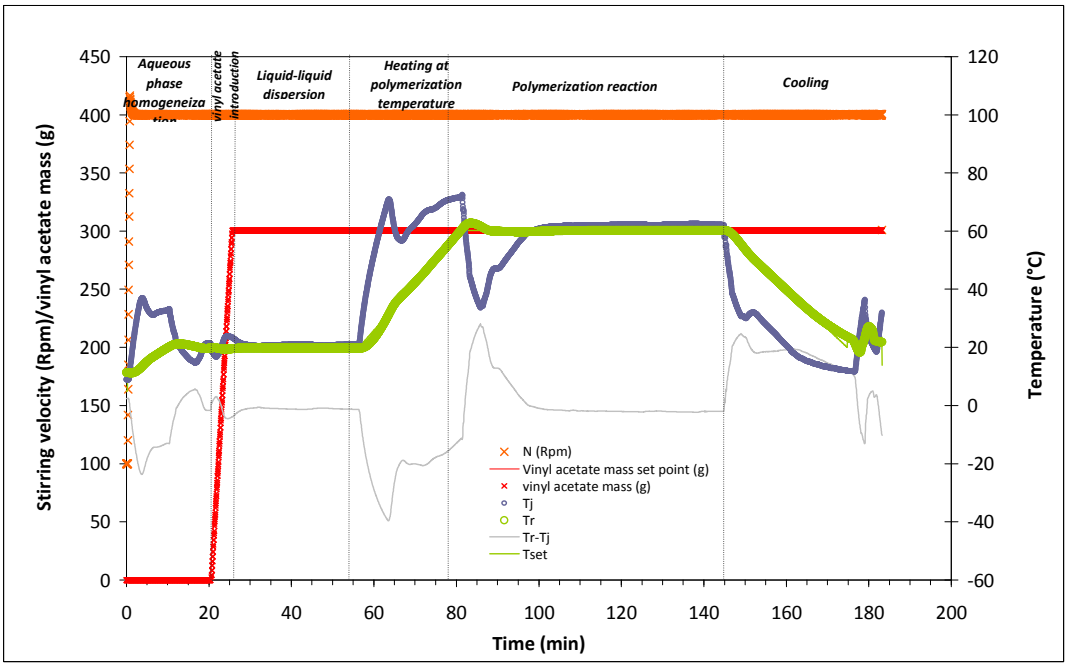

Figure VI- 6 : monitoring for the Batch 03 test

The different process steps are indicated on each graph. The time length for each step can be evaluated. We focused on the heating and polymerization times (see Table VI- 2).

At the end of the heating time, in both cases, we observed a small peak of the reactive mixture temperature. The vinyl acetate suspension polymerization is exothermic (ΔH_r=-88 kJ.mol^{-1}). This peak is attributed to the exothermicity of the reaction. The difference between both temperatures is high (around 35°C). At the end of the reaction the jacketed temperature is equal to the polymerization temperature. No more heat is emitted by the reaction. The reaction is then complete.

III.2. ***Conversion***

The conversion is obtained by comparing the product mass to the initial monomer vinyl acetate introduced.

The following table summarizes the results obtained for the three runs performed.

Test number	Heating time (min)	Polymerization time (min)	Tmax °C	Tmoy °C	Conversion X (% mass)
Batch01	14	61.7	62.3	56.6	72.5%
Batch02	14.2	46	72.6	58.5	83%
Batch03	24.5	33.4	62.7	59.7	67%

Table VI- 2 : some characteristic times and temperatures of the reaction and their corresponding conversion for the different tests

For batch02 and 03 tests, the evolution of the conversion is logical: less polymerization time in the same condition leads to a lower conversion. In addition, the maximum reactive temperature reached is higher for batch 02 test which contributes to the faster decomposition of the initiator and then to obtain higher conversion.

Regarding batch01 and batch03 tests the conversion difference is due to the longer reaction time in the batch01 test.

III.3. ***Solid characterization***

The solid is characterized after filtration under vacuum and drying under vacuum at 20°C. Unfortunately, this treatment leads to the formation of agglomerates and the granulometry cannot be obtained by laser diffraction measurement (Malvern Mastersizer 2000).

The samples are observed thanks to SEM (Figure VI-7).

The particles are well spherical and present a smooth surface. Larger particles are obtained in the Batch01 test which seems the more polydispersed. It is logical because less primary suspending agent was used and the liquid-liquid dispersion was created at a lower stirring velocity N. A residual small skin is sometimes observed on the agglomerates.

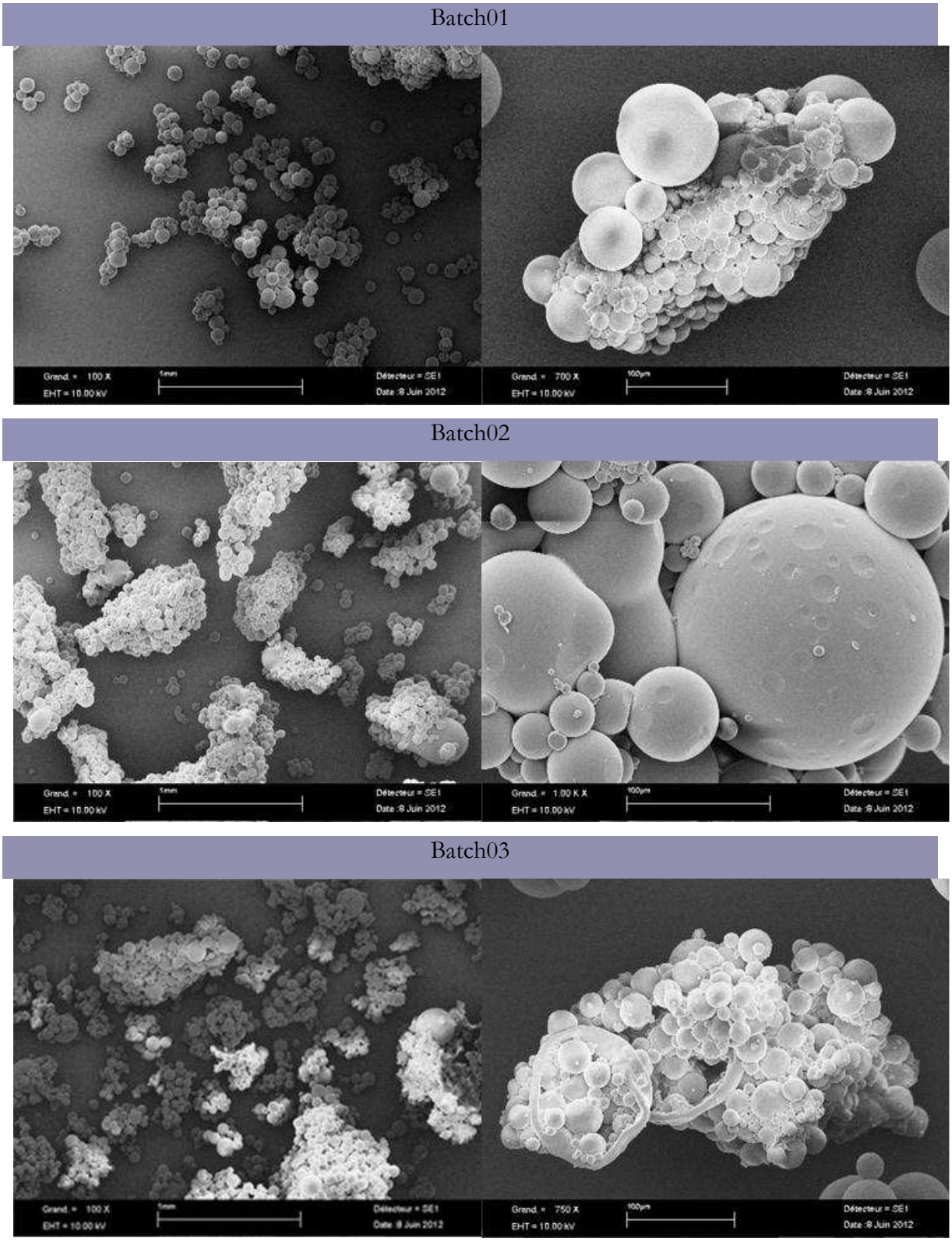

Figure VI- 7 : SEM observation of the suspension vinyl acetate polymerization in batch reactor

IV. CONTINUOUS S-PVAC POLYMERIZATION IN OSCILLATORY BAFFLED REACTOR

IV.1. ***Operating conditions***

Globally five polymerization tests have been carried out. Two of them led to a mass polymerization in the column due to a lack of stirring (bubbles). The different test conditions are summed up in Table VI- 3.

	Test PVAM-3	Test PVAM-4	Test PVAM-5
Q_{VAM} g.min^{-1}	59.82	21.97	22.31
$Q_{demi\ water}$ g.min^{-1}	111.73	111.24	111.56
$Q_{prémix}$ g.min^{-1}	5.77	5.77	10.66
Initiator /VAM %mol	0.02	0.06	0.11
PVAI/VAM ppm	448	1220	2250
Jacketed temperature section3-5 (°C)	22	22	22
Jacketed temperature section 6-9 (°C)	61	61	61
Jacketed temperature section 10-12 (°C)	56	56	56
Jacketed temperature section13 (°C)	10	10	10

Table VI- 3: Operating conditions

The reaction kinetics is affected by both the temperature and the initiator concentration. Moreover due to high flowrate fluctuation during the test PVAM-3, the permanent flowrate was never reached.

In Figure VI- 8, the time evolutions of the temperatures at the different positions in the reactor are reported for the test PVAM-4.

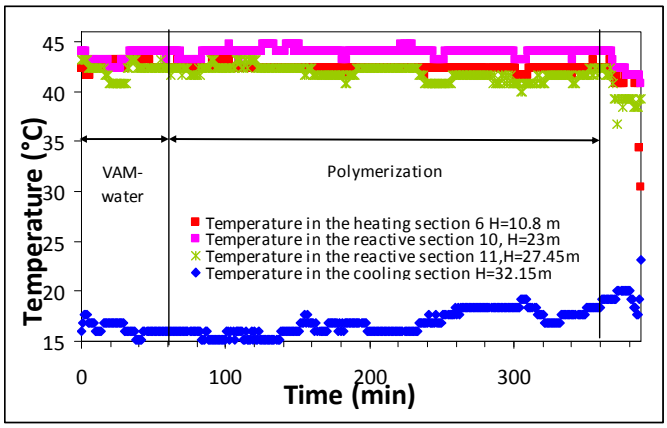

Figure VI- 8 : Product temperature profile test PVAM-4

As it can be seen, the heat loss is important. Indeed, the temperature in the reactor is about 44°C whereas the jacketed temperature ranges from 61°C to 55°C, respectively in the heating and reaction zones. The temperature profile of the other tests is exactly the same and is then not presented.

Thanks to the check valve, the flowrate is regulated. Unfortunately only the water and vinyl acetate flowrates are monitored. The check valves and counter-pressure allow to ensure a constant flowrate (see Figure VI- 9).

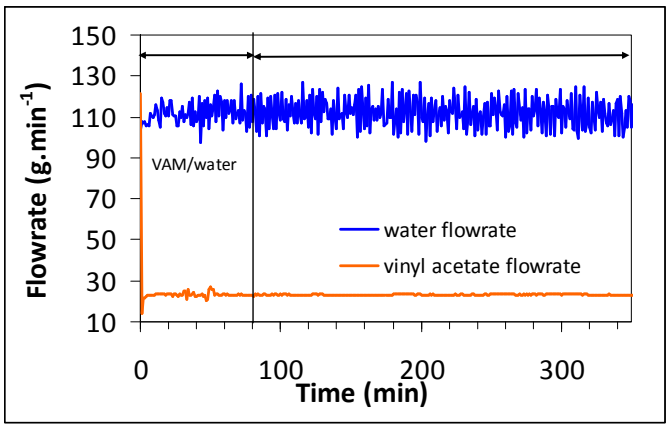

Figure VI- 9: Flowrate test PVAM-4

During a test, the reactor is filled of demineralized water. Then the vinyl acetate is introduced during 45 min to stabilize the flow and the temperature. The premix enters in the reactor.

Thanks to the glass section, we can observe what happened inside the reactor. The liquid-liquid dispersion as well as the polymerization lead to an opaque flow (Figure VI- 10).

Figure VI- 10 : overview of the column in course of polymerization, L-L means liquid-liquid dispersion, H corresponds to the start of the reaction (heating zone) and P at the polymerization continuation

However, in course of polymerization, some degassing has been observed, nevertheless less important than the initial degassing which conducted to the stop of the stirring and to the mass polymerization. It could not be avoided under the operating conditions investigated. The bubble creation starts from section 8 until the outlet of the reactor. The vapor creates liquid/gas interface in the small cells and the polymer tends to attach to the glass wall at this interface and above as observed in Figure VI- 11.

Figure VI- 11 : zoom on two sections – observation of the encrusting

This encrusting is non-desirable for the continuous process. However, the wall of the reactor is made of glass and no coating was applied. We remind that in batch a coating is applied between each charge and the reactor is made of enamel or stainless steel.

The tests presented here are just feasibility tests. So, in the future, the material effect will have to be investigated.

*IV.2. **Steady-state regime***

The time required to reach the stationary flow is evaluated. Samplings are collected to estimate the conversion (see chapter II section VI).

The following graph presents the conversion evolution according to time at the P5 sampling which corresponds to the reactor outlet.

The stationary regime is reached after 3 hours. Generally, after each sampling, the flow is disturbed and a degassing is observed from the section 8.

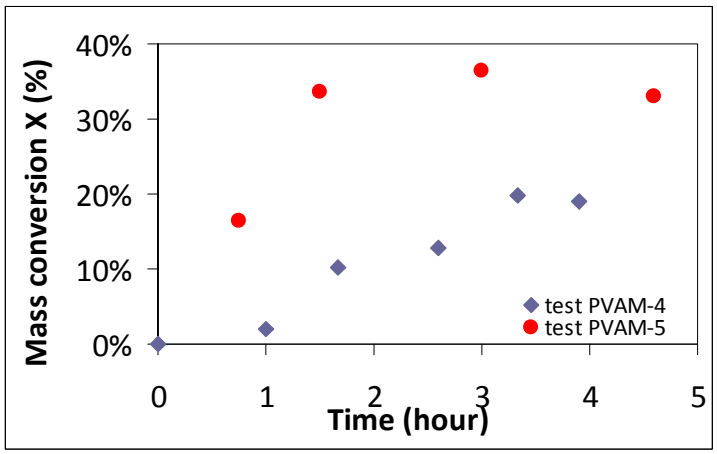

Figure VI- 12 : Permanent regime

IV.3. ***Conversion along the reactor***

Samples are collected all along the reactor and dried (chapter II-section IV) in order to evaluate the conversion profile. The conversion profiles are reported on Figure IV-13 and Figure IV-14. In both figures, the result of modeling is also represented.

The kinetic model used is the free radical homogeneous model. The kinetic constant used are those presented in Table VI- 1. It is a simple approximation.

For the test PVAM-4 the model fits well, but it is not the case for the second test.

However, the 30%mass of conversion obtained in this test seems convenient because of a higher initiator amount. But unexpectedly, the beginning of the reaction seems to be slowed down. Contrary to the previous tests, more degassing was observed which probably was disturbing the flow.

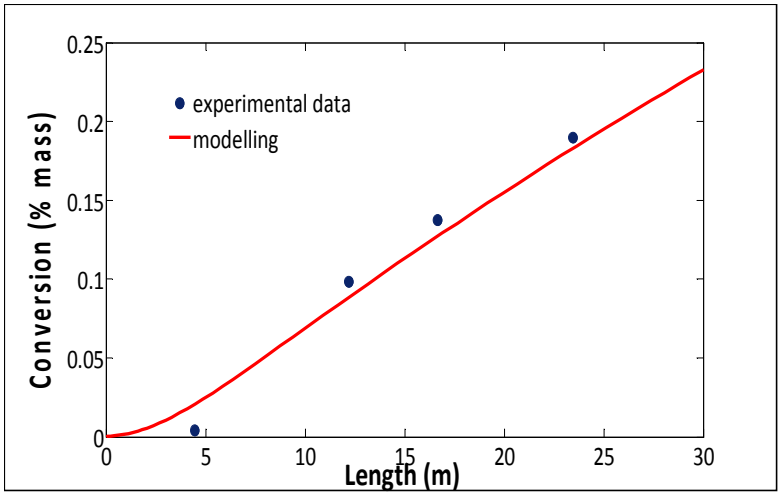

Figure VI- 13 : test PVA-4

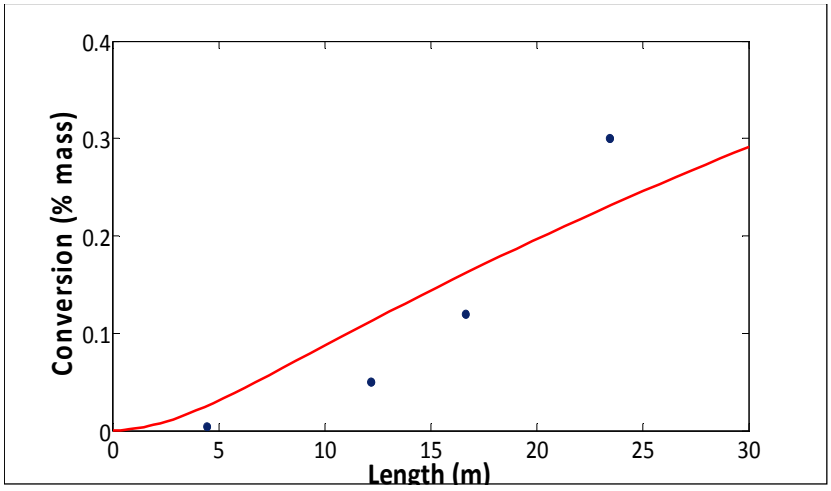

Figure VI- 14 : test PVA5

IV.4. ***Solid characterization with the conversion***

The different samples have been analysed via the SEM (Hitachi TM 3000) for the reacting droplet and microscopy Zeiss AX 10 for the liquid-liquid dispersion.

By drying the sample with the rotary evaporator at 20°C under vacuum, the particle forms a film in the bottle. The SEM picture is provided whereas the same sample dried on a stub in the desiccator leads to the picture on the right.

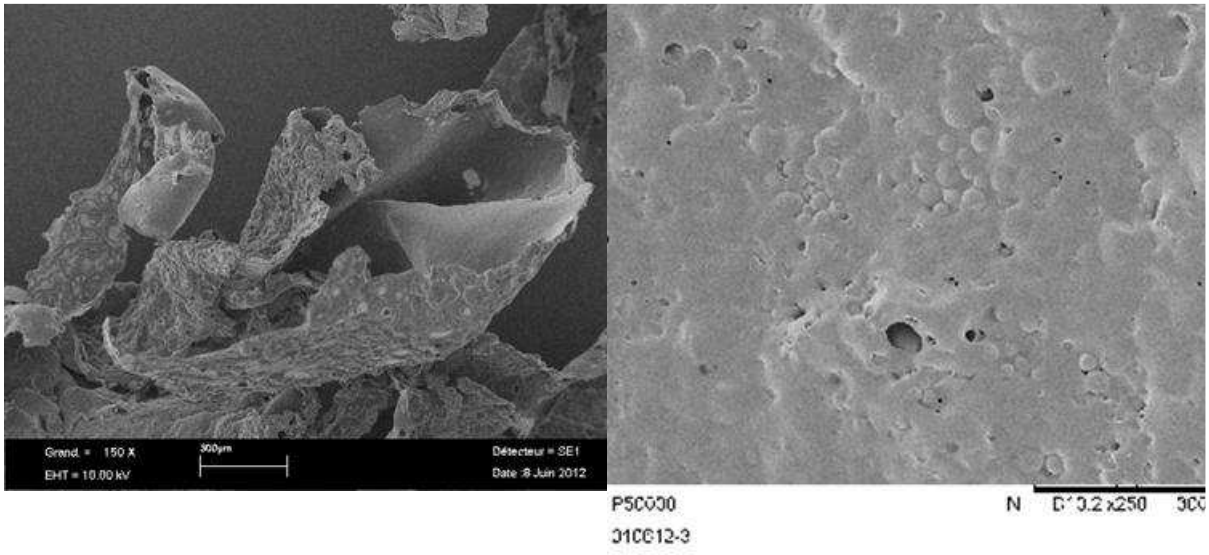

Figure VI- 15 : analysis of the same sample with two different drying techniques

By drying the sample after centrifuging under vacuum at 20°C, we obtained a kind of gel which is not analyzable (see Figure VI- 16).

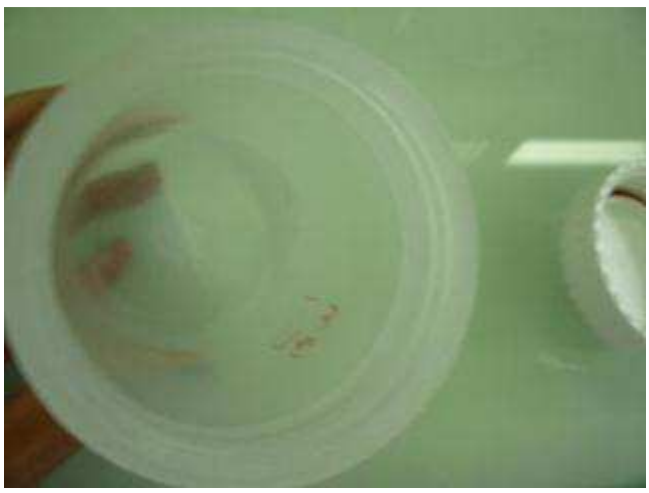

Figure VI- 16 : centrifuging and drying under vacuum at 20°C of the test PVA5-sample at 30% mass of conversion

To observe the particles formed during the polymerization, a drop of the suspension is deposed on a carbon scotch stuck on a stub.

The different samples are prepared and placed in a desiccator. Then each sample is observed via the TM3000 (Hitachi) without metallization by using the charge up reduction mode and with a beam of 15kV under the compo mode (see chapter II).

Figure VI- 17 and Figure VI- 18 represent the visualization of the different samples at same enlargement for each type of microscope. Consequently for a given test, the particle evolution can be compared and the difference from a test to another too.

On test PVAM-4, the liquid-liquid dispersion obtained seems to be multimodal. Large drops are observed (100µm) on the left picture and very small droplets on the right picture.

These larger droplets are not observed in the liquid-liquid dispersion of test PVAM-5. There is less PVA I suspending agent in the test PVA-4 than in the PVAM-5 test. It is then possible that the droplets in PVAM-4 are not well stabilized. Consequently larger particles are also observed.

Liquid-liquid dispersion – P1 sample

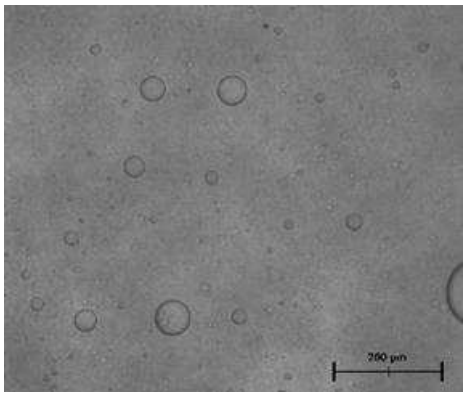

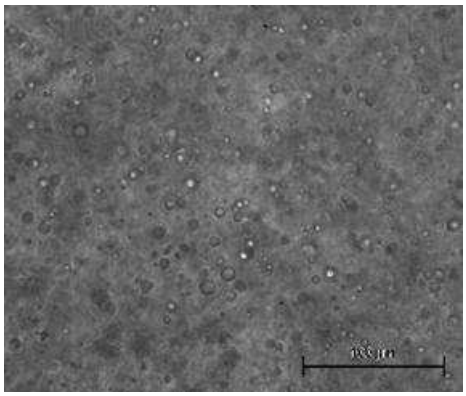

Liquid-solid suspension – sampling along the column

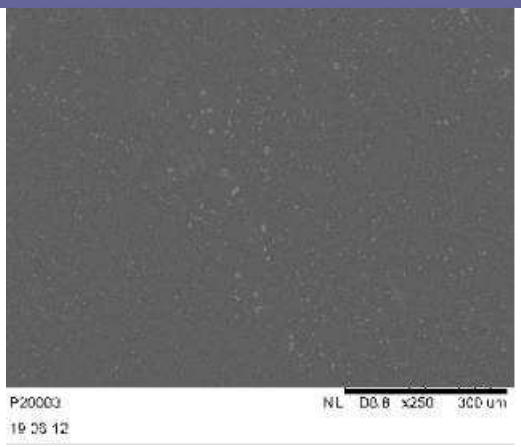

P2 – X=0.41%

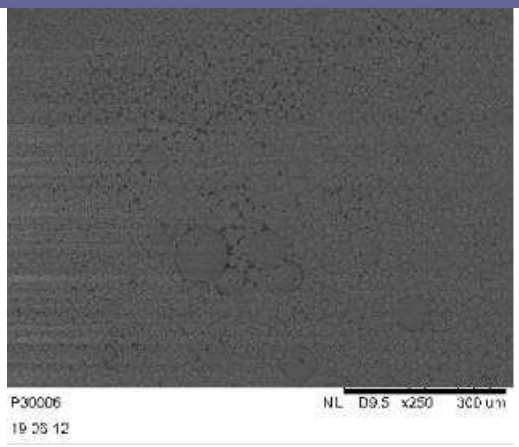

P3-X=10%

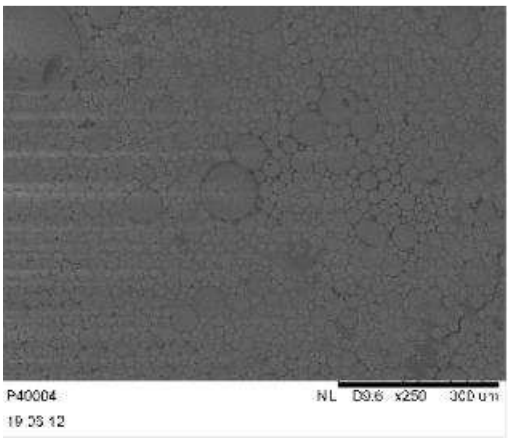

P4-X=14%

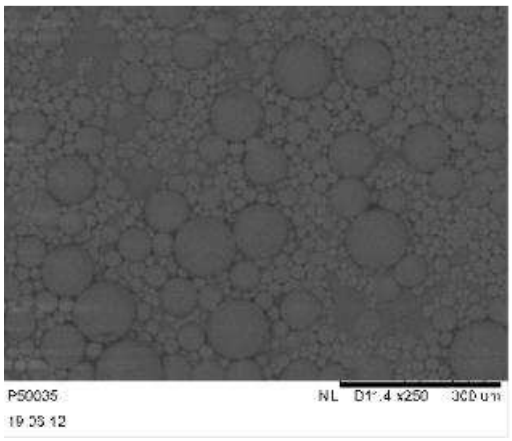

P5-reactor outlet-X=19%

Figure VI- 17 : test PVA-4- evolution of the dispersion/suspension along the column

Liquid-liquid dispersion –P1

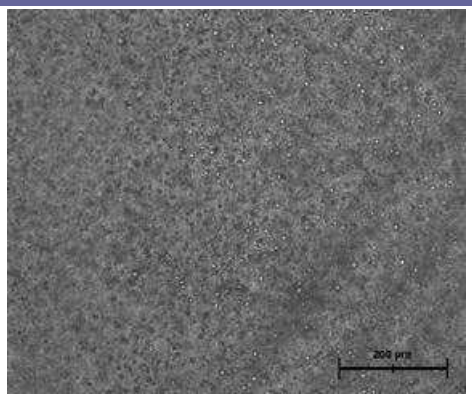

Liquid-solid suspension – sampling along the column

P2-X=0.4%

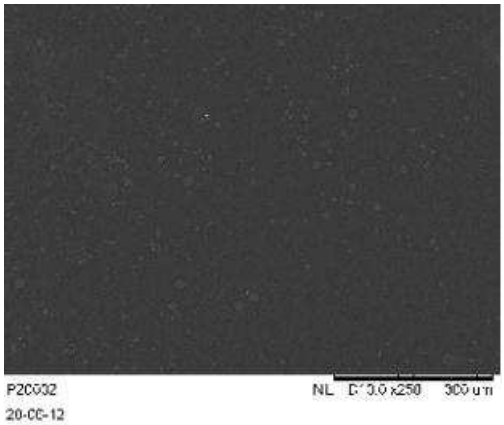

P3-X=5%

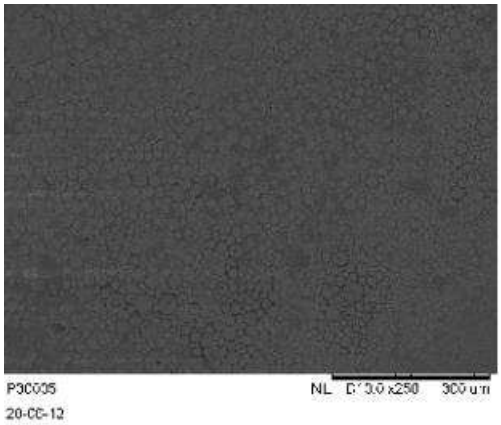

P4-X=12%

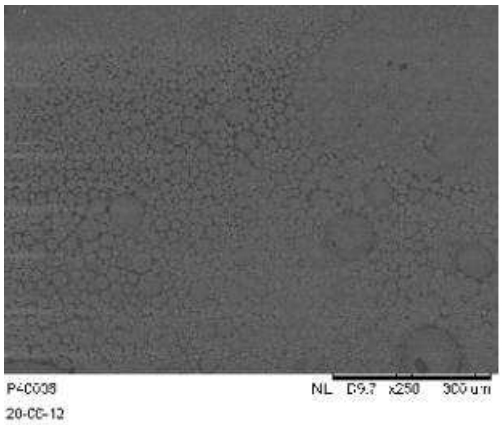

P5-X=30%

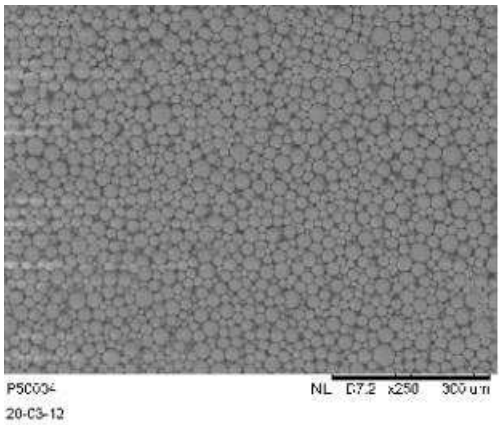

Figure VI- 18 : test PVA-5-evolution of the dispersion/suspension along the column

Concerning the first solid sample P2 in both figures, the conversion is very low and the same observation is made: dissymmetric particles are observed, they are in fact the initiator particles. Indeed, a stub of liquid-liquid dispersion is sampled and dried in the desiccator. No solid is created because the reaction temperature is not reached. However, solid is observed. Consequently, it is confirmed as being the initiator (Figure VI- 19).

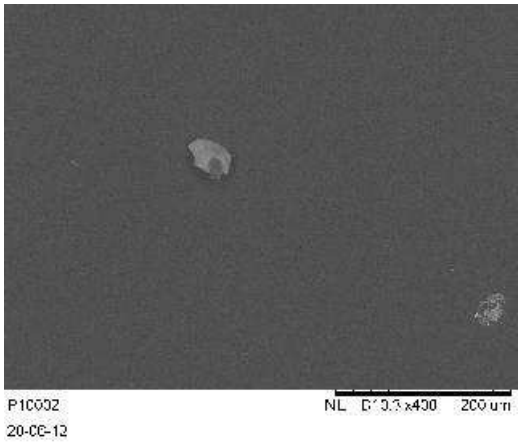

Figure VI- 19 : Observation of the liquid-liquid dispersion sample after drying in the desiccator-test PVAM 5

Then small particles are obtained. It seems that the particles are surrounded by a film. Figure VI- 20 presents a larger enlargement.

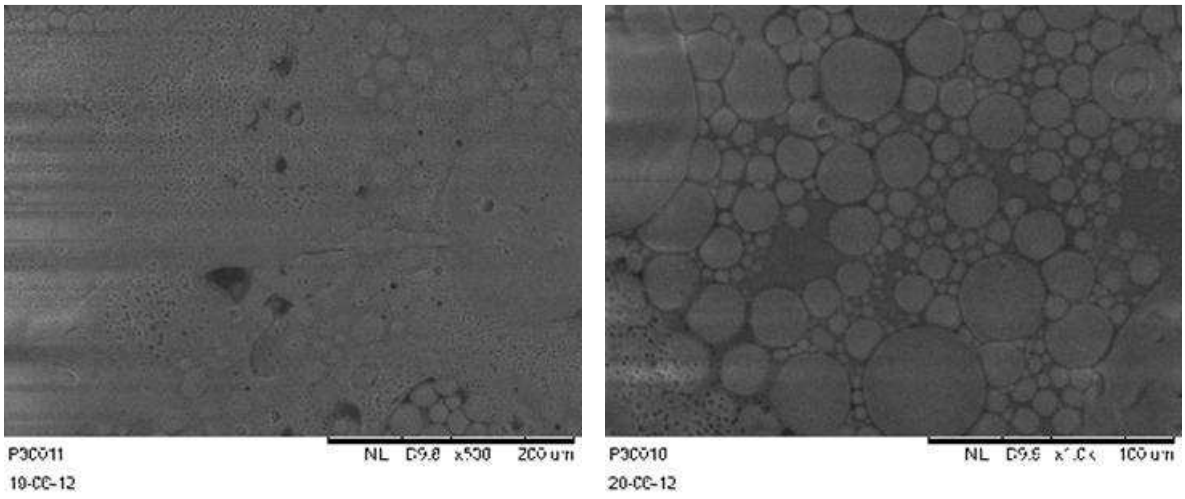

Test PVA-4 – X=10% Test PVA-5-X=5%

Figure VI- 20 : Observation of the skin on the sample at low conversion for the tests PVAM-4 and PVAM-5 (be careful both enlargements are different)

If we have a look on the evolution with the conversion for a given test, it seems that the particle size does not evolve.

The polymerizing grains obtained are well spherical and mainly with a continuous and smooth aspect. As large droplets were created, large solid particles are also observed (Figure VI- 17). Sometimes grains with a porous aspect are observed as well with a skin (Figure VI- 21).

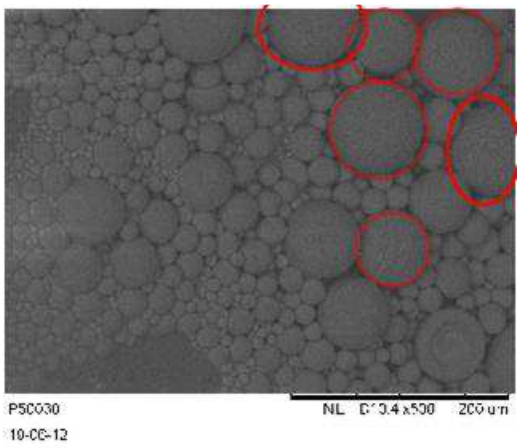

Test PVA-4 X=19%

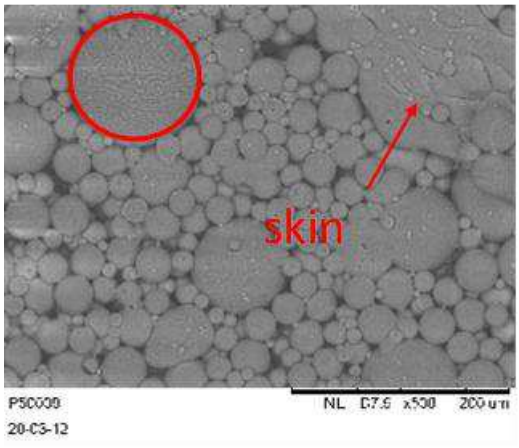

Test PVA-5 X=30%

Figure VI- 21: Observation of the smooth and sporadic porous grains on the sample at the outlet of the column for the tests PVAM-4 and PVAM-5

As it was not observed in the batch test, we assume that the porous aspect and the skin disappear with conversion.

V. CONCLUSION

The carrying out of a continuous suspension polymerization was challenging. Lots of problems have been encountered and all are not solved actually. Indeed, the premix introduction is not regulated and it is a key parameter for the good achievement of our process. The primary suspending agent controls the droplets size and a good distribution of the initiator allows to obtain the homogeneity of the properties for all the grains (conversion, polymerization degree…).

The goal of this chapter was clearly not to provide a complete vinyl acetate polymerization study but first to see the feasibility of a continuous mode and to identify future beacons of work. The polymerization was carried out until 30% of mass conversion which corresponds to the sticky stage (see chapter I part I-3). Some polymer deposit was observed. So the combination of glass wall and pulsation do not allow to avoid encrusting. Coating is necessary in these conditions. Some researches have to be carried out concerning the material encrusting in course of polymerization.

Moreover, the pilot needs some additional improvements: the addition of on-line gas purge can allow to regularly degas and then avoid the formation of bubbles which contributes to the encrusting, the interface constituting a preferential sticking point.

To conclude, these preliminary tests provide however some encouraging results for the batch to continuous transposition of the suspension polymerization.

Conclusion

The vinyl chloride suspension polymerization process is one of the most successfully complete batch processes in the industry. The physico-chemistry and particle formation knowledge is very well documented and described in literature. Manufacturers master the different recipes with various additives in order to produce particles of particular properties (porosity, size, use…) for specific applications.

In front of a so well optimized batch process, the batch to continuous transposition is then all the more complicated and represents a real challenge As regard the droplet/particle formation, three steps can be clearly identified. The first step deals with the liquid-liquid dispersion creation. The expected mean droplet size ranges from 30 to 50µm and the droplet size distribution has to be as narrow as possible. The suitable continuous device for this step will then be able to create monodispersed droplet size distribution and high energy dissipation or high shear rate must be experienced by all droplets.
From the second steps, the reactive medium reached its temperature and the exothermic reaction started. From literature, polymerizing drops exhibit a sticky behaviour from 5 to 30% of conversion. The particles can then agglomerate. Moreover, the sticky particles can cause encrusting and fouling at the reactor wall. It is the most crucial step for the continuous process. The agglomeration has to be accurately controlled to obtain the suitable particle size and the encrusting must be avoided. Currently some coatings are applied on the batch wall reactor. At the end of this step, the particles have reached their final size. In the last step, the particles size must be maintained and the homogeneity of the reaction and particles properties have to be ensured. The reaction is carried out until 80-90% of conversion depending on the required final product properties.

In our research, the two classical ways are investigated to develop a continuous suspension vinyl chloride suspension polymerization process:

- **The continuous stirred tank reactors**: this way will be easily implementable at plant scale given that the available tanks. It raises several questions concerning the dispersion creation, the polymerizing medium transfer and the residence time distribution.
- The **tubular plug-flow reactor**: this way is the most innovative and is a real technological breakthrough. It allows a total plug-flow behaviour and a better control

of the operating parameters (temperature control, higher surface to volume ratio…). However, encrusting must be avoided.

These two ways are investigated at lab scale. The implementation of these steps at lab-scale has required the development of many different pilots: static mixers at the lab-scale and at the pilot scale, disc and doughnut pulsed column and COBR for the liquid dispersion and for the solid suspension as well with and without reaction. The liquid-liquid dispersion was first studied in static mixers which allow the creation of an emulsion of controlled size in a very short residence time. Then, the liquid-liquid dispersion was studied into two different pulsed devices: the vertical discs and doughnuts pulsed column and the horizontal continuous oscillatory baffled reactor. Both experimental rigs were then modified to study the transport of the solid-liquid suspension and the continuous suspension polymerization at the sticky stage.

Besides, to control the droplets/particles properties, lots of analytical techniques have been used and/or developed. The physico-chemical properties of our systems were characterized, especially the transient interfacial tension. It was indeed necessary to measure the interfacial tension at a precise time corresponding to the respective residence times inside the different equipments, some of them being inferior to 1 second. Therefore, it was required to develop specific methods for that purpose. Liquid-liquid dispersion analyses were carried out as well on line (On-Line Turbiscan) as off-line with laser diffraction measurement and microscopic observation. The particles properties were assessed in term of size and shape, thanks to laser diffraction and scanning electronic microscopy.

These different experimental studies have allowed us to acquire preliminary and valuable results for the future development of the continuous process.

Concerning the CSTR way, the Sulzer® static mixers are proposed to create fast a dispersion of controlled size and then the stirred tank reactors are devoted to the reaction. The static mixers are considered for the loading of the current batch reactor or for the loading of the stirred tank reactors in series.

As for tubular reactor, the pulsed column is proposed to develop the entire process from step 1 to step 3 in a first time. Their abilities to perform liquid-liquid dispersion, transport homogeneously solid-liquid suspension and to prevent from encrusting issues are studied.

The studies were carried out at lab scale by using model fluids for safety reasons. When possible, they are implemented at Mazingarbe pilot scale to improve the device by using the industrial reactive system.

First, the **CSTR way** is investigated. We focus on the liquid-liquid dispersion creation for batch or CSTR loading. In a first time, the liquid-liquid dispersion is studied in static mixers at lab scale. Different models systems are investigated by changing the dispersed phase or continuous phase (effect of the physico-chemical parameter) or the surfactant nature (effect of the interfacial tension). Moreover, for practical industrial reason, the system must be highly concentrated in dispersed phase to avoid the post treatment of the organic phases. Consequently, the dispersed phase fraction in volume range from 10 to 60%. The residence time in the mixer is extremely short. It ranges from 0.04 to 0.08 second to obtain mean droplet size in the expected range.

The required specifications on the liquid-liquid dispersion are satisfactory:

- To ensure a mean droplet size of 30-50μm, the corresponding flowrate for this equipment size is of 400 to 550 $L.h^{-1}$. For extrapolation at same design characteristic, the pressure drop must be preserved;
- The droplet size distribution are narrow;
- The creation is faster than in batch.

Moreover, these lab scale tests allow to establish a correlation that will take into account the physico-chemical parameters of the systems based on Middelman's correlation (1974).

The main physico-chemical parameters are the interfacial tension. A special attention has been paid to measure interfacial tension in the range of the residence time to improve our understanding of this parameters for fast emulsification process.

Given their convincing results, static mixers are implemented at the Mazingarbe's pilot plant. The goal of these tests is to perform the direct emulsification loading in a batch and to carry on the polymerization. It is expected to decrease the loading time in batch and the time to obtain the dispersion. The droplet size distribution is perfectly controlled and their uses at pilot scale have led to the improvement of the current batch process. One of the major results concerns the reduction of the batch loading time which corresponds to a decrease of the energy costs and an increase of the productivity. The other properties of the final particles and an improvement of the different additives were noticed.

This loading mode is foreseen to be implemented in the industrial reactor of 40 m^3 in volume.

Concerning **the tubular plug-flow reactor**, all the identified steps are studied either in co-current up-flow disc and doughnut pulsed column or in continuous oscillatory baffled reactor. The liquid-liquid dispersion in pulsed column has provided very promising results. The mean droplet size obtained ranged in the expected sizes (30-50 μm) whatever the dispersed phase concentration operated. The pulsed columns (disc and doughnuts column or COBR) can then generate the dispersion and maintain it on large residence time. The experimental tests have

led to establish correlations depending on the hydrodynamics and physico-chemical properties of the phases.

The ability of pulsed columns to maintain an homogeneous solid-liquid suspension transport by avoiding settling and particles segregation was also demonstrated.

Those reactor types allow then to work in biphasic fluid flow, liquid-liquid or liquid-solid.

These results demonstrate that pulsed column can be considered as a suitable S-PVC reactor.

The crucial step remains the sticky stage. If this step succeeds, the polymerization can entirely be carried out in pulsed column. Some preliminary tests were conducted in continuous oscillatory pulsed column. The conversion does not exceed 30% in mass, but the covered range is representative of the sticky stage. Encrusting was observed but the polymerization was nevertheless successful. The main difficulties inhere to the equipment. A continuous oscillatory baffled reactor has to be constructed with proper materials for baffle and wall.

These research works demonstrate that the different identified steps for continuous vinyl chloride suspension polymerization reaction can be successfully carried out by using continuous technologies.

However, the different steps have been studied with model fluids which depict the vinyl chloride/PVC physical properties at a given step. It is obvious that tests must be carried out by using vinyl chloride to conclude on the reliability of the equipment.

Our results contribute to a better understanding of the biphasic flow properties at high dispersed phase concentration, particularly in liquid-liquid flow. Correlations have been established but it is obvious that they are improvable. To design a S-PVC continuous pilot, some additional systems will be studied as well as the scale-up effects on the liquid-liquid dispersion or suspension properties and on the reaction characteristics in the different equipments (pulsed column and static mixer).

These future developments should lead to the design of pilot scale system to carry out tests with vinyl chloride.

This research project has yet led to some short term transfer. The current batch process can be improved by using static mixer for the batch loading. It is a real time saving operation which can contribute to an increase of the productivity. However, concerning the CSTR way, some pending questions are still under investigation, the main issue being the transfer problem.

Concerning the development of the tubular continuous process, some additional tests are needed to understand the effect of the different parameters. A suitable pilot is required to investigate the suspension polymerization of vinyl chloride. Safety studies are required as well as the development of on-line monitoring for the reaction conversion.

.

Annex 1

The flow type must first be identified. So the Kolmogoroff's length scale η is calculated thanks to the following expression:

$$\eta = \left(\frac{\upsilon_c^{\,3}}{\varepsilon_m} \right)^{1/4}$$

Where υ_c is the kinematic viscosity of the continuous phase, and ε_m the mean energy dissipation rate per fluid mass unit.

The table gives the Kolmogoroff's length scale for the four systems.

S_1: Water/Tween80/Cyclohexane	5 - 8
S_2: Water/Tween80/Toluene	5 - 8
S_3: Water/PVA/Toluene	5 - 7
S_4:Water-Glycerol 25%m./PVA/Toluene	8 - 12

Consequently, the turbulent inertial regime takes place in our static mixers given that $\eta_K < d_{32} < d_h$.

The coalescence efficiency P is defined by the following formula (Coulaloglou, 1975)

$$P = \exp(-\frac{t_{drainage}}{t_{contact}})$$

For non-deformable rigid sphere, the contact time $t_{contact}$ is estimated by the following expression (Levich, 1962) in turbulent system:

$$t_{contact} \approx \frac{d^{2/3}}{\varepsilon_m^{\,1/3}}$$

The drainage time is estimated by integrating the model corresponding to the rigid drop of Chester (1991) which gives for the interaction force F:

$$F = \frac{3\pi\mu_C R^2}{2h}\left(-\frac{dh}{dt}\right)$$

Where R is the radius of a droplet, and h represents the film thickness between two droplets.

For F constant, h is defined as follows:

$$h = h_0 \exp\left(-\frac{t}{t_{ch}}\right)$$

Where t_{ch} is the characteristic time defined by:

$$t_{ch} = \frac{3\pi\mu_C}{2F}$$

The drainage time corresponds to the time at which the critical thickness h_c is reached.

h_c is given by:

$$h_c \approx \left(\frac{AR}{8\pi\sigma} \right)^{1/3}$$

Where A is the Hamacker constant taken equal to 10^{-20} J.

Consequently, $t_{drainage}$ is calculated by integrating the expression (14) with $h=h_c$ and $t=t_{drainage}$.

References

ALOPAEUS,V.,KOSKINEN,J.,KESKINEN,K.I.,MAJANDER,J.,(2002).Simulationofthe population balances forliquid–liquid systems in a non ideal stirred tank.Part 2—parameter fitting and the use of the multiblock model fo rdense dispersion,. *Chem.Eng.Sci.57*(10),1815–1825.

ALEXOPOULOS, A.-H. AND KIPARISSIDES, C. (2007). On the prediction of internal particle morphology in suspension of vinyl chloride Part I : the effect of primary particle size distribution, *Chemical engineering science*, 62, issue 15, 3970-3983

ALLSOPP, M.-W. AND VIANELLO, G.-V. (2005). Poly(Vinyl Chloride), Ullmann's encyclopedia of industrial chemistry, Wiley-VCH Verlag GmbH&Co

ALOPAEUS,V., KOSKINEN,J., KESKINEN K.I., MAJANDER J., (2002). Simulation of the population balances for liquid–liquid systems in a nonideal stirred tank. Part 2—parameter fitting and the use of the multiblock model for dense dispersions, *Chemical Engineering Science*, Vol. 57, Issue 10, 1815-1825

AL TAWEEL, A.-M. AND CHEN, C.-A. (1996). A novel static mixer for the effective dispersion of immiscible liquids. *Trans IchemE* 74, Part A, 445-450.

AL TAWEEL, A.-M. AND WALKER, L.-D. (1983). Liquid dispersion in static in line mixers. *Can. J. Chem. Eng.,* 61, 527-533.

ANGLE, C.-A., DABROS, T., HAMZA, H.-A. (2006). Predicting the sizes of toluene-diluted heavy oil emulsions in turbulent flow Part 1: application of two adsorption kinetic models for σ^E in two size predictive models. *Chem. Eng. Sci.,* 61, issue 2, 7309-7324.

ANGLE, C.-A., HAMZA, H.-A. (2006). Predicting the sizes of toluene-diluted heavy oil emulsions in turbulent flow Part 2 : Hinze-Kolmogorov based model adapted for increased oil fraction and energy dissipation in a stirred tank. *Chem. Eng. Sci.,* 61, 7325-7335.

AOUN NABLI, M.-S. (1995), Simulation numérique de l'hydrodynamique et du mélange axial dans les colonnes d'extraction pulsées à garnissage disques et couronnes, PhD thesis, INP Toulouse

ARAI, K., KONNO, M., MATUNAGA, Y., SAITO, S. (1977). Effect of dispersed phase viscosity on the maximum stable drop size for breakup in turbulent flow. *Jour. Chem. Eng. of Japan,* 10, 325-330.

AZIZI AND AL TAWEEL (2011). Inter-Phase Mass Transfer in Turbulently Flowing Liquid-Liquid Dispersions: A comparative Analysis of Models. *Chemical engineering journal*, 179,231-241

BABAK V.-G., DESBRIÈRES J. AND TIKHONOV V.-E. (2005). Dynamic surface tension and dilational viscoelasticity of adsorption layers of a hydrophobically modified chitosan, *Colloids Surf. A*, 255, 119-130

BAHARGAVA, G.-S., KHAN, H.-U., BHATTACHARYYA, K.-K. (1979). SAN copolymer by suspension polymerization. II. Bead size distribution and molecular weight, *Journal of applied polymer science*, 23,1181-1187

BAIRD, M.-H.-I.; STONESTREET, P. (1995). Energy dissipation in oscillatory flow within a baffled tube, *Chemical engineering research and design*, 73, issue A5, 503-511

BAO YZ; BROOKS BW. (2001). Phase-equilibrium behavior of vinyl chloride/n-butane and its application in determination of vinyl chloride heterogeneous polymerization kinetics, *Journal of polymer science part A – polymer chemistry*, 39, 2179-2188

BARTON, J.-A. AND NOLAN, P.-F. (1989). Incidents in the chemical industry due to thermal runaway chemical reactions, Hazards X : Process safety in fine and specialty chemical plants, Symposium series, 115, 3-18

BERKMAN, P.-D., CALABRESE, R.-V. (1988) Dispersion of viscous liquids by turbulent flow in a static mixer, *AIChE J.* 34, N°4, 602-609

BIRD, R.-B., STEWART, W.-E., LIGHTFOOT, E.-N. (1924). Transport Phenomena, 2nd edition, John Wiley and Sons, New York, Chapter 6, 177-184

BOHNET, M., KALBITZ, H., NÉMETH, J., PAZMANY, J. (1990). Improvement of forced convection heat transfer by using static mixers. *Proceeding Int. Act. Conference,* INTC, Jerusalem, 315-320.

BORWANKAR, R.-P., CHUNG, S.-I., WASAN, D.-T.(1986). Drop sizes in turbulent liquid-liquid dispersions containing polymeric suspension stabilizers. I. The breakage mechanism. *Jour. of Applied Polymer Sci.* 32, 5749-5762

BOSCHER VIRGINIE (2009). Modélisation de la polymérisation en suspension du chlorure de vinyle : étude granulométrique en ligne par spectroscopie acoustique d'émulsion modèles stabilisées par des PVA, PhD thesis, Université de Haute Alsace

BOYADZHIEV L.(1973) On the movement of a spherical particle in vertically oscillating liquid. *J.Fluid Mech.*, 57 (3), pp 545-548.

BRACOU, H. (1995). Etude hydrodynamique d'une colonne d'extraction influence de la mouillabilité, PhD thesis, INP Toulouse

BROOKS, B.-W. (2005) Free radical polymerization: suspension, chapter 5, *handbook of polymer reaction engineering*, Wiley-VCH Verlag GmbH&Co

BRUNET, L. AND PRAT, L.E. AND CASAMATTA, G.AND CARVIN, P. Use of the pulsation to control a polydispersed particles flow in a new type of pulsed column. (2007*) Chemical Engineering and Technology*, vol. 3 (n° 11). pp. 1571-1575.

BRUNOLD C.R.; HUNNS J.C.B.; MACKLEY M.R.. (1989). Experimental observations on flow patterns and energy losses for oscillatory flow in ducts containing sharp edges, *chemical engineering science*, 44, issue 5, 1227-1244

BURATTI M.F. (1988) Etude des phénomènes de mélange axial dans les colonnes pulsées équipées de garnissage disques-couronnes. *Thèse de Doctorat d'Etat, Institut National Polytechnique de Lorraine.*

BURGESS, R.-H. (1982). Suspension polymerization of vinyl chloride, chapter 1, *Manufacturing and processing PVC*, Applied sciences publishers, London

BURON, H., MENGUAL, O., MEUNIER, G., CAYRÉ, I., SNABRE, P. (2004) Review Optical Characterization of concentrated dispersions: applications to laboratory analyses and on-line process monitoring and control. *Polym. Int.* 53, 1205-1209.

CALABRESE, G.-S. AND PISSAVINI, S. (2011). From batch to continuous flow processing in chemicals manufacturing, *AIChE Journal*, vol.57, no. 4, 828-834

CARVALHO ASCM., CHICOMA D., SAYER, C., GIUDICI, R. (2006). Comparison of vinyl acetate butyl acrylate emulsion copolymerization conducted in a continuous pulsed sieve plate column reactor and in a batch stirred tank reactor, *Macromol. Symp.* 243, 147-158

CEBOLLADA, A.-F., SCHMIDT, M.-J, FARBER, J.-N., CAPIATI, N-J., VALLES, E.-M. (1989). Suspension polymerization of vinyl chloride I. Influence of viscosity of suspension medium on resin properties, *Journal applied polymer science*, 37, 145-166

CHANDRA, K.-G., KALE, D.-D. (1995). Pressure drop for two-phase air-non-Newtonian liquid flow in static mixers, *Chem. Eng. Jour.*, 59, 277-280.

CHATZI E.-G., KIPARISSIDES, C. (1994). Drop size distributions in high holdup fraction dispersion systems : effect of the degree of hydrolysis of PVA stabilizer, *Chem. Eng. Sci.*, 49, 5039-5052

CHATZI, E.-G., KIPARISSIDES, C. (1995). Steady-state drop-size distributions in high holdup fraction dispersion systems, *AIChE Jour.*, 41, 1640–1652.

CHARTON,S., DUHAMET, J, BORDA,G. ODE,D. (2011). Axial dispersion in a pulsed column, *Chemical engineering science*, vol.75, 468-477

CHEN, S.J., LIBBY, D.R., (1978). Gas liquid and liquid-liquid dispersions in a Kenics mixer, *71st Annual AIChE Meeting.*

CHEN,Z.,PRUSS,J.,WARNECKE,H.J.,(1998).Apopulationbalancemodelfordispersesystems:drop size distribution in emulsion.*Chem.Eng.Sci.53*(5), 1059–1066.

CHESTERS, A.-K. (1991). The modelling of coalescence processes in fluid-liquid dispersions: a review of current understanding. *Trans IChemE* 69, part A, 259-270.

CHUNG S.-I. AND WASAN D.-T. (1988). Dynamic Stability of Liquid-Liquid Dispersions Containing Polymeric Suspension Stabilizers, *Colloids and Surfaces*, 29, 323-336

COULALOGLOU, C.-A. (1975). Dispersed phase interactions in an agitated vessel, PhD thesis, Illinois Institute of Technology, Chicago.

COULALOGLOU, C.-A., TAVLARIDES, L.-L. (1976). Drop size distributions and coalescence frequencies of liquid-liquid dispersions in flow vessels, *AIChE Jour.*, 22, 289-297.

COULALOGLOU, C.-A., TAVLARIDES, L.-L.(1977). Description of interaction processes in agitated liquid-liquid dispersions, *Chemical Engineering Science*, 32, issue 11, 1289-1297

DAVIES R.H., SCHONBERG J.A., RALLISSON J.M., (1989) The lubrification force between two viscous drop. Physics of Fluid A1, 77-81

DAS, P.K., LEGRAND, J., MORANÇAIS, P., CARNELLE, G., 2005. Drop breakage model in static mixers at low and intermediate Reynolds number. *Chem. Eng. Sci.* 60, 231-238.

DE, B., MANDAL, T.K., DAS, G., 2010. Experimental studies on phase inversion in a small diameter horizontal pipe. *Chem. Eng. Res. Des.* 88, 819-826.

DESNOYER, C., MASBERNAT, O., GOURDON, C. (2003). Experimental study of drop size distributions at high dispersed phase ratio in liquid-liquid dispersions. *Chem. Eng. Sci.*, 58, 1353-1363.

DOWDING P.J.; GOODWIN J.W.; VINCENT B. (2000). Production of porous suspension polymers using a continuous tubular reactor, *Colloid and polymer science*, 278 Issue: 4, 346-351

EASTOE, J., DALTON, J.-S. (2000). Dynamic surface tension and adsorption mechanisms of surfactants at the air–water interface, *Advances in Colloid and Interface Science*, Volume 85, Issues 2–3, 31, 103-144

EASTWOOD, C.D., ARMI, L., LASHERAS, J.C.(2004). The breakup of immiscible fluids in turbulent flows. *J. Fluid Mech.* 502, 309–333.

FILIPPOV, L.-K. (1994). Dynamic Surface Tension of Aqueous Surfactant Solutions 1. Diffusion-Convective Controlled Adsorption, *J. Colloid Interface Sci.*, 163, 49-60

FILIPPOV, L.-K. (1994). Dynamic Surface Tension of Aqueous Surfactant Solutions 2. Diffusion-Kinetic-Convective Controlled Adsorption, *J. Colloid Interface Sci.*, 164, 471-482

FITCH, A.-W., HONGBING J., NI, X. (2005). An investigation of the effect of viscosity on mixing in an oscillatory baffled column using digital particle image velocimetry and computational fluid dynamics simulation, *Chemical Engineering Journal*, Vol. 112, Issues 1-3, 1997-210

GÄBLER A., WEGENER M., PASHEDAG,A.R., KRAUME,M. (2006) The effect of pH on experimental and simulation results of transient drop size distributions in stirred liquid-liquid dispersions. *Chem. Eng. Sci.* 61 (9), 3018-3024

GARTON, A., GEORGE, M.-H. (1974). Effect of oxygen on the polymerization of vinyl chloride. II. Polymer properties, *J. Polym. Sci. Polym. Chem.*, Vol. 12, 2779 – 2788.

GEIL P.H. (1977). Polymer morphology, *Journal of macromolecular science-chemistry*, A11, issue 7, 1271-1280

GOURDON, C. (1989), Les colonnes d'extraction par solvant : modèles et comportement, PhD thesis, INP Toulouse

GOURDON C. AND CASAMATTA G., (1994). in *Liquid-liquid extraction equipment*, ed. by Godfrey and Slater

GUSTIN, J.-L. (2005). Understanding vinyl acetate polymerizations accidents, *Chemical Health and Safety*, 36-46

HAAS, P.A., (1987). Turbulent dispersion of aqueous drops in organic liquid. *AIChE J.* 33, 987-995.

HASHIM S., BROOKS B.W. (2002). Drop mixing in suspension polymerization. *Chemical Engineering Science* 57, 3703-3714

HASHIM S., BROOKS B.W. (2004). Mixing of stabilized drops in suspension polymerisation. *Chemical Engineering Science* 59, 2321-2331

HE, Y., HOWES, T. AND LITSTER, J.-D. (2004). Dynamic Interfacial Tension of Aqueous Solutions of PVAAs and Its Role in Liquid-Liquid Dispersion Stabilization, J. *Chem. Eng. Jpn*, 37, 181-186

HESKETH, R.P., ETCHELLS, A.W., RUSSELL, T.W.F., (1991). Experimental-observations of bubble breakage in turbulent-flow. *Ind. Eng. Chem. Res.* 30 (5), 835–841.

HEYOUNI, A., ROUSTAN, M., DO-QUANG, Z. (2002). Hydrodynamics and mass transfer in gas-liquid flow through static mixers. *Chem. Eng. Sci.,* 57, 3325-3333.

HINZE, J. O. (1955). Fundamentals of the hydrodynamic mechanism of splitting in dispersion processes. *A.I.Ch.E. Journal*, 1(3), 289–295.

HIRSCHBERG, S., KOUBEK, R., MOSER, F., SCHÖCK, J. (2009). An improvement of the Sulzer SMX static mixer significantly reducing the pressure drop. *Chem. Eng. Res. Dev.,* 87, 524-532.

HOEDEMAKERS (1990) Continuous emulsion polymerization in a pulsed packed column, PhD thesis, Eindhoven

HOUNSLOW, M.-J., NI, X. (2004). Population balance modelling of droplet coalescence and break-up in an oscillatory baffled reactor, *Chemical Engineering Science*, Vol. 59, Issue 4, 819-828

HUA, X.-Y. AND ROSEN, M.-J. (1988). Dynamic Surface Tension of Aqueous Surfactant Solutions. 1. Basic Parameters, *J. Colloid Interface Sci.*, 124, 652-659

HÜTTINGER, K.-J., HOHMANNWIEN, S., KREKEL, G. (1992). A method for the determination of the acid-base interaction and the work of adhesion at a solid-liquid interface, *Journal of adhesion science and technology*, 6, n°3, 317-331

IOANNOU, K., NYDAL O.J., ANGELI, P., (2005). Phase inversion in dispersed liquid liquid flows. *Experimental Thermal and Fluid Sci.* 29, 331-339.

JAHANZAD, F., SAJJADI, S., BROOKS, B.-W. (2005). Characteristics interval in suspension polymerization reactors : an experimental and modelling study, *Chemical Engineering Science*, 60, 5574-5589

JAHANZAD, F., SAJJADI, S., BROOKS, B.-W., (2004). On the evolution of particle size average and size distribution in suspension polymerization processes, *Macromolecular symposia*, 206, 255-262

JAHYA, A., STEVENS, G.-W., PRATT, H.-R.-C. (1999). Pulsed disc and doughnuts column performance, *Solvent extraction ion exchange*, 27, 63-82

JEALOUS, A.-C., JOHNSON, H.-F. (1955), Power requirements for pulse Generation in Pulsed Columns, *Industrial and engineering chemistry*, 47, No. 6, 1159-1166

KALBANOV, A.-S., MAKAROV, K.-N., PERTZOV, A.-V., SHCHUKIN, E.-D. (1990). Ostwald Ripening in Emulsions, *Jour. Colloid Interface Sci.*, 138, 98-104.

KALFAS, G., YUAN, H., RAY, W.-H. (1993). Modelling and experimental studies of aqueous suspension polymerization process II. Experiments in batch reactor, *Ind. Eng. Chem. Res.*, 32, 1831-1838

KIPARISSIDES C.; MACGREGOR J.F.; HAMIELEC A.E. (1979). Continuous emulsion polymerization modelling oscillations in vinyl-acetate polymerization*, Journal of applied polymer science*, 23, issue 2, 401-418

KIPARISSIDES C; DASKALAKIS G; ACHILIAS DS. (1997). Dynamic simulation of industrial poly(vinyl chloride) batch suspension polymerization reactors, *Industrial and engineering chemistry research*, 36, issue 4, 1253-1267

KOTOULAS, C., KIPPARISSIDES, C. (2006). A generalized population balance model fro the prediction of particle size distribution in suspension polymerization reactor, *Chemical Engineering Science*, 61, 332-346

KUMAR, S., KUMAR, R. AND GHANDI, K.-S. (1993). A new model for coalescence efficiency of drops in stirred dispersion, *Chem. Eng. Sci.,* vol.48, n°11, 2025-2038

KUMAR, A., HARTLAND, S. (1988). Prediction of Dispersed Phase Hold-up in Pulsed Perforated-Plate Extraction Columns, *Chemical Engineering process*, 23, 41-59

KUMAR, A., HARTLAND, S. (1996). Unified correlations for the prediction of drop size in liquid-liquid extraction columns, *Industrial and engineering chemistry research*, 35, issue 8, 2682-2695

KUNII D. AND LEVENSPIEL O. (1990) *Fluidization Engineering* (Wiley, 2*nd* Edition)

LANKVELD, J.-M.-G. AND LYKLEMA, J. (1972). Adsorption of polyvinyl alcohol on the paraffin-water interface. I. Interfacial tension as a function of time and concentration, *Journal of Colloid Interface Sci.*,41, 454-465

LANKVELD J.-M.-G. AND LYKLEMA, J. (1972). Adsorption of Polyvinyl Alcohol on the Paraffin-Water Interface III. Emulsification of Paraffin in Aqueous Solutions of Polyvinyl Alcohol and the Properties of Paraffin-in-Water Emulsions Stabilized by Polyvinyl Alcohol, *J. Colloid Interface Sci.*, 41, 475-483

LAWTON S., STEELE G.; SHERING P. (2009). Continuous Crystallization of Pharmaceuticals Using a Continuous Oscillatory Baffled Crystallizer, *Organic process research and development*, 13, issue 6, 1357-1363

LEGARREC S.(1993), Modélisation et simulation numérique de l'écoulement et de la dispersion d'un contaminant dans une colonne pulsée. Thèse de Doctorat, Conservatoire National des Artset Métiers

LEGRAND, J., MORANCAIS, P., CARNELLE, J. (2001). Liquid-liquid dispersion in a SMX-Sulzer static mixer, *Inst. Chem. Eng.*, vol. 79, part A, 949-956

LEMENAND, T., ZELLOUF, Y., DELLA VALLE, D., PEERHOSSAINI, H. (2001). Formation de gouttelettes dans un mélange turbulent de deux fluides immiscibles (Droplet formation in the turbulent mixing of two immiscible fluids), *15ème Congr. Fr. Méc.*, Nancy 3-7 septembre, 494-499

LEMENAND, T., DELLA VALLE, D., ZELLOUF, Y., PEERHOSSAINI, H. (2003). Droplet formation in turbulent mixing of two immiscible fluids in a new type of static mixer, *Int. J. Multiphase Flow* 29, 813-840.

LEMENAND, T., DUPONT, P., DELLA VALLEE, D., PEERHOSSAINI, H. (2005). Turbulent mixing of two immiscible fluids, *Trans. Am. Soc. Mech. Eng.*, 127, 1132-1139.

LEVICH, V.-G. (1962). Physiochemical Hydrodynamics. Prentice Hall, Englewood Cliffs, NJ, 464

LEVY, L.-B. AND HINOJOSA, L. (1992). Effect of oxygen on vinyl acetate polymerization, *Journal of applied polymer science*, vol 45., 1537-1544

LI, H.-Z., FASOL, C., CHOPLIN, L. (1997). Pressure drop of Newtonian and non-Newtonian fluids across a Sulzer SMX static mixer. *Trans IchemE* 75, part A, 792-796.

LIAO, Y., LUCAS, D., (2009). A literature review of theoretical models for drop and bubble breakup in turbulent dispersions. *Chem. Eng. Sci. 6*4 (15), 3389–3406

LIAO, Y., LUCAS, D. (2010). A literature review on mechanisms and models for the coalescence process of fluid particles, *Chemical Engineering Science*, 65, 2851-2864

LIU, S., LI, D. (1999). Drop coalescence in turbulent dispersions, *Chem.Eng.Sci*, vol. 54, 5667-5675

LOBRY E., THERON,F., GOURDON C., LESAUZE N., XUEREB C., LASUYE T.(2011) Turbulent liquid–liquid dispersion in SMV static mixer at high dispersed phase concentration. *Chemical Engineering Science*, 66 (23),5762-5774

LONGSDAIL, D.-H., THORNTON, J.-D., PRATT, H.-R.C. (1957). , Liquid-liquid extraction part XIV : The effect of column diameter upon the performance and troughput of pulsed plate columns *Trans. Inst. Chem. Eng.* 35, 301

MACKLEY, M.-R., NI, X. (1991). Mixing and dispersion in a baffled tube for steady laminar and pulsatile flow, *chemical engineering science*, 46, issue 12, 3139-3151

MACKLEY, M.-R., SMITH, K.-B., WISE, N.-P. (1993). The mixing and separation of particle suspensions using oscillatory flow in baffled tubes, *Chemical engineering research and design*, Vol. 71, Issue A6, 649-656, Times Cited 39

MACKLEY, M.-R., NI, X. (1993). Experimental fluid dispersion measurements in periodic baffled tube arrays, *Chemical Engineering Sciences*, Vol. 48, Issue 18, 3293-3305

MAASS S.; KRAUME M. (2012). Determination of breakage rates using single drop experiments, *Chemical Engineering Sciences, 70, 146-164*

MATE, A., MASBERNAT, O., GOURDON, C. (2000). Detachment of a drop from an internal wall in a pulsed liquid-liquid column, *Chemical engineering science*, 55, 2073-2088

MATSUMURA, K., MORISHIMA, Y., MASUDA, K., IKENAGA, H. (1981). Some performance data of the Hi-Mixer-An In-line mixer, *Chem. Ing. Tech.*, 53, N°1, 51-52.

MEYER ROBERT F.; ROGERS W. BENJAMIN; MCCLENDON MARK (2010). Producing Monodisperse Drug-Loaded Polymer Microspheres via Cross-Flow Membrane Emulsification: The Effects of Polymers and Surfactants, *Langmuir*, 26 Issue: 18, 14479-14487

MIDDLEMAN, S. (1974). Drop size distributions produced by turbulent pipe flow of immiscible fluids through a static mixer, *Ind. Eng. Chem. Process Des. Develop.*, 13, N°1, 78-83.

MINO, G. (1956). Copolymerization of styrene and acrylonitrile in aqueous dispersion, *Journal polymer science*, 22, 369-383.

NAHRINGBAUER, I. (1995). Dynamic surface tension of aqueous polymer solution, I. Ethyl(hydroxyethyl) cellulose (BERMOCOLL cst-103), *Journal colloid interface science*, 176, 318-328

NASS, L.-I., HEIBERGER, C.-A. (1986). PVC process and manufacture, chapter 3, *Encyclopedia of PVC volume 1 : resin manufacture and properties*, M. Langsam, 2nd edition revised and expanded Marcel Dekker

NARSIMHAN, G., GUPTA, J.P., RAMKRISHNA, D., (1979). Model for transitional breakage probability of droplets in agitated lean liquid–liquid dispersions. *Chem. Eng. Sci.* 34 (2), 257–265.

NI, X., ZHANG, Y., MUSTAFA, I. (1999). Correlation of polymer particle size with droplet size in suspension polymerization of methylmethacrylate in a batch oscillatory baffled reactor, *Chemical engineering science*, 54, 841-850

NI, X., JOHNSTONE, J.-C., SYMES, K.-C., GREY, B.-D., BENNETT, D.-C. (2001). Suspension polymerization of acrylamide in an oscillatory baffled reactor: from drops to particles, *AIChE Journal*, 47, issue 8, 1746-1757

NI, X., SOMMER DE GELICOURT, Y., BAIRD, M.-H-.-I., RAMA RAO, N.-V. (2001). Scale-up of single phase axial dispersion coefficients in batch and continuous oscillatory baffled tubes, *The Canadian Journal of chemical engineering*, vol. 79, R&D Note

NI, X., BROGAN, G., STRUTHERS A., BENNETT, D.-C., WILSON S.-F. (1998). A systematic study of the effect of geometrical parameters on mixing time in oscillatory baffled columns, *Chemical Engineering Research and design*, Vol. 76, Issue 5, Oil and nature gas production, 635-642.

NI, X., MURRAY, K.-R., ZHANG, Y., BENNETT, D., HOWES, T. (2002). Polymer product engineering utilising oscillatory baffled reactor, *Powder Technology*, 124, 281-286.

NILSSON, H., SILVEGREN, C., AND TÖRNELL, B. (1985). Suspension Stabilizers for PVC production I : Interfacial Tension Measurements, *J. Vinyl Technol.*, 7, 112-118.

OH W.Z. (1983) Analyse du fonctionnement hydrodynamique d'une colonne pulsée à disques et couronnes : étude du champ des vitesses. Thèse de Doctorat, Institut National Polytechnique de Toulouse.

ORMONDROYD S. (1988), The influence of polyvinylalcohol suspending agents on suspension polyvinyl chloride morphology, *Br. Polymer journal*, 20 Issue: 4 , 353-359.

OUSMANE, S., MABILLE, I., MOSCOSA-SANTILLAN, M., MAMADOU, T., AMOUROUX, J. (2011). Study of mass transfer and determination of drop size distribution in pulsed extraction column, *Chemical engineering research and design,* 89, issue 1, 60-68.

PADOVAN, D. AND WOODS, D.-R. (1986). Polyvinyl alcohol as a suspending agent for PVC production, *AIChE Symp. Ser.*, 82, 91-99.

PALMA M.AND GUIDICI R.(2003). Analysis of axial dispersion in a continuous oscillatory flow reactor*, chemical engineering journal*,94,189-198.

PAQUET D.A.; RAY W.H. (1994). Tubular reactors for emulsion polymerization. I. experimental investigation, AICHE JOURNAL, 40, Issue: 1,73-87.

PAUWELS, K.-F.-D. (2004). New aspects of the suspension polymerization of vinyl chloride in relation to the low thermal stability of poly(vinyl chloride), Ph.D. thesis, University of Groningen, Netherlands.

PEIXOTO, L.-S, MELO, P.-A., NELE, M., PINTO, J.-C (2009). Expanded Core/Shell Poly(vinyl acetate)/Poly(vinyl alcohol) Particles for Embolization, *Macromolecular materials and engineering*, vol. 294, Issue: 8, 463-471

PENLIDIS A.; MACGREGOR J.F.; HAMIELEC A.E. (1985). Dynamic modelling of emulsion polymerization reactors, *AiChE Journal*, 31 Issue: 6,881-889.

PENLIDIS A; MACGREGOR J.F.; HAMIELEC A.E. (1989), Continuous emulsion polymerization – design and control of CSTR trains, *chemical engineering science*, 44 Issue: 2 ,273-281.

PEREIRA, N.-E., NI, X. (2001). Droplet size distribution in a continuous oscillatory baffled reactor, *Chemical engineering science*, 56, 735-739.

PEREIRA, N.-E. (2002). Characterisation of a continuous oscillatory baffle tubular reactor, PhD thesis, Heriot-Watt University, Edinburgh, U. K.

PIZZINO, A., CATTÉ, M., VAN HECKE, E., SALAGER, J.-L., AUBRY, J.-M. (2009). On-line backscattering tracking of the transitional phase inversion of emulsions. *Colloids and surfaces A: Physicochem. Eng. Aspects* 338, 148-154.

RAMA RAO, N.V., BAIRD, M.H.I., HRYMAK, A.N., WOOD, P.E., (2007). Dispersion of high-viscosity liquid-liquid systems by flow through SMX static mixer elements. *Chem. Eng. Sci.*, 62, 6885-6896.

RAWLINGS J.B.; RAY W.H. (1988). The modelling of batch and continuous emulsion polymerization reactors. II. Comparison with experimental data from continuous stirred tank reactors,*Polymer engineering and science*, 28 Issue: 5,257-274.

REIS,N.;HARVEY,A.P.;MACKLEY,M.R.;VINCENTE,A.A.,TEIXEIRA,J.A.(2005). Fluid mechanics and design aspects of a novel oscillatory flow screening mesoreactor, *Chemical engineering research and design*, 83, 357-371.

RIBEIRO, M.M., REGUEIRAS, P.F., GUIMARAES, M.M.L., MADUREIRA, C.M.N., PINTO, J., (2011). Optimization of breakage and coalescence model parameters in a steady-state batch agitated dispersion. *Ind. Eng. Chem. Res. 50* (4), 2182–2191.

RICHARDSON J.F. AND ZAKI W.N. (1954) Sedimentation and fluidization: Part I. *Trans IChemE,Part A*, 32, 35-53.

ROSS, S.M.(1983). Stochastic processes, Wiley Series in Probability and Mathematical Statistics/Probability and Mathematical StatisticsWiley, New York (309 pp.)

ROTUREAU, E., LEONARD, M., DELLACHERIE, E. AND DURAND, A. (2004). Amphiphilic derivatives of dextran: Adsorption at air/water and oil/water interfaces, *J. Colloid Interface Sci.*, 279, 68-77

RUIZ, M.C., PADILLA, R., (2004). Analysis of breakage functions for liquid-liquid dispersions. *Hydrometallurgy* 72 (3-4), 245-258

SAEKI, Y., EMURA, T. (2002). Technical progresses for PVC production, *Progress in polymer science*, 27, issue 10, 2055-2131

SAYER, C., PALMA, M., GIUDICI, R. (2002). Modelling continuous vinyl acetate emulsion polymerization reactions in a pulsed sieve plate column, *Ind.Eng.Chem.Res.*, 41, 1733-1744

SCREENIVASULU, K., VENKATANARASAIAH, D., VARMA, Y.-B.-G. (1997). Drop size distributions in liquid pulsed columns, *Bioprocess engineering*, 17,189-195

SHAH, N.-F., KALE, D.-D. (1991). Pressure drop for laminar flow of non-newtonian fluids in static mixers, *Chem. Eng. Sci.,* 46, N°8, 2159-2161.

SHAH, N.-F., KALE, D.-D. (1992). Pressure drop for laminar flow of viscoelastic fluids in static mixers. *Chem. Eng. Sci.*, 47, N°8, 2097-2100.

SHAH, N.-F., KALE, D.-D. (1992). Two-phase, gas-liquid flows in static mixers. *AIChE J.*, 38, N°2, 308-310

SHINNAR, R, (1961). On the behaviour of liquid dispersions in mixing vessels, *Journal of Fluid mechanics*, Vol.10, 259-275

SHIRAISHI, M. AND TOYOSHIMA, K. (1973). Use of polyvinyl alcohol in the manufacture of polyvinylchloride, *Br. Polym. J.* , 5, 419-432

SHVAREV, E.-B., KOTLYAR, I.-B. AND ZAKHAROVA, Z.-S. (1966). Production of PVC using a polyvinylalcoholas a dispersing agent, *Plasticheskie Massy*, 7, 66-67
Singh et al (2009)

SMALLWOOD P.V. (1986). The formation of grains of suspension polyvinyl chloride, *Polymer*, 27 issue 10, 1609-1618

SNABRE, P., ARHALIASS, A. (1998). Anisotropic scattering of light in random media. Incoherent backscattered spot light, *Applied Optics* 37 (18) 211 – 225.

SNABRE, P., MENGUAL, O., MEUNIER, G. (1999). Optical characterization of concentrated suspensions, *Colloids and Surfaces*, A 152, 79–88.

SPROW, F.-B. (1967). Distribution of drop sizes produced in turbulent liquid-liquid dispersion, *Chemical engineering science*, vol. 22, 435-442

STAMENKOVIC, I.-S., BANKOVIC-ILIC, I.-B., JOVANIC, P.-B., VELJKOVIC, V.-B., SKALA D.-U. (2010). Hydrodynamics of a cocurrent upflow liquid–liquid reciprocating plate reactor for homogeneously base-catalyzed methanolysis of vegetable oils, *Fuel*, vol.89, 3971-3984

STEPHENS, G.-G. (1996). Suspension polymerization in oscillatory flow, PhD thesis, Cambridge university

STEPHENS, G.-G., MACKLEY M.-R. (2002). Heat transfer performance for batch oscillatory flow mixing, *Experimental Thermal and Fluid Science*, 25, 583-594.

STONESTREET P., VAN DER VEEKEN, P.M.J. (1999). The Effects of Oscillatory Flow and Bulk Flow Components on Residence Time Distribution in Baffled Tube Reactors, *Chemical Engineering Research and Design* 77 (8), 671-684.

STORK, M., (2005). Model-based Optimization of the Operation Procedure of Emulsification. Dissertation Thesis. Technical University Delft, Delft.

STREIFF, F.-A. (1977). In-line dispersion and mass transfer using static mixing equipment, *Sulzer Technol. Rev.*, 108-113.

STREIFF, F.-A., MATHYS, P., FISHER, T.-U. (1997). New Fundamentals for liquid-liquid dispersion using static mixers. *Réc. Progr. Génie Proc.* 11, 307-314.

TADROS, T.-F., VINCENT, B. (1983). Encyclopedia of Emulsion Technology, Paul Becher Edition, Vol. 1, Marcel Dekker, New York.

TAYLOR, G.-I. (1932). The viscosity of a fluid containing small drops of another fluid, *Proceedings of the Royal Society of London*, vol. 138, 41-48.

TAYLOR, T.-W., REICHERT, K.-H. (1985). The influence of reactor type and operating conditions on the molecular weight distribution in vinyl acetate polymerization, *Journal of applied polymer science*, 30, 227-250.

TEYMOUR F. (1989). The dynamic behavior of free radical solution polymerization in a continuous stirred tank reactor. Ph. D. Thesis, University of Wisconsin Madison.

THAKUR, R.-K., VIAL, CH., NIGAM, K.-D.-P., NAUMAN, E.-B., DJELVEH, G. (2003). Static mixer in the process industries - a review, *Trans IChemE*, 81, part A, 787-826.

THERON, F., LE SAUZE, N., RICARD, A. (2010). Turbulent liquid-liquid dispersion in Sulzer SMX mixer, *Ind. Eng. Chem. Res*, 49, 623-632.

THERON, F., LE SAUZE, N. (2011). Comparison between three static mixers for emulsification in turbulent flow *International Journal of Multiphase Flow*, Volume 37, Issue 5, Pages 488-500.

THOMSEN F., BILKE-KRAUSE (2006) *KRUSS Application note* An251e.

TIDHAR, M., MERCHUK, J.C., SEMBIRA A.N., WOLF D., 1986. Characteristics of a motionless mixer for dispersion of immiscible fluids - II. Phase inversion of liquid-liquid systems. *Chem. Eng. Sci.* 41, N°3, 457-462.

TORAB-MOSTAEDI, M., GHAEMI, A., ASADOLLAHZADEH, M. (2011). Flooding and drop size in a pulsed disc and doughnut extraction column, *Chemical Engineering Research and Design*, 83, 2742-2751.

TOURBIN, M. (2006). Caractérisation et comportement de suspensions concentrées de nanoparticules sous écoulement, Application aux processus d'aggrégation et de rupture, PhD thesis, INP Toulouse.

TURUNEN, I. (1994). Mass transfer in tubular reactors equipped with static mixers*, Chem. Eng. Sci.*, 49, N°24B, 5257-5269.

UEDA, T., TAKEUCHI, K., KATO, M. (1972). Polymer particle formation in suspension polymerization of vinyl chloride and vinyl acetate, *Journal of polymer science-Part A1 : Polymer chemistry,* vol 10, 2841-2852.

VAN DELDEN, M.-L., KUIPERS, N.-J.-M., DE HAAN, A.-B. (2006). Extraction of caprolactam with toluene in a pulsed disc and doughnut column - Part I: Recommendation of a model for hydraulic characteristics, *solvent extraction and ion exchange*, 24, issue 4.

VAN DELDEN, M.-L., KUIPERS, N.-J.-M., DE HAAN, A.-B. (2006). Extraction of caprolactam with toluene in a pulsed disc and doughnut column - Part II: Experimental evaluation of the hydraulic characteristics, *solvent extraction and ion exchange*, 24, 519-538.

VANKOVA, N., TCHOLAKOVA, S., DENKOV, N.D., VULCHEV, V.D., DANNER, T.(2007). Emulsification in turbulent flow 2. Breakage rate constants. *J. Colloid Interface Sci.* 313 (2), 612–629.

VILLERMAUX, E., (2007). Fragmentation. *Annu. Rev. Fluid Mec*h. 39, 419–446.

WALSTRA, P. (1993). Principles of emulsion formation, *Chem. Eng. Sci.,* Vol. 480, n°2, 333-349.

XIE, T.-Y., HAMIELEC, A.-E., WOOD, P.-E., WOODS, D.-R. (1991). Experimental investigation of vinyl chloride polymerization at high conversion: mechanism, kinetics and modelling, *Polymer*, 32, issue 3, 537-557.

YAMAMOTO, T., KAWASAKI, H., KUMAZAWA, H. (2007). Relationship between the dispersed droplet diameter and the mean power input for emulsification in three different type of motionless mixers, *J. Chem. Eng. Jpn*, 40, 673-678.

YARRANTON, H.-W., MASLIYAH, J.-H. (1997). Numerical simulation of Ostwald Ripening in emulsions. *Jour. Colloid Interface Sci.*, 196, 157-169.

YASUDA M., GODA T., OGINO H., GLOMM W.R., TAKAYANAGI, H. (2010). Preparation of uniform monomer droplets using packed column and continuous polymerization in tube reactor. *Journal of colloid and interface science* 349, 392-401.

YUAN, H.-G., KALFAS, G., RAY, W.-H. (1991). Suspension polymerization, JMS, *Rev. Macromol. Chem. Phys.*, C32 (2&3), 215-299.

ZERFA, M. AND BROOKS, B.-W. (1996). Prediction of vinyl chloride drop sizes in stabilized liquid-liquid agitated dispersion, *Chem.Eng.Sci.*, vol 51., n°12, 3223-3233.

ZERFA, M. AND BROOKS, B.-W. (1996).Vinyl chloride dispersion with relation to suspension polymerisation, *Chemical Engineering Science*, Volume 51, Issue 14, 3591-3611.

ZHOU, G., KRESTA, S.-M. (1997) Correlation of mean drop size and minimum drop size with the turbulence energy dissipation and the flow in an agitated tank, *Chem. Eng. Sci.*, 53, 2063-2079.

US 20050054795A1 (Akzo Nobel)
US 3004013, 1961, Detrex corporation
US 4487898, 1984, Kanegafuchi Chemical industry
US 5282680, 1994, Shin Etsu Chemical
US 6252016B1 (2001, Rhom and Haas Company)
US4424301, 1984, Hoechst
US4456735, Juin 1984, Hoechst
WO03/054040 2002 Akzo Nobel
WO2007110350A1 2007, Akzo Nobel)